Central Asian Snow Cover Characteristics between 1986 and 2012 derived from Time Series of Medium Resolution Remote Sensing Data

Inaugural-Dissertation zur Erlangung der Doktorwürde der

Philosophischen Fakultät I der Julius-Maximilians-Universität Würzburg

vorgelegt von

Dipl. Geograph Andreas Jürgen Dietz

aus Hammelburg

München, 2013

Erstgutachter: Professor Dr. Christopher Conrad

Zweitgutachter: Professor Dr. Jürgen Rauh

Tag des Kolloquiums: 18.12.2013

Acknowledgments

The presented thesis was only made possible due to the support of my supervisors, colleagues, and friends. First of all I want to thank Prof. Dr. Christopher Conrad from the University of Würzburg, who assisted in many research questions related to the study region of Central Asia. His extensive knowledge about the situation in place, the water related issues, the political framework, combined with the most profound experience in the processing and analysis of remotely sensed data turned out to be all but unpayable. At the same time, I want to thank Prof. Dr. Stefan Dech from the German Remote Sensing Data Center of the German Aerospace Center for the support. His far-reaching experience in the processing and handling of medium resolution remote sensing data – AVHRR in particular – would have been an irreplacebale store of knowledge. Finally, I want to thank Dr. Claudia Künzer from the Department of Land Surface, German Remote Sensing Data Centre of the German Aerospace Center for her continuous assistance and advice, and for allowing me to be part of a most motivating, open-hearted, and cooperative team.

All the colleagues from this team also deserve my special thanks and appreciation, notably - though not exclusively - Dr. Tuan Vo Quoc, inspiring with his exhilarant spirit, Dr. Ursula Gessner for supporting me during the realization of my first paper, Igor Klein for his help with the Russian Translation, Dr. Vahid Naemi for his help and comments regarding IDL programming, Dr. Corinne Frey and Patrick Leinenkugel for enduring to share the office with me, and finally my colleagues Malte Ahrens, Manuel Fabritius, Tim Funkenberg, and Marco Ottinger for diversifying discussions and activities also outside the office.

I want to thank Gerhard Gesell from the Department of Atmosphere, German Remote Sensing Data Center of the German Aerospace Center for his most valuable support during the processing of AVHRR data, the patient introductions to the APOLLO software, and the provision of the required computer infrastructure to facilitate my processing.

Further thanks go to Thomas Eiglsperger who supported the study by collecting field data, the colleagues from the German Research Centre for Geoscience (GFZ) in Potsdam who managed and were involved in the CAWa project, the German Ministry of Foreign Affairs for financing this project, as well as all the interns and administrational staff for doing all the work that usually stays all but unnoticed.

Finally, I want to thank my parents Gabi and Gunter Dietz for their long-time support. The presented thesis was only made possible due to your patience, assistance, and compliancy for so many years.

Table of contents

List of figures

List of tables

Glossary

AATSR	Advanced Along Track Scanning Radiometer
ACQWA	Assessing Climate impacts on the Quantity and quality of Water
AMSR-E	Advanced Microwave Scanning Radiometer - Earth Observing System
ANSA	Air ForceWeather Agency/NASA Snow Algorithm
AO	Arctic Oscillation
APOLLO	AVHRR Processing scheme Over Land, cLoud and Ocean
ARSIS	Amélioration de la Résolution Spatiale par Injection de Structures
ATSR-2	Along Track Scanning Radiometer 2
AVHRR	Advanced Very High Resolution Radiometer
CAWa	Central Asian Water
CLASS	Comprehensive Large Array-data Stewardship System
CLAVR	Clouds from AVHRR
CLPX	Cold Land Processes Field Experiment
DEM	Digital Elevation Model
DFD	Deutsches Fernerkundungsdatenzentrum / German Remote Sensing Data Center
DLR	Deutsches Zentrum für Luft- und Raumfahrt / German Aerospace Center
DMSP	Defense Meteorological Satellite Program
ECA&D	European Climate Assessment & Dataset
ECV	Essential Climate Variable
ESPON	European Spatial Planning Observation Network
ETM	Enhanced Thematic Mapper
GCOS	Global Climate Observing System
GCP	Ground Control Points
GLIMS	Global Land Ice Measurements from Space
GMS	Geostationary Meteorological Satellites
GOES	Geostationary Operational Environmental Satellites
GPCC	Global Precipitation Climatology Centre
HRPT	High Resolution Picture Transmission
HSDSD	Historical Soviet Daily Snow Depth
HUT	Helsinki University of Technology

ICSU	International Council for Science
IMS	Interactive Multisensor Snow and Ice Mapping System
IOC	Intergovernmental Oceanographic Commission
IPCC	Intergovernmental Panel on Climate Change
IR	InfraRed region of the spectrum
ISODATA	Iterative Self-Organizing Data Analysis Technique
LAC	Local Area Coverage
LDCM	Landsat Data Continuity Mission
LST	Land Surface Temperature
MAE	Mean Absolute Error
MBE	Mean Bias Error
MERIS	Medium Resolution Imaging Spectrometer
MIR	Medium InfraRed region of the spectrum
MLP	Multi-Layer Perceptron
MODIS	Moderate Resolution Imaging Spectroradiometer
MSC	Meteorological Service of Canada
NAO	North Atlantic Oscillation
NASA	National Aeronautics and Space Administration
NCEP	National Centers for Environmental Prediction
NDSI	Normalized Difference Snow Index
NDVI	Normalized Difference Vegetation Index
NESDIS	National Environmental Satellite, Data, and Information Service
NIR	Near InfraRed region of the spectrum
NLR	Norwegian Linear-Reflectance
NOAA	National Oceanic and Atmospheric Administration
NOHRSC	National Operational Hydrologic Remote Sensing Center
NSIDC	National Snow and Ice Data Center
PM	Passive Microwave
PPL	Post Processing Level
PPMW	Parts Per Million by Weight
QSCAT	QuickSCAT
RIHMI	Russian Institute for Hydrometeorological Information
RMSE	Root-Mean-Square-Deviation

SCD	Snow Cover Duration
SCDA	Simple Cloud Detection Algorithm
SCI	Snow Cover Index
SCI_{ES}	Early Season Snow Cover Index
SCI_{LS}	Late Season Snow Cover Index
SCM	(Date of) Snow Cover Melt
SCMD	Snow Cover Melting Date
SCOD	Snow Cover Onset Date
SCS	(Date of) Snow Cover Start
SD	Snow Depth
SMMR	Scanning Multichannel Microwave Radiometer
SNODAS	Snow Data Assimilation System
SNOTEL	Snow Telemetry
SPARC	Single Pixel Aggregate Rating of Cloudiness
SRTM	Shuttle Radar Topography Mission
SSM/I	Special Sensor Microwave Imager
SST	Sea Surface Temperature
ST	Skin Temperature
SWE	Snow Water Equivalent
SYKE	Finnish Environment Institute
SZ	Solar Zenith Angle
TGI	Temperature Gradient Index
TIR	Thermal InfraRed
TIROS-1	Television and InfraRed Observation Satellite
TM	Thematic Mapper
TOA	Top-Of-Atmosphere
UNEP	United Nations Environment Programme
UNESCO	United Nations Educational Scientific and Cultural Organization
USGS	U.S. Geological Survey
VIS	Visible range of the spectrum
VGT	SPOT-4 VEGETATION
VHRR	Very High Resolution Radiometer
WMO	World Meteorological Organization

Abstract

The eminent importance of snow cover for climatic, hydrologic, anthropogenic, and economic reasons has been widely discussed in scientific literature. Up to 50% of the Northern Hemisphere is covered by snow at least temporarily, turning snow to the most prevalent land cover types at all. Depending on regular precipitation and temperatures below freezing point it is obvious that a changing climate effects snow cover characteristics fundamentally. Such changes can have severe impacts on local, national, and even global scale. The region of Central Asia is not an exception from this general rule, but are the consequences accompanying past, present, and possible future changes in snow cover parameters of particular importance. Being characterized by continental climate with hot and dry summers most precipitation accumulates during winter and spring months in the form of snow. The population in this 4,000,000 km² vast area is strongly depending on irrigation to facilitate agriculture. Additionally, electricity is often generated by hydroelectric power stations. A large proportion of the employed water originates from snow melt during spring months, implying that changes in snow cover characteristics will automatically affect both the total amount of obtainable water and the time when this water becomes available. The presented thesis explores the question how the spatial extent of snow covered surface has evolved since the year 1986. This investigation is based on the processing of medium resolution remote sensing data originating from daily MODIS and AVHRR sensors, thus forming a unique approach of snow cover analysis in terms of temporal and spatial resolution. Not only duration but also onset and melt of snow coverage are tracked over time, analyzing for systematic changes within this 26 years lasting time span. AVHRR data are processed from raw Level 1B orbit data to Level 3 thematic snow cover products. Both, AVHRR and MODIS snow maps undergo a further post-processing, producing daily full-area mosaics while completely eliminating inherent cloud cover. Snow cover parameters are derived based on these daily and cloud-free time series, allowing for a detailed analysis of current status and changes. The results confirm the predictions made by coarse resolution predictions from climate models: Central Asian snow cover is changing, posing new challenges for the ecosystem and future water supply. The changes, however, are not aimed at only one direction. Regions with decreasing snow cover exist as well as those where the duration of snow cover increases. A shift towards earlier snow cover start and melt can be observed, posing a serious challenge to water management authorities due to a changed runoff regime.

Zusammenfassung (Abstract in German)

Die Bedeutung von Schneebedeckung hinsichtlich klimatischer, hydrologischer, anthropogener und ökonomischer Gesichtspunkte wurde in der wissenschaftlichen Literatur bereits umfassend diskutiert. Bis zu 50% der Nördlichen Hemisphäre sind zeitweise schneebedeckt. Abhängig von Niederschlag und Temperaturen unter dem Gefrierpunkt beeinflussen Veränderungen des Klimas zwangsläufig die Charakteristik der Schneeverteilung. Solche Veränderungen können weitreichende Folgen auf lokalem, nationalem und sogar globalem Maßstab haben. Zentralasien stellt in diesem Zusammenhang keine Ausnahme dar, denn die Konsequenzen vergangener, aktueller und möglicher zukünftiger Schneebedeckungsveränderungen sind hier besonders gravierend: Wegen des kontinentalen Klimas und den damit verbundenen trocken-heißen Sommern fällt der Hauptteil des verfügbaren Niederschlages in den Winter- und Frühlingsmonaten in Form von Schnee. Die Bevölkerung in der etwa 4.000.000 km² großen Region ist in besonderem Maße von Bewässerungslandwirtschaft abhängig. Darüber hinaus wird ein Großteil der Elektrizität durch Wasserkraftwerke erzeugt. Das für diese Zwecke verwendete Wasser generiert sich hauptsächlich durch Schneeschmelze im Frühling. Veränderungen im Schneehaushalt haben unmittelbare Auswirkungen auf die Menge des zur Verfügung stehenden Wassers sowie den Zeitpunkt, zu dem dieses frei wird. Die vorgestellte Arbeit wird der Frage nachgehen, wie sich die räumliche Ausdehnung schneebedeckter Flächen seit dem Jahr 1986 entwickelt hat. Diese Untersuchung basiert auf der Analyse mittelaufgelöster Fernerkundungsdaten der Sensoren MODIS und AVHRR, die mit der verbundenen zeitlichen und räumlichen Auflösung einen einmaligen Ansatz darstellen. Nicht nur die Schneebedeckungsdauer, sondern auch Beginn und Ende der Schneesaison werden über die Zeit hinweg verfolgt, um systematische Veränderungen innerhalb der 26 Jahre andauernden Zeitreihe analysieren zu können. Rohe AVHRR Daten werden in thematische Produkte überführt, die dann zusammen mit den MODIS Schneeprodukten prozessiert werden um tägliche, wolkenfreie Mosaike der kompletten Region zu erzeugen. Die Ergebnisse bestätigen Vorhersagen grob aufgelöster Klimamodelle: Die Schneebedeckung in Zentralasien verändert sich und stellt damit die Ökosysteme und Wasserplanungsbehörden vor neue Herausforderungen. Die Änderungen sind jedoch nicht ausschließlich negativ: Regionen mit reduzierte verringerter Schneebedeckung existieren neben solchen, in denen die Bedeckung zunimmt. Eine generelle Verschiebung der Schneebedeckung hin zu früherem Beginn und früherem Ende der Saison kann ebenfalls beobachtet werden. Gerade diese Verschiebung stellt die Behörden und Wasserplaner vor deutliche Herausforderungen, da mit diesen Verschiebungen auch eine Änderung des zugrundeliegenden Abflussregimes einhergeht.

резюмé (Abstract in Russian)

Значение снежного покрова с климатической, гидрологической, антропогенной и экономической точки зрения в научной литературе широко обсуждалось. До 50% северное полушарие временами покрыта снегом. Поэтому снег являетса, по крайней мере временно самым распространенным покрытием земли. В замисимости от осадков и температур ниже градуса звмерзения, изменения климата воздействуют на характеристику распределения снега. Такие изменения могут иметь далеко идущие последствия местного, регионального и даже глобального масштаба. Центральная Азия в данном моменте не являетса исключенная, потому что последствия прошлых, настояших, и возможных будушщих изменений покрова снега значительны серьезные: из-за континентального климата и связанного с этим сухого жаркого лета, основная часть осадков падает на зимние и весенние месяцы в виде снега. Жители этого примерно 4.000.000 км² региона, в большой степени зависят от оросительной системы. Кроме того, большая часть электричества производится с помощью электростанций. Используемая для этого вода образуется от тайния снега весной. Изменение количества снега оказывает непосредственное влияние на каличество готовой для использования воды и на время её образования.

Представленная работа рассматривает вопрос как развивалось пространственное расширение снежного покрова площадей с 1986 года. Эти иследования базироваться на процессиворании данных сеисоров MODIS и AVHRR которые представляют связанные временем и пространством показыват беспримерную методику. Не только время снежного покрова, но и начало и конец снежного сезана наблюдались в течение продолжительного времене, чтобы анализировать систематические изменения произошедшие в течение 26 лет. Результаты подтверждают предсказание модель климата с низким разрешением: снежный покров Центральной Азии изменяетса и ставит экологическую систему и управление водных планирования перед новыми задачами. Однако изменения направленн не только в одну сторону: регионы с уменьшением снежного покрова существовать рядом с такими, в которых величена снежного покрова увеличивается. Всеобщим сдвиг снежного покрова в сторону раннего начала и раннего окончания сезона так же наблюдается. Как раз эти сдвиги ставят а власти и хозяйства вода планирования перед сложные задачи, так как с этими сдвигами связаны и изменения в системе сточных вод.

1. Introduction and aims of the thesis

Up to 50% of the Northern Hemisphere – around 47,000,000 km² - is covered by snow during winter months (Hall et al., 1995; Levinson and Lawrimore, 2007; Romanov et al., 2000). Another 10% of the total land surface are permanently covered by ice (Lemke et al., 2007). Figure 1.1 gives an example of the maximum (left: January 15th) and minimum (right: August 15th) snow and ice cover extent for 2010 on the Northern Hemisphere. GlobSnow snow extent product (Solberg et al., 2011), GLIMS glacier inventory (Armstrong et al., 2011), and Sea Ice Concentrations from Nimbus-7 Scanning Multichannel Microwave Radiometer (SMMR) and Defense Meteorological Satellite Program (DMSP) Special Sensor Microwave Imager (SSM/I) (Cavalieri et al., 1996) were used to produce Figure 1.1. The comparison between both months reveals the tremendous dynamics that occur within Earth's cryosphere every year.

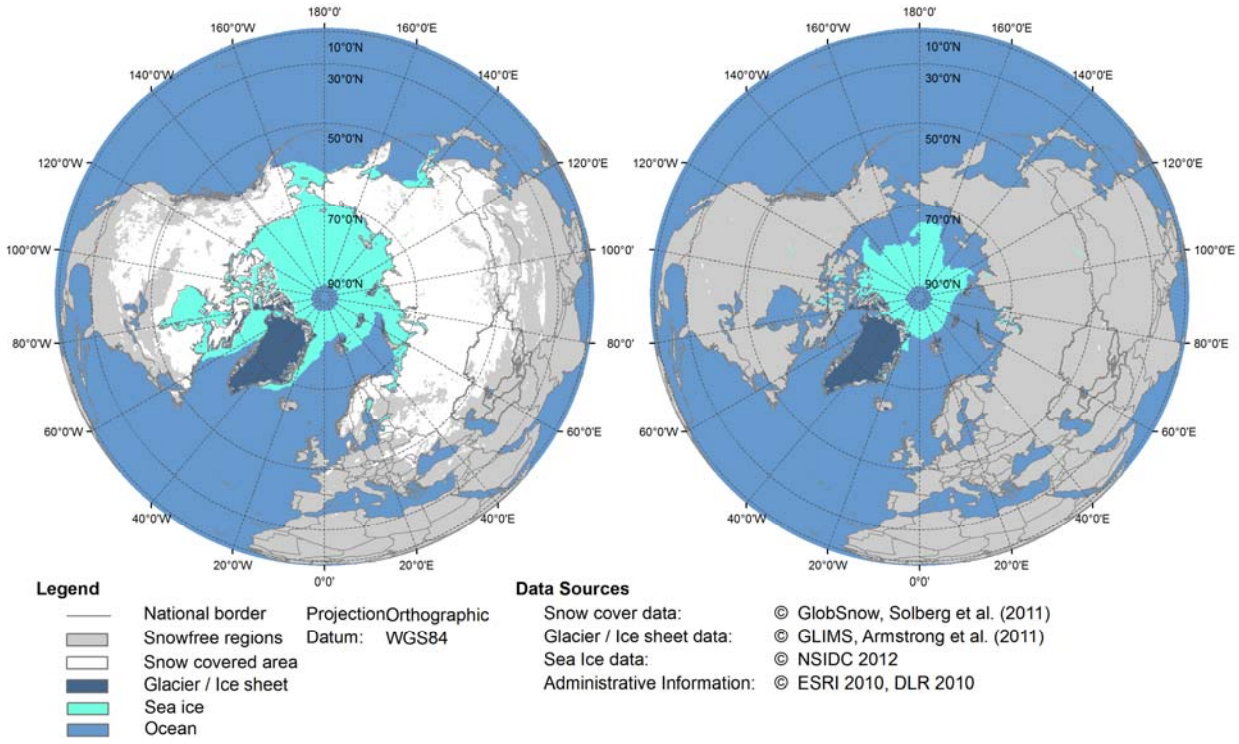

Figure 1.1: Northern Hemisphere snow and ice cover extent in January (left) and August (right) 2010

The high reflectivity of snow covered areas (up to 90% of incoming solar radiation are reflected) constitutes an important factor for the overall radiation budget of the Earth's surface (Barnett et al. 1989; Groisman et al. 1994; Groisman et al. 1994a; Klein et al. 2000; König et

al. 2001; Winther et al. 1999; Hall & Martinec 1985). On a more regional scale, snow cover is important for the local water availability, river runoff, groundwater recharge, and glacier mass balance (Jain et al. 2008; Akyürek & Sorman 2002; Zhang et al. 2010). Vegetation growth is influenced by snow cover duration (SCD) and thickness because snow has an isolating effect during cold months, preventing plant roots from freezing (Peng et al., 2010). Forest greening in water-limited mid-elevation zones of mountainous regions is influenced by snowpack variability (Trujillo et al., 2012). Permafrost is affected by this effect as well, controlling ground temperatures by keeping them warmer than air temperature once snow is deep enough (Stieglitz et al., 2003). Agriculture is depending on the quantity and character of snow cover (Richter, 1960). Besides, natural disasters such as floods, droughts, or avalanches can be triggered through abnormal snow cover events (Thurman 2011; Nature Protection Ministry Republic of Kazakhstan 2006; Muntán et al. 2009).

Climate change is affecting the distribution and duration of snow coverage, generally leading to a reduction of the parameters (Barry 2008; Ross D. Brown 2000; Jylhä et al. 2008; Brown & Mote 2009; Lemke et al. 2007). The average snow cover extent and SCD for the Arctic is projected to decrease by up to 20% until the year 2050 (Callaghan et al., 2011). Model simulations proof that snow cover will develop variably, depending on the position and the prevailing changes in temperature and precipitation (Räisänen, 2007). Therefore, snow cover has been identified within the Global Climate Observing System (GCOS) as an Essential Climate Variable (ECV) where satellite observations can make significant contributions (WMO and GCOS, 2011). The GCOS, initiated by the World Meteorological Organization (WMO), the Intergovernmental Oceanographic Commission (IOC) of the United Nations Educational Scientific and Cultural Organization (UNESCO), the United Nations Environment Programme (UNEP), and the International Council for Science (ICSU) aims to provide comprehensive scientific information on the entire climate system (GCOS, 2012). The systematic observation requirements for satellite-based data products for climate as a part of GCOS describe the standards which should be conformed during the processing of ECVs. They constitute the aspired standards for the presented thesis and are based on the fact that snow coverage is highly sensitive to changes in temperature and precipitation. Changed snow cover characteristics may lead to significant feedbacks due to changed planetary albedo and energy balance (WMO and GCOS, 2011). Continuous monitoring of snow is therefore an important aspect for understanding the effects of climate change on the cryosphere. The target requirements of GCOS are included in Table 1.1.

Table 1.1: Target Requirements for ECV snow cover extent

Variable/ Parameter	Horizontal Resolution	Vertical Resolution	Temporal Resolution	Accuracy	Stability
Snow areal extent	1km; 100m in complex terrain	N/A	daily	5% (maximum error of omission and commission in snow area); location accuracy better than 1/3 IFOV with target IFOV 100m in areas of complex terrain, 1km elsewhere	4% (maximum error of omission and commission in snow area); location accuracy better than 1/3 IFOV with target IFOV 100m in areas of complex terrain, 1km elsewhere

Source: (WMO and GCOS, 2011)

The Intergovernmental Panel on Climate Change (IPCC) stated in their assessment report of 2007 that, besides the shrinking of glaciers and arctic sea ice, SCD and extent has decreased significantly since 2001 (Lemke et al., 2007). These changes followed earlier developments of decreasing snow cover extent observed since 1966 and are related to shifts towards later snow cover onset in autumn and earlier melting in spring seasons. Since 1972, the mean date of snow cover melt (SCM) has shifted two weeks onwards (Dye, 2002). Earlier SCM results in changed runoff patterns and decreased surface albedo. The consequences on a regional scale may, however, differ from these general statements.

How is Central Asia affected by snow cover changes and what consequences may evolve from these changes for the region? Kazakhstan, Kyrgyzstan, Tajikistan, Turkmenistan, and Uzbekistan form the approximately 4,000,000 km² large region of Central Asia (Figure 1.2) – a region whose economic development strongly depends upon water availability. The shrinking Aral Sea, an immense cotton production with high demands for irrigation, retreating glaciers, and the proceeding desertification are only few examples for actual threats the region is facing (Lioubimtseva & Henebry 2009; Aizen et al. 2006). Precipitation in this mostly arid and continental region occurs mainly during winter and spring months (Klein et al. 2012), constituting regular and sufficient snow cover a strongly required source of freshwater. The main source of water for rivers originating in Central Asian mountains is melt water from both seasonal snow cover and glaciers (Aizen et al. 1995). The water scarcity in the region was even described to have the potential to intensify international tensions between Uzbekistan and Kazakhstan (Bernauer & Siegfried 2012). This explains why status and changes of snow cover characteristics are of particular research interest.

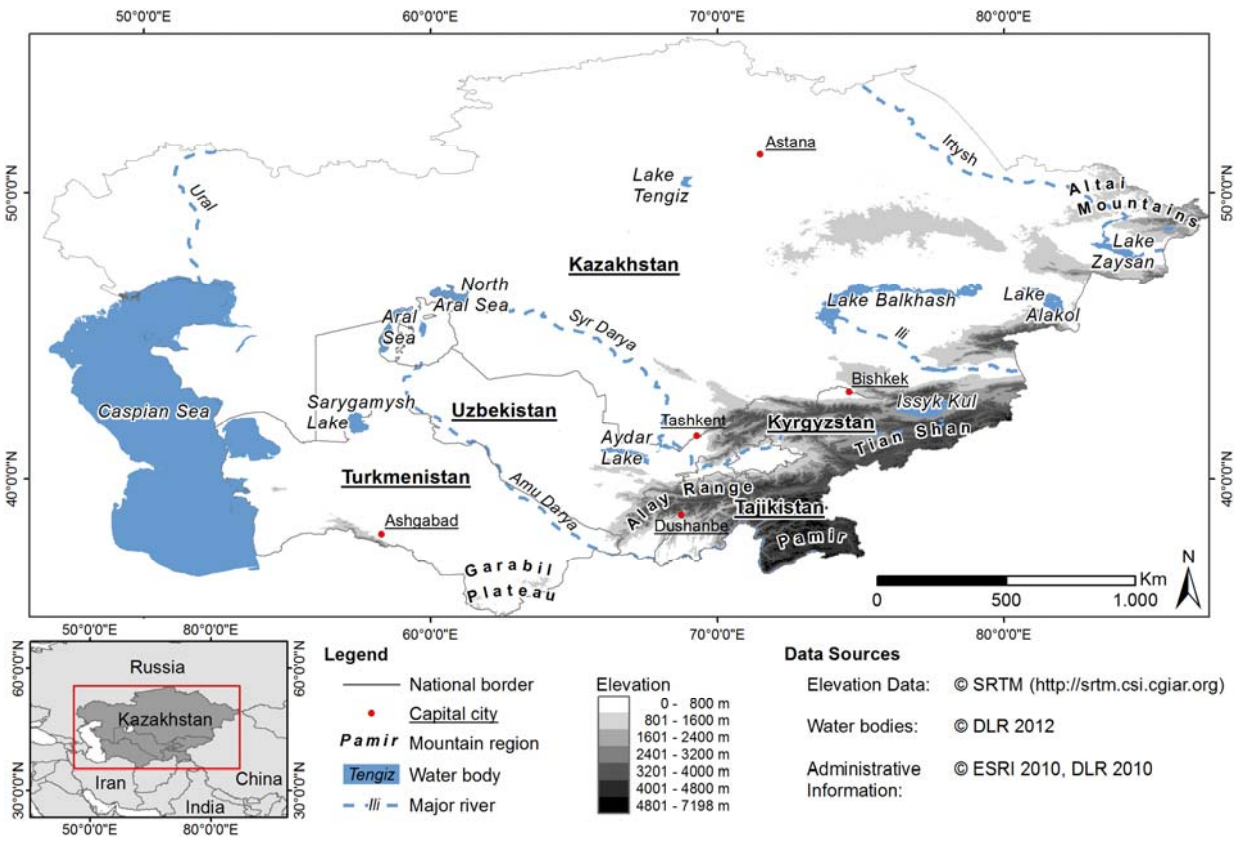

Figure 1.2: Overview of Central Asia

Climate change has caused a temperature increase of 1-2 °C in Central Asia since the beginning of the 20th century (Lioubimtseva and Henebry, 2009), affecting SCD, snow cover start (SCS), and SCM. Precipitation trends point towards increased values during winter/spring and decreased values in summer months (Mokhov et al., 2006). All these dynamics confirm a strongly susceptible and variable ecosystem where monitoring and forecasting of actual and possible future changes is of major importance for environment and population. Changing snow cover characteristics inevitably affect the status of glaciers, which play an important role in the hydrological cycle of Central Asia (e.g. Aizen et al., 1997). The locations of the upstream hydro-catchments of Amu Darya and Syr Darya Rivers coincide with the glacier springs – rivers which form the lifelines of Central Asia. Irrigation, drinking water, electric power generation, pastoral economy, and the establishment and management of artificial water reservoirs: All these aspects are directly affected by changing snow cover parameters. It is of utterly importance to identify past and present snow cover characteristics for the whole area, providing high temporal and spatial resolution. Only then becomes an analysis of the snow cover changes within the study region possible. The aims of the presented thesis evolve from this background and include the following questions:

- Which techniques are available that allow the mapping of snow cover on a daily basis, for the whole area of Central Asia, while fulfilling the demands made with regards to spatial resolution and product accuracy? A review of snow mapping techniques is required to complete this task.
- Once the adequate techniques have been identified during the review: How do the snow cover characteristics (including the parameters SCD, SCS, and SCM) of Central Asia look like today? The processing of the snow cover parameters based on the methods identified during the review will allow answering this question.
- How did each of the snow cover parameters develop over time? The processing of a time series of daily snow cover data for the longest possible period is required to account for this question.
- Given that a time series of daily snow cover parameters is available: How may the future snow cover conditions look like when coming from the results prepared during the processing of this long term time series? What are the possible consequences with regards to future water availability?

Because of the large extent of the study area and the requirement to use daily data (otherwise snow cover parameters cannot be calculated) the only possible data source is remotely sensed data. The next chapters will outline a detailed description about the study region (chapter 2), the physical background of how snow cover can be monitored from space using different observation techniques (chapter 3), and the data sources analysed during the thesis (chapter 4). The methods used to derive the desired snow cover parameters will be outlined (chapter 5) before the results will be presented and discussed (chapter 6). Finally, the conclusions (chapter 7) will complete the presented thesis.

Some scientific publications have already emerged from the presented study or are currently under review: It was a priority objective from the very beginning that all the conducted analyses and results should be made available to the scientific community as soon as possible. It does not make sense to gain insight in cryospherical/hydrological processes of a region without sharing and discussing these insights with the affected people and other experts from the same research field. Within the framework of the presented thesis, the following publications emerged or are currently under way:

Publications:

- Dietz, A.J., Kuenzer, C., Gessner, U., and Dech, S. (2012): Remote Sensing of Snow – a review of available methods. *International Journal of Remote Sensing*, 13, pp. 4094-4134.
- Dietz, A.J., Wohner, C., and Kuenzer, C. (2012): European Snow Cover Characteristics between 2000 and 2011 Derived from Improved MODIS Daily Snow Cover Products. *Remote Sensing*, 4, pp. 2432-2454.
- Dietz, A.J., Kuenzer, C., and Conrad, C. (2013): Snow-cover variability in Central Asia between 2000 and 2011 derived from improved MODIS daily snow-cover products. *International Journal of Remote Sensing*, 34, pp. 3879-3902.
- Dietz, A.J., Gesell, G., Conrad, C., Kuenzer, C., and Dech, S. (submitted in 2013): Processing of daily snow cover products from NOAA-AVHRR data for Central Asia using APOLLO. Submitted to *Remote Sensing of Environment* and accepted with major revisions (as of March 22nd, 2013).
- Dietz, A.J., Kuenzer, C., Conrad, C., and Dech, S. (prepared in 2013): Changes of Snow Cover Characteristics in Central Asia between 1986 and 2012 derived from AVHRR and MODIS time series. Prepared for *Hydrological Processes* (as of May 2nd, 2013).

Conference contributions:

- Dietz, A.J., Conrad, C., and Kuenzer, C.: Snow cover variability in Central Asia during the last decade derived from MODIS. Oral presentation at *International Geographical Congress (IGC) Cologne*: 28.08.2012.
- Dietz, A.J., Kuenzer, C., and Dech, S.: European Snow Cover Characteristics between 2000 and 2011 derived from improved MODIS Daily Snow Cover Products. Poster presentation at *ESA Earth Observation and Cryosphere Science Conference*. 13-16.11.2012, Frascati (Rome), Italy.
- Dietz, A.J., Kuenzer, C., Conrad, C., and Dech, S.: Changes of Snow Cover Characteristics in Central Asia between 1986 and 2012 derived from AVHRR and MODIS time series. Oral presentation prepared for the *70th Eastern Snow Conference*. 04-06.06.2013, Huntsville (Ontario), Canada.

2. Region of interest – Central Asia

The term “Central Asia” itself is ambiguous because it is no established definition and was used for different regions in literature. (Cowan, 2007) introduced to the diverse usages of “Central Asia” and “Middle Asia” and reviewed various publications referring to these regions. It appears that in recent years, the traditional meaning of “Central Asia” (Western China, Outer and Inner Mongolia) has shifted towards what was initially defined as “Middle Asia” (Kazakhstan, Turkmenistan, Uzbekistan, Tajikistan, Kyrgyzstan). When referring to “Central Asia” in a political context, the term can include Turkmenistan, Uzbekistan, Tajikistan, and Kyrgyzstan while in a more geographical context, “Central Asia” is also used to describe Xinjiang in China (Cowan, 2007). (Glantz, 2005) asserts that “Central Asia” can comprise Afghanistan, as well. In the presented thesis however, the region of interest – “Central Asia” - is congruent with the countries included in the CAWa project (Figure 1.2) and includes Kazakhstan, Turkmenistan, Uzbekistan, Tajikistan, and Kyrgyzstan.

Snow cover characteristics are influenced by several factors: Temperature and precipitation are most important variables concerning amount, duration, start, and melt of snow cover. Besides, land cover type and topography constitute additional, more static parameters. While the land cover type can influence the snow mapping accuracy (this aspect will be outlined in section 3.2), topography also determines duration, start, and stop of snow coverage through elevation, slope, and aspect. The geology does not influence the presence of snow and is therefore excluded from closer examinations. The same is true for soils, which are of course impacted by temperature and precipitation – the two most important aspects when it comes to snow cover monitoring – but which stand in no direct connection among each other. The following sub sections will summarize the most relevant aspects of Central Asia in terms of snow cover occurrence.

2.1 Climate, climate change, and hydrology

The aridity of the region with maximum precipitation during winter and spring months has already been addressed to in the introduction. Figure 2.1 illustrates the detailed precipitation characteristics for Central Asia during Spring (March, April, May), Summer (June, July, August), Autumn (September, October, November), and Winter seasons (December, January, February). As data source for Figure 2.1, the Global Precipitation Analysis Product of the Global Precipitation Climatology Centre (GPCC) between 1980 and 2009 was used

(Schneider et al., 2010). Climate station data from up to 47,000 different locations (in 1986) were incorporated in this product that is made available in 0.5° and 2.5° resolutions.

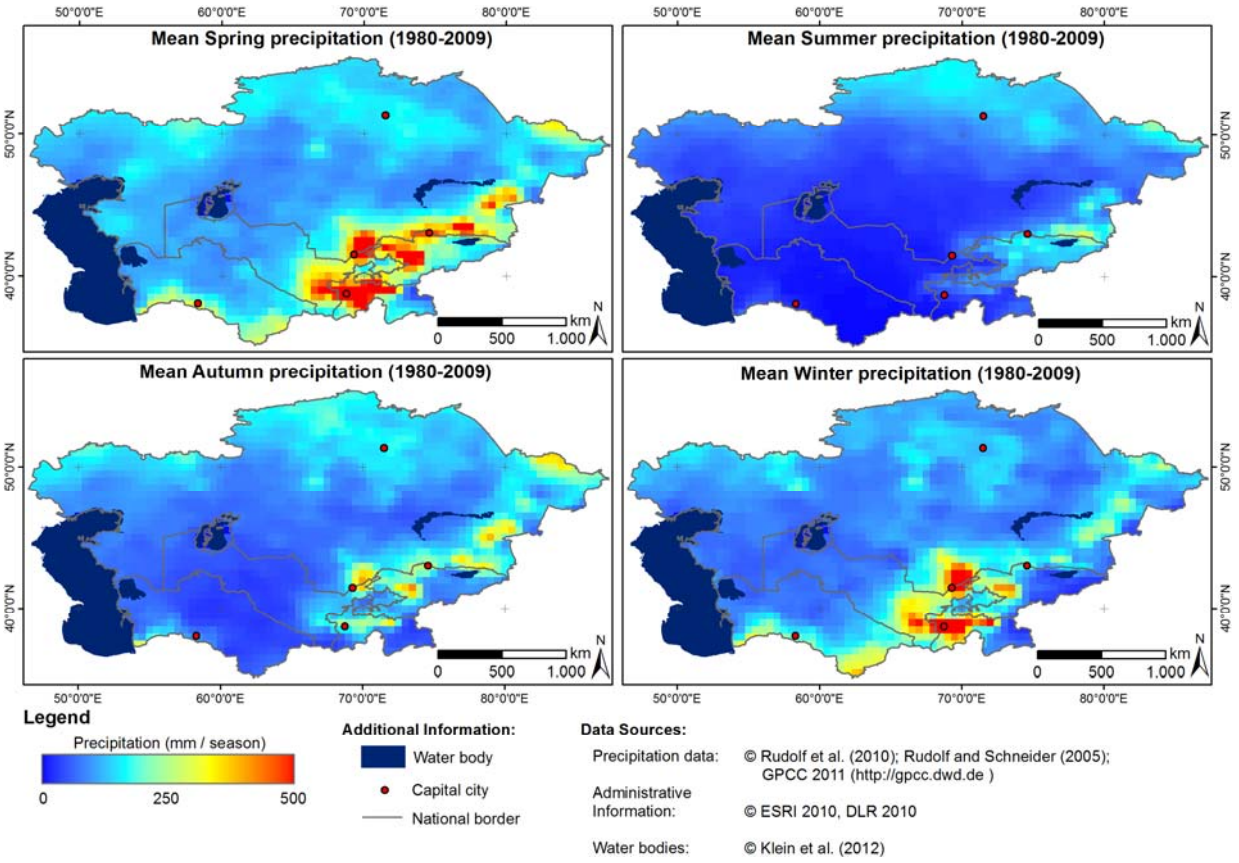

Figure 2.1: Seasonal precipitation characteristics of Central Asia

The precipitation patterns of Figure 2.1 describe an absolute maximum during spring months, followed by winter and autumn. Summer is the season with least precipitation. Mountainous regions stick out due to extraordinary high rates especially in spring and winter months. The mountainous region in the South and South-East receive the largest part of available precipitation.

The hydrological catchments of Amu Darya, Syr Darya (both tributaries to the Aral Sea), and Ili River (tributary to the Lake Balkhash) obtain most of their inflow from these mountainous regions. Figure 2.2 gives a detailed overview of the sub-catchments within the three hydrological entities. These sub-catchments will be referred to later in the presented thesis. They are divided into three categories: Upstream-, Intermediate-, and Downstream-catchments (see blue, orange, and red boxes in Figure 2.2). Detailed information about the size and elevation range of each catchment is also presented in Table 2.1.

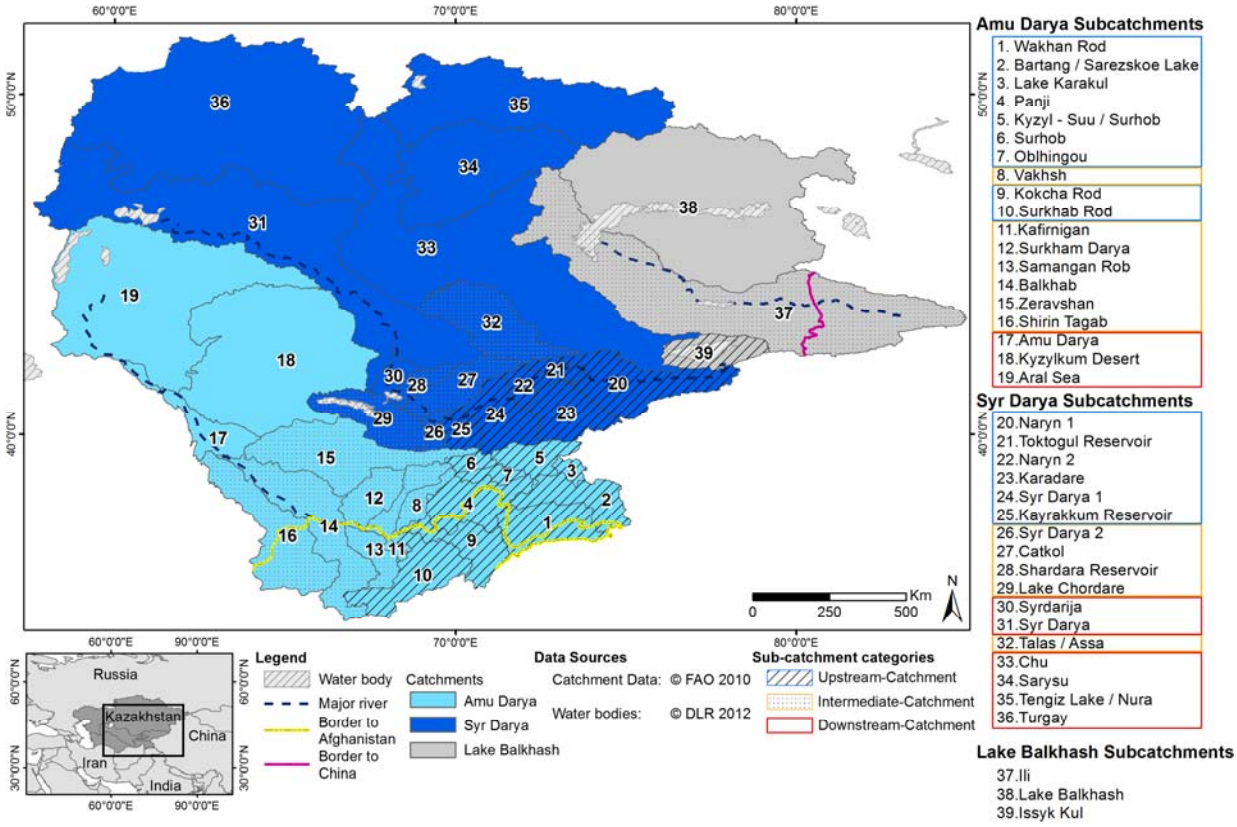

Figure 2.2: Sub-catchments of Amu Darya, Syr Dayra, and Lake Balkhash, classified in Upstream- (blue rectangles), Intermediate- (orange rectangles), and Downstream-catchments (red rectangles)

The rivers of Amu Darya and Syr Darya are the most important sources of fresh water for Central Asia. Forming in the mountainous regions of Kyrgyzstan and Tajikistan, these rivers represent one of the few natural resources of these countries. A detailed register containing all tributaries, catchments sizes and runoff amounts can be found in a summary provided by UNECE (2007, see also Table 2.1). The transboundary character of Amu Darya River - with 70 to 77 km³ total runoff per year twice as much as Syr Dayra River (Glantz, 2005; Ososkova et al., 2000) - constitutes a severe political issue due to increased water consumption and regulation in the upstream area and the diverse consequences that finally led to the Aral Sea disaster: Desiccation of the Aral Sea, salinization, pollution (Micklin, 2007) – a development that was already initiated by the vast expansion of water infrastructure since the 1950s. Since that time and under the reign of the former Soviet Union, water consumption for irrigation from Amu Darya and Syr Darya Rivers increased continuously. While in 1960s, 56 km³ water reached the Aral Sea through Amu Darya River, the amount was reduced to only 6 km³ in the 1980s (Diebold and Sehring, 2012).

Table 2.1: Sub-catchments of Central Asia, basic information and classification into three categories: Upstream (UP), Intermediate (IN), and Downstream (DO) catchments

Code	Sub-catchment Name	Mean elevation	Min. elevation	Max. elevation	Area (km²)	Catchment*
1	Wakhan Rod	4,320	1,982	7,241	31,369	AM - UP
2	Bartang / Sarezskoe Lake	4,355	1,992	6,368	27,818	AM - UP
3	Lake Karakul	4,521	3,955	6,513	4,464	AM - UP
4	Panji	2,438	410	6,185	32,387	AM - UP
5	Kyzyl - Suu / Surhob	3,891	1,755	6,865	16,790	AM - UP
6	Surhob	2,790	1,158	4,856	5,610	AM - UP
7	Oblhingou	3,418	1,167	7,198	6,619	AM - UP
8	Vakshs	939	320	3,627	9,718	AM - IN
9	Kokcha Rod	2,722	315	6,455	25,381	AM - UP
10	Surkhab Rod	2,281	307	5,644	38,491	AM - UP
11	Kafirnigan	1,317	290	4,466	17,269	AM - IN
12	Surkham Darya	1,245	272	4,396	20,319	AM - IN
13	Samangan Rob	1,316	272	4,030	14,550	AM - IN
14	Balkhab	963	173	4,520	60,605	AM - IN
15	Zeravshan	1,137	188	5,376	63,061	AM - IN
16	Shirin Tagab	760	174	3,652	58,705	AM - IN
17	Amu Darya	167	85	392	23,105	AM - DO
18	Kyzylkum Desert	219	67	2,006	163,969	AM - DO
19	Aral Sea	80	58	416	179,028	AM - DO
20	Naryn 1	2,986	1,173	5,095	45,935	SY - UP
21	Toktogul Reservoir	2,253	1,038	4,083	6,875	SY - UP
22	Naryn 2	1,525	403	4,132	10,384	SY - UP
23	Karadare	2,185	437	4,904	27,391	SY - UP
24	Syr Darya 1	1,556	355	5,282	27,984	SY - UP
25	Kayrakkum Reservoir	1,564	321	5,397	10,544	SY - UP
26	Syr Darya 2	1,280	272	4,923	6,578	SY - IN
27	Catkol	1,709	252	4,244	24,212	SY - IN
28	Sardara Reservoir	514	248	2,542	9,354	SY - IN
29	Lake Chordare	561	248	4,087	31,476	SY - IN
30	Syrdarija	280	197	578	7,997	SY - DO
31	Syr Darya	218	65	4,043	207,637	SY - DO
32	Talas / Assa	910	329	4,316	45,426	SY - IN
33	Chu	587	125	4,772	213,051	SY - DO
34	Sarysu	473	223	1,063	83,917	SY - DO
35	Tengiz Lake / Nura	540	324	1,485	110,438	SY - DO
36	Turgay	212	74	1,095	248,426	SY - DO
37	Ili River	1,266	402	5,296	202,012	BA - IN
38	Lake Balkhash	706	487	4,409	221,629	BA - DO
39	Issyk Kul	135	43	244	21,953	BA - UP

*AM, SY, and BA are abbreviations for Amu Darya, Syr Darya, and Lake Balkhash, respectively. Information was in parts extracted from

Today and during dry years, the water resources of Amu Darya and Syr Darya are consumed completely for irrigation, causing the rivers to run dry before they even reach the Aral Sea (Ososkova et al., 2000). The efficiency of irrigation techniques is often low, wasting considerable amounts of the most precious resource (Awan et al., 2011; Tischbein et al.,

2013). Evaporation and groundwater discharge add to an estimated water loss of 40% or more for irrigated areas along Amu Darya River (Conrad et al., 2007). Hydroelectric power production is another large consumer of water (~27% of Central Asia's electricity is generated by hydropower plants (Kipshakbaev et al., 2004)). Because electric power is needed throughout the year, water discharges for electric power production increase during winter months. This water is then missing during the irrigation period (Ibatullin et al., 2009). 90% of Kyrgyzstan's electricity is produced by hydroelectric sources (Diebold and Sehring, 2012). Tajikistan generates 98% of its electricity from hydropower and plans exist to extend hydropower generation and export energy to China and Pakistan (Jalilov et al., 2011) - an indirect export of water in a manner of speaking. Especially China seems to have increased interest in Central Asia as a trading partner and energy exporter since the country is investing in the development of future hydropower facilities in the region (Granit et al., 2010). This so-called water-energy nexus (UNEP et al., 2005) creates serious tensions among the Central Asian states: More energy is needed, and fossil fuels are too expensive (and in the case of Kyrgyzstan rather finite) when compared to hydropower. It is only consequential that the upstream countries of Tajikistan and Kyrgyzstan prefer hydropower generation to fossil fuel power generation, leaving the downstream nations short of water in dry years. Tajikistan and Kyrgyzstan are the only Central Asian states with positive water balance: More water is generated through to precipitation, snow- and glacier-melt than it is withdrawn. For Kazakhstan, Uzbekistan, and Tajikistan, the opposite is true (UNEP et al., 2005).

Turkmenistan is seeking for foreign investors to finance a $1 billion expansion in cotton industry until 2016 (Gurt, 2012). The situation may even get worse since Afghanistan will most likely establish or reconstruct irrigation canals and water management facilities in the upstream regions of Amu Darya catchment (Glantz, 2005), draining additional water from the already narrow resource. Former international agreements between the USSR and Afghanistan have not been renewed after the collapse of the Soviet Union (Vinogradov and Langford, 2001), posing additional uncertainty to the already tense situation. The Fergana Valley, which is located in the Syr Darya catchment, is the most densely populated region of whole Central Asia. Population is even projected to increase by 40% until 2050 (Siegfried et al. 2011). Social problems are triggered by water scarcity, including economic, civil rights, and health issues (Strickman and Porkka, 2008). More than 290 water reservoirs have been constructed until 2010 in Central Asia, regulating and managing runoff from rainfall, snow and glacier melt. Many of these reservoirs were constructed under Soviet regime in the 1960s and 1970s, primarily for cotton production in Tajikistan and Uzbekistan (Karaev, 2005). Plans for even more reservoirs are raising issues among the countries (Rakhmatullaev et al., 2010). It was already mentioned in the introduction that changes in water management, population, water demand,

and available fresh water runoff may increase the tensions between the neighbouring countries in this region (Bernauer & Siegfried 2012). It is especially this region within the Amu Darya and Syr Darya River catchments that is susceptible to these tensions. A citation from (Glantz, 2005) is perhaps best suited to conclude this paragraph:

> *"[…] the Greater Central Asian Republics, collectively speaking, are dependent on the flow of two major rivers […] for their long-term survival. Upstream-midstream-downstream issues will strongly influence the way these states interact, whether it is through cooperation, litigation or conflict."*

Figure 2.2 excludes two regions without information about their hydrological affiliation: The western area between the Caspian Sea and the Aral Sea catchments is draining to the Caspian Sea. The region of northern and north-eastern Kazakhstan is part of the Irtysh River catchment, draining northwards into Ob River and, finally, into the Arctic Ocean. Water generated in these regions is lost for the irrigated areas of Central Asia (location of irrigated areas will be included in Figure 2.5 of section 2.2).

Runoff in Central Asia in general is dominated by snowmelt – regardless of the hydrological catchment that is being observed. This means that the ratio of snowfall to annual runoff is larger than 0.5 for the whole area (it often even exceeds 0.8 (Barnett et al. 2005) and even nearly reaches 1 in some areas (Adam et al. 2009)). Melt from seasonal snow cover is more important for Syr Darya River while in the Amu Darya River catchment, melt water from both snow and glacier ice emerge simultaneously (Ososkova et al., 2000). The importance of snow for Central Asia becomes apparent from these facts and they also make clear that changes in snow cover characteristics pose a serious threat to the political stability as well as the growing population.

Besides precipitation, glacier melt is an important contributor to available runoff water especially during spring season. Figure 2.3 gives an overview of glaciers in Central Asia based on the Global Land Ice Measurements from Space (GLIMS) dataset (Raup et al. 2007; Armstrong et al. 2011). This dataset was established by more than sixty institutions throughout the world to provide an inventory of all existing glaciers and is growing continuously. Glaciers form an important part of the hydrological cycle but in Pamir, Tian Shan, and Altai mountains, climate change causes a significant retreat in both volume and length. While during the 1950s glacier melt was artificially intensified to increase water availability in downstream catchments by depositing coal dust to the glacier surfaces (Kotlyakov and Dolgushin, 1973), the glacier retreat is seen most unfavourable today and has been investigated by various researchers:

Khromova et al. (2006) found that glaciers in eastern Pamir have receded substantially between 1978 and 2001 (Zulumart glacier at ~38°N, 72°E e.g. lost 17.5% of glaciated area). Aizen et al. (2006) analysed tacheometric and photogrammetric measurements as well as remotely sensed data of Akshiirak and Ala Archa glaciers in Tian Shan. They concluded that over the last 140 years, both glaciated regions sustained a recession. In total, the area covered by glaciers in Tian Shan mountains decreased by 12-14% only within the last 40 to 60 years (Aizen et al. 2007). Surazakov et al. (2007) investigated glaciers in the Siberian Altai Mountains at the border between Kazakhstan, Mongolia, Russia, and China between 1952 and 2006. Again, a reduction of glaciated area was observed. The recession of glaciers is projected to continue in the future with a volume reduction of up to ~31% (depending on the scenario) until 2050 (Siegfried et al. 2011). Glacier melt will contribute to a significant increase in river runoff until 2050, but this will only be a short term incident. Water amounts will decrease to only one third of today's values before 2100 (Watson et al., 1998).

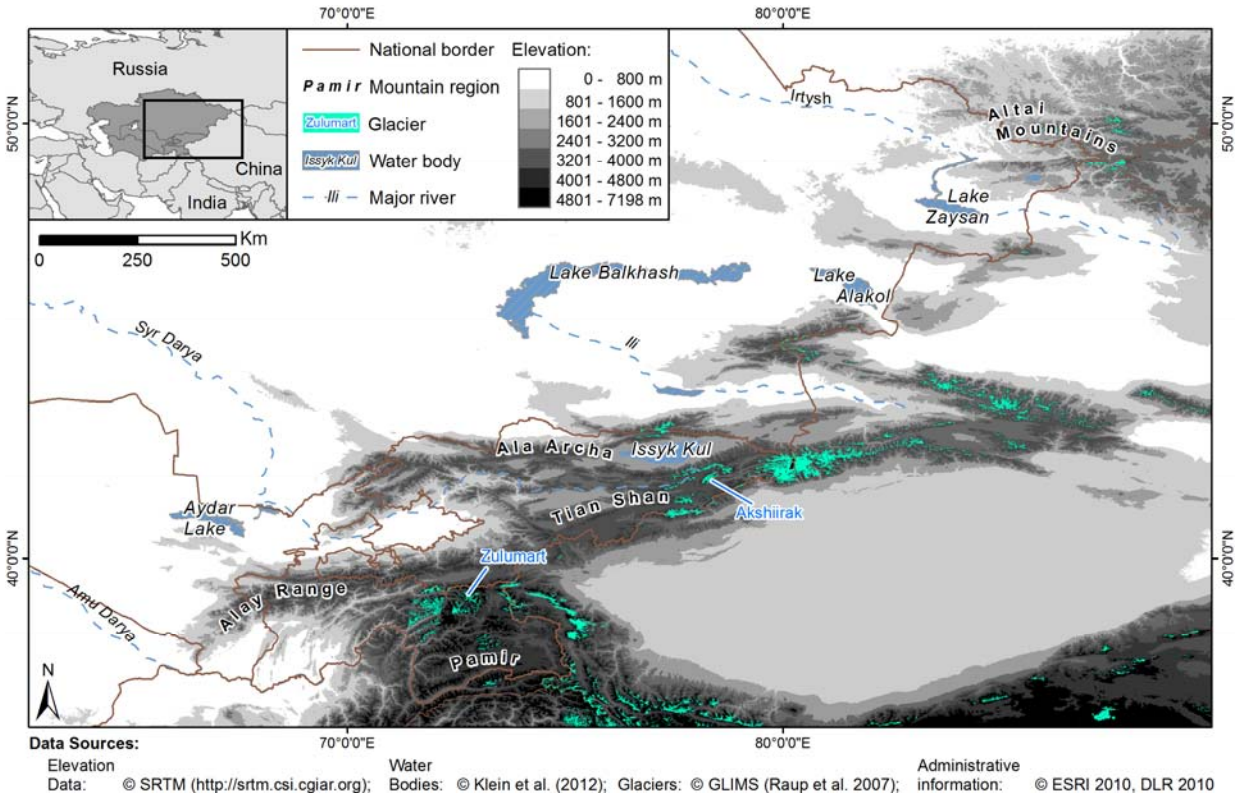

Figure 2.3: Glacier inventory of Central Asia and adjacent regions (GLIMS data set)

The presented thesis does not focus on glaciers or their possible development in the future. However, because they are depending on snowfall on one hand and contribute significantly to runoff on the other hand, glaciers are a necessary part of the cryospheric and hydro-

logical system of Central Asia. Neglecting their existence would prevent a holistic summary of the actual conditions. Therefore, this short overview of glaciers in Central Asia was included in this section.

Surface temperature is a limiting factor with regards to snow cover persistence. Only while temperature stays below freezing point an accumulation of snow on the surface is possible. Figure 2.4 depicts the mean surface temperature for each month as provided by the *Worldclim* dataset (Hijmans et al., 2005). The temperature was interpolated from climate station data for the years between 1950 and 2000 with a spatial resolution of 30 arc seconds (around 1 km – depending on the distance to the equator). The authors of the *Worldclim* data declare that the quality of the product varies, depending on station density and topography.

Because station density in Central Asia is generally low, the product must be interpreted with care (Hijmans et al., 2005). The same is true for the precipitation product from the GPCC (Figure 2.1). The quality of the already sparsely distributed stations is another issue. Giese & Moßig (2004) pointed to the problem that some of the stations provide biased data because they have been moved to other locations, changed the instruments/measuring techniques, or stopped/interrupted operation after the collapse of the Soviet Union in 1989. Savitskaya (2010) confirmed that consistent time series of meteorological data are limited for Central Asia. Libert et al. (2008) support the conclusion that especially since the separation of the Central Asian States from the former Soviet Union, the number of climate stations decreased substantially.

However, because Figure 2.1 and Figure 2.4 only serve as an overview to understand the general climatic background, the problems related to the generation of the GPCC and *Worldclim* data can be neglected. The information from these two figures suggests that although temperature is below freezing point for large parts of Kazakhstan, Tajikistan, Uzbekistan, and Kyrgyzstan during November, the lack of autumn precipitation may prevent from early snow cover onset.

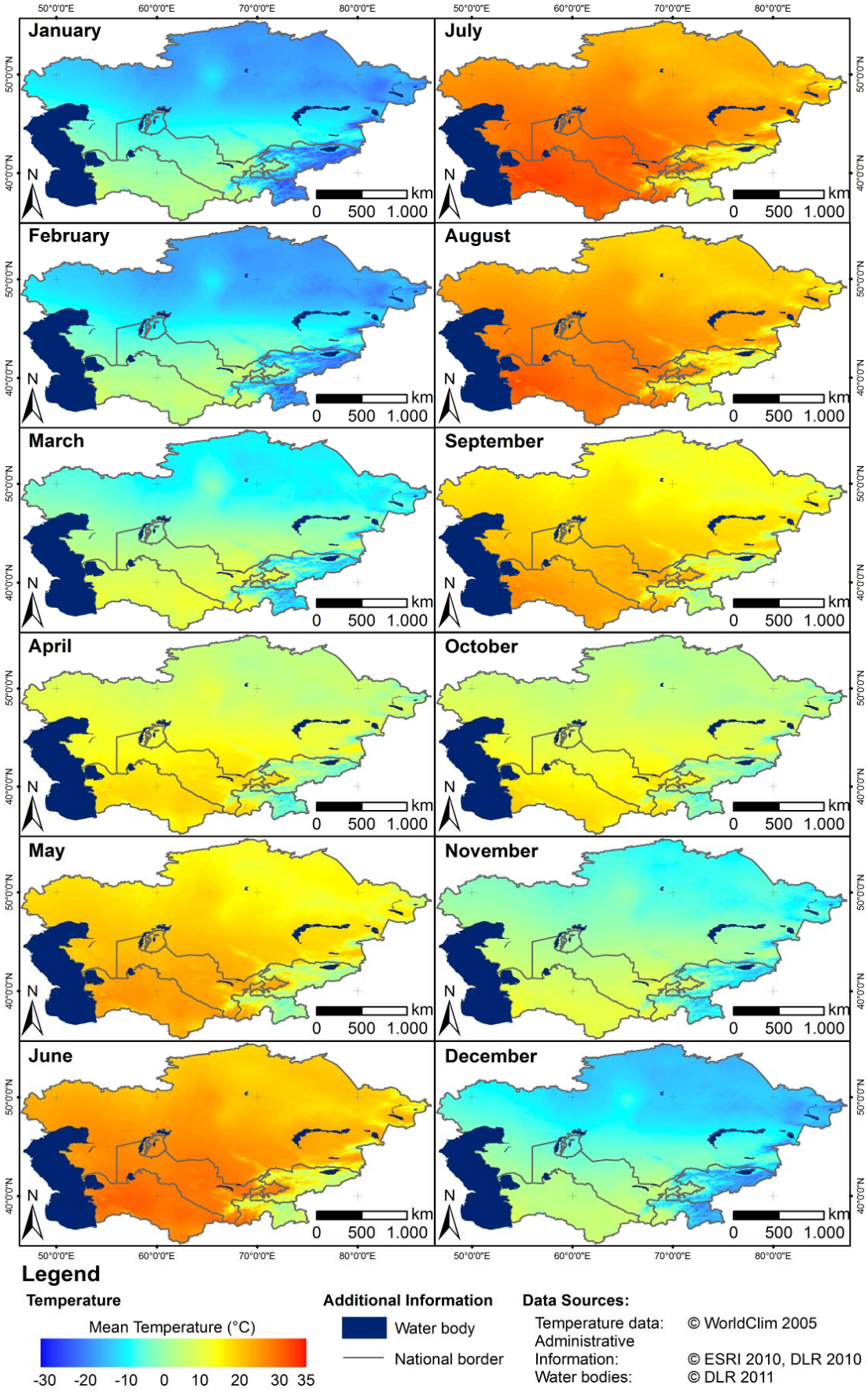

Figure 2.4: Mean surface temperature per month

The amount of precipitation is particularly low in Uzbekistan and southern Kazakhstan. With the beginning of December, snowfall can be expected to increase under normal conditions as can be interpreted from Figures 2.1 and 2.4. From this point on, the temperature increase in spring will be the dominant factor ending the snow season.

Climate change is an important topic not only in Central Asia. Reconsidering the hydrological situation with problems like water scarcity, increasing water demand and transboundary water issues the possible effects of climate change on the region of Central Asia become evident. Some basic facts about climate change in Central Asia have already been presented in the introduction: Distribution and duration of snow coverage are affected by climate change, leading to a reduction of the parameters in most regions of the world (Barry 2008; Brown 2000; Jylhä et al. 2008; Brown & Mote 2009; Lemke et al. 2007). Räisänen (2007) analysed various climate model simulations and concluded that in some regions, changed temperature and precipitation will lead to more snow. The borderline between increasing and decreasing snow cover coincides with the -20°C cold season isotherm. In regions with warmer temperatures, a reduction of SCD and Snow Water Equivalent (SWE) can be expected. This was also confirmed by Hosaka et al. (2005) who projected an increase in SWE for northern parts of Siberia and North America, only.

A temperature increase of 1-2°C since the beginning of the 20th century in Central Asia inevitably affects SCD (Lioubimtseva and Henebry, 2009). The velocity of climate change was analysed by Loarie et al. (2009): For Central Asia, temperature increase proceeds with ~ 0.7 km/year. In other words: If today, mean surface temperature at a certain location is 0° C for March, the same temperature conditions will only be found 7 km further to the North after ten years. An increase in precipitation especially during winter and spring months was observed (Mokhov et al., 2006), potentially leading to an earlier SCS. Fallot et al. (1997) confirmed that this increase in precipitation led also to higher snow depths rates in northern Kazakhstan. Kim et al. (2012) detected a trend towards earlier spring thawing and longer non-frozen seasons for the Northern Hemisphere, affecting also parts of Kazakhstan, Uzbekistan, and Central Asian mountain regions. Aizen et al. (1997) observed increasing temperatures and precipitation in Tian Shan Mountains. If precipitation increases due to climate change, snow cover may start earlier. Higher temperatures in spring, however, would even out- or overcompensate this effect. It was predicted by Siegfried et al. (2011) that changes in precipitation and temperature will lead to earlier SCM. This development may cause the runoff peak in the upstream catchments of Amu Darya and Syr Darya Rivers to shift 30 to 60 days towards an earlier date. Such changes would result in severe consequences for reservoir management. Savitskaya (2010) emphasized that changes in the discharges of Central Asian rivers are of great importance for

millions of people. Water content in Amu Darya and Syr Darya Rivers will decrease in the future because glacier melt - which compensated the increased temperatures and changed snowmelt pattern in the past - will not be able to contribute to a balanced water budget in the future. Glaciers have already melted for the most part and cannot alleviate future water shortage (Savitskaya, 2010). These predictions are, however, based on calculations from climate models. An in-depth analysis of snow cover time series processed from medium resolution remote sensing data could serve as a more solid proof for these conclusions.

2.2 Land cover and topography

Land cover is an important aspect when considering the accuracy of snow cover classifications derived from remotely sensed data. Especially the presence of forests (Hall et al. 2002) or large shrubs (Lucas & Harrison 1990; Rittger et al. 2012) can limit the reliability of the classification (section 3 will outline these limitations in more detail). The land cover information from Figure 2.5 was taken from Klein et al. (2012). Forested areas are only present in eastern and most northern Kazakhstan as well as in mountain valleys of Kyrgyzstan. They account for 1.8 % of the total area (~39,000 km² needleleaved evergreen trees and ~34,000 km² broadleaved deciduous trees). A decreasing forest cover fraction trend was observed by Yesserkepova (2010) and Klein et al. (2012) that is caused by logging, forest fires, and climate change. Shrubs are distributed along a large belt stretching from the Caspian Sea in the West over the Aral Sea region and Lake Balkhash to the East.

These shrubs are composed of the classes *closed to open shrubland* (~40,500 km²; ~1% of total area), *open shrubland* (~264,000 km²; ~6.6% of total area), and *sparse shrubs and sparse herbaceous vegetation* (~472,000 km², ~11.8% of total area). In general it could be stated that compared to other regions like Russia, Europe or North America, Central Asia is an ideal region for snow cover mapping concerning the prevailing land cover. The sparse forested regions are especially advantageous in this context.

Irrigated areas concentrate along the major rivers and irrigation channels of Central Asia: They are represented within the *cultivated aquatic or regularly flooded area* class and primarily located within Amu Darya and Syr Darya catchments (Klein et al., 2012; UNEP et al., 2005). These regions have no direct influence on the accuracy of snow cover mapping. They are, however, potentially affected by changes in snow cover characteristics since they depend on the melt water during spring and summer months.

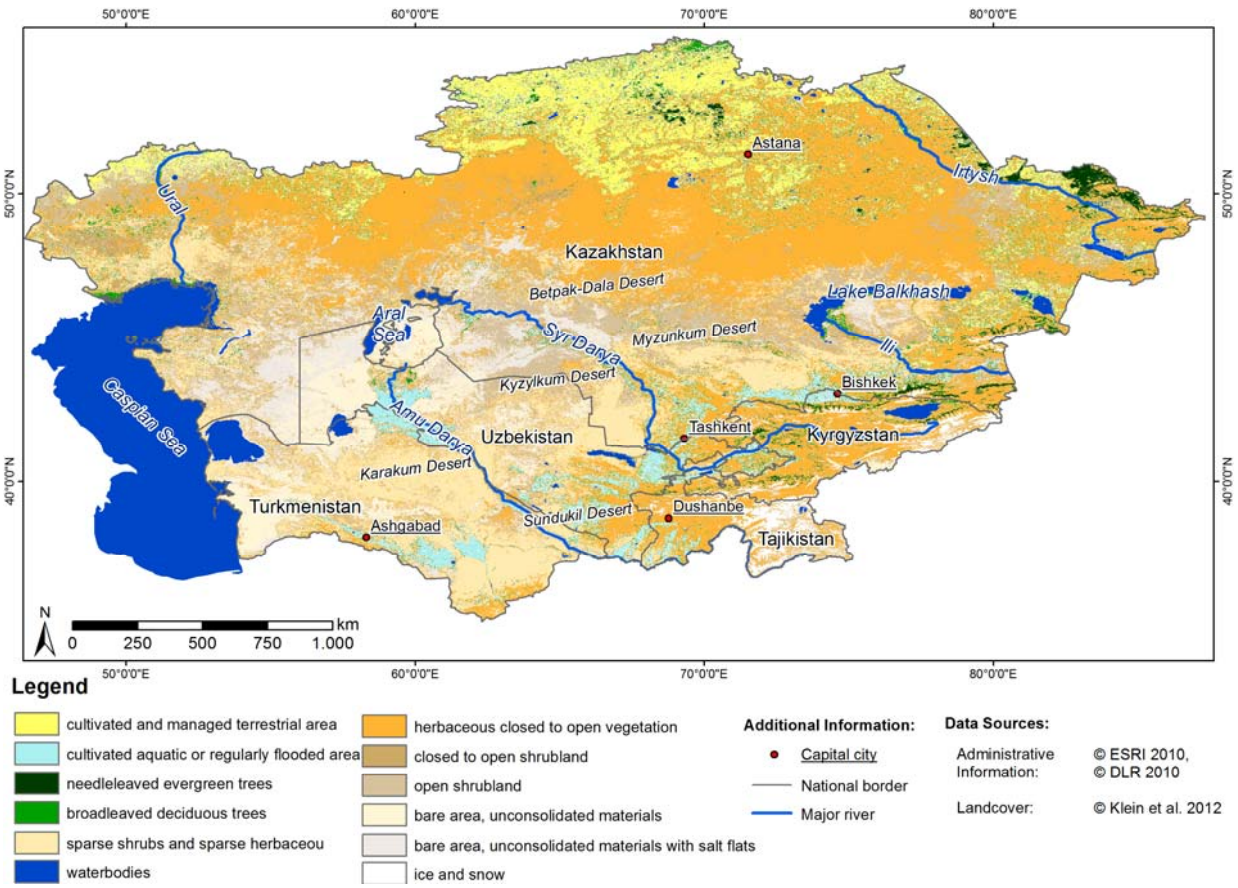

Figure 2.5: Land cover of Central Asia (2009)

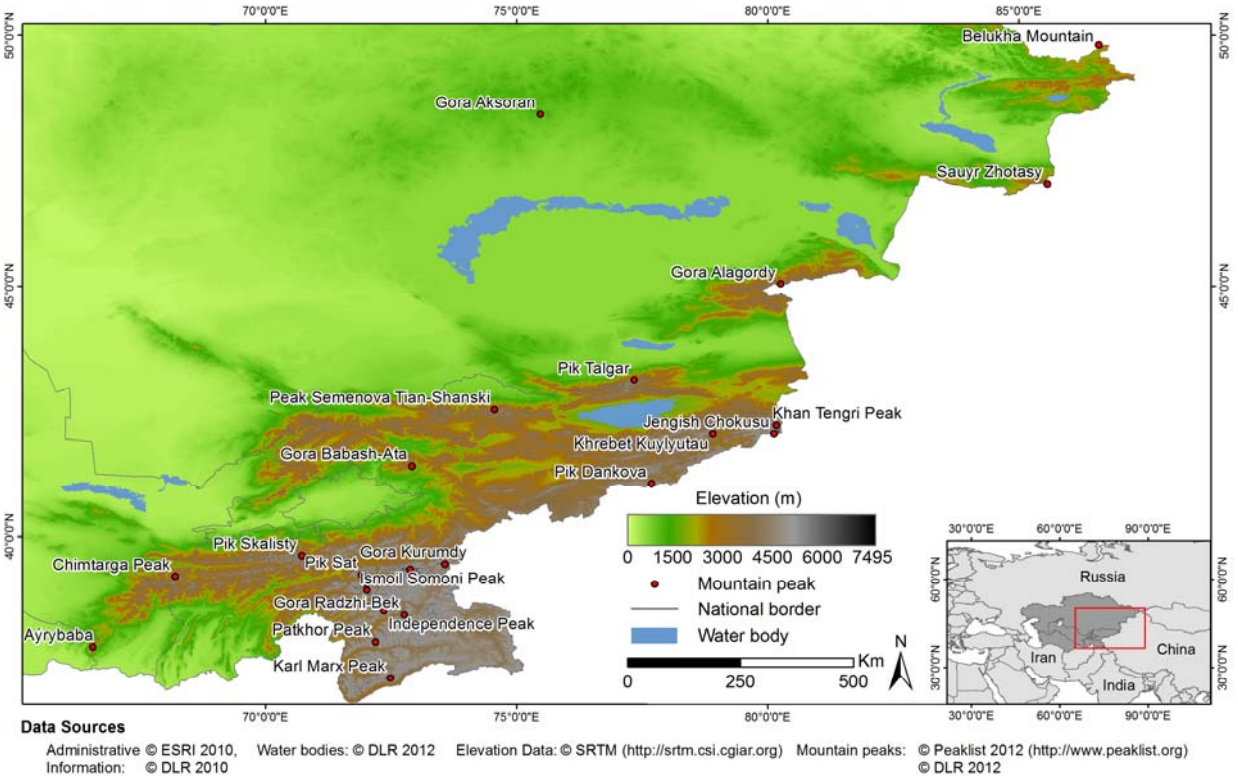

Figure 2.6: Mountainous regions and mountain peaks of Central Asia

Topography is another influencing factor with regards to snow cover classification accuracy. This will also be illustrated in section 3.2. A general overview about the topography of Central Asia is included in Figure 1.2 which already reveals that a pronounced topography is only present in the south-eastern area. Figure 2.6 depicts a detailed relief of this region. Major mountain peaks are represented in this figure as well. A list of these highest peaks of Central Asia is given in Table 2.2. Besides snow mapping accuracy, topography also influences snow accumulation. Temperature decreases by ~ 0.7°C per 100 m elevation above an altitude of 2,000 m in Central Asian Mountains (Severskiy et al. 2000a). The dependence of SCD on elevation is well known and documented (e.g. in Dietz, Wohner, et al. (2012)). Slope orientation is another factor: Solar insolation and heat input are affected by the slope orientation. A study in the Zailiyskiy Alatau (~43°N, ~77°E; ~50 km north of Issyk Kul lake; near Pik Talgar mountain peak in Figure 2.6) revealed that a slope with southern orientation received 2.8 times more heat input than a northern slope at the same location (Severskiy et al. 2000b). The topography of a region is an important parameter when assessing snow cover parameters and should be considered during the analysis.

Table 2.2: List of mountain peaks in Central Asia

Name	Elevation (m)	Lat.	Lon.	Region	Mountain system
Ismoil Somoni Peak	7495	38°55'00" N	72°01'00" E	Tajikistan	Pamir
Jengish Chokusu	7439	42°02'15" N	80°07'30" E	Kyrgyzstan	Tian Shan
Ibn Sina Peak (Lenin Peak)	7134	39°20'33" N	72°52'39" E	Tajikistan	Pamir
Peak Korzhenev-skaya	7105	39°03'27" N	72°00'30" E	Tajikistan	Pamir
Khan Tengri Peak	6995	42°12'39" N	80°10'30" E	Kyrgyzstan	Tian Shan
Independence Peak	6940	38°30'36" N	72°21'15" E	Tajikistan	Pamir
Karl Marx Peak	6723	37°09'45" N	72°28'54" E	Tajikistan	Pamir
Gora Kurumdy	6614	39°27'00" N	73°34'00" E	Tajikistan	Pamir
Patkhor Peak	6083	37°53'21" N	72°11'21" E	Tajikistan	Pamir
Pik Dankova	5982	41°03'33" N	77°41'00" E	Kyrgyzstan	Tian Shan
Pik Sat	5900	39°14'09" N	71°54'39" E	Tajikistan	Pamir
Gora Radzhi-Bek	5735	38°25'30" N	72°45'36" E	Tajikistan	Pamir
Pik Skalisty	5621	39°37'09" N	70°43'12" E	Kyrgyzstan	Alay Mountains
Chimtarga Peak	5489	39°11'45" N	68°11'45" E	Tajikistan	Alay Mountains
Pik Tandykul	5544	39°26'54" N	71°05'00" E	Kyrgyzstan	Alay Mountains
Khrebet Kuylyutau	5281	42°02'09" N	78°54'27" E	Kyrgyzstan	Tian Shan
Pik Talgar	4979	43°07'06" N	77°20'27" E	Kazakhstan	Tian Shan
Peak Semenova Tian-Shanski	4895	42°31'12" N	74°33'22" E	Kyrgyzstan	Tian Shan
Gora Alagordy	4622	45°02'30" N	80°15'27" E	Kazakhstan	Tian Shan
Belukha Mountain	4506	49°48'27" N	86°35'24" E	Kazakhstan	Altai
Gora Babash-Ata	4428	41°24'39" N	72°54'42" E	Kyrgyzstan	Tian Shan
Sauyr Zhotasy	3840	47°02'57" N	85°34'00" E	Kazakhstan	Tian Shan
Aýrybaba	3138	37°47'15" N	66°33'24" E	Uzbekistan	Alay Mountains
Gora Arlan	1880	39°40'24" N	54°32'36" E	Turkmenistan	(Karakum Desert)
Gora Aksoran	1565	48°25'11" N	75°28'07" E	Kazakhstan	Kyzylarai

3. Principles of snow cover monitoring using remotely sensed data

Remotely sensed data was used to map snow cover parameters since April 1960 when the Television and InfraRed Observation Satellite (TIROS-1) became operational (Lucas & Harrison 1990). Since that time, many new sensors and snow mapping methods have been established – a development that still continues. Several review papers about available techniques to identify extent, status, depth, and water content of snow have been published in the past (Hall & Martinec 1985; Bernier 1987; Rott 1987; Lucas & Harrison 1990; Massom 1991; König et al. 2001; Solberg et al. 2006; Amlien 2008). Following this practice, an additional review paper was established within the framework of the CAWa project and the thesis at hand: Dietz, Kuenzer, et al. (2012). Within this publication, recently developed methods from optical, active, and passive microwave remote sensing are contrasted with each other to identify the best available data source and method for the given project definition. The findings from this publication will in parts be reflected as citations in the subsequent sections of the thesis, indicated by double greater-than-/smaller-than signs (>>…<<).

>>Spectral reflectivity and scattering characteristics of snow depend on many different factors such as snow grain size and shape, liquid water content, SD, impurity of snow, temperature, ice content, depth hoar (result of snow metamorphism from low to moderate density; (Domine et al., 2007)) and the consistency of the surface beneath the snow cover (Hall & Martinec 1985; Sturm et al. 1995; Tait 1998; Kelly et al. 2003; Foster et al. 2005; Painter et al. 2009). Depending on the chosen sensor type and resolution, the interference of all these factors on the retrieval of snow parameters may vary. The following subsections will outline the details.<<

3.1 Physical and spectral properties of snow

>>Snow reflects a high proportion of the radiation in visible (VIS) wavelengths. Depending on the impurity, grain size and age of the snow, this proportion can reach 80% (Winther et al. 1999; Klein et al. 2000; König et al. 2001), 90% (Hall & Martinec 1985), and even up to 97% (Hadley and Kirchstetter, 2012) for freshly fallen, pure snow. With high snow age, the percentage of reflected insolation decreases. The reasons for this decrease arise from various facts. First, the impurity of the snow cover increases with time, leading to de-

creased reflectance. Aoki et al. (2000) suggested that the fallout of atmospheric aerosols is the main contributor to the impurity of the snow surface. Aoki et al. (2007) measured the impurity of different snow stages and found impurity concentrations of 2–8 parts per million by weight (ppmw) during accumulation period and up to 100 ppmw and more during the melt period.<< Black carbon contamination of snow was calculated to cause a radiative forcing of ~ 0.05 W/m² when averaged on a global scale (Hadley and Kirchstetter, 2012). Huang et al. (2011) however suggested that the contamination of snow with black carbon is strongly controlled by the distance to anthropogenic sources, e.g. heavily industrialized regions. >>Secondly, melting and refreezing processes within the snow lead to an increased grain size, which then leads to reduced reflectance (Hall & Martinec 1985; Rango 1996; Foster et al. 1999).<<

>>For longer wavelengths, the reflectance of snow declines significantly, reaching near-zero values in the region of the near-infrared (NIR) (Pepe et al. 2005; Wang et al. 2005). Figure 3.1 shows a typical reflectance curve of snow. The observed spectrum of Landsat 7 is also shown in Figure 3.1: The curves are similar, but the coarse spectral resolution of Landsat inhibits a detailed analysis of the spectral behaviour of surface features such as – in this case – snow. This demonstrates that the modelled reflectance curves differ from the actual satellite measurements. The low spectral resolution of Landsat 7 (acquisition date: March 5th, 2002) and the saturation of the VIS channels make it more difficult to recognize the distinctive features that characterize snow.<<

>>Different grain sizes lead to high variability in the reflection properties of snow, especially in regions around 1 and 1.2–1.3 µm, whereas the characteristics remain similar in the region below 0.8 and 1.5 µm (Hall & Martinec 1985; Dozier 1989; König et al. 2001). Figure 3.2 shows the influence of snow grain size on the reflectance of snow. The signatures from Figure 3.2 have been adopted from Choudhury & Chang (1979). While in the VIS part of the spectrum the differences of the signatures are small, the differences increase for longer wavelengths with a maximum in the region from 0.95 to 1.40 µm. For a detailed description of the spectral reflectance of snow and how the optical depth of a snowpack can be calculated, refer to Dozier (1989).<<

>>As mentioned above, impurity and age of snow can also influence the spectral behaviour. Figure 3.3 gives an example of the spectral behaviour of different snow and ice surfaces for the range 0.4–1.2 µm (based on Zeng et al. (1983), modified). Fresh snow reflects up to 100% in this figure, which was adopted and modified from Zeng et al. (1983). While a snowpack ages, the amount of reflected radiation decreases. For ice surfaces, this amount is further reduced, reaching a minimum for dirty glacier ice with only 15–20% reflection. The measurements given in Figure 3.3 have been collected from a study area in North China from

1980 to 1982, using a spectral radiometer with a wavelength range of 0.38–1.20 µm and a spectral resolution of 0.01 µm. The snowpack can change its spectral characteristics considerably within even a few hours. Figure 3.4 shows this behaviour for the same study area in North China, derived from Zeng et al., (1983). For signatures “A” and “B” in Figure 3.4, the temperature was below 0°C and the time span between the measurements was 40 hours. Although air temperatures were below freezing point, the snow had undergone slight snow crystal metamorphosis, increasing snow grain size and snowpack density and therefore altering the reflection for up to 10% in the IR region. Signatures “C”, “D”, and “E” refer to slightly wet, wet, and water saturated snow packs, respectively (Zeng et al., 1983).<<

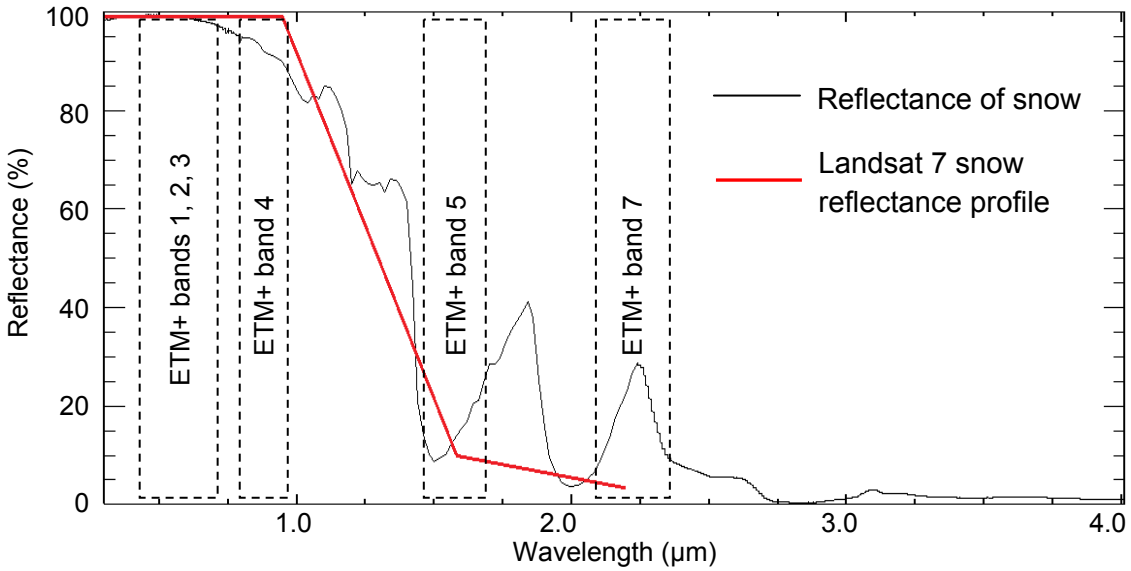

Figure 3.1: Reflectance of snow compared to Landsat 7 observations

>>One of the major challenges in snow mapping is the discrimination between clouds and snow. Although other land cover classes can be easily discriminated from clouds in the VIS wavelengths, snow may behave similarly to clouds in the reflective and thermal part of the spectrum (Akyürek & Sorman 2002; Wang et al. 2005; Hyvärinen et al. 2009; Hall et al. 2010; Miller & Lee 2005). Figure 3.5 gives an example of spectral signatures for different clouds (*r* = particle radii) and snow. The major differences between the reflective characteristics of clouds and snow have been described by Dozier (1989); water drops (10 µm) or ice crystals (40 µm) within clouds are smaller than typical snow grains (300–500 µm, (Chang et al. 1987)). The smaller particle size and the water content cause less absorption in the spectral region from 1.55 to 1.70 µm (Hall et al. 2002; Pepe et al. 2005). However, ice-containing clouds cannot be discriminated from snow by this feature. Because snow cover is usually optically thicker than

cloud cover, it reflects a larger proportion of the VIS radiation. This criterion can help to distinguish between thin cirrus clouds and snow. <<

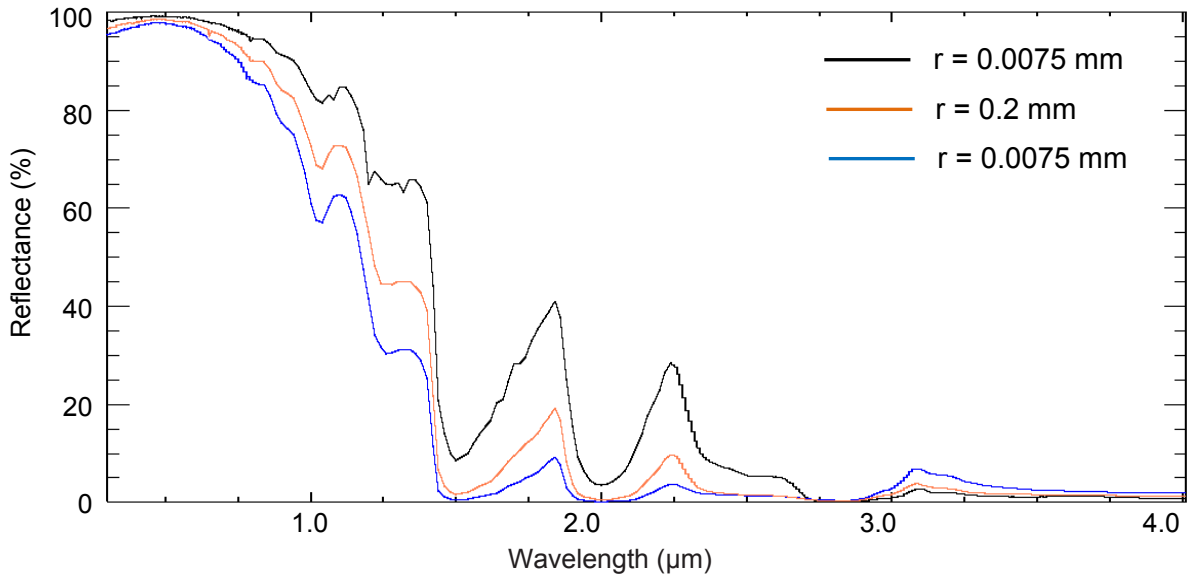

Figure 3.2: Influence of different snow grain sizes on the reflectance of snow

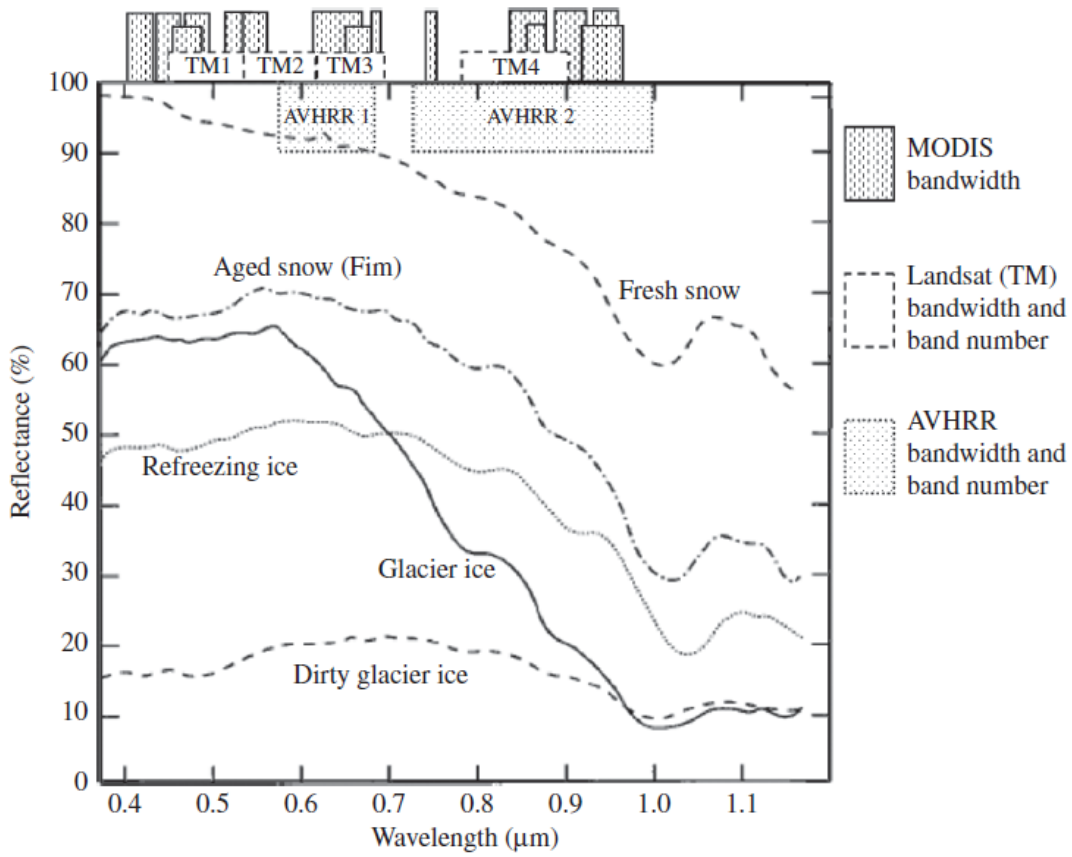

Figure 3.3: Reflectance of different surface types related to snow

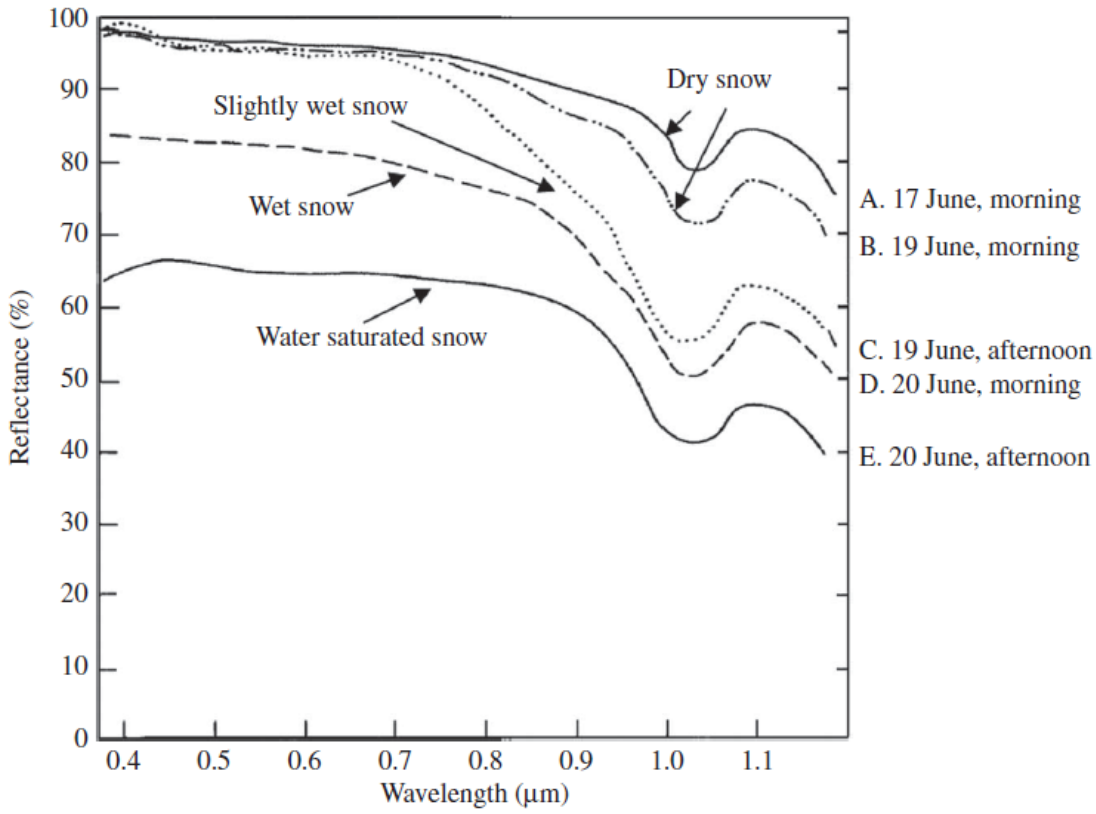

Figure 3.4: Reflectance of different snow age and wetness stages

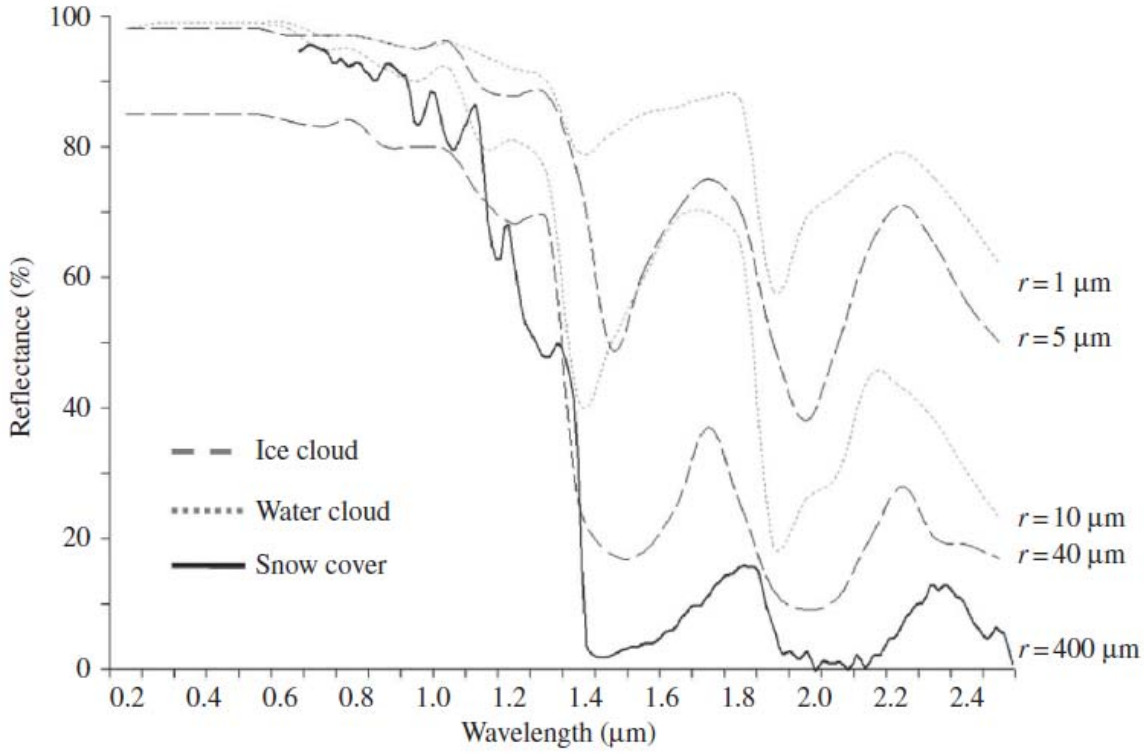

Figure 3.5: Spectral behaviour of different cloud types compared to snow

>>The characteristic decline of snow reflectance towards short-wave IR can be useful to distinguish between the cloud and snow because most clouds reflect a higher proportion of the short-wave IR (Hall et al. 2002; Pepe et al. 2005). Sensors such as the Advanced Very High Resolution Radiometer (AVHRR), the Moderate Resolution Imaging Spectroradiometer (MODIS) or Landsat provide the appropriate spectral channels to utilize the properties mentioned above. Table 3.1 gives an overview of the optical sensors reviewed in section 3.2 and also includes the most relevant characteristics. Usually, using only one spectral channel to discriminate between clouds and snow can lead to errors (Miller & Lee 2005). To identify the low and high, thin and thick, warm and iced clouds correctly and avoid confusion with snow cover, a combination of multiple spectral bands is advisable (Ackerman et al., 2010; King et al., 1997). But even then, confusion between clouds and snow can occur (Hall et al. 2002; Klein & Barnett 2003). If cloud coverage exceeds certain threshold percentages, a satellite scene can become useless for snow detection. Rodell & Houser (2004) have identified a maximum cloud coverage of 94% of an entire MODIS scene to be the upper limit beyond which successful snow-cover delineation is unfeasible.<<

Table 3.1: Characteristics of optical sensors for snow detection

Satellite / Sensor	Operational since / until	Spectral bands	Spatial Resolution	Swath width	Data acquisition
Landsat 1-3 / MSS	1972 / 1983	0.5-0.6µm, 0.6 - 0.7µm, 0.7-0.8µm, 0.8-1.1µm	79m	185km	every 18 days
Landsat 4-5 / TM	1982 / present	0.45-0.52µm, 0.52-0.6µm, 0.63-0.69µm, 0.76-0.9µm, 1.55-1.75µm, 2.08-2.35µm, 10.4-12.5µm	30m (band 6: 120m)	185km	every 16 days
Landsat 7 / ETM+	1999 / present	0.45-0.52µm, 0.53-0.61µm, 0.63-0.69µm, 0.78-0.9µm, 1.55-1.75µm, 2.09-2.35µm, 10.4-12.5µm, 0.52-0.9µm	30m (band6: 60m; band 7: 15m)	185km	every 16 days
Terra & Aqua / MODIS	2000 & 2002 / present	36 bands from 0.62µm to 14.38µm	bands 1-2: 250m; bands 3-7: 500m; bands 8-36: 1000m	2330km	2 per day
NOAA / AVHRR	1978 / present	0.58-0.68µm, 0.72-1.0µm, 1.58-1.64µm, 3.55-3.93µm, 10.3-11.3µm (10.5-11.5µm)*, 11.5-12.5µm**	1090m	2399km	daily
GOES	1975 / present	0.52-0.72µm, 3.78-40.3µm, 6.47-7.02µm, 10.2-11.2µm, 11.5-12.5µm	band 1: 1000m, bands 2-4: 4000m, band 5: 8000m	Full Earth disk	every 3 hours
SPOT / Vegetation	1998 / present	0.43-0.47µm, 0.61-0.68µm, 0.78-0.89µm, 1.58-1.75µm	1150m	2200km	1-2 days
ERS-2 / ATSR-2	1995 / present	0.55µm, 0.66µm, 0.87µm, 1.6µm, 3.7µm, 10.8µm, 12.0µm	1000m	512km	2-3 days
Envisat / AATSR	2002 / present	0.55µm, 0.66µm, 0.87µm, 1.6µm, 3.7µm, 11.0µm, 12.0µm	1000m	500km	2-3 days
Envisat / Meris	2002 / present	15 bands from 0.39µm to 1.04µm	300m	1150km	2-3 days

* Valid for AVHRR/2 instead of 10.3 – 11.3µm band

** Only valid for AVHRR/3 (NOAA-15 to NOAA-19)

So far, properties useful for the visible interpretation of snow have been introduced. Because Earth continuously emits microwave radiation from its surface, passive microwave (PM) sensors can be facilitated to measure these emissions (König et al., 2001). SMMR, the SSM/I and the Advanced Microwave Scanning Radiometer – Earth Observing System (AMSR-E) collected such data, thus providing a large and continuous time series on a global scale (see Table 3.2 for details about the sensors).

>>Snow-covered areas attenuate the emitted microwave radiation from the underlying surface for wavelengths similar to the snow grain size (Chang et al. 1987). This attenuation of

microwave radiation depends principally on the snow mass of a respective snowpack; the more the snow covers an area, the less the microwave radiation will reach the satellite sensor (Chang et al. 1987; König et al. 2001; Clifford 2010). A snowpack consists of air, ice and in some cases liquid water. Because the air does not influence the microwave signal (or at least can be neglected, see Mätzler & Wegmüller (1987) and Mätzler (1994)), the propagation of microwaves in a snowpack depends on the dielectric constants of ice and water, which are extremely different. Liquid water content, grain size and grain shape may influence the signal that reaches the sensor (Foster et al. 1999; Clifford 2010). For dry snow, the scattering is caused by the dielectric discontinuities of snow grains and air. Microwave absorption within dry snow is low, resulting in volume scattering of the snowpack (Amlien, 2008).<<

Table 3.2: Passive microwave sensors and their characteristics

	SMMR	**SSM/I**	**WindSat**	**AMSR-E**
Operational since / until	1978 / 1987	1987 / present	2003 / present	2002 / 2011
Platform	Nimbus-7	DMSP	Coriolis	Aqua
Frequencies and IFOV (km x km)	6.6 GHz; 156 x 156 10.7 GHz; 97 x 97 18.0 GHz; 60 x 60 21.0 GHz; 60 x 60 37.0 GHz; 30 x 30 *N/A*	*N/A* *N/A* 19.3 GHz; 69 x 43 22.2 GHz; 60 x 40 37.0 GHz; 37 x 29 85.5 GHz, 15 x 13	6.8 GHz; 39 x 71 10.7 GHz; 25 x 38 18.7 GHz; 16 x 27 23.8 GHz; 30 x 30 37.0 GHz; 8 x 13	6.9 GHz; 74 x 43 10.6 GHz; 51 x 30 18.7 GHz; 27 x 16 23.8 GHz; 31 x 18 36.5 GHz; 14 x 8 89.0 GHz; 6 x 4
Polarizations	H / V	H / V*	Full **	H / V
Incidence angle (°)	49	53	49.9 – 55.3	53
Data acquisition	every other day	daily	daily	daily
Swath width	780 km	1400 km	1000 km	1600 km
Sensitivity (K)	0.9 – 1.5	0.8 – 1.1	0.2 – 0.7	0.3 – 1.1

* 22.2 GHz channel is only available in vertical polarization

** Dual polarization for 6.8 GHz and 23.8 GHz channels

>>PM sensors map the surface in different frequencies and polarizations. Vertically polarized data are more sensitive to the snow volume and are therefore capable of mapping shallow snow cover. However, because there could be confusion between snow and underlying dry soils, horizontally polarized data are usually used to map snow cover (Amlien, 2008; Grody and Basist, 1996). The frequency is crucial for the wavelength and the spatial resolution of the signal. The higher the frequency, the finer is the resolution of the resultant pixel, but the wavelength also decreases with increasing frequency.<<

>>The maximum snow depth (SD) that can be derived from PM sensors depends on the wavelength of the signal. The 37 GHz channel, for example, which is often used to derive SWE (Chang et al. 1987; Josberger & Mognard 2002), has a wavelength of 0.8 cm, limiting the maximum SD that can be measured to 10–100 times the wavelength, thus ∼100 cm (Clifford, 2010) and a respective SWE of 250 mm (Foster et al. 2005). Derksen (2008) observed that SWE measurements derived from the 37 GHz channel inherit an increasing uncertainty with rising SWE; volume scattering is reduced at SWE values greater than 120 mm. Scattering effects are also decreased when the wavelength of the signal becomes greater than the grain size of the snow crystals. Increasing the wavelength of the sensors will therefore not improve the ability to map deeper snow. At wavelengths greater than 5 cm, not scattering but absorption will be the dominant process (Chang et al. 1987). The minimum SD that can be recognized by PM sensors has been identified at 2 cm (Che et al., 2008). The snow crystal properties can influence the signal and may lead to an overestimation of the SWE. Initially, a fixed snow crystal diameter and snow density was assumed for the calculations, for example, 1 mm crystal size and 300 kg m−3 snow density (Rott & Nagler 1995). Large divergences from these fixed values can lead to wrong assumptions. Foster et al. (1999) have shown that the shape of the snow crystals has little to no impact on SD and SWE estimations derived from the PM radiometry. The crystal size is a more sensitive factor. Especially in regions with plate-like depth hoar crystals, an overestimation of SWE has been observed (Clifford, 2010). The analysis of PM data is subject to some other major restrictions. Forests tend to mask out the snow cover, leading to underestimation of SD and SWE (Hall et al. 1982; Foster et al. 1991). The vegetation absorbs microwaves in the 37 GHz region, thereby suppressing the scattering signal emitted from the snow surface underneath (Derksen 2008). Liquid water increases the dielectric losses within the snowpack, which strongly increases the absorption of microwaves within the snowpack. Volume scattering is therefore completely prevented leading to strongly degraded SD estimation (Rott & Nagler 1995; Amlien 2008). Algorithms to estimate SD under wet snow conditions are, therefore, still being researched (Kelly 2009). Furthermore, owing to its coarse resolution, PM data are more suitable for global monitoring of snow properties than it is for a regional scale (Vikhamar & Solberg 2002). Although the resolution may be the biggest disadvantage of PM sensors, their ability to map snow even in the presence of clouds makes them a valuable tool for snow-cover mapping. The possibility to estimate SD and SWE is another big advantage of this sensor type.<<

>>Active microwave data may be used to analyse snow cover as well, though the application is limited by the fact that only wet snow can be recognized reliably (Wang et al. 2008). Under dry conditions, it is not the snow crystals but the ground beneath the snow cover that forms the major source for the backscattering signal (König et al., 2001). Liquid water reduces the penetration depth of the microwaves from around 20 m in dry conditions to only 13.8 cm with 1% of liquid water content (Rott & Nagler 1994). Active sensors can come with much higher spatial resolutions than PM sensors, reducing swath (50–500 km) and revisit frequency (24 days for RADARSAT SAR, 35 days for Envisat ASAR, 11 days for TerraSAR-X; (König et al. 2001; Nghiem & Tsai 2001; Strozzi et al. 2009). Ice layers within refrozen snow bodies can be recognized by scatterometers such as QuickSCAT (QSCAT) using the Ku band at 13.4 GHz, as shown by Nghiem et al. (2005). Additionally, the beginning of snowmelt can be recognized because of the liquid water content that appears within the snowpack. This feature is exploited in combination with optical and PM sensors by Foster et al. (2011) and the same is reviewed in section 3.2. Table 3.3 gives an overview of the different active microwave sensors and their characteristics. The interest in analysing the scatterometer data for snow-cover mapping has increased in recent years (Foster et al. 2011). However, because the use of active microwave data for snow-cover detection is limited to the existence of liquid water content, methods to use these data are excluded from detailed examination.<<

Table 3.3: Characteristics of selected active microwave sensors

Satellite / Sensor	Operational since / until	Bands	Spatial resolution	Swath width	Data acquisition
ADEOS I / NSCAT	1996 / 1997	Ku band (14.0 GHz)	50 km	2x 600 km	every other day
QuickSCAT/ Seawinds	1999 / 2009	Ku band (13.4 GHz)	25 km	1800 km	daily
ADEOS II / SeaWinds	2002 / present	Ku band (13.4 GHz)	25 km	1800 km	daily
MetOp / ASCAT	2005 / present	C band (5.25 GHz)	25 km, 50 km	2x 550 km	every other day
RADARSAT / SAR	1995 / present	C band (5.3 GHz)	8m - 100m	45 km - 500 km	every 24 days
RADARSAT2 / SAR	2007 / present	C band (5.4 GHz)	3m - 100m	20 km - 500 km	every 24 days
Envisat / ASAR	2001 / present	C band (5.3 GHz)	30m, 150m, 1000m	60 km - 100 km, 400 km	every 35 days
JERS 1 / SAR	1992 / 1998	L band (1.275 GHz)	18m	75 km	every 44 days
TerraSAR-X, TanDEM-X / SAR	2007 / present	X band (9.6 GHz)	1m, 3m, 18m	10 km, 50 km, 150 km	every 11 days

3.2 Methods to map snow using remotely sensed data

>>The algorithms and methods to map snow parameters from remotely sensed data vary primarily depending on the sensor type, but may also be influenced by the most prevalent land cover type, topography and climatic conditions. This section gives an overview of the most important methods to map snow extent, SD and SWE. It is not possible to include every single method in a clearly arranged manner, so only the most recent or most commonly applied and published methods are reviewed. Table 3.4 summarizes the methods discussed in this review. Additional details such as resolution, accuracy of the product and respective authors who investigated the methods are also included.<<

3.2.1 Discrete methods for snow cover mapping with optical sensors

>>*Snowmap* is an algorithm that was developed especially for MODIS (Hall et al., 1995). The MODIS daily, 8-day and monthly snow cover products provided by the National Snow and Ice Data Center (NSIDC) are based on this algorithm. It uses the reflectance of VIS and IR radiation to calculate the normalized difference snow index (NDSI):

$$NDSI = \frac{b_4 - b_6}{b_4 + b_6}, \quad (1)$$

where b_4 and b_6 refer to MODIS bands 4 (0.54–0.56 µm) and 6 (1.62–1.65 µm), respectively (Hall et al. 2002). The NDSI was first introduced by Crane & Anderson (1984) for experimental DMSP data. Dozier (1989) used Landsat bands 2 (0.53–0.61 µm) and 5 (1.55–1.75 µm) in a similar study.<<

>>Because band 6 on Aqua MODIS is non-functional, $NDSI_{(Aqua)}$ is calculated using band 7 (2.10–2.15 µm). The correlation between MODIS bands 6 and 7 over land is high. However, the reflectance magnitude of band 7 is lower. Additionally, the spatial misregistration between bands 7 and 4 accounts for 0.3 pixels compared to a misregistration of only 0.1 pixels for bands 6 to 4 (Salomonson & Appel 2006). Riggs & Hall (2004) confirmed that switching the bands greatly improved the accuracy for the Aqua MODIS product. The snow patterns from Terra and Aqua MODIS are now very similar with differences of 0 to 5%. Biggest deviations are observed in dense forests and low illuminated areas (Riggs & Hall 2004).<<

$$NDSI_{(Aqua)} = \frac{b_4 - b_7}{b_4 + b_7}, \quad (2)$$

>>The NDSI is used to automatically distinguish between clouds and snow; while the reflectance of clouds remains high for MODIS band 6 (7 for Aqua), the reflectance of snow drops to near zero in this spectral region (Hall et al. 1995). To map snow extent automatically with NDSI, a threshold value of NDSI >0.4 is used to indicate snow coverage. This value has been suggested by Hall et al. (1995) after extensive analyses for the USA. Klein & Barnett (2003) validated daily MODIS snow cover maps and proved that an NDSI value >0.4 indicates snow covered surfaces. For forested areas, both underestimation and overestimation errors can occur. To prevent underestimation, the NDSI threshold must be decreased because forests tend to mask out snow covered ground. Hall et al. (2002) found that NDSI values <0.4 also indicate snow if the normalized difference vegetation index (NDVI) is around 0.1. Snow tends to lower the NDVI, and an NDVI ~0.1 is therefore an indication of snow covered forests even if NDSI <0.4 (Hall et al. 2002). To prevent overestimation, the reflectance in MODIS band 4 (Landsat TM band 2) must exceed 10% to be mapped as snow (Klein et al. 1998). This additional reflectance test is required because dark surfaces such as forests significantly reduce the reflectance values and therefore cause the denominator of the NDSI equation (1) to be quite small. Small increases in the VIS wavelengths would lead to NDSI values high enough to indicate snow (Klein et al. 1998; Hall et al. 2002). The *Snowmap* algorithm only works for pixels with at least a 50% snow cover fraction (Hall et al. 2002). Trying to catch smaller subpixel fractions of snow can lead to the erroneous assignment of bright, snow free surfaces as snow (Hall et al. 1995). Fractional snow mapping techniques described later in this section can improve these results (Salomonson & Appel 2004). An additional source of error is the incorporation of the MODIS cloud mask product MOD35 L2 in the snow cover processing. These cloud masks tend to overestimate actual cloud coverage, leading to an underestimation of snow cover (Bormann et al. 2010; Riggs et al. 2006). Despite all these problems, the overall accuracy of the daily MODIS snow cover product (MOD10A1) reaches 93% for clear-sky conditions, even though it varies according to the land cover type and snow conditions (Hall & Riggs 2007). Accuracy is lower for forested areas (~90%) and higher for “nonforest” land cover (nearly 100%). The transition zone between snow covered and snow-free area is prone to higher error rates, again (85% accuracy for forest, 95% for “nonforest”) (Hall et al. 2001). The overall accuracy including all-weather conditions, and if clouds are treated as classification errors, is lower, reaching 31% for Aqua (MYD10A1) and 45% for Terra (MOD10A1) MODIS daily products (Gao et al. 2010).<<

>>Rosenthal & Dozier (1996) presented a decision-tree based classification model to map snow cover and fractional snow cover from Landsat TM data. The method was developed for Landsat TM 5 scenes taken from 1983 to 1993 in the Sierra Nevada in California, USA. Within this decision-tree, a large number of threshold and ratio tests (21 terminal nodes for the

full cloud classification tree) are accomplished to first identify cloud contamination. A second tree derives snow cover from the TM scenes with an additional 11 terminal nodes. Mainly, discrete threshold tests including TM bands 1, 2, 4 and 5 (Rosenthal & Dozier 1996) are used. This second tree decides whether a pixel is covered by snow, water or 'other' surface types. A subsequent regression tree estimates fractional snow cover; this step is explained later in section 3.2.2. The accuracy of the decision-tree based classification of Landsat TM is similar to the one achieved with high-resolution aerial photography. A linear relationship between these snow cover estimates has been detected with a determination coefficient R2 = 0.979.<<

>>*Snowcover* is an algorithm developed by Fernandes & Zhao (2008) especially for AVHRR data over the Northern Hemisphere (Zhao and Fernandes, 2009). They used top-of-atmosphere (TOA) reflectance of AVHRR channels 1 and 2, NDVI, clear-sky surface broadband albedo, skin temperature (ST), solar zenith angle (SZA) and a cloud mask for their analysis. As ground truth, SD measurements were taken from both the Meteorological Service of Canada (MSC, 67 in situ sites) and the Historical Soviet Daily Snow Depth Version 2 (HSDSD, 260 in situ sites). Initially designed to be used with the 1 km AVHRR imagery, the *Snowcover* algorithm was also used to derive snow cover from 5 km AVHRR land grid cells. Three steps were performed to acquire the final snow cover product: (1) temporal filtering and interpolation of each grid cell by an adaptive rank filter, (2) normalization of channel 1 to standard acquisition geometry and (3) snow detection. The temporal stability of each pixel is analysed per year for this snow detection step. Samples of snow-free and snow covered surface temperature and NDVI time series are used to define the threshold that will be used for the final snow cover classification. A pixel is classified as snow only if it is above the threshold for snow-free ground. The analysis of the whole time series of each pixel allows for the estimation of snow cover under clouds or cloud shadows as well. A final temperature threshold eliminates misclassification during summer and autumn months.<<

>>*Snowcover* is capable of producing snow cover maps for 90% of the period from 1982 to 2008 over the Western Arctic. The accuracy reaches values of 87% for 50% of the test sites (Fernandes and Zhao, 2008). *Snowcover* avails itself of the Single Pixel Aggregate Rating of Cloudiness (SPARC) routines to discriminate clouds from snow. Within this procedure, several tests including a brightness temperature test (T-test), a reflectance brightness test (B-test) and a reflectance test (R-test) are accomplished to derive the likelihood of cloud cover for each pixel (Khlopenkov and Trishchenko, 2007). The SPARC routine has successfully been applied to the European Alps using AVHRR data by Hüsler et al. (2012) with a mean snow cover classification accuracy of 90%. The need for additional input layers (skin temperature) limits the adaptability to regions where such data are available on an operational basis.<<

>>The National Operational Hydrologic Remote Sensing Center (NOHRSC) used AVHRR data from the National Oceanic and Atmospheric Administration (NOAA) to map snow extent for North America with the multi-band snow classification algorithm *theta*. Each pixel of an input AVHRR scene is treated by theta as a vector quantity consisting of the selected bands. To map snow cover extent, the National Operational Hydrologic Remote Sensing Center (NOHRSC) conducted two individual classifications, both connected to a user-defined reference vector. First, a three-space vector was initialized using AVHRR bands 3, 4 and 5 to identify clouds while, as a second step, AVHRR bands 1–4 were used to identify snow and cloud extent. To construct the final snow cover classification, the results from the first step must be subtracted from the second step. The success of the theta algorithm depends on the selected input bands and the reference vector. Assuming that suitable input parameters have been found, this method is capable of screening both cirrus and cumulus clouds, and besides that it distinguishes cirrus clouds above snow cover. Mixed pixels, cloud shadow and the presence of forested areas may influence the effectiveness. Furthermore, the method is not fully automated because the user must set thresholds for both steps of cloud and cloud/snow classifications (Maxson et al., 1998).<<

Table 3.4: Overview of reviewed methods and their characteristics

Sensor(s)	Method(s)	Author(s)	Spatial Resolution	Temporal Resolution	Accuracy	Parameters
MODIS	Snowmap; NDSI; multispectral enhancement; ARSIS; SnowFrac; Snowl; Aqua + Terra composite	Hall *et al.* 1995, 2002; Riggs and Hall 2004,2007; Salomonson and Appel 2003, 2006; Klein and Barnett 2003; Parajka *et al*. 2010; Sirguey *et al*. 2008; Vikhamar and Solberg 2002; Wang and Xie 2009a	500m (250m)	daily, 8-day, monthly	~95% (clear sky) 31-45% (all weather conditions)	SC, SCF
Landsat	NDSI; Decision-trees; SnowFrac	Rosenthal and Dozier 1996; Vikhamar and Solberg 2002	30m	every 16th day	R^2 = 0.979	SC, SCF
AVHRR	Snowcover; theta	Fernandes and Zhao 2008; Maxson *et al.* 1998	1100m, 5000m	Daily	~87% (for 50% of test sites)	SC
	APOLLO	Saunders and Kriebel 1988, Gesell 1989	1100m	Daily	Unknown	SC
	SPARC	Khlopenkov & Trishchenko 2007, Hüsler et al. 2012	1100m, 5000m	Daily	90% for Europe	SC

Sensor(s)	Method(s)	Author(s)	Spatial Resolution	Temporal Resolution	Accuracy	Parame-ters
MERIS+ AATSR	Supervised fuzzy statis-tical classifi-cation	Pepe *et al.* 2005	260m * 290m	every three days	95-98%	SC, SCF
AMSR-E	SWEMAP	Chang and Rango 2000; Kelly 2009	25km	daily, 5-day, monthly	3.7cm error	SWE, SD, SC
SMMR	Spectral gradient (Tb18 – Tb37) * c	Foster *et al.* 1996; Derksen 2008; Chang *et al.* 1987	25km	daily, 5-day	2.2cm; 1.5cm error; R^2 = 0.75-0.8	SWE, SD
SMM/I	Snow Emis-sion Model-Based Au-tomatic In-version Al-gorithm	Pulliainen and Hal-likainen 2011; Goïta *et al.* 2003; Derksen *et al.* 2003a,b	25km	daily, 5-day	2.3cm; 1.4 - 3.3cm; 1.5cm error	SWE, SD
MODIS+ AMSR-E	combination of products	Liang *et al.* 2008; Gao *et al.* 2010	500m	daily	~85%	SC
MODIS	MODSCAG	Painter *et al.*2009	500m	daily	SC: 95%, Albedo: 95% Grain size error: 51 µm	SC, SCF, Albedo, Snow grain size
GOES+ SSM/I	combination of products	Romanov *et al*. 2000	4km	every 30 minutes	~85%	SC
ATSR-2 / AATSR	NLR and SCAmod	Solberg and Ander-sen 1994; Metsämäki *et al.* 2005	0.01°	daily	compara-ble to MODIS snowmap results	SC, SCF
MODIS+ AMSR-E + QSCAT	ANSA	Foster *et al.* 2011	25km	daily	better than the single base products	SC, SWE, SD, SCF, Snowmelt

>>Today, NOHRSC uses the Snow Data Assimilation System (SNODAS) with a snow mass and energy balance model as the major source of information. The snow model runs in steps of 1 hour and assimilates the estimates of the last 18 hours to produce a 30 arc second snow cover product. Remotely sensed data are only incorporated to map the boundaries be-tween snow and snow-free ground for cloud-free pixels (Barrett, 2003).<<

The AVHRR Processing scheme Over Land, cLoud and Ocean (APOLLO) is one of the oldest fully automated classification procedures able to derive snow covered surfaces from remotely sensed data. Developed between 1986 and 1988, the software is still operational at the German Remote Sensing Data Center (DFD) of the German Aerospace Center (DLR). APOLLO involves all available spectral channels to detect cloud coverage from AVHRR imagery (Saunders and Kriebel, 1988). The initial version of APOLLO has been modified within the years, adding a routine to discriminate between clouds and snow (Gesell, 1989) and increasing cloud and snow detection accuracy (Kriebel et al., 2003).

APOLLO uses a straightforward classification scheme, starting with calibrated reflectances and brightness temperatures to detect cloud and snow covered surfaces in a first step. Within this step, up to five tests are applied to the (daytime-) data. Figure 3.6 gives an overview of the full daytime algorithm (as adopted from Saunders & Kriebel (1988)). T_{min} in test 1 (Gross cloud check) is the mean Sea Surface Temperature (SST) from 5 days over water while over land, the initial threshold was defined interactively from the data. In test 2 (Spatial coherence test), the standard deviation of brightness temperatures within a 3 x 3 pixel window must not exceed a threshold (0.2° K over water). This test is only applied to water bodies during daytime. For test 3 (Dynamic visible threshold test), the threshold is defined automatically from a 50 x 50 moving window: A cloud-free peak is identified from the histogram of the input pixels and all pixels with reflections above this peak are considered as cloud covered. Test 4 (NIR / VIS ratio test) uses different thresholds for water and land surfaces again. For clouds, the ratio will even out close to unity because reflectance is only slightly less in NIR than in VIS (compare Figure 3.5). Cloud free land reflectance will be greater in NIR than in VIS over vegetated regions and even over deserts, causing the ratio in test 4 to be greater than under cloud covered conditions. Over water, however, an alternative threshold must be used because reflectance in VIS is usually much higher than in NIR due to increased backscattering in shorter wavelengths. The final test (Thin cirrus test) is dependent on the satellite zenith angle (θ) and a lookup table of typical temperature difference values for different atmospheres under clear sky conditions. Depending on the atmosphere, temperature differences of up to 6° K can be observed between bands 4 and 5 for cloud covered pixels (Saunders and Kriebel, 1988).

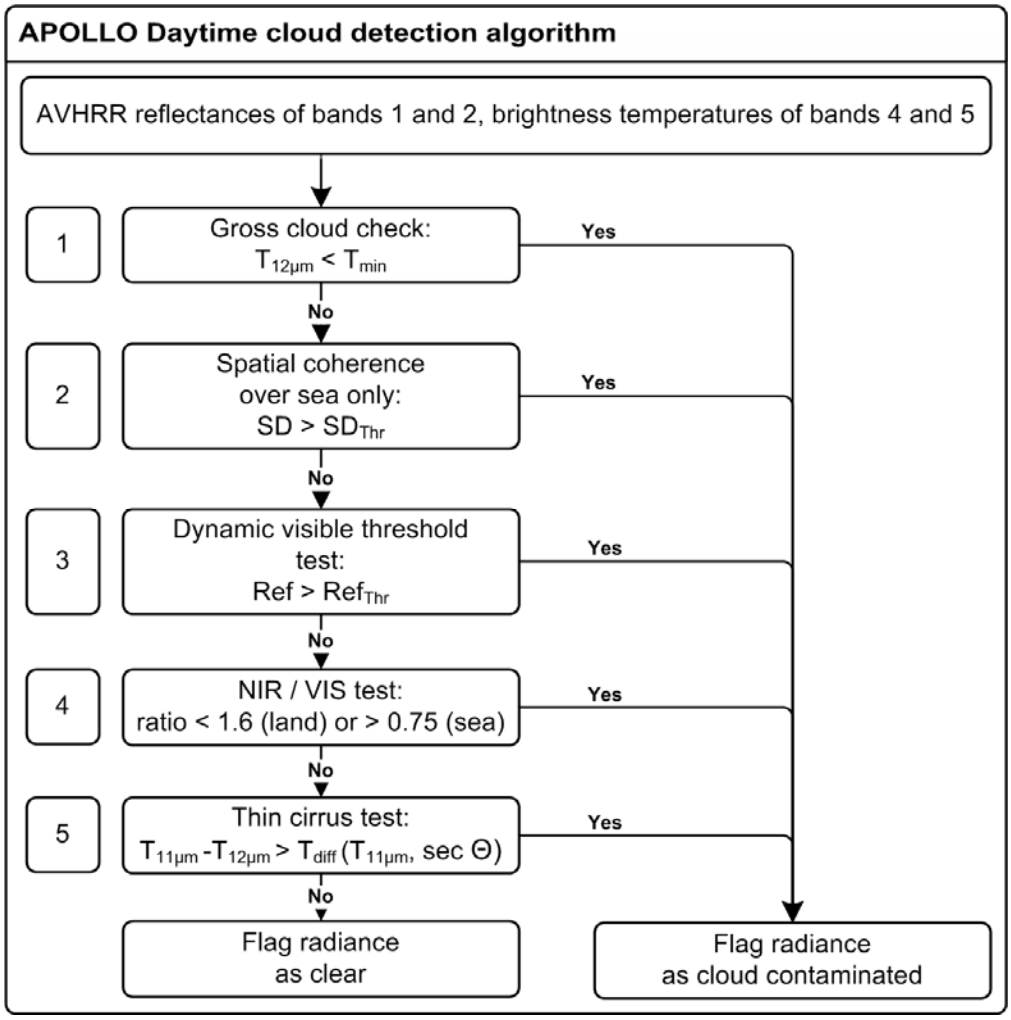

Figure 3.6: Apollo Daytime cloud detection algorithm

Figure 3.6 only depicts the first cloud detection algorithm. All pixels flagged as clouds after this procedure will be processed by an additional algorithm to estimate cloud cover fraction from each pixel as well. This algorithm will not be included here because it is of little relevance for the snow detection scheme that follows in the next step:

The APOLLO cloud detection algorithm (Figure 3.6) cannot distinguish between clouds and snow. Tests 3, 4, and 5 will classify snow covered surfaces as clouds because the spectral properties exploited within these tests are similar for both, clouds and snow (Gesell, 1989). Therefore, up to 12 additional tests are applied to the results produced from the cloud detection algorithm. These tests are part of the APOLLO snow and ice extension and illustrated in Figure 3.7. DVT (Dynamic Visible Threshold), $Ratio_{C1/C2}$ and T45T (Thin cirrus test) are adopted from the cloud algorithm (Figure 3.6). The other tests are based on thresholds exploiting the spectral and thermal differences between clouds and snow and have been developed by Gesell (1989).

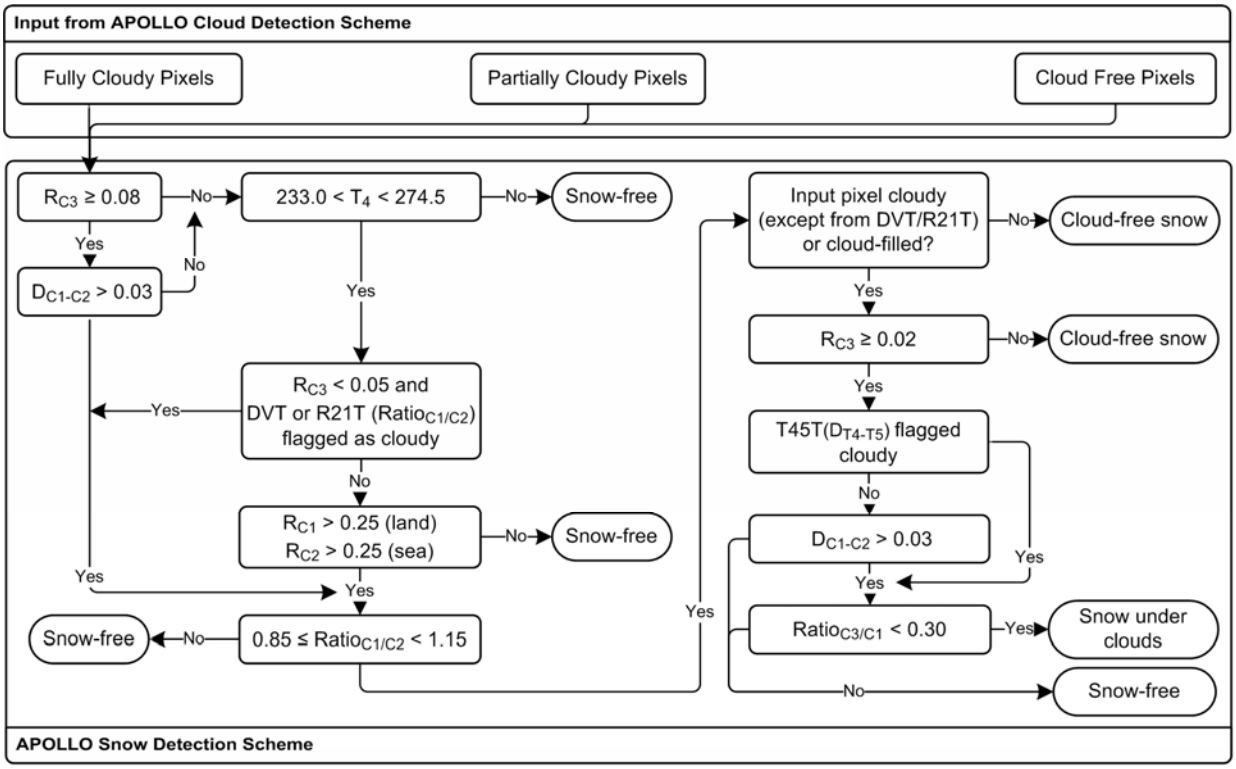

Figure 3.7: APOLLO Snow detection scheme

Though operational since 1989 the snow and ice extension has never been validated thoroughly. Initial tests conducted by the author of the extension suggest that the algorithm shows only few uncertainties in the presence of thin cirrus clouds over water. Additionally, water clouds with ice tops may in rare cases be misclassified as snow (Gesell, 1989). A second algorithm exists that is capable of detecting ice covered surfaces as well. It is not included in this summary since ice cover is not the subject of the thesis. As a concluding remark it should be stated that - though the APOLLO routine may seem a bit outdated – the ability to process AVHRR data from all available satellite generations offers a good tool to process consistent time series of snow cover data. In contrast to other AVHRR processing schemes, APOLLO does not need additional input like *Snowcover*/SPARC. It runs fully automated (in contrast to *theta*) and therefore offers a good perspective for the processing of long time series. However, because the accuracy of the snow cover classification is not known in detail, an accuracy assessment would be required before APOLLO could be utilized.

>>One limitation that is common to most of the products mentioned so far is their relatively coarse resolution. A pixel size of 500 m × 500 m may be inapplicable for local or small scale snow cover analysis or for complex terrain conditions. Sirguey et al. (2008) developed a method to improve the spatial resolution of MODIS in the context of snow cover mapping. As a basis, the “Amélioration de la Résolution Spatiale par Injection de Structures” concept (ARSIS) was used to fuse MODIS channels with different spatial resolutions into one improved snow

cover product. ARSIS is a multi-scale method that constructs a high resolution for a low-resolution band from the information given by an additional high-resolution band (Ranchin and Wald, 2000). Because no panchromatic band is available, the high-resolution band that is the closest to the respective lower resolution channel was chosen for the transformation (MODIS b1: b3 and b4; MODIS b2: b5, b6, b7). After the new 250 m MODIS channels were computed, corrections for the topography and atmosphere were conducted, and a linear constrained unmixing was also applied for eight endmembers to produce subpixel snow cover information. As a result, significantly better snow cover products were generated. Compared to a 15 m Aster reference image, the overall overestimation of the snow covered area decreased from 4.1% to 1.9%, the mean absolute error decreased by 20% and the global quality index (Q, introduced by Wang & Bovik (2002) as a universal image quality index) increased by 3%. The number of endmembers limits the use of the procedure to smaller regions with known land cover circumstances. On the other hand, the method is beneficial for environmental or hydrological implementations in steep terrain, where coarser resolutions may lead to significantly increased misinterpretations of snow cover and fractional snow cover (Sirguey et al., 2008).<<

The Interactive Multisensor Snow and IceMapping System (IMS) was initiated in 1997 by NOAA/NESDIS. It includes the longest time series of continuous snow cover extents which was intended to serve as an input parameter into numerical forecasting at the National Centers for Environmental Prediction (NCEP). These snow data are also often used as input for studies about climate change impacts on snow (e.g. (Brown & Mote 2009; Dahe et al. 2006; Gutzler & Rosen 1992; Liston & Hiemstra 2011)) and therefore also included in this review. The earliest datasets range back to 1966 when they were derived through manual construction based on photographic copies of visible imagery (Robinson et al. 1993; Robinson 1993). In 1972 when the Very High Resolution Radiometer (VHRR) became operational the accuracy of the weekly digitized snow cover product increased substantially. The quality of the boundary between snow covered and snow free area did not show too much detail before 1972, making the product suitable for studies not exceeding the continental scale (Kukla & Robinson 1979). Between 1972 and 1997, snow and ice charts were still derived manually and on a weekly basis. The resolution of the weekly maps ranged from 125 to 200 km, depending on the latitude. Only after the initiation of the IMS in 1997, daily snow cover products were made available using GIS technology, replacing most of the manual work by automated classification routines (Helfrich et al., 2007). The data sources utilized for IMS come from optical and passive microwave sensors (15 separate input sources in total). Geostationary data originating from Geostationary Operational Environmental Satellites (GOES), METEOSAT, and Geostationary Meteorological Satellites (GMS) are combined with SSM/I, AVHRR, station data, and additional data layers (vegetation, land cover, elevation) (Ramsay, 1998). The SSM/I data are usually

only referred to during darkness or cloud coverage. The resolution of IMS snow extent data is 4 km since 2006 (Helfrich et al., 2007).

>>Additional methods exist to map snow cover also from different sensors. (Pepe et al., 2005), for example, researched the ability to use the two Envisat instruments, the Medium Resolution Imaging Spectrometer (MERIS) and Advanced Along Track Scanning Radiometer (AATSR), to monitor snow cover in Alpine regions. SPOT VEGETATION data can be used to map snow cover, as shown by Lissens et al. (2000), and compared to MODIS, as shown by Simic et al. (2004). It is not possible to include all these approaches in this summary. For a detailed description, the reader should refer to the individual authors.<<

3.2.2 Fractional snow cover algorithms

>>Because binary information about snow cover can produce large uncertainties, especially within hydrologic runoff models, it is desirable to produce fractional snow cover maps from medium resolution satellite data – in particular, during the accumulation or ablation period of snow, but also in forested areas such approaches are reasonable (Vikhamar & Solberg 2002; Salomonson & Appel 2004; Salomonson & Appel 2006). Rosenthal & Dozier (1996) used a regression tree to estimate fractional snow cover from Landsat TM data, and their results were as accurate as those obtained from aerial photography. Endmember selection or snow grain size, shape or SWE had no impact on the algorithm. Topography-induced illumination differences have only little or no effect on the results. In summary, the regression tree tests whether a pixel in VIS wavelengths reflects more or less radiation than is defined by a given threshold. If it reflects more, the pixel will be assigned to a higher snow cover fraction. The contrary is performed for the IR wavelengths; the higher the reflection, the lower the snow cover fraction will be (Rosenthal & Dozier 1996).<<

>>A supervised fuzzy classification approach was used by Pepe et al. (2005) to estimate fractional snow cover from MERIS data. Based on an interactively chosen training sample, the probability of a pixel belonging to a respective land cover class is derived. As a result, a soft classification map for each land cover class is created containing a value that describes the likelihood of a pixel representing the respective land cover class. Fisher & Pathirana (1990) showed that such soft classification maps can be used to estimate fractional land cover information. The approach was not done in the context of snow cover and was arranged for Landsat 5 data, which is different in spatial and temporal resolution from other sensors usually consulted to map snow cover. One conclusion, however, was that land cover classes with well-defined spectral behaviours can be estimated with a comparatively high accuracy (r =

0.984 for water, r = 0.945 for wetland). Land cover classes with a wide variety of spectral signatures on the other hand provide poor correlations (r = 0.472 for built-up area, r = 0.504 for open area). Because snow cover is characterized by a very strict spectral behaviour (high reflectance with up to 90% in the VIS region, reflectance values near zero in the near IR region; see Hall & Martinec (1985), Pepe et al. (2005), and Wang et al. (2005)), the fractional snow cover estimations derived from fuzzy classification results should provide good accuracy.<<

>>Salomonson & Appel (2006) developed a method to retrieve fractional snow cover information for Aqua MODIS satellite data. The 500 m MODIS snow cover product was used as the source. To retrieve the snow cover fraction within a MODIS pixel, a concurrent Landsat scene was used and registered to the same 500 m grid as MODIS. Every Landsat pixel was then classified as snow or snow-free ground, and the percentage of snow cover within each MODIS pixel (fractional snow cover) was generated. By comparing multiple such results, a relationship between fractional snow cover and NDSI was computed depending on the used satellite:<<

$$FRA6T = -0.01 + 1.45 * (NDSI), \quad (3)$$

$$FRA7U = -0.64 + 1.91 * (NDSI), \quad (4)$$

>>Here, 6 and 7 refer to the used bands in the calculation of NDSI, while *T* (Terra) and *U* (average of two combined relationships for Aqua) stand for the used satellite. The performance of these algorithms has been tested using different Landsat 7 ETM+ scenes. The correlation coefficients were located between 0.88 and 0.94 with a root-mean-square-deviation (RMSE) between 0.07 and 0.15. Accuracy was similar for both Terra and Aqua MODIS, but with Terra having some slight advantages that may result from the misregistration of 0.3 pixels between Aqua MODIS bands 7 and 4. Possible improvements of the method include the use of land cover and terrain information to adjust equations (3) and (4). Atmospheric correction may also further improve the accuracy (Salomonson & Appel 2006). The algorithm is included in the MODIS standard product and provides fractional snow cover in an operational way depending on the NDSI value of the respective pixel (Solberg et al. 2006).<<

>>Vikhamar & Solberg (2002) focused on the problem of decreased snow cover detection accuracy in forested areas. A subpixel snow cover mapping technique called *SnowFrac* was developed, which is based on a linear spectral mixture model *(SnowFor*). *SnowFor* simulates the pixel reflectance of forests. The signal that reaches the satellite sensor consists of a function from trees, snow, bare ground and irradiance. Each of these

components describes a function itself; for example, trees are a function of density, species and chlorophyll content and bare soil is a function of rock or soil type and vegetation. Irradiance depends on the satellite position, incidence angle and sensor characteristics. This results in a large number of variables, but the *SnowFor* method uses additional inputs to limit their number. A digital forest cover map and several endmember fractions are estimated by submodels prior to the run of the *SnowFor* model. Depending on the predominant tree types, a general forest reflectance model is adjusted. In the case of this study for Norway, spruce, pine and birch were the most prevalent tree species. The modelled pixel reflectance thus consists of the sum of the area proportions occupied by the respective tree type, snow or bare soil.<<

>>The additional submodels mentioned before are *BirchMod*, *ShadMod* and *DiffusMod*. *BirchMod* calculates the effective branch area of leafless birch trees as a function of tree height and also takes into account the solar elevation angle. *ShadMod* estimates the cast shadows on the snow cover caused by trees depending on the solar position. *DiffusMod* computes the amount of diffuse radiation that is shielded by the tree crowns and therefore does not reach the sensor. By unmixing the whole *SnowFor* model, the snow cover fraction can be estimated once the other variables are known. It was concluded that each additional submodel continuously improved the results. *ShadMod* brought the biggest improvements, increasing R2 from 0.48 to 0.62 for birch forest (Vikhamar & Solberg 2002).<<

>>The *MODSCAG* (MODIS Snow-Covered Area and Grain size) model was developed and tested by Painter et al. (2009). It is capable of deriving fractional snow cover, grain size and snow albedo from MODIS data. A library of modelled snow endmembers is used as the input together with endmembers for rock, soil, vegetation and lake ice. *MODSCAG* now analyses the linear spectral mixtures for each combination of two or more endmembers from the library. Snow covered area percentage and snow grain size are selected for each pixel according to the result of the linear spectral mixture analysis and the model that fits best for each endmember. Snow albedo can finally be determined using the snow cover fraction and grain size of each pixel as input. Validation was derived using Landsat observations for the fractional snow cover part while field measurements were available for grain size validation. Energy balance towers were used to assess the accuracy of the albedo estimates. The RMSE for fractional snow cover ranges from 1 to 13% with a mean RMSE of 5%. For grain size, the *MODSCAG* method constantly overestimates actual snow grain radii by a Mean Absolute Error (MAE) of 51 µm and a mean error of 30 µm (with mean actual snow grain size between 83 and 268 µm). For snow albedo, the MAE was 4.2% with a mean error of 3.6% (Painter et al., 2009).<<

>>In the context of the GlobSnow project funded by the European Space Agency (ESA), fractional snow cover products are generated on a daily, weekly and monthly basis using Along Track Scanning Radiometer 2 (ATSR-2) and AATSR data (see table 1 for details) for the complete Northern Hemisphere (Solberg et al. 2011). The Simple Cloud Detection Algorithm (SCDA) developed by the Finnish Environment Institute (SYKE) is used to recognize clouds. Once clouds, water bodies and glaciers have been masked out, the snow cover fraction is calculated using two algorithms, one for mountainous areas (>2◦ local slope) above the tree line (Norwegian Linear-Reflectance-to-snow cover algorithm NLR; developed by the Norwegian Computing Centre) and another for open areas and forested regions (*SCAmod*; developed by the SYKE). The NLR algorithm was developed for AVHRR data initially (Solberg & Andersen 1994). It uses only two endmembers (100% snow cover and 0% snow cover) for linear spectral unmixing to derive the snow cover fraction. The C-correction method (Meyer et al., 1993) is used to correct for topographic effects.<<

>>The *SCAmod* algorithm was designed to be suitable for most optical sensors and first applied to AVHRR data (see Metsamaki et al. (2005) for details). In the context of GlobSnow, it uses AATSR/ATSR-2 bands 1 and 4 (see Table 3.1) to derive fractional snow cover information for non-mountainous regions. Before the algorithm can be applied, a transmissivity map must be generated that serves as a reference for 100% (dry) snow covered conditions. Depending on this map, the snow cover fraction for each pixel is calculated by a semi-empirical reflectance model using reflectance values for wet snow, forest canopy and snow free ground as input parameters. The accuracy of the fractional snow cover product was evaluated against MODIS and Landsat snow maps. Good overall agreement was found for both analyses with GlobSnow overestimating snow cover fraction especially in June. Besides, discrepancies were recognized at the border of the mountain mask that also forms the border between the two algorithms (*NLR* and *SCAmod*) where a smooth transition of the results was expected but not always achieved (Solberg et al. 2011).<<

3.2.3 Algorithms to estimate snow cover below clouds

>>Because cloud cover hinders an optical sensor from measuring surface reflectance, various methods have been developed to estimate ground conditions underneath clouds. For hydrological models, it is important to have daily gapless information about the snow-cover extent. Rango (1996) mentioned that there is a definite need to develop techniques for snow-cover mapping beneath clouds. This is why so many methods have been developed to interpolate snow extent below cloud cover.<<

>>*SnowI* is an algorithm that determines the regional snow line based on the MODIS snow cover product (Parajka et al., 2010). The mean elevation of all snow covered pixels is opposed to all snow free pixels. If a clouded pixel lies above the regional snow line, it can be stated as snow covered. Otherwise, it will be reclassified as snow-free. This method is capable of decreasing cloud cover in a standard MODIS snow cover product from 60 to 20%. If cloud cover is too large in proportion to the entire scene, this method will not work properly. The threshold that is used to determine whether a scene can be processed by *SnowI* or not (because of too much cloud cover) determines the accuracy of the final result. This accuracy ranges from 48.7% to 81.5% depending on the cloud threshold (Parajka et al., 2010).<<

>>A method that combines both Terra MODIS and Aqua MODIS to reduce the impact of cloud obscuration is presented by Wang & Xie (2009). With their method, only ~2.5 days are needed to create a cloud-free snow extent from MODIS. The resultant Aqua–Terra composite achieved an accuracy of 90% when compared with in situ measurements at 20 meteorological stations. On average, the snow cover duration was 9 days higher than that suggested by the in situ data. This overestimation was due to the compositing technique that combined several days and therefore produced uncertainties. A second source for the overestimation may be the imbalance in scale that always exists when point-ground measurements are compared with pixel sizes of – in this case – 500 m × 500 m. Similar approaches were undertaken by Wang et al. (2009) and Parajka & Blöschl (2008) to combine Aqua and Terra MODIS snow cover products.<<

>>Gafurov & Bárdossy (2009) interpolated snow cover below clouds using six successive steps. Their methods are based on the MODIS daily snow cover product, which is determined using the *Snowmap* algorithm, described earlier in this thesis. In the first step, the snow cover products from Terra and Aqua MODIS are combined according to the method of Wang & Xie (2009). The temporal combination of snow cover information is the second step. Up to 2 days in the past and 1 day into the future or 1 day in the past and 2 days into the future are analysed for cloud-free classification results. In the third step, the maximum and minimum elevations of snow cover are evaluated similar to the method described by Parajka et al. (2010) earlier in this section. This method was only used for scenes with less than 30% cloud cover because determination of snow lines can lead to the wrong results if too many pixels are obscured by clouds. In step four, the snow condition of the four neighbouring pixels of each cloud covered pixel is analysed. If at least three of them are classified as snow, the centre pixel will also be classified as snow covered. Step five is similar to step four; here the eight neighbouring pixels of each cloud covered pixel are analysed. If a pixel is snow covered and a direct neighbour is obscured by clouds but has a higher altitude, the cloudy pixel is also

considered to be snow covered. Qobilov et al. (2001) suggested an alternative implementation of this step: if a pixel or segment of pixels is cloud covered, the nearest cloud-free pixel with the same elevation, azimuth and slope angle is used as a replacement. They used this method for AVHRR-processing only (Qobilov et al., 2000).<<

>>In step six, the time series of each pixel for the whole snow season is analysed to determine the start date of snow accumulation and the end date of complete snowmelt. Cloud covered pixels were then reclassified depending on the results of the time series analysis. The effects of short intermediate snow fall or melting are not respected. The sixth step automatically removes all remaining cloud covered pixels and is therefore placed at the end of the processing chain. To validate the results, several MODIS snow cover products with little cloud cover were artificially filled with cloud cover from other, more clouded scenes. It was reasoned that step one, the combination of Terra and Aqua MODIS, produced the highest improvements. Step four eliminated the smallest amount of cloudy pixels, whereas step six revised most. The accuracy of steps two to five accounts for 90–96% if they are accomplished in the given order. The accuracy of step one was not evaluated because it only depends on the accuracy of the snow classification results. Step six produced the lowest accuracy (78%) but removed the largest amount of clouds (Gafurov and Bárdossy, 2009).<<

3.2.4 Identification of snow cover and SWE with PM sensors

>>PM sensors are capable of mapping the surface beneath clouds and in darkness, and they are therefore valuable in the context of daily time series analysis. Especially when clouds are present for many consecutive days, interpolation techniques presented in section 3.2.3 become uncertain. Additionally, PM data can provide useful information on snowpack properties such as grain size or liquid water content (Rott & Nagler 1995). Various sensors provide global coverage with PM imagery. Refer to Table 3.2 for a detailed overview. The drawbacks of these sensors include their coarse resolution, the maximum SD of ~1 m that can be mapped, difficulties in mapping through precipitating clouds and the inability to map SD when snow is containing liquid water (Chang & Rango 2000; König et al. 2001; Josberger & Mognard 2002).<<

>>Clifford (2010) gives an overview of available PM sensors and methods to map SWE, which is defined as the mass of water included in the snowpack per area unit. In theory, the spectral gradient between different microwave channels is used as an indicator for SWE:<<

$$SWE = c * (T_{b18H} - T_{b37H}) \quad (5)$$

>>SWE is given in millimetres, T_{b18H} and T_{b37H} refer to the horizontally polarized brightness temperature of 18 GHz and 37 GHz microwave channels and c represents the slope of the linear fit: 4.8 mm K^{-1} (Chang et al. 1987). The brightness temperature at 37 GHz is prone to volume scattering of the snowpack whereas the frequency of 18 GHz is sensitive to the underlying surface. Volume scattering is the basic source of information for SWE as long as the snow is dry and not interspersed with liquid water, which would prevent volume scattering and lead to absorption of the microwaves (Che et al., 2008; Tait, 1998).<<

>>Not only horizontal but also vertical polarization can be used to retrieve SWE, but as Armstrong & Brodzik (2001) showed, the vertical polarization overestimates SWE in areas of desert soil or frozen ground whereas horizontal polarization only underestimates in early winter. The snow density is presumed to be 300 kg m^{-3}, which is a representative estimate for mature snow in North America, although the density can range from 100 kg m^{-3} for freshly fallen snow to 500 kg m^{-3} for very old snow (Foster et al. 1996). In a similar way like SWE, the SD can be derived:<<

$$SD = 1.59 * (T_{b18H} - T_{b37H}) \quad (6)$$

>>For the snow grain size, constant values of 0.3 and 0.5 mm are assumed. Because grain size and density are fixed, this method can be ranked as a static model. Foster et al. (1996) showed that the static algorithm from Chang et al. (1987) underestimates snow mass in North America by more than 50% for the period from December to March.<<

>>Other aspects limit the feasibility of SWE and SD retrievals; the snow grain size is an important factor that influences the PM signal. To achieve higher accuracy with SWE products, the evolution of the snowpack including its grain size and structure should be incorporated. Che et al. (2008) confirmed that a grain size of 0.3 mm would result in a coefficient c = 1.59 for SD estimations (see equation 6). However, a grain size of 0.4 mm would change the coefficient to c = 0.78 (Che et al., 2008).<<

>>A second point is the handling of vegetation. Not only forest fraction but detailed information about how vegetation interacts and influences microwave signals is required for better SWE estimations (Derksen 2008; Clifford 2010). Contrary to crystal size, the snow crystal shape has little to no influence on SWE and SD estimations from PM sensors, as shown by Foster et al. (1999). Derksen (2008) described how deep snowpacks with SWE values greater 120 mm can cause the measurements from the 37 GHz regions to become

unreliable. Volume scattering does not increase after this point. Additionally, the 18 GHz frequency can be influenced by volume scattering itself at SD greater 30 cm (Markus et al. 2006). The 10 GHz frequency can compensate for this problem if available, but the resolution is usually coarser than in the 18 GHz region (Table 3.2).<<

>>The basis of SWE and SD estimations with PM data is always related to equations (5) and (6). These formally static approaches have developed during the years, leading to fundamental improvements. Josberger & Mognard (2002) used air temperature as an additional input to estimate snow metamorphism. Their method was tested for the Northern Great Plains in the USA, which are characterized by very flat terrain, only very sparse forested areas and a large number (285) of climate stations.<<

>>The analysis of Tb19–Tb37 GHz gradient maps showed that the gradient stays near zero until the first snow occurs on the ground, which causes the gradient to increase. Abrupt changes in the gradient signal where the difference between the channels falls back to zero again indicate a warming event with liquid water arrival. These impacts of changing air temperature induced Josberger & Mognard (2002) to develop a temperature gradient index (TGI) that describes the grain size metamorphism of snow crystals within a snowpack. This index is defined as the temperature difference between the bottom and the top of the snow surface divided through the snow thickness for a whole snow season. The index is then correlated with the spectral gradient of the snow covered area during the snow season, and the congruence was found to be quite high because the spectral evolution of the snow covered area followed that of the TGI. Therefore by including the TGI, SD and SWE can be calculated from PM data and air temperature measurements.<<

>>Josberger & Mognard (2002) concluded that TGI can be used as an indicator for snow grain size metamorphism. This conclusion was also used for the first development of the AMSR-E SWE Algorithm (*SWEmap*) that is utilized to produce daily, 5-day and monthly global snow storage index maps (Chang & Rango 2000). Because the vertical structure of a snowpack can consist of different layers of densities, grain sizes and underlying surface conditions, the upwelling microwave radiation can vary extremely. This is why a number of different snowpack profiles have been selected to create a database that can be used with a multi-layer perceptron (MLP) type artificial neural network.<<

>>Chang & Tsang (1992) describe the idea behind the neural network approach to map SWE: because the neural network must be trained before using, simulated SWE data are integrated into the network. The microwave brightness temperature is the only input layer to the network. One or more hidden layers are used to process the data and there is again only

one output layer. As a result, the sum of all input signals to a hidden layer is processed by the sigmoid function. A back-propagation algorithm is used to train the network. This algorithm compares the results of the process with the training datasets included at the beginning.<<

>>The training of the network is done by calculating different combinations of the three input parameters: snow crystal size, snow density and SD. Snow temperature is fixed at 265 K, and three additional atmospheric models are included: Mid-latitude winter, sub-Arctic winter and Arctic winter atmospheres. 720 sets of input–output pairs are generated out of these variables and used for training of the neural network. SWEmap is then prepared to derive the SWE estimates. First, the attributes of the respective pixel are gathered, including snow classes, fractional forest cover, land use, elevation, probability of snow, SWE history and land–water mask. Second, a number of tests are conducted. A snow probability test determines whether the occurrence of snow is possible for a respective pixel or not by – amongst others – analysing snow frequency maps for the last 10 years. A surface temperature test is added, deciding whether the presence of snow is possible. SWEmap consists of a number of tests again. First, the surface temperature derived from IR bands or even PM data are tested, which has a reported accuracy of 1.2–2.5° C for SSM/I data (Pulliainen et al. 1997). The AMSR-E imagery is then tested for precipitation followed by a wet snow test. Fractional forest cover is included in a last step to linearly fit the maximum albedo of a pixel depending on the forest fraction with values of 0.8 for no forest fraction and 0.2 for 100% forest cover within a pixel.<<

>>The algorithm for determining SWE from AMSR-E has evolved in recent years. Because the 18 GHz frequency is affected by volume scattering for deep snowpacks (Derksen 2008), the 10 GHz frequency can be used instead (Kelly 2009). Additionally, the 89 GHz frequency can be included to map shallow snowpacks in combination with the 23 GHz frequency from the AMSR-E sensor. Because the 89 GHz region is prone to atmospheric contamination, additional tests are required to ensure the reliability of the shallow snow detection (Kelly 2009). Unfortunately, the AMSR-E sensor aboard the Aqua satellite stopped the acquisition of data on October 4th, 2011.<<

>> Pulliainen & Hallikainen (2001) presented a study to retrieve regional SWE from PM observations in the Kemijoki drainage area in Finland. An algorithm called the Snow Emission Model-Based Automatic Inversion Algorithm was used to retrieve SWE, and the results were compared to conventional spectral and polarization difference procedures. The algorithm was developed at the Helsinki University of Technology (*HUT*) and will from now on be called the *HUT* algorithm. *HUT* is an emission model-based iterative algorithm that takes into account the average SD, density and grain size of snow. The details of the model are described by

Pulliainen et al. (1999). The emission behaviour of snow is a function of grain size, density and SWE. The brightness temperature of each pixel is also modelled depending on the forest fraction to take into account the loss factor of the canopy. Atmospheric transmissivity, soil emission contribution and the effect of multiple reflections between the soil–snow and snow–air boundaries are also modelled using additional methods developed by Pulliainen et al. (1993); Pulliainen et al. (1997), and Ulaby et al. (1981). When compared with independent experimental data and tower-based experiments, *HUT* modelled results agreed well with in situ data. In comparison to SSM/I-derived brightness temperature, the *HUT* model predictions showed correlation coefficients of 0.82 for vertically (V) and 0.76 for horizontally (H) polarized frequencies. Only observations with a daily maximum temperature greater than 0° C were allowed. If all observations regardless of temperature were analysed, the accuracy decreased to r = 0.79 (V) and r = 0.69 (H).<<

>>Because the emission model was now validated to produce admissible results, *HUT* was finally used to retrieve SWE from SSM/I data. Three SSM/I channels were used in a modified inversion scheme instead of the original method that tried to fit the modelled brightness temperature into the seven SSM/I channels (this led to unsatisfactory results). The modified scheme used the differences between the channels and polarizations instead of the raw SSM/I brightness temperatures (37 GHz (V), 19 GHz (V) and 19 GHz (H) were used) and also included the snow grain size and the standard deviation of the SSM/I brightness temperatures (2 K as shown by Hollinger et al. (1990) who verified that SSM/I is a stable and well-calibrated microwave sensor). The results from the Kemijoki drainage area in Finland for night-time observations during the winter of 1993–1994 showed that *HUT* produces reasonable results (r = 0.93) when compared to in situ data. When calculated for the midwinter seasons from 1993–1994 to 1997–1998, the correlation coefficient for *HUT* was 0.75 (for observations with temperatures less than 0° C) to 0.62 (all midwinter observations) and therefore better when compared to the results of conventional SWE retrieval methods. That is why the authors conclude that the performance of the algorithm depends mainly on the weather conditions and that additional information such as near-surface air temperature could still improve the results. Data for snow characteristics would also be useful to replace the fixed values such as snow grain size and snow density (Pulliainen & Hallikainen 2001).<<

>>The *HUT* model is also incorporated in the GlobSnow project to estimate SWE values for the complete Northern Hemisphere for the years from 1979 until present. Daily, weekly and monthly products are generated from SMMR, SSM/I and AMSRE data (Luojus, Pulliainen, Takala & Lemmetyinen 2010). The method applied for the GlobSnow product is described by Pulliainen (2006). By combining ground-based observations with spaceborne PM

data, the accuracy of SWE and SD estimates improves significantly. The analysis of spaceborne PM data alone is subject to major restrictions as the brightness temperature saturates at large SD values. The new assimilation technique estimates snow grain size at the ground-based stations and determines SWE and SD values at these stations while interpolating (Kriging interpolation) between their locations (Pulliainen 2006).<<

>>Derksen, Walker & Goodison (2003) compared 18 winter seasons of in situ data and SWE derived from PM instruments in Western Canada. For the years from 1978 to 1996, 5-day average SWE estimates derived from SSM/I and SMMR have been crosschecked with in situ data. In regions with small forest cover, the agreement between the different results was good, whereas in heavily forested areas or at times when the SD exceeded 75 mm, SWE was systematically underestimated. Interannual performance variability was also observed when the accuracy of different years was evaluated. Whereas during the winter season of 1991–1992, the mean bias error (MBE) was only ~5 mm, in the following season the MBE was nearly 25 mm (Derksen, Walker & Goodison 2003).<<

>>Derksen, Walker, LeDrew, et al. (2003) also presented a method to combine SSM/I and SMMR data for Central North America to derive an SWE time series. There is only a 6-week overlap of this time series because the SMMR sensor only operated until August 1987 with SSM/I starting in June 1987. It is desirable to have consistent and comparable time series of SWE estimations, and this is why this study is focused on the comparison of the two sensors. SD data from climate stations served as in situ data and have been converted to SWE using an average snow density described by Brown (2000).<<

>>In summary, both SMMR- and SSM/I-derived SWE estimates showed a consistent relative agreement with in situ data with none of the sensors being more accurate than the other. Both sensors underestimated SWE in heavily forested areas for more than 15 mm. However, the SMMR sensor was found to underestimate SWE values significantly stronger than SSM/I. It was demonstrated that SWE magnitudes calculated from SSMR brightness temperature differ from the ones derived from SSM/I and that this circumstance should be accounted for in order to evaluate longer time series of SWE metrics (Derksen, Walker, LeDrew, et al. 2003).<<

3.2.5 Combination of PM and reflective data to map snow cover

>>Because PM data has the capability to estimate snow cover underneath clouds, advanced combination methods of both PM and optical data are desired (König et al. 2001; Simic et al. 2004; Liang et al. 2008). Data from optical and thermal sensors alone cannot

provide cloud-free snow cover information on a daily basis. A combination of these sensors with PM sensors is therefore most desirable (Romanov et al., 2000) and recommended (Rango 1996).<<

>>Romanov et al. (2000) presented a system for automated mapping of snow cover for North America with a combination of VIS and IR data from the GOES and PM data from SSM/I. As measurements in the medium IR region of the spectrum (MIR) were not available from geostationary satellites until the launch of GOES-8, attempts to map snow cover from these sources encountered serious difficulties. Since 1994, the MIR range measurements are available and have been used in this study to automatically map snow extent for North America.<<

>>The GOES observations are available every 30 minutes. By compositing these individual images using the pixel with maximum 11 µm brightness temperature and minimum MIR, cloud coverage is mitigated. To identify a snow covered pixel, two steps are established after a water mask is applied to exclude all water bodies from the analysis; the ratio between the VIS and the MIR channels is calculated, producing a snow index SI that indicates snow cover. To eliminate the influence of iced clouds and semi-transparent cirrus clouds, which is the most challenging problem, an additional temperature threshold is applied. This threshold is based on the surface temperature forecast of the NCEP regional operational Eta Model. Because these model estimations can also be erroneous, the threshold is decreased by 10 K. Additionally, the IR brightness temperature must be lower than 283 K for a pixel to be mapped as snow. In the second step, all snow-free pixels are now classified either as land or as cloud. If the IR brightness temperature is lower than 283 K and VIS or MIR reflectance is high (at least 25% for VIS, 10% for MIR), the pixel is classified as cloud. Otherwise, the pixel is assumed to be cloud free.<<

>>The compositing of multiple GOES observations per day minimizes cloud coverage but does not eliminate it. This is why SSM/I-derived snow cover data are used additionally. The SSM/I snow cover maps are provided by NOAA as an automatically derived product. The resolution of the SSM/I snow cover dataset is 30 km and is remapped to 4 km GOES resolution. To prevent false classification near water, all pixels as close as 30 km to water bodies are excluded. Precipitating clouds can also cause misclassifications and therefore, ‘no data’ is assumed for SSM/I where such precipitation is acknowledged. In a case where neither SSM/I nor GOES provides useful results, the previous day’s classification is used.<<

>>For validation, 1,000 climate stations reporting SD from the US cooperative network are compared to the blended snow cover product for the period from February to April 1999.

The GOES clear-sky classifications produced the most accurate results with 88% correct interpretations. The SSM/I snow maps only provide 80%. The blended product of GOES and SSM/I is 3% better than SSM/I, leading to an overall accuracy of 85% (Romanov et al., 2000).<<

>>Gao et al. (2010) combined MODIS and AMSR-E and also added an additional cloud mitigation step by combining Aqua and Terra MODIS prior to AMSR-E fusion (see 3.2.3; Wang & Xie (2009); Wang et al. (2009)). The overall cloud coverage of the MODIS products (60.0% for Aqua and 55.0% for Terra MODIS) was reduced to 47.8% by the combination of both Aqua and Terra MODIS. The 25 km pixels of AMSR-E were downscaled to 500 m. The SWE values from the original AMSR-E product were then recalculated using the actual number of snow covered pixels taken from the fused MODIS snow cover product. A linear distribution of SWE within the snow covered pixels retrieved from MODIS was assumed, and the original SWE estimations were recomputed using:<<

$$SWE_n = SWE_0 * 2(\frac{2500}{N_{snow}}), \quad (7)$$

>>where SWE_n represents the new SWE value for the respective 500 m pixel, SWE_0 refers to the AMSR-E 25 km SWE value and N_{snow} stands for the number of snow covered MODIS pixels within the AMSR-E pixel. The scaling factor 2 is used because SWE data taken from NSIDC (in this case AE_DySno) is scaled down by the factor 2.<<

>>The accuracy of the combined product was tested for the region of Fairbanks and Upper Susitna Valley, Alaska, and found to be better than any of the original snow cover datasets. When compared to in situ data for the period from 1 October 2006 to 30 September 2007, the snow accuracy of the merged snow cover product reached 86% and is therefore much better than the combined Terra–Aqua MODIS snow cover product (49%) and still slightly better than the AMSR-E snow accuracy (85%). The accuracy for the no-snow period was also better for the combined product (95%) when compared to the original datasets (55% for Aqua–Terra MODIS product, 94% for AMSR-E product). During snow accumulation, the accuracy increased by 12–16% (compared to AMSR-E), and during melting the increase was 1–38% (compared to AMSR-E). Even when compared to the blended product of Liang et al. (2008), who tested the combination of Terra MODIS and AMSR-E for China, the accuracy was higher (75.4% for Liang et al. (2008); 86.0% for (Gao et al., 2010)).<<

>>The accuracy of SWE estimations did not change significantly during the midwinter season for the combined product. This is because the 25 km AMSR-E pixels were completely

filled with snow, and the linear redistribution to 500 m pixels did not have much impact. During transition periods in autumn and spring, however, the accuracy improved because the snow cover was thin, patchy and in some cases wet. The final conclusion was that the combined product of Aqua and Terra MODIS together with AMSR-E can improve snow cover and SWE estimations and that the product can contribute to hydrological and meteorological modelling (Gao et al. 2010). Liang et al. (2008) developed a similar method. They concluded that the combined snow cover products of Terra MODIS and AMSR-E can improve the accuracy of daily snow cover estimations. Hall et al. (2007) also concluded that the combination of the MODIS snow cover product with AMSR-E snow estimations will produce a higher accuracy than any of the original data alone for the Lower Great Lakes region in North America.<<

>>Foster et al. (2011) combined VIS, PM and scatterometer data to produce a single snow cover dataset containing SWE, snow extent, fractional snow cover, snowpack ripening, onset of snowmelt and actively melting areas. The algorithm is called *ANSA* (Air ForceWeather Agency/NASA Snow Algorithm). MODIS, AMSR-E and QSCAT data were included to provide daily datasets for the whole Earth. The use of scatterometer data differentiates between this new product and prior approaches. Some basic facts about how snow covered areas affect scatterometer observations are presented in section 3.1. The MODIS snow cover product was the default to estimate snow extent because it provided the best accuracy under clear-sky conditions. For clouded pixels, AMSR-E was used to derive the snow extent. SWE was inherited from the AMSR-E SWE product version T08. The 89 GHz frequency was only included for clear-sky regions to prevent negative effects of atmospheric contamination. Diurnal amplitude variations of the 37 GHz and 19 GHz frequencies were analysed to identify the onset of snowmelt. Information about forest fraction was finally included to improve the PM accuracy. The QSCAT backscatter from the Ku band was used additionally to determine snowmelt onset and actively melting areas. The accuracy of the blended ANSA product was better than both MODIS and AMSR-E alone (Foster et al. 2011).<<

3.3 Summary and discussion of presented methods

After an overview about the available methods to map snow cover using remotely sensed satellite data has now been established it is about time to reconsider the advantages and drawbacks of the available sensor types and algorithms. This step is important in order to identify the most suitable set of data and methods for the given task: To be able to analyse snow cover parameters of Central Asia with both, sufficiently high temporal and high spatial

resolution of the results. Additionally, the accuracy of the snow cover products should be as high as possible.

>>The *Snowmap* algorithm is used to produce MODIS snow cover products at various temporal and spatial resolutions. Daily, 8-day and monthly products are available and have been validated by various researchers and for many different parts of the Earth. Klein & Barnett (2003) compared the MODIS snow cover with in situ snow telemetry (SNOTEL) data from NOHRSC for the Upper Rio Grande basin. The MODIS product achieved an overall accuracy of 94% (with 4.4% omission and 25.5% commission errors). Maurer et al. (2003) compared the MODIS product with station data from the Missouri River basin and the Columbia River basin. GOES and AVHRR snow cover estimates from NOHRSC were used as well to evaluate the accuracy of the MODIS product, and it was found that the MODIS snow cover product was more accurate than the NOHRSC product. Parajka & Blöschl (2006) evaluated the daily MODIS product for Austria using station data from 754 SD stations. The agreement of MODIS reached 95% for cloud-free days with the highest error rates in January (15%) and the lowest error in summer months (1%). Huang et al. (2011) tested the MODIS product for Northern Xinjiang, China, and again the overall accuracy reached 95% when compared to ground measurements and Landsat data. Nearly the same result was found by Simic et al. (2004) for Canada; accuracy was 93% compared to ground-truth data. All these accuracy values were calculated analysing clear-sky scenes.<<

>>The *Snowmap* algorithm had similar problems for each analysis. In mountainous regions, snow cover is often underestimated if no digital elevation map (DEM) is used to adjust for local solar illumination (Dozier & Marks 1987; König et al. 2001; Jain et al. 2008; Dozier & Painter 2004). Jain et al. (2008) therefore prepared an aspect map from a DEM including eight classes for orientations. However, Parajka & Blöschl (2006) did not observe any significant influence of the topography on the MODIS snow cover accuracy. A problem that was confirmed not only from Parajka & Blöschl (2006) but also from Simic et al. (2004) and Klein & Barnett (2003) is the lower accuracy during transition periods. In autumn when snow cover starts to accumulate or during spring when snow cover is melting, the accuracy of the MODIS product is affected by more fractional snow cover or decreased reflection of the snow surface due to impurity. Vegetation is the third parameter that may lead to a decreased accuracy of the MODIS snow cover product. Maurer et al. (2003), Klein & Barnett (2003) Huang et al. (2011), and Simic et al. (2004) confirmed this behaviour, especially for forested regions. But scrubland also can influence the accuracy of the MODIS product, as Huang et al. (2011) described. Thin snow cover can also introduce serious underestimation of actual snow cover with accuracy values of only 5% for 1 cm 15% for 2 cm, 28% for 3 cm and 56% for 4 cm of SD (Wang et al.

2008).<< Liang et al. (2008) reported the same. Their study will be reviewed in section 3.4.2 since the study region of Northern Xinjiang lies very close to the Central Asia and is therefore of special interest.

>>Despite the problems outlined so far, the MODIS snow cover product processed by the *Snowmap* algorithm is the most accurate product these days. Only a few alternative products are available in a similar temporal and spatial resolution and for the whole Earth: The fractional snow cover product facilitated by the GlobSnow project covers the complete Northern Hemisphere for the years from 1995 until present. The daily, weekly and monthly snow maps are derived from ATSR-2 and AATSR data (Table 3.1). Two different algorithms are utilized for both mountainous and plain terrain. This differentiates between the GlobSnow product and the MODIS approach. When compared to the MODIS snow cover product, the agreement was quite high. GlobSnow was overestimating snow cover for mountains during June. Additionally, the transition zone between the results from the two algorithms is not smooth in some regions, leading to inaccurate discrepancies in these areas. The cloud detection (SCDA) does not work for cold and high cloud tops consistently. In some cases, clouds are mistakenly detected along the border between snow cover and snow-free ground (Solberg et al. 2010a; Solberg et al. 2010b). The product is freely available and produced every 24 hours in near real time, making GlobSnow an alternative to the MODIS product. The coarser resolution of 0.01° and the less elaborate cloud detection may limit the usability when compared to MODIS. Validation of the accuracy is required to clarify the advantages and weaknesses of the GlobSnow product. The forest transmissivity map that is used as an input by the SCAmod algorithm is based on the GlobCover land cover map, which does not represent very dense and very sparse forests correctly. Snow cover fraction for these land cover types, especially in North America and Siberia, can therefore be underestimated (Solberg et al. 2010b). The handling of mountainous areas with a unique algorithm may on the other hand yield higher accuracy for these regions. Additionally, the use of the SCAmod algorithm for plain terrain may produce better snow cover results for forested regions than MODIS because the algorithm was initially designed especially for the boreal forest zone (Metsamaki et al., 2005).<<

>>SPOT-4 VEGETATION (VGT) snow maps are available every other day at 1 km resolution and since 1998. The overall accuracy of this product is 83% as has been tested by Simic et al. (2004) for Canada. Because the accuracy decreases to 41% for snow covered forested areas, the product is not suited for regions with extensive forest cover. The algorithm can be adjusted to the respective region of interest to increase the accuracy, as shown by Dankers & De Jong (2004). They used the red instead of the green band and changed the NDSI threshold. However, the original VGT-S1 product should be used with care. The algo-

rithm (not reviewed in this thesis) is therefore not recommended for use on a global scale but better suited for regional applications and after prior analysis of the correct thresholds and band combinations.<<

>>Snow maps derived from AVHRR data are an additional alternative to MODIS. AVHRR data are available since the early 1980s, providing a long time series of daily observations.<< Three methods to process snow cover from AVHRR data were reviewed in section 3.2: *Snowcover*, *theta*, and APOLLO. >>The accuracy of *Snowcover* products has been evaluated by Fernandes & Zhao (2008) for the Western Arctic and identified as 87% for 50% of the test sites (67 sites provided by the MSC and 260 sites from the HSDSD 2). The theta algorithm was originally designed for North America (Maxson et al., 1998) but has been successfully transferred to Turkey by Akyürek & Sorman (2002). Theta was able to recognize most clouds and discriminate between clouds and snow, which is often a problem for AVHRR because of the sparse selection of available bands. The coarser resolution of AVHRR (~1,000 m compared to 500 m from MODIS) also leads to an increased uncertainty due to mixed pixels (Maxson et al. 1998). Additionally, the method is not fully automated because some thresholds must be set manually. When compared to unsupervised classification results using the Iterative Self-Organizing Data Analysis Technique (ISODATA), theta was more accurate for the eastern part of Turkey (Akyürek and Sorman, 2002).<< APOLLO is able to process data from all available AVHRR data without any manual interaction or additional input layers. The algorithms were developed in the 1980s, but they have been updated within the years for continuous improvement. The snow and ice extension that was evolved to discriminate between clouds and snow within the APOLLO scheme has not been investigated for possible systematic classification errors. Therefore, though on the first look APOLLO seems to be suited for the processing of long time series of daily snow cover data, an accuracy assessment of the product would be necessary in a first step.

>>While for large scale analyses of snow covered areas the resolution of 500 m (or 1,000 m for AVHRR and VGT) is sufficient, it may be too coarse for local investigations. In such cases, the ARSIS concept can be used to increase the resolution of MODIS to 250 m as shown by Sirguey et al. (2008). The resultant snow cover product was more accurate than the 500 m product with the mean absolute error decreased by 20%. Because a large number of endmembers are needed for unmixing, this procedure can only be applied on a local scale due to increased computing time. However, the ARSIS concept is a good alternative for steep terrain where the 500 m product may be disturbed by serious misinterpretations.<<

>>In summary, it can be stated that the MODIS snow cover product should be preferred where available. The accuracy of AVHRR is constantly lower, often underestimating

snow covered areas seriously (Molotch and Margulis, 2008). Lower resolution and the smaller selection of available spectral channels are the main reasons for this fact. The lesser geolocation accuracy of AVHRR (±1,000 m) when compared to MODIS (±250 m) adds to this circumstance (Butt and Bilal, 2011). The GlobSnow product may serve as an alternative for MODIS. The coarser resolution, simple cloud detection and the lack of an intensive evaluation for different regions and snow cover conditions of GlobSnow still put the MODIS product ahead. The IMS daily snow cover maps have a coarser resolution (4 km). Although PM, station data and atmospheric models are used to generate cloud free data, errors can be introduced, especially in the ablation phase and for thin, cloud covered snowpacks (Helfrich et al., 2007). Frei & Lee (2010) compared the MODIS snow extent to the IMS snow cover product and found that MODIS consistently achieved better accuracy.<<

>>The decision tree based classification of Landsat data is an example of high resolution snow products. Because Landsat observations are only available every 16 days and the thresholds can require much manual work to adjust for a new region of interest, this method is not intended to be used operationally. Once correctly adjusted, the accuracy of the decision tree is very good (R2 = 0.979; Rosenthal & Dozier (1996)). This makes Landsat snow cover maps an ideal ground truth source for medium resolution products.<<

>>Mixed pixels of snow covered and snow free ground are often a source of over- or underestimation of actual snow cover from medium resolution data. Algorithms to estimate the snow cover fractions from Landsat (Rosenthal & Dozier 1996), MERIS (Pepe et al., 2005) and MODIS (Salomonson & Appel 2004; Salomonson & Appel 2006) were reviewed in section 3.2.2. All these approaches lead to higher accuracy of snow cover classification results. They usually require additional input data such as land cover maps (Salomonson & Appel 2006) or even detailed information about the composition of forests including different tree types and density (Vikhamar & Solberg 2002). If such ancillary data are available, fractional snow cover algorithms can add to the accuracy of snow cover products. Hydrologic models such as snowmelt runoff simulations can benefit from fractional snow cover information in particular (Bales et al. 2008). On the other hand, computing time and data volume are most likely to increase during these calculations.<<

>>Methods to estimate snow cover below clouds are presented in section 3.2.3. Unlike the products derived from PM sensors, these methods use the combination of multiple acquisitions (Wang & Xie 2009), neighbourhood analysis (Gafurov and Bárdossy, 2009) or terrain-dependent rules (Parajka et al., 2010) to mitigate the impact of cloud cover. Additionally, a seasonal filter can be applied to eliminate even the final cloud proportion (Gafurov and Bárdossy, 2009). The quality of these methods varies. The combination of different observa-

tions yields the best accuracy because the snow cover classification is produced from the actual Earth observations and not modelled like that from the other methods. The combination of Terra and Aqua MODIS allows for cloud free observations every 2.5 days, whereas without this step, 8 days are required to acquire the same result (Wang & Xie 2009). *SnowI* is an algorithm that estimates snow cover below clouds according to the terrain elevation of cloud-free pixels. The accuracy depends on prior defined thresholds and ranges from 48.7% for a progressive approach to 95.0% for a conservative approach (Parajka et al., 2010).<<

>>For observations made from the reflective part of the spectrum, clouds turn out to be the most inhibiting factor regarding accuracy and reliability of the results. There are two major reasons for this problem: First, clouds obscure the surface and do not allow for surface condition estimations from optical sensors. This limits the capability of snow cover detection algorithms and can cause high errors of omission, depending on the size of the cloud covered area and the number of consecutive days the surface was obscured. Especially at the beginning and the end of the snow season, when conditions can change dramatically within few days, false interpretations of snow cover can occur. The second problem is linked to the likelihood of confusion between clouds and snow. Because the spectral signature of clouds and snow is similar especially for the VIS part of the spectrum, these confusions cannot be foreclosed. The use of additional wavelengths from the IR region can mitigate the misclassification of clouds but still, misinterpretation can occur between clouds and snow. Land cover constitutes an additional error source of snow mapping with optical sensors. Water bodies and lake ice can induce false snow cover recognition. Forested regions, however, turned out to be the most inhibiting land cover class. Depending on the density of the forests and to some degree also depending on the tree types, the underlying snow cover is obscured by the canopy and cannot be estimated from space. Forests also tend to prevent the surface from direct sun insolation, conserving the enclosed snow from melting longer than the snow from the neighbouring unobstructed areas. Both facts tend to underestimate the actual snow extent. The low reflection of dark forests such as spruce can cause the NDSI to reach values similar to snow. This can lead to overestimation of snow extent if no threshold for VIS bandwidths is included. Terrain conditions such as elevation, slope and aspect account for a third error source. In mountainous regions, different illumination effects can occur depending on both satellite and solar zenith angle. Snow distribution may also vary according to local wind regimes, leading to snow free areas in the direct neighbourhood of snow accumulation zones. The use of a DEM can help to minimize these problems.<<

>>PM data can be used to calculate SD and SWE with high temporal resolution and for the whole Earth. Their ability to record data during darkness and cloud cover makes them a

valuable tool in snow cover mapping. Derksen et al. (2003) presented a method to combine SMMR and SSM/I, which was problematic because acquisition periods of the sensors only overlapped for a short time (6 weeks). Algorithms to map SWE with AMSR-E ensure a gapless time series from 1978 till present. Because the individual sensors operate at different frequencies, resolutions and overpasses, the change between different sensors must be handled with care. The first methods to map SWE and SD used a static model with fixed values for snow density (300 kg m^{-3}) and snow crystal size (0.3–0.5 mm). Only frequencies around 18 GHz as background and 37 GHz as scattering signal were incorporated, which created serious uncertainties (Clifford, 2010). These algorithms have developed over time, leading to version T08 of AMSR-E as the latest product. By including 89 GHz for shallow snow detection and 10 GHz for SWE greater than 120 mm, the accuracy was improved. An additional test for snow temperature and information about the forest fraction of each pixel is also applied (Foster et al. 2011).<<

>>The GlobSnow SWE product is generated from SMMR, SSM/I and AMSR-E data and provides daily, weekly and monthly datasets from 1979 till present. The method used to derive SWE was chosen after testing several possible algorithms, including the AMSR-E standard algorithm (Kelly et al. 2003), the algorithm of Chang et al. (1987) and the methods from Derksen, Walker & Goodison (2003) and Derksen, Walker, LeDrew, et al. (2003). It was found that the algorithm of Pulliainen (2006) worked best when applied to the whole Northern Hemisphere. The Pulliainen algorithm (HUT) induced an RMSE of 43.2 mm for Eurasia, 29.8 mm for Finland and 24–77 mm for Canada (Luojus, et al. 2010). When the algorithms were compared against each other, the latest version of the AMSR-E operational SWE algorithm was not yet developed. Because this new version now includes methods for improved SWE detection under shallow and deep snowpack conditions, the comparison may have led to a different conclusion. However, since AMSR-E stopped acquiring data on October 4th, 2011, SWE products after this date will again have to rely on SSM/I data.<<

>>SWE and SD estimates derived from PM data are subject to various restrictions. The coarse resolution can introduce large uncertainties due to mixed pixel effects. Water bodies limit the significance of the product, as observed by Dong et al. (2005). Volume scattering of snowpacks saturates at SWE values greater than 120 mm (Derksen 2008) to 150 mm (Luojus, Pulliainen, Takala & Lemmetyinen 2010), leading to major underestimations of SWE for deeper snowpacks. Finally, forest cover can reduce the accuracy of SWE and SD estimations. Validation of these SWE and SD values is also a problem. To assess the accuracy correctly, at least nine point measurements would be required for a 1° by 1° grid. An analysis for the Northern Great Plains gave proof that single-point measurements used as ground truth can

imply error rates as high as 22 cm for SD. Using ten test sites instead of only one, the error was reduced to 7 cm (Chang et al. 2005). Because dense station networks measuring SD are not available for the whole Earth, validation of SWE and SD derived from coarse resolution PM data may not be possible without extensive field campaigns. In some studies (e.g. Derksen (2008) with more than 25 km spacing between test sites; (Kelly 2009) with only ~250 test sites scattered over the whole Earth), this problem could not be solved. Kelly (2009) reported RMSE values between 17 and 23 cm for SD, Derksen (2008) RMSE values of 27–35 mm for SWE, both derived from AMSR-E. The combination of observations from different sensor types is suggested by several authors (e.g. König et al. (2001); Simic et al. (2004); Foster et al. (2011); Liang et al. (2008)) as it can utilize the benefits of the respective sensors. Their individual drawbacks can often be mitigated at the same time. Liang et al. (2008) combined MODIS and AMSRE and found that the overall accuracy of this blended product was much higher (75.4%) than for the Terra MODIS daily snow cover product alone (33.7% for all-weather conditions if clouds were treated as error). Similar results were found by Gao et al. (2010), who calculated even 86% overall accuracy for the blended MODIS–AMSR-E product, whereas the combination of only Aqua and Terra MODIS only yielded 49% accuracy. Foster et al. (2011) blended MODIS, AMSR-E and QSCAT data to produce a daily dataset of snow extent, SWE, snow cover fraction and information about snowmelt on a global scale. The authors again concluded that the combined dataset was more accurate than MODIS, AMSR-E or QSCAT alone.<<

It must be noted here, however, that the interpretation of cloud covered pixels as erroneous classification results is somehow controversial: If clouds are present, the obscured pixels may be interpreted as missing data instead. When calculating parameters like SCD, SCS, or SCM (equations 8 to 11 in section 3.4.2), data gaps will, however, lead to errors in these parameters. It is therefore – and with special respect to the presented thesis – a valid statement to count data gaps caused by cloud coverage as potential error sources, although the classification result itself is correct.

>>Existing spaceborne sensors do not have the capability to derive the whole bandwidth of snow cover parameters from a single platform on their own. This is why the National Aeronautics and Space Administration (NASA) accomplished the Cold Land Processes Field Experiment (CLPX) from winter 2002 to spring 2003 (NSIDC, 2013). Field data and airborne and spaceborne remotely sensed data were collected for the same regions. Multispectral, hyperspectral, passive and active microwave data have been acquired and can be accessed from the website of NSIDC (http://nsidc.org/data/clpx). These data serve as a basis for future algorithms and validations. Different algorithms and products are presented and discussed. It depends on the region and research subject which of the methods should be preferred. In ret-

rospect, it seems that snow cover products blended from reflective, PM and maybe even scatterometer data are the best choice. The accuracy is higher than for the individual products and the bandwidth of the available snow cover characteristics that can be determined is broader. In fact, these are conclusive arguments, and because the development of the combined algorithms has advanced during the recent years, they seem appropriate. However, the coarse resolution of the PM datasets can limit the usefulness of derived and combined products. Molotch & Margulis (2008) confirmed that PM data are not suited to small scale analysis of SWE. The coarse resolution generalizes SWE in mountainous regions and can attenuate the SWE variations. Additional input data such as forest fraction maps and information about water bodies are needed. Additionally, the validation of blended snow products can be problematic depending on the region and availability of in situ data.<<

>>The 10 GHz frequency is not facilitated by the SSM/I sensor while the 89 GHz region was not included for the SMMR sensor. It depends on the location whether these frequencies are recommended or not. The 10 GHz data for example is not necessarily needed when SWE will not exceed 120–150 mm. However, the decision on which sensor to choose when relying on PM data should be easy. For the years before 1987, SMMR was the only available data source. From 1987 to 2002, SSM/I was the only sensor to measure the Earth's surface in the PM region and after 2002, AMSR-E should be preferred because it provides a larger bandwidth of frequencies than SSM/I. A comparison between different SWE retrieval algorithms derived in 2009 suggested that the method developed by Pulliainen (2006) fits best on a global scale (Luojus, Pulliainen, Takala, Derksen, et al. 2010). Because the latest version of the AMSR-E SWE algorithm (Kelly 2009) was not included in this comparison, it cannot be assured that this assessment still applies. Further analyses are required here. For optical sensors, MODIS seems to be the best choice as it provides the highest resolution and accuracy among the available sensors. For the years before 2000, AVHRR should be used, which has been available since 1978. Methods to map snow extent from AVHRR have been developed by various researchers, and the data are freely available. VGT (since 1998) or ATSR (since 1991 for ATSR-1) data may be an alternative, but they cover a shorter time span and cannot be accessed for free easily. The *Snowcover* algorithm developed by Fernandes & Zhao (2008) can be applied to the AVHRR data. Results have been demonstrated to be quite accurate, but the algorithm needs additional input data such as ST. The *theta* algorithm (Maxson et al., 1998) may also be used, but it requires manual intervention. APOLLO runs automatically and without any additional input but the quality of the snow cover products has never been systematically assessed.<<

Snow mapping algorithms for active microwave sensors have not been considered in the overview because, as stated in section 3.1, they are limited by several severe restrictions. In a study accomplished by Tedesco & Miller (2007), optical, active and passive microwave snow extent data were compared. The results from the active sensors stood out due to the highest uncertainties (forests with less than 30% tree density as an exception). Active microwave data will not further be attended during the presented thesis.

3.4 Existing Snow Cover Studies

Because snow cover is such an influencing parameter, many studies have been conducted throughout the world addressing aspects like SCD, SCS, SCM, or the Snow Cover Index (SCI), which was introduced by Wang & Xie (2009). It is neither useful nor is it possible to reflect all of these studies here. Many very small scale analyses of snow cover parameters deal with problems and methods specifically designed for a single mountain range or river catchment not related to the region of Central Asia. Examples include the studies of Bales et al. (2008) about fractional snow cover monitoring in the Colorado and Rio Grande basins, Bormann et al. (2012) introducing a regional snow detection algorithm suited especially for Australia, or Salminen et al. (2009) describing the challenges of monitoring snow cover in the boreal forest zone. There are, however, several small and large scale studies that are relevant in some respects. They will be reflected in this section, starting with the large to global scale analyses.

3.4.1 Large scale snow cover studies

Impacts of climate change on snow cover have been analysed by Gutzler & Rosen (1992), Groisman et al. (1994a), Groisman et al. (2006), Brown (2000), Brown & Mote (2009), Frei & Robinson (1999), Liston & Hiemstra (2011), and Ye et al. (1998) – to name only a selection. The study regions range from hemispherical to continental scale while the spatial resolution of the analysed remote sensing data is usually relatively coarse (100-200 km, depending on the latitude and used snow cover product). Some studies rely on data from snow stations (e.g. Ye et al. (1998)) while others incorporate snow cover estimates from climate models (e.g. Liston & Hiemstra (2011)). The aim of such large scale studies is often the identification of regions with changing snow cover characteristics due to a changing climate and the derivation of trends. A long time series of continuous observations is therefore required to ensure sophisticated and reliable results.

The study of Ye et al. (1998) about spatial snow cover parameters in Russia is based on SD station data from the HSDSD collection (Armstrong 1999). Daily SD information for the years from 1936 to 1983 were analysed to find possible trends of changing snow cover characteristics. The authors identified increasing snow depth in latitudes above 60° N and decreasing snow depth south of 60° N. On average, the increase in the North more than compensates the decrease in the South, leading to an overall increase of 0.5% to 1.0% of global water accumulation on land (Ye et al. 1998). Because only 119 SD stations were available for the processed years the results reflect a very coarse overview of Russian snow cover changes. Additionally, the development after 1983 is unknown.

Bulygina et al. (2011) analysed the same region (Russia) using station data but the authors also processed remotely sensed data to calculate trends in snow cover characteristics. The weekly snow cover extent provided by NOAA NESDIS was chosen for this study. This data is available since 1972 (actually since 1966 but with a few gaps that hinder from steady trend calculations) and has a spatial resolution between ~125 km and ~200 km – depending on the latitude (Robinson et al. 1993). The authors found similar snow patterns as Ye et al. (1998) but concluded that since the early 1990s, the decrease of snow cover extent has ceased. This result could not be obtained in the study of Ye et al. (1998) because the time series of station data only lasted until 1983. Bulygina et al. (2011) also stated that – with the European part of Russia as an exception – snow cover increased over most of Russia. This development stands in clear contrast to Canada and Alaska where snow extent and duration have decreased by 18% (Alaska) since 1966 (Callaghan et al., 2011).

The reason for the contrary snow cover development in Russia is the decrease of Arctic ice cover during summer, leading to increased water vapour in the polar atmosphere at the beginning of the cold season and consequently to more precipitation in northern Russia and Siberia. The effect was described by Groisman & Soja (2009): Ice extent of the Arctic Ocean is reducing since the 1970s, changing regional albedo and influencing cold season heat fluxes “dramatically”, as it was described by Groisman & Soja (2009). As a result, more water vapour is available in early winter season, leading to an increased snow accumulation in parts of Russia. As the reduction of warm season ice cover extent for the Arctic Ocean is predicted to continue (Serreze et al., 2007), the increase of early winter snow accumulation may also persist through the future.

A connection between northern snow cover extent during summer/autumn and weather conditions of the upcoming winter is generally accepted by researchers (Kerr, 2003): Extensive Eurasian snow cover can serve as an indicator for colder surface temperature in the next winter season especially in the US (Cohen & Saito 2003). The changing snow cover especially

in Eurasia provokes feedbacks in the North Atlantic and Arctic Oscillation (NAO and AO). Early Eurasian snow cover onset during autumn causes weaker polar vortex in the stratosphere, positive feedback on pressures/heights in the Arctic troposphere, and negative pressures/heights in mid-latitudes troposphere (Saito et al., 2001). A detailed description of atmospheric feedbacks caused by anomalous snow cover characteristics goes beyond the scope of the presented thesis. The short excursion was meant to affirm the relevance of snow cover monitoring and to emphasize the possible long range consequences and interactions, changing snow cover extents may have with regards to the global climate.

Brown & Mote (2009) used the same snow cover data from NOAA NESDIS as Bulygina et al. (2011) to derive possible trends of Northern Hemisphere snow coverage. Data from climate stations in Canada, monthly snow cover and SWE estimates from climate models (CMIP3 from the World Climate Research Programme, see Meehl et al. (2007)) were also included in this study. The results depict a very complex response of snow cover to a changing climate: SCD and SWE are most sensitive to temperature increases in low elevated regions with a maritime winter climate. The more continental areas are not as sensitive and potential changes in snow cover characteristics pass off slower. In mountainous regions, local factors such as slope, aspect, vegetation, or snow transport through wind are an important part of the possible future development. Increased SWE and decreased SCD are likely to occur in drier mountain regions. Brown & Mote (2009) derived future snow cover trends as calculated from remotely sensed data during autumn, spring, and full season. Central Asia does not appear to be as sensitive towards temperature increase as e.g. the west coast of Canada or Scandinavia. There is, however, a small band of sensitive area between 40° N and 45° N that stretches from the Caspian Sea eastwards until it reaches the Balkhash Sea and the border to China. The south-eastern mountains ranges also fall into this region.

To conclude chapter 3.4.1, the study of Groisman et al. (2006) will be reflected in a few sentences: Data from 1,811 climate stations provided by the Russian Institute for Hydrometeorological Information (RIHMI) were analysed and compared to the NOAA snow cover product derived from remotely sensed data (Robinson et al. 1993). The aim of this study was to investigate snow cover, frozen and unfrozen ground between 1936 and 2004 with respect to the influence of climate change. The results agree with those from the earlier reviewed studies: Increase of SCD for northern Russia, decrease of SCD especially in spring for parts of Siberia and the former Soviet Union, and slowdown of declining trends during the last decade of the 20th century.

The overall conclusion that can be drawn from the reviewed large scale studies while taking into consideration the scope of the presented study about snow cover changes in Central Asia is the fact that climate change is affecting the entire Northern Hemisphere. Mutual feedbacks between NAO/AO and hemispherical snow coverage exist, suggesting that the currently observed changes in snow cover characteristics will persist in the future. The consequences for Central Asia may be that SCD increases in northern Kazakhstan at the transition to Siberia while it is suggested to decrease in the more southern regions, where snow coverage is more sensitive to the increasing temperature. The coarse resolution of large scale analyses, however, hinders from detailed assessments on a regional scale or for mountains. As stated by WMO & GCOS (2011), the minimum resolution of snow cover datasets should meet 1 km in flat areas and 100 m in complex terrain. Once it was managed to produce an inventory of daily snow cover data at such resolutions and for a long enough time series, extensive conclusions on regional snow cover responses to a changing climate will be possible.

3.4.2 Small scale snow cover studies

On a more regional scale, Khan & Holko (2009) presented a study about snow cover characteristics in the Aral Sea Basin, which consists of the catchments of Amu Darya and Syr Darya rivers. Figure 3.8 shows positions and extents of these river catchments which nearly entirely fall inside the region of Central Asia. Only small upstream parts of Amu Darya River fall within the frontiers of Afghanistan and Pakistan. Therefore, the study of Khan & Holko (2009) is of major interest even though the main focus was put on the relation between snow cover and river runoff. SWE and snow depth data from climate models (ERA-40 ECMWF, NCEP/DOE and JRA-25) were used for the study and combined with the snow extent derived from remotely sensed data. The satellite data has a spatial resolution of ~25 km and is available on a weekly basis from NSIDC (Armstrong & Brodzik 2005). Aims of the study were the investigation of long-term snow cover trends and the comparison between snow cover and river runoff trends.

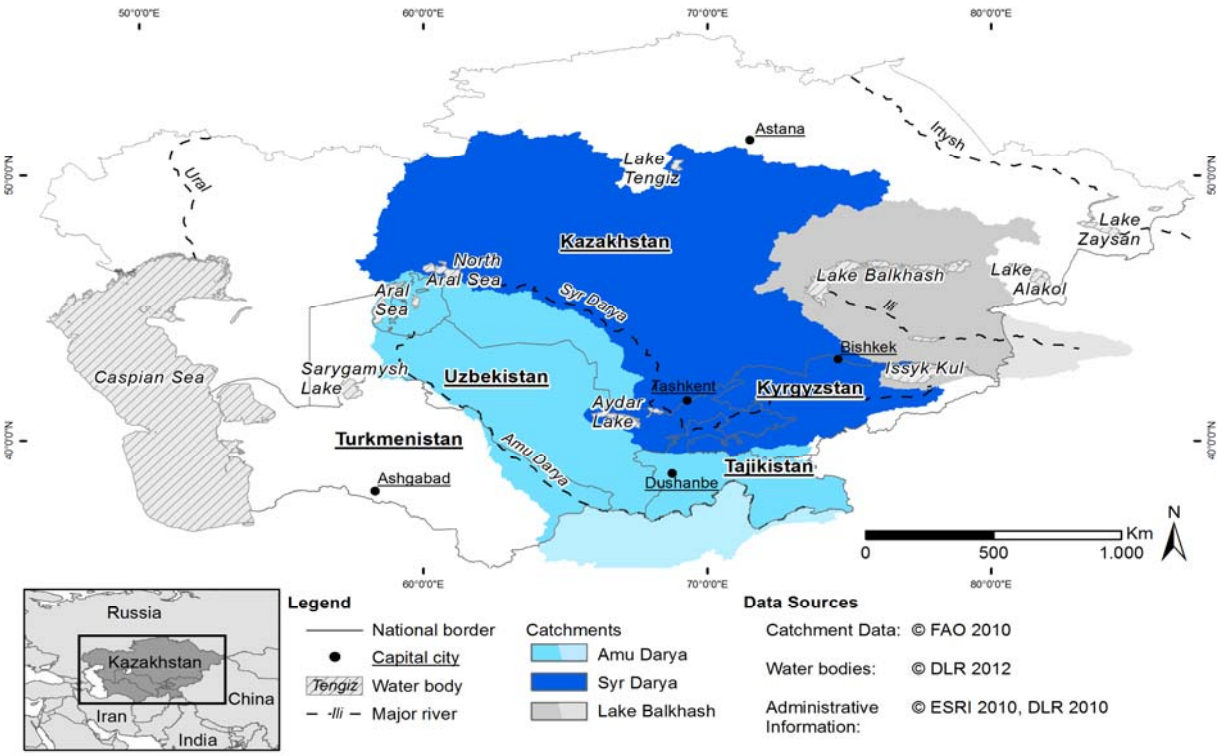

Figure 3.8: Overview of hydrological catchments of Central Asia

It had turned out that all reanalysis data inherited from the climate models underestimate the actual snow cover conditions especially in the mountainous regions above 1,000 m elevation. The trends of SWE within the basin range from -0.04 to -0.57 mm/year. Snow cover extents provided by NSIDC are characterized by strong inter-annual variability but are still marked with a significantly decreasing trend of -56.5 km²/year between 1971 and 2006, merged for the whole Aral Sea Basin. In contrast, runoff in Amu Darya and Syr Darya Rivers followed a positive trend within the same time span. The authors suggest that water from accelerated glacier melting contributes to this contrary development (Khan & Holko 2009). The 25 km snow extent data is an alternative source for the biased results: The resolution may be too coarse to estimate the snow cover status in mountainous regions correctly. As already described by Dozier (1989), severe problems can occur while analysing snow coverage in mountainous terrain – especially if fixed thresholds for e.g. NDSI are used for classification. The 25 km satellite adds to the effect: The resolutions of MODIS (500 m) and even Landsat (30 m) may be too coarse to derive mountain snow cover status correctly (Rittger et al., 2012). Thus, how can 25 km data produce reliable results? Against this background it's no wonder that uncertainties emerged within the presented study.

Several studies about snow cover in China have been published in recent years, including some from Northern Xinjiang which borders Kazakhstan, Kyrgyzstan and Tajikistan and is therefore of interest for the presented thesis: Liang et al. (2008) investigated the quality of the MODIS daily snow cover product MOD10A1 (Hall et al. 2002) by comparing it with in situ snow depth measurements from climate stations. The obtained overall accuracy of the MODIS snow cover product was 98.5%. Only one station which is located in an urban area stood out due to a significantly reduced snow mapping accuracy (77.8%). Another effect that was investigated is the influence of snow depth on the classification accuracy. Klein & Barnett (2003) already reported that the *Snowmap* algorithm used to classify the snow (see section 3.2.1) in MOD10A1 is subject to (considerable) underestimation of actual snow cover if the SD falls below (0.5 cm) 3.5 cm. In the study of Liang et al. (2008) MOD10A1 does not detect any snow below SD of 0.5 cm, which agrees to Klein & Barnett (2003). The snow mapping accuracy at SD between 1 and 2 cm is 45.2% - 76.2%, increases to 94.3% at SD of 3 cm, and reaches 98.6 – 99.6% above SD of 4 cm. If SD increases further to more than 40 cm, snow mapping accuracy peaks at 100% (Liang et al. 2008). An important aspect described by the authors is the effect of cloud coverage on the MOD10A1 product. Because clouds accumulated especially during the snow season they severely limited the snow cover detection. The use of the 8-day composite MODIS snow cover product MOD10A2 helped to reduce this problem, but some cloud covered pixels even persisted here. Another drawback of MOD10A2 also mentioned by the authors is the fact that only the maximum snow cover extent during the 8 days of observation will be represented in the product (Hall et al. 2001).

Another promising study about new methods to analyse snow cover variability in Northern Xinjiang, China, was published by Wang & Xie (2009). The authors chose the Tian Shan Mountains at the border between China, Kyrgyzstan, and Kazakhstan to calculate parameters like SCD (equation 8), snow cover onset date (SCOD, equation 9), snow cover melting date (SCMD, equation 10), and the new introduced SCI (equation 11):

$$SCD = \sum_{i=0}^{N} (D_{i2} - D_{i1}) , \tag{8}$$

$$SCOD = D - SCD' , \tag{9}$$

$$SCMD = D + SCD' , \tag{10}$$

$$SCI = \sum_{i=0}^{P} A * SCD_i , \tag{11}$$

where *N* is ne number of days per hydrological year while D_{i1} and D_{i2} refer to the beginning and ending dates of the year, respectively. *SCD'* is the snow cover duration before (after) a fixed date (December 1st in the case of this study) in equation 9 (10). *A* is the pixel size, *P* the number of pixels, and SCD_i is snow cover duration for pixel *i*.

As data basis, the authors used a combination of MOD10A1 and MYD10A1 between 2000 and 2006. The products from Aqua and Terra platforms were combined to reduce cloud coverage after 2002 (since Aqua was only operational from July 4th, 2002, Table 3.1). Additional temporal combinations of multiple days further reduced (but not completely eliminated) cloud cover percentage. A comparison between station and satellite derived parameters of SCD, SCOD (from now on abbreviated SCS – Snow Cover Start), and SCMD (from now on abbreviated SCM – Snow Cover Melt) revealed that station- and MODIS-SCD agree well (90%). SCS and SCM were shifted for ~1 week forward and backward, respectively. Transient snowfall events are responsible for these shifts as the authors declare. The SCI is promoted as an ideal variable to describe the impact of snow on a hydrological entity: Consisting only of one single number to describe SCD and snow extent within e.g. a hydrological catchment, it can serve as a tool for easy analysis of inter-annual snow cover variability. The comparison of the 6 hydrological years that were processed during the study revealed that the season of 2001-2002 had the most snow from the 6 year time series. 2005-2006 constituted the minimum (Wang & Xie 2009).

3.4.3 Conclusions: Transferability of the findings to Central Asia

The presented selection of already conducted snow cover studies includes different scales, data basics, methods, and objectives. The findings from the large scale snow cover studies in section 3.4.1 are quite generalized when examining the conditions of Central Asia. Statements comprise a moderate sensitivity of Central Asian snow cover to an increasing temperature (Brown & Mote 2009). While snow cover and SD are projected to increase in northern Russia, the trend points towards decreased snow coverage especially in spring seasons for the remaining Northern Hemisphere. AO/NAO are affecting snowfall characteristics in Eurasia. Driven by changed sea ice duration and extent, these pressure patterns lead to more snowfall especially in Siberian early winter season. It is difficult to estimate the effect on Central Asia: the region is located at the transition to Siberia, leading to possible increases of snow cover in the most northern part of the area. The Mountains to the South and Southeast are difficult to evaluate due to the complex terrain. Typical resolutions of 25 km per pixel and more cannot produce reliable results for these regions, which are most important in terms of freshwater generation.

Small scale studies about snow cover characteristics in Central Asia are rare. The few examples presented in section 3.4.2 either rely on improper data sources (Khan & Holko 2009) or investigate regions outside of Central Asia. The general statements made by the authors are that snow coverage is variable in terms of extent and duration. The overall trend between 1971 and 2006 – at least for the Aral Sea basin – appears to be negative when derived from coarse resolution snow cover data. In northwestern China, 2001-2002 was richest in snow coverage between 2000 and 2006 as analysed by Wang & Xie (2009). 2005-2006 had least snow in this study that relied on the MODIS 500m daily snow cover products MOD10A1 and MYD10A1. These findings may be helpful when processing the respective years from neighbouring Kazakhstan and Kyrgyzstan. The accuracy of MOD10A1 and MYD10A1 was assessed by Liang et al. (2008) and found to be above average for north-western China. For Central Asian regions with similar land cover, these findings may as well apply to. However, because a detailed analysis of the snow cover characteristics of whole Central Asia has never been derived until now, the selection of transferable results is sparse.

4. Data Sources

The following subsections will include details about the data sources that were used for the analysis of snow cover characteristics in Central Asia. The review of available snow mapping methods in section 3.2 provided insight into the variety of possible data sources. Those suited best for the aims of the thesis were subsequently selected: MODIS snow cover products processed by the *Snowmap* algorithm for the years after 2000 and AVHRR data before 2000. Because no operational snow cover product from AVHRR is available, the snow maps will be processed using the APOLLO scheme. Unfortunately, the accuracy of this algorithm has not been assessed systematically. Therefore, Landsat data will be used as source for accuracy assessment. Shuttle Radar Topography Mission (SRTM) will be utilized as a digital elevation model in order to reduce cloud coverage according to the methods reviewed in section 3.2.3 and finally, in situ data from hydrological and climate stations is involved into the analysis of results and accuracy as well. The following sections will outline the details of all these data sources.

4.1 AVHRR LAC Level 1B Data

Basic characteristics of NOAA/AVHRR data were described in section 3.1 (Figure 3.3 and Table 3.1). AVHRR sensors observe the Earth's surface since 1978 from sun-synchronous orbits. Numerous sensors were brought to space since that time when TIROS-N was launched and started an unprecedented and still ongoing time series of daily earth observation data. Although similar in band widths and amount of available spectral channels, the configuration of the sensors constantly changed, following the technical improvement. Table 4.1 includes a detailed overview of available AVHRR sensors and their differences. The decision to choose AVHRR as data source before 2000 was easy to make: AVHRR constitutes the only time series of daily medium resolution data that is available for Central Asia. With MODIS being operational since early 2000, the switch to the higher resolution and accuracy is mandatory.

Table 4.1: Spectral band widths (µm) and operational phases of AVHRR sensors

Channel *	TIROS-N	NOAA-6,-8, -10	NOAA-7,-9, -11,-12,-14,**	NOAA-15,-16, -17,-18,-19
1 (VIS)	0.55-0.90	0.58-0.68	0.58-0.68	0.58-0.68
2 (NIR)	0.725-1.10	0.725-1.10	0.725-1.10	0.725-1.00
3A (MIR)	-	-	-	1.58-1.64
3B (MIR)	3.55-3.93	3.55-3.93	3.55-3.93	3.55-3.93
4 (TIR)	10.50-11.50	10.50-11.50	10.30-11.30	10.30-11.30
5 (TIR)	-	-	11.50-12.50	11.50-12.50
Operational	05/1978 - 01/1980	06/1979 - 09/1991	08/1981 - 10/2002	10/1998 - present

* VIS: Visible spectrum; NIR: Near infrared; MIR: Medium infrared; TIR: Thermal infrared.
** NOAA-13 never became operational due to a spacecraft power supply malfunction after launch. All information taken from (NOAA/NESDIS, 1998, 2009).

For the region of Central Asia, AVHRR Local Area Coverage (LAC) data have been acquired from the Comprehensive Large Array-data Stewardship System (CLASS) of NOAA (http://www.class.noaa.gov). LAC was used because High Resolution Picture Transmission (HRPT) data was not disposable for Central Asia. The difference between LAC and HRPT is that HRPT is transmitted to the receiving station in real-time while LAC is recorded on board of the satellite and transferred later. The maximum LAC record length per orbit accounts for ten minutes. The resolution of 1.1 km (nadir) can degrade towards 6.5 km at maximum off-nadir areas. All available LAC data before August 31st, 2000 have been selected for the region from 34° N to 56° N and 45° E to 89° E. Although operational since 1998, data from NOAA-15 (NOAA-K) was not available for download from CLASS. The format of the obtained datasets is Level 1B, meaning that the data has been quality controlled and information about Earth location (Ground Control Points; GCPs) and calibration is included, but not applied to the raw data (NOAA/NESDIS, 1998). The unit of the pixel values is digital counts.

The number of obtained Level 1B scenes is ~ 27,000. However, because of the LAC specific transmission procedure without any operational ground station within the receiving range, the amount of available scenes varies from year to year. Figure 4.1 depicts the amount of AVHRR scenes per year and clearly demonstrates that data availability is poor during the 1980s, though the absolute numbers from Figure 4.1 may pretend the opposite: 750 scenes for e.g. 1985 may seem enough to ensure daily coverage of the area of interest. This number, however, includes all available scenes from the CLASS archive, comprising night scenes as well as damaged/biased data and scenes with only very few scan lines falling within the study region. Additionally, one overpass is not enough to cover the complete area, meaning that especially for the years between 1985 and 1990, full coverage is not available for every day of the year.

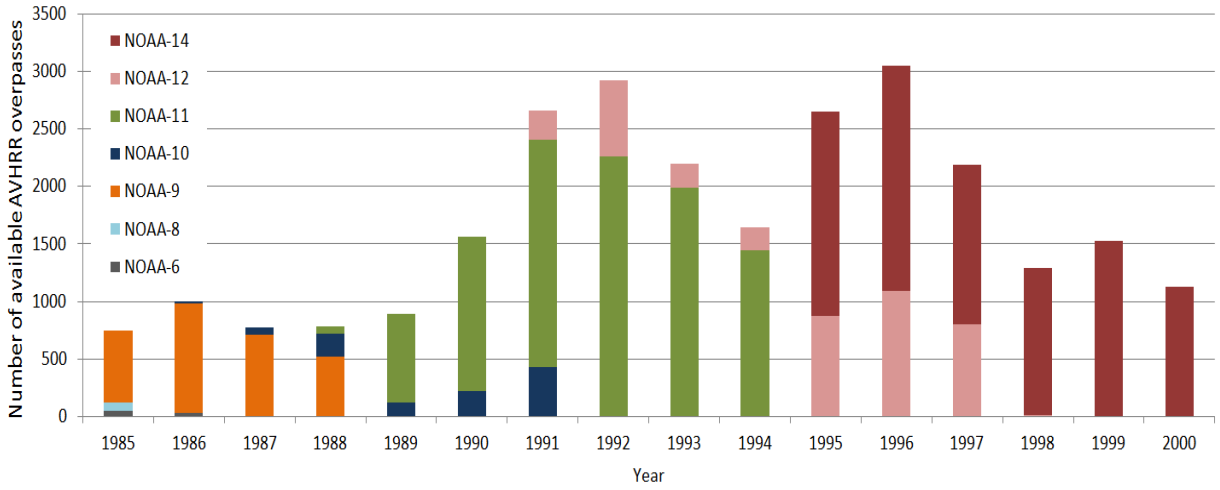

Figure 4.1: Number of available NOAA/AVHRR datasets per year

Unfortunately, AVHRR data before 1985 is not available for Central Asia and the data from 1985 contains mostly unusable observations from NOAA-9. The aim to extend the generated time series of daily snow cover data to the longest possible period therefore merges into 1986. The amount of data is still limited for the early years between 1986 and 1992. Possible reasons and consequences that emerge from this circumstance will be presented in section 6. Since all available AVHRR scenes have been acquired from the archive, no alternative exists to extend the data sources any further.

4.2 MODIS daily snow cover products MOD10A1 and MYD10A1

As described in section 3.2.1, the MODIS snow cover products processed by the *Snowmap* algorithm should be preferred as data source where available due to their high accuracy. Eight MODIS tiles are required to cover Central Asia entirely as it is demonstrated in Figure 4.2. To be able to derive SCD, SCS, and SCM it is essential to rely on daily snow cover data. The MODIS daily snow cover products MOD10A1 (from Terra MODIS) and MYD10A1 (from Aqua MODIS) provided by NSIDC are the ideal source for this task. MOD10A1 and MYD10A1 are operational, thematic products. Information about pixel values and their respective classes is included in Table 4.2. The number of acquired scenes nearly reaches 66,000, including all days from August 31st, 2000 until January 16th, 2013.

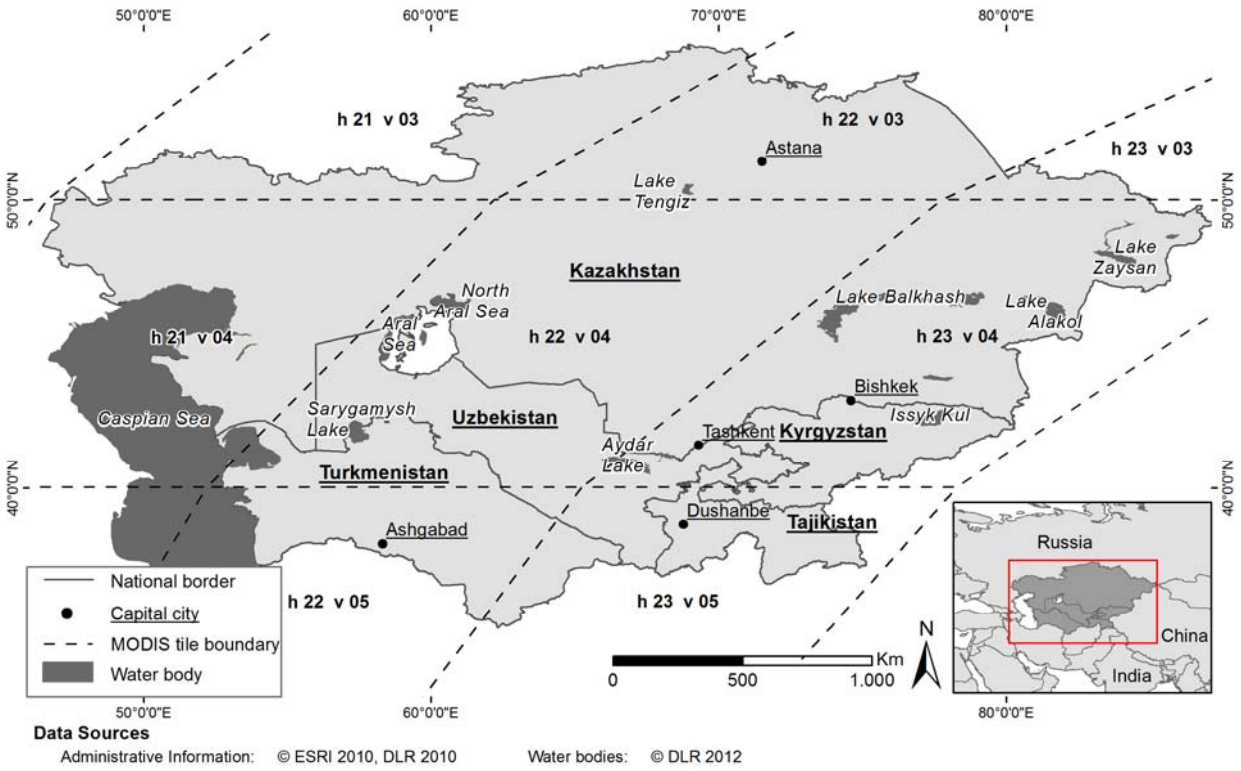

Figure 4.2: MODIS tile coverage for Central Asia

Table 4.2: Class values of MOD10A1 and MYD10A1 products

Pixel value	Land cover class	Pixel value	Land cover class
0	data missing	50	cloud obscured
1	no decision	100	snow covered lake ice
11	darkness, terminator, or polar	200	snow covered land
25	snow-free land	254	detector saturated
37	lake or inland water	255	fill
39	open water		

Some observations are missing between 2000 and 2013 as it is summarized in Table 4.3. After 2002, the missing observations occur on different dates so that Aqua and Terra MODIS complement one another. That is not the case for the years 2000 to 2002 where only Terra MODIS is available. To fill the gap in the year 2000 (October 28th), the observation prior to the missing date was used. In 2001, 18 observations are missing beginning with June 15th, 2001 and ending with July 2nd, 2001. Fortunately, this time span falls within the summer season where snow cover dynamic is minimal. For 2002, Terra observations from March 20th to March 28th are missing. Because Aqua was only operational from July 4th on the tiles from 2001 and 2002 cannot be replaced like it was possible after 2002. The missing observations from 2001 and 2002 were therefore treated as 100% cloud covered.

Table 4.3: Dates of missing MODIS observations per year (days of year)

	2000	2001	2002	2003	2004	2005	2006
Aqua	-	-	256; 257	132; 170; 334	-	-	-
Terra	301	166-183	079-087; 105	032; 351-358	050	-	235
	2007	**2008**	**2009**	**2010**	**2011**	**2012**	**2013**
Aqua	336	-	-	-	-	-	-
Terra	-	355-358	-	-	-	-	-

4.3 SRTM data

SRTM data was collected from a space shuttle in February 2000, using C-band and X-band radar. The aim of this mission was to produce a near-global topography dataset spanning from 60° N to 60° S in a 1 arc second resolution (Rabus et al., 2003). The performance requirements (maximum vertical error: 16 m for 90% of the data; maximum geolocation error: 15 m for 90% of the data) were met and often exceeded by a factor of 2 (Rodríguez et al., 2005). The elevation information contained in the SRTM data is utilized to estimate snow cover below clouds as introduced in section 3.2.3. The data was obtained from the CGIAR-CSI SRTM 90 m Database (Jarvis et al. 2008), where it is freely available. Figure 1.2, Figure 2.3, and Figure 2.6 also contain SRTM data as an input source for the illustration of elevation.

4.4 Landsat

Because detailed accuracy information about the APOLLO snow cover product is not available, a suitable data source for intercomparison and accuracy assessment is required. Level 1 data from Landsat Thematic Mapper (TM) 5 and Enhanced TM (ETM+) 7 have been acquired for this task from the U.S. Geological Survey (USGS). The Landsat program started in 1972, providing high resolution remote sensing data for the whole globe. Eight satellites have been launched until today (with Landsat 6 failing to achieve its orbit) with the recently started (February 2013) Landsat 8 mission (Landsat Data Continuity Mission; LDCM) constituting the latest version of the program (USGS, 2012).

The use of high resolution Landsat data is common practice in validating medium resolution snow cover products. This technique was also used to assess the absolute accuracy of the MODIS snow cover products (Hall & Riggs 2007). Figure 3.3 in section 3.1 already referred to some of the available spectral bandwidths of Landsat. A detailed overview is included in Table 4.4.

Table 4.4: Landsat spectral channels and resolution

Band	Landsat 4, 5	Landsat 7
1 - blue	0,45 - 0,52 µm - 30 m	0,45 - 0,52 µm - 30 m
2 - green	0,52 - 0,60 µm - 30 m	0,53 - 0,61 µm - 30 m
3 - red	0,63 - 0,69 µm - 30 m	0,63 - 0,69 µm - 30 m
4 - NIR	0,76 - 0,90 µm - 30 m	0,78 - 0,90 µm - 30 m
5 - MIR	1,55 - 1,75 µm - 30 m	1,55 - 1,75 µm - 30 m
6 - MIR	2,08 - 2,35 µm - 30 m	2,09 - 2,35 µm - 30 m
7 - TIR	10,4 - 12,5 µm - 120 m	10,4 - 12,5 µm - 60 m
8 - PAN	-	0,52 - 0,90 µm - 15 m

Table 4.5: Landsat scenes acquired for the accuracy assessment

Nr.	Scene Name	Path/Row	Date	Snow cover (%)
1	LT51470311998259BIK00	147/031	16.09.1998	41.39
2	LT51500321999027XXX02	150/032	27.01.1999	43.23
3	LT51510311998319AAA01	151/031	15.11.1998	27.18
4	LT51440251998142ULM00	144/025	22.05.1998	29.83
5	LT51510321998319AAA01	151/032	15.11.1998	7.19
6	LT51520331999105XXX02	152/033	15.04.1999	85.6
7	LT51520331999217AAA02	152/033	05.08.1999	17.95
8	LT51530311999016XXX02	153/031	16.01.1999	71.09
9	LT51540301999023XXX02	154/030	23.01.1999	38.15
10	LT51510301996298XXX01	151/030	24.10.1996	8.06
11	LT51490351999116AAA01	149/035	26.04.1999	67.13
12	LT51510341999114XXX02	151/034	24.04.1999	88.95
13	LT51510351999114XXX02	151/035	24.04.1999	70.96
14	LT51530311998141XXX01	153/031	21.05.1998	17.91
15	LT51550291999030AAA02	155/029	30.01.1999	44.49
16	LT51550291999078AAA02	155/029	19.02.1999	25.18
17	LT51460291998140ULM00	146/029	20.05.1998	16.25
18	LT51520341999057AAA02	152/034	26.02.1999	65.83
19	LE71560282000064SGS00	156/028	04.03.2000	38.67
20	LE71560272000064SGS00	156/027	04.03.2000	86.88
21	LE71560262000064SGS00	156/026	04.03.2000	89.41
22	LE71560252000064SGS00	156/025	04.03.2000	84.01
23	LE71560242000064SGS00	156/024	04.03.2000	87.13

Landsat faces a few drawbacks when used for accuracy assessment of snow cover products: The visible bands tend to saturate quickly over snow covered surfaces (NASA, 2006). Providing a resolution of 30 m, Landsat is reported to be an imperfect source for validating medium resolution snow cover products due to classification errors for mixed pixels

(Rittger et al., 2012). The saturation problem is solved exerting a manual inspection and correction of possible classification errors. Mixed pixels, however, may still cause uncertainties in the transition zone between snow covered and snow free regions. A list of all 23 acquired Landsat scenes is presented in Table 4.5.

4.5 In situ data

In situ data is only sparsely available for Central Asia. This problem was already addressed to in section 2.1. The Historical Soviet Daily Snow Depth Version 2 (HSDSD) product is one example for a generally very promising data source: Snow depth was recorded on a daily basis for 284 stations throughout the former Soviet Union between 1881 and 1995 (Armstrong 1999). On a second view, however, several problems occur while working with the data: The instruments used to measure snow depth include snow measuring rods and visual observations, both subject to uncertainties. Besides, some stations especially in the former Soviet States of Central Asia did not continue operation after the collapse of the Soviet Union. Figure 4.3 illustrates the location of all snow depth stations that fall within Central Asia. The density is low (only 43 stations for ~4,000,000 km²) and only 38 stations operated until 1995 – some of them with considerable data gaps. However, because the HSDSD data constitute the only source of snow stations for Central Asia, they are included in the accuracy assessment of the APOLLO snow products.

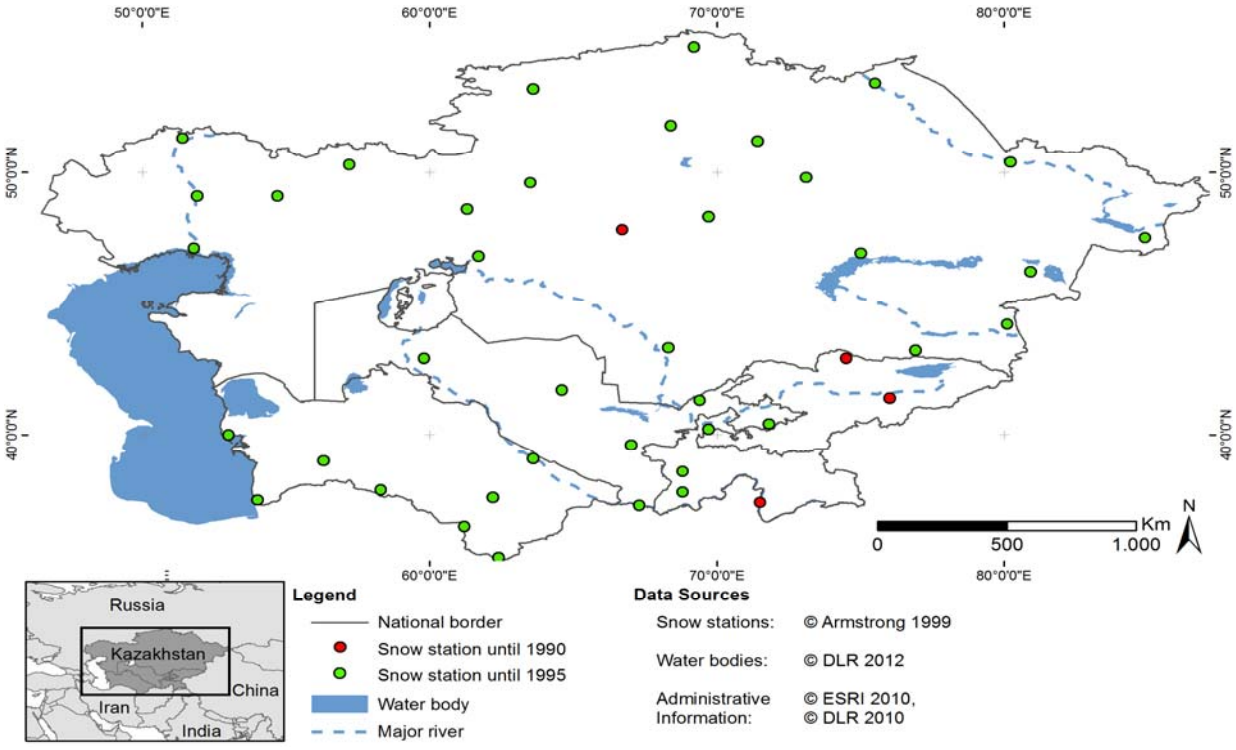

Figure 4.3: Location of Historical Soviet Daily Snow Depth (HSDSD) stations

A field trip was organized to support the snow cover processing. On December 6th, 2010 and between December 12th and December 15th, 2010, snow depth was recorded by an independent contractor along a route through Kazakhstan: The trip started near Almaty and progressed northwards, surrounding Lake Balkhash and leading to the Capital city of Kazakhstan: Astana. Snow cover status was recorded for more than 170 locations along the ~1,150 km transect according to a field protocol that was prepared especially for this task. The structure of this protocol is included in Figure 4.4. Elevation, snow depth, temperature, cloud cover conditions, snow cover fraction, and land cover type were the basic elements of the survey. The data are exploited to assess the accuracy of the cloud reduction scheme which is described later in section 5.2.

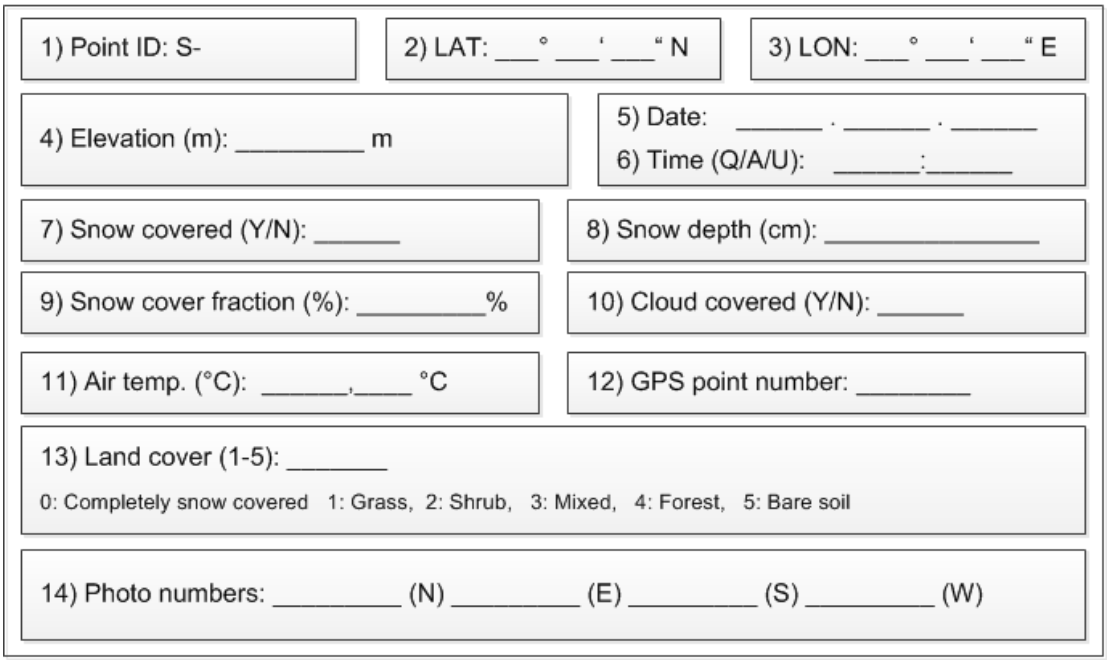

Figure 4.4: Field protocol for snow cover in Central Asia

The European Climate Assessment & Dataset Project (ECA&D) provides snow depth measurements from 1094 climate stations (as of July 2012. In the meantime, additional stations were added for Russia). These data are available for Europe and parts of Russia, only. Information taken from these station data are used to assess the accuracy of snow cover products within the framework of a transferability study in Europe, where the same processing steps were applied to as in Central Asia. This procedure allows for an indirect accuracy assessment of the results for Central Asia, where no station data is available.

5. Methods

In this section, the methods that were applied to the data sources to process and analyse snow cover characteristics of Central Asia will be described. Many of these methods were already introduced in section 3.2. The sections are ordered chronologically according to the time series, beginning with the processing of AVHRR data. Some of the figures and descriptions about the applied methods have already been published in International Journal of Remote Sensing (Dietz et al., 2013). Comments will be included for content that is adopted from this publication.

5.1 AVHRR processing

APOLLO was chosen to process daily snow cover information from AVHRR Level 1B data because it is operational at the German Remote Sensing Data Center (DFD) of the German Aerospace Center (DLR) since more than 15 years, processing cloud information for daily Normalized Difference Vegetation Index (NDVI), Sea Surface Temperature (SST), and Land Surface Temperature (LST) products for Europe from AVHRR HRPT data (Dech et al., 1997; Dech et al. 1998; Kriebel et al. 2003; Tungalagsaikhan et al. 2003). Other schemes like SPARC or Clouds from AVHRR (CLAVR) require additional input parameters like skin temperature, surface type maps, and monthly surface climatological fields (Hüsler et al., 2012; Khlopenkov and Trishchenko, 2007; Stowe et al., 1998). Details about APOLLO were already described in section 3.2, including the algorithms for cloud cover detection (Figure 3.6) and snow detection (Figure 3.7).

In a first step and before APOLLO can be applied to the AVHRR data obtained from CLASS, the configuration of the original APOLLO settings must be changed. The initial system settings were designed specifically for Europe, involving HRPT data format instead of LAC. Preprocessing, which relies on the TeraScan software (http://www.seaspace.com/) requires different parameters for both formats (LAC command for LAC format, HRPTIN command for HRPT format).

The workflow for this thesis continues with the calibration of digital counts from the AVHRR data, producing top of atmosphere (TOA) reflectance of channels 1 and 2 as well as brightness temperatures of channels 4 and 5. The TeraScan software ensures sophisticated calculation of these parameters, including regularly updated calibration coefficients for all AVHRR channels. The continuous post-launch calibration is required to ensure that all spuri-

ous trends are removed from the data (NOAA/NESDIS, 1998). Channel 3 is calibrated to simple radiances using TeraScan since APOLLO requires the reflective part of channel 3 as input. This parameter is most useful for separating snow and clouds (Dozier 1989) and is calculated within the APOLLO software package from channel 3 radiances and channel 4 temperatures (Gesell, 1989).

Table 5.1: Snow mask values after APOLLO utilization

Pixel value	Land cover class	Pixel value	Land cover class
0	partially cloudy sea	14	cloud-free snow pixel over land
1	totally cloudy sea	16	partially cloudy ice pixel over sea
2	partially cloudy land	17	totally cloudy ice pixel over sea
3	totally cloudy land	18	partially cloudy ice pixel over land
4	partially cloudy pixel in the sunglint	19	totally cloudy ice pixel over land
5	totally cloudy pixel in the sunglint area	20	partially cloudy snow on ice pixel over sea
6	partially cloudy snow pixel over land	21	totally cloudy snow on ice pixel over sea
7	totally cloudy snow pixel over land	24	cloud-free ice pixel over sea
8	cloud-free sea	26	cloud-free ice pixel over land
		28	cloud-free snow on ice pixel over sea
10	cloud-free land		
12	cloud-free pixel in the sunglint area, sunglint pixel	31	sun below/above 5 degrees elevation (day/night)

After calibration is accomplished, the APOLLO algorithms to detect cloud covered pixels (Figure 3.6) are conducted, followed by the snow and ice detection scheme (Figure 3.7). The result is a thematic product with classes according to Table 5.1. The pixel values from Table 5.1 are recoded in order to conform to the MODIS daily snow cover product specifications from Table 4.2. The recoding scheme is included in Table 5.2. This step is required to compare or combine both products.

Table 5.2: Recoding scheme for APOLLO snow masks

Pixel value(s) from APOLLO	New pixel value conforming to MOD10A1
0; 1; 2; 3; 4; 5; 7; 12; 16; 17	50
18; 19; 20; 21; 31	50
24; 26	100
8	37
10	25
6; 14; 28	200

Once recoded to MODIS snow cover product pixel values, the APOLLO products are converted to georeferenced GeoTiff format using geolocation information from APOLLO (processed using GCPs and an internal watermask to compensate possible pixel shifts). The georeferenced format is a prerequisite in order to build daily or multi-temporal composites. After georeferencing, the snow product is defined as “Post-Processing Level 1” or PPL1. It will be referred to as PPL1 for the rest of the presented study.

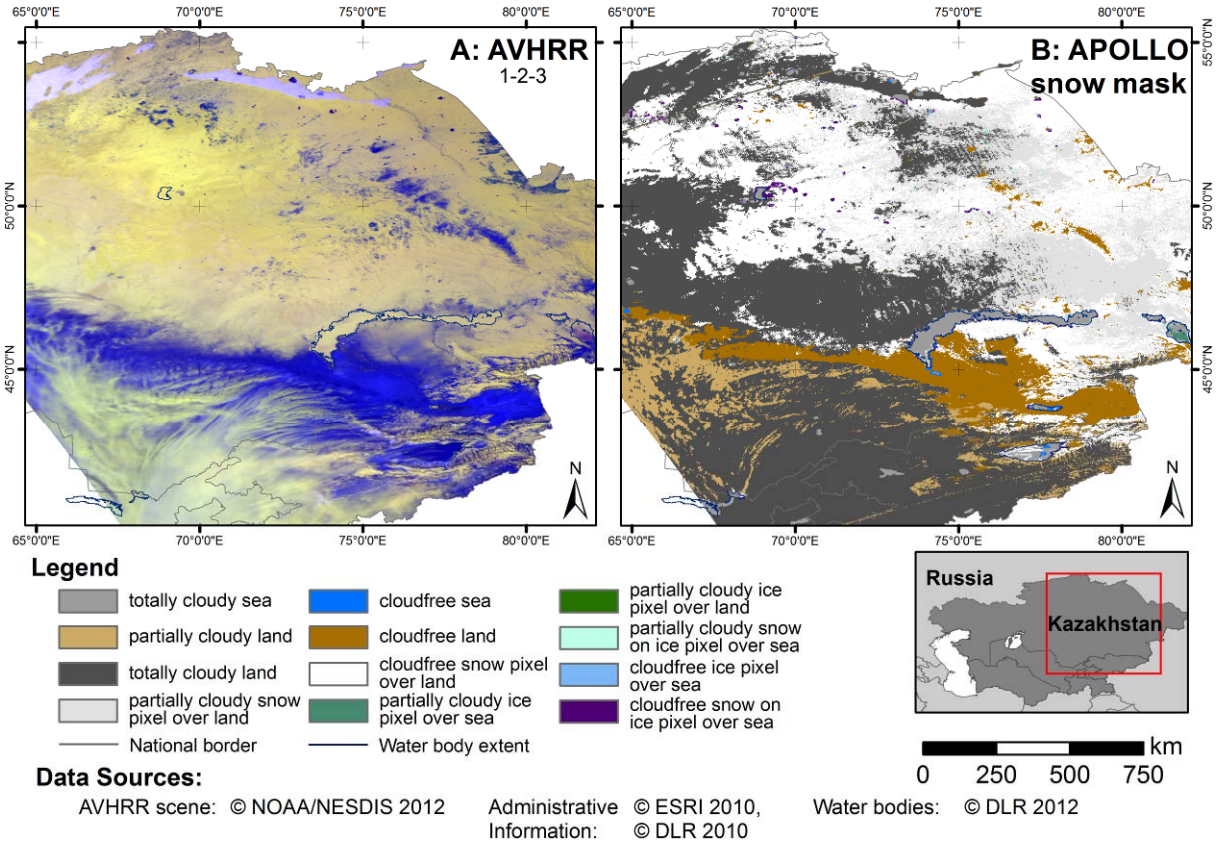

Figure 5.1: Example of APOLLO snow product for March 4th, 2000 (NOAA-14)

The PPL1 can now be considered the same level as the MODIS daily snow cover products, though the accuracy of APOLLO is still unknown. That is why in a typical study, an accuracy assessment of the obtained results would follow at this point. This procedure is slightly changed for the presented thesis for one reason: The processing of the snow products is not yet finished. Several post-processing steps, affecting both PPL1 and MODIS data, will be applied to the snow products to remove cloud coverage. An accuracy assessment will then be accomplished for all processed snow cover products, including also the APOLLO products prepared during AVHRR processing. The results from this accuracy assessment will be included in sections 6.1 and 6.3.

Figure 5.1 is an example for an APOLLO PPL1 product based on an AVHRR scene from NOAA-14 (March 4th, 2000). The difference between snow covered pixels and clouds is difficult to identify from the northern parts of Figure 5.1 “A”, which is depicted in the band combination 1 – 2 – 3 (Red – NIR – MIR). The classification, however, readily distinguishes between clouds and snow Figure 5.1 “B”.

5.2 Cloud reduction in AVHRR and MODIS snow data

The biggest problem for analyzing daily snow cover time series is cloud coverage. Clear sky conditions are rare, especially in the winter season. Figure 5.2 displays the total number of cloud covered observations in the MOD10A1 product for the hydrological year 2000/2001 (September 1st, 2000 through August 31st, 2001). 200 cloud covered days or more are not an exception in northern Kazakhstan or the southeastern mountain ranges. The calculation of e.g. SCD is impossible relying only on the original MOD10A1 source. Large uncertainties would arise with more than 50% data gaps in the time series. Additionally, most of the cloud coverage is concentrated on winter and spring months, as can be learned from Figure 5.3 (adopted from Dietz et al. (2013)). In this figure, mean cloud cover percentage for each month of MOD10A1 is depicted between 2000 and 2011 for three selected MODIS tiles (see Figure 4.2 for information about tile location).

The overall mean cloud cover percentage in MOD10A1 varies from 58% for tile h21v03 (northwestern tile) over 40% for tile h22v04 (center tile) down to 29% for tile h23v05 (southeastern tile). Maximum cloud coverage is concentrated during winter and spring months, significantly limiting the ability to map the exact number of snow covered days. Against this background, methods to reduce cloud coverage as introduced in section 3.2.3 become necessary. The aim is to completely remove all cloud covered pixels from the time series. Some of the methods from section 3.2.3 cannot fulfill this task when applied solitary. The combination of Aqua and Terra MODIS as described by Wang & Xie (2009) e.g. only results in an improved product if either Aqua or Terra MODIS observed the surface under cloud free conditions on a respective day. If clouds persisted during both observations this method will fail. The same is true for temporal combinations comprising several days. If the surface remains cloud covered for multiple days, this method will again fail to estimate the actual snow cover conditions on the surface. Such scenarios do not appear too unlikely while reconsidering Figure 5.2 and Figure **5.3** (adopted from Dietz et al. (2013)).

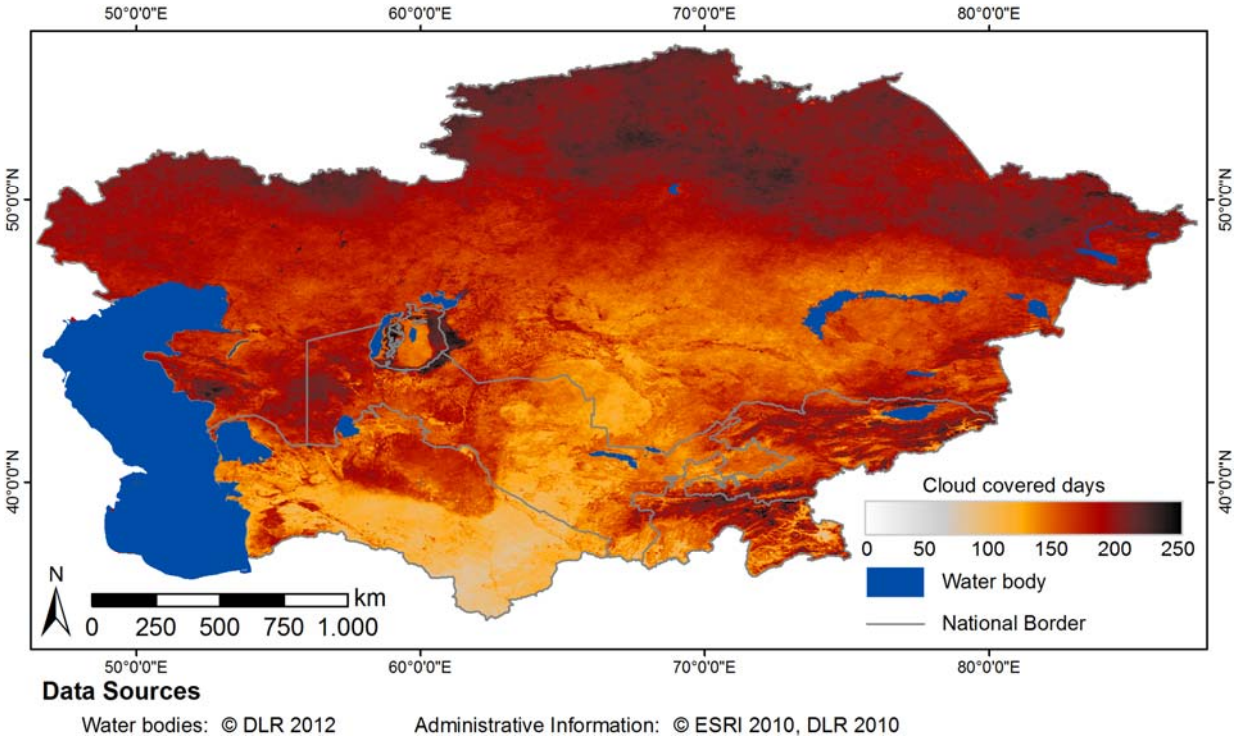

Figure 5.2: Number of cloud covered days in MOD10A1 between Sept. 1st, 2000 and Aug. 31st, 2001

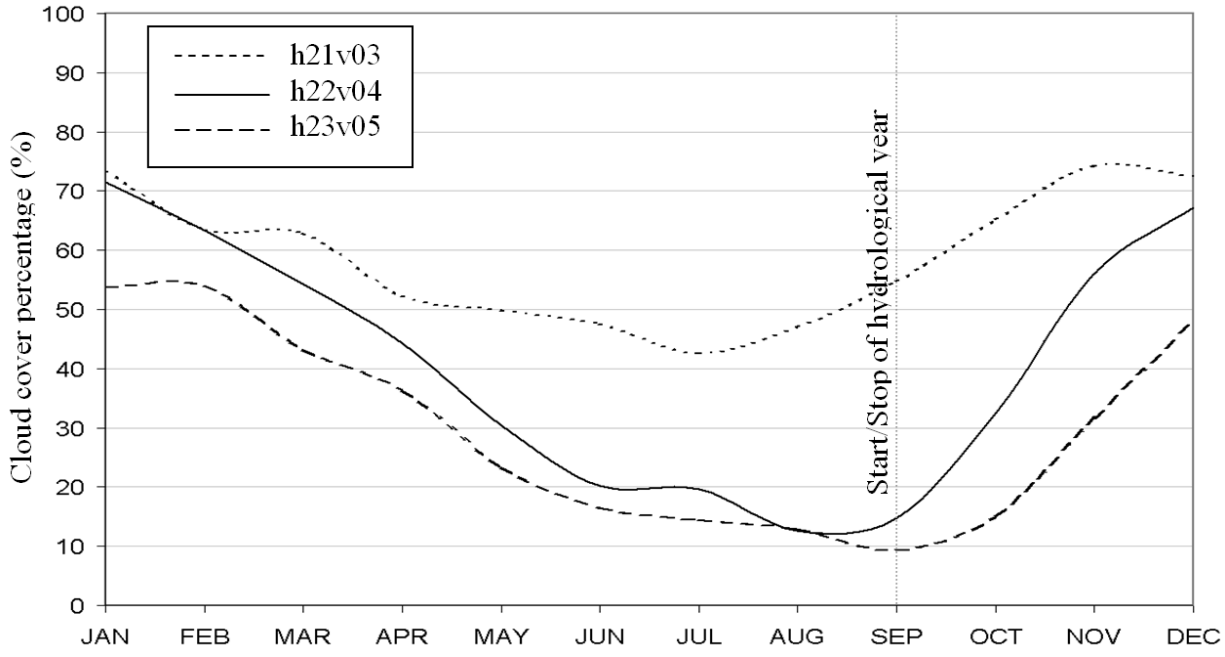

Figure 5.3: Mean cloud cover distribution for selected MODIS tiles of Central Asia

Therefore, a combination of several methods to reduce cloud coverage from the time series is applied to the APOLLO PPL1 and MODIS snow cover products. Similar approaches were followed by Gafurov & Bárdossy (2009), Wang et al. (2009) or Parajka & Blöschl (2008). These authors applied temporal, spatial, and sensor combinations to MODIS snow cover products to reduce cloud coverage. For the presented thesis, a combination of four successive steps will be implemented. A workflow of these steps is included in Figure 5.4.

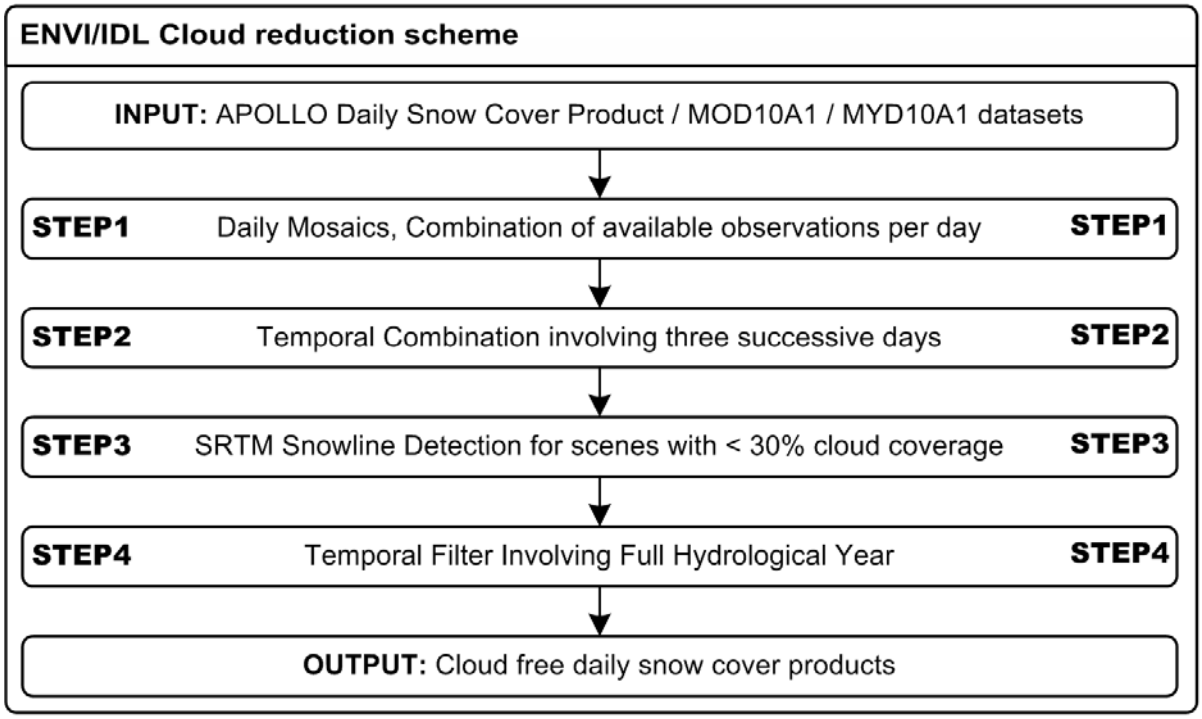

Figure 5.4: ENVI/IDL cloud reduction scheme

Because detailed information about the applied steps is already contained in section 3.2.3, instructions about these steps will be condensed to a minimum at this point: First, all available snow cover products for each specific day will be combined. These combined snow masks are further processed by a temporal filter, merging cloud cover pixels over three successive days (one day prior and one day after the currently processed day). The result from the temporal filter is then committed to the SRTM snowline detection if total cloud cover percentage of the snow mask does not exceed 30% (otherwise, the scene will automatically be transferred to the last step). After snowline detection is applied, the cloud-reduced daily snow cover product is defined as “Post-Processing Level 2” or PPL2. In this stage, the product is still retraceable back to its original observation date (± 1 day). Finally, a second temporal filter involving the full hydrological year is applied to the time series, combining scenes until the first scene with a cloud free surface flag is reached.

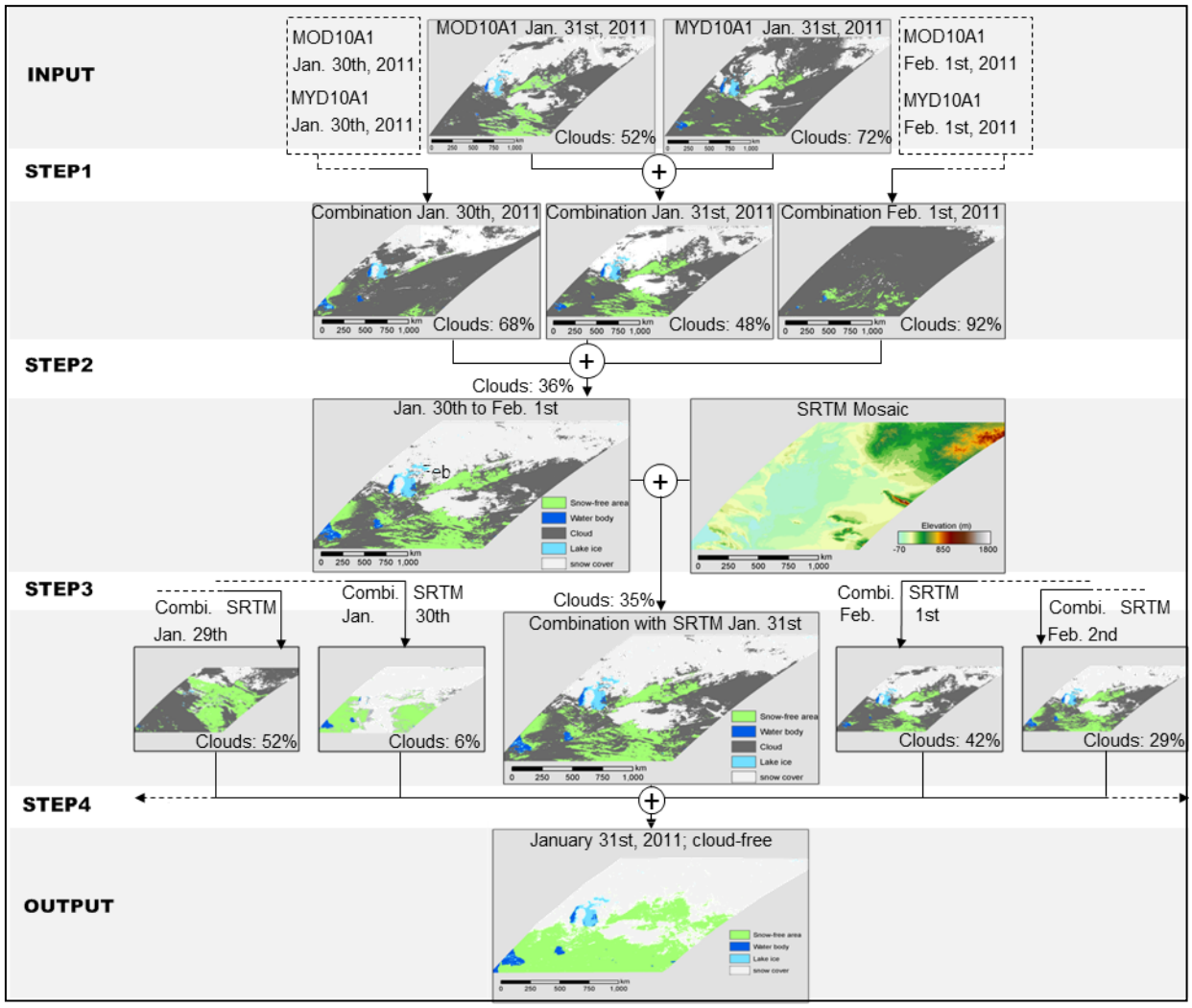

Figure 5.5: Workflow example for an application of the cloud reduction scheme

Figure 5.5 illustrates the workflow of the cloud reduction scheme in a more figurative way, relying on MODIS as input data source. Cloud contamination is reduced step by step. The input data sets contain 52% (MOD10A1) and 72% (MYD10A1) cloud covered pixels, rendering them quite useless when it comes to the quantitative analysis of snow cover. Step 1 (daily mosaics) already reduces the cloud cover fraction to 48%. Since this step is based on actual satellite observation data (acquired during different day times), the accuracy of the combined product is not afflicted with additional uncertainties. Step 2 (temporal combination) further reduces the cloud coverage to now 36%. This step affects the accuracy of the product especially during fall or spring, where snow covered areas are most dynamic and can change rapidly from one day to another. The snowline detection (step 3) only clears 1% of cloud coverage from the presented example. This rate is comparably low but the method is included since it produces reliable results (step 3 is only applied to scenes with less than 30% cloud coverage. In Figure 5.5, the input scene contains more than 30% cloud covered pixels but is

processed by the S*nowl* algorithm anyway due to illustration purposes). Step 4 removes the last 35% of clouds. In the presented example, most cloud covered pixels during this step are cleared based on the day prior to the processed file: The result from the *snowl* algorithm for January 30th. Though Figure 5.5 only illustrates the cloud reduction scheme for a MODIS example it must be underlined here that the procedure is applied to AVHRR data in exactly the same manner. Resolution and number of input data sets vary, but the algorithms behind the cloud reduction stay the same.

The cloud reduction scheme is implemented in the ENVI/IDL software environment, allowing automated processing of the time series. No user interaction is required between input and output of data. All available MOD10A1 and MYD10A1 as well as all APOLLO PPL1 snow maps containing pixels with solar elevations of more than 10° are processed by the cloud reduction scheme. The resulting, completely cloud-free daily snow cover datasets from APOLLO are defined as “Post-Processing Level 3” or PPL3 and will be referred to using this abbreviation for the rest of the thesis. The cloud reduction scheme must be designed to handle large amounts of data. 27.000 AVHRR and 66.000 MODIS datasets require post-processing. This amount of data is unique when it comes to the calculation of medium resolution snow cover time series. The size of the study region (~ 4.000.000 km²) and the period (more than 26 years) explain the need for such an input data extent.

5.3 Calculation of snow cover parameters

As indicated in section 1, the snow cover parameters SCD, SCS, and SCM are desired results for the presented thesis. The aim is to prepare these parameters for each year of the time series. The equations used to derive the parameters (equations 8 to 10) have been defined in section 3.4.2, referring to a study published by Wang & Xie (2009). All prepared products are based on hydrological years, beginning with September 1st of a given year and ending with August 31st of the following year.

SCD is a relatively stable and uncritical parameter. Consisting of the total number of snow covered days per year SCD is only depending on the accuracy of the underlying snow cover product. This is not necessarily the case for SCS and SCM. These parameters are based on the number of snow covered days before and after a fixed date. This date was set to December 1st in the original study by Wang & Xie (2009) but changed to January 15th for the presented thesis because maximum snow cover extent occurred around this date. However, the fact that only the sum of snow covered days before or after this date is calculated does not

consider intermediate snow cover events. If snowfall occurs e.g. on December 10th of a given year, snow cover may persist for one week before an abrupt temperature increase may lead to extensive snow cover melt. If snow cover returns two weeks later and remains through January, the SCS is calculated from the total number of snow covered days before January 15th, leading to a biased result as illustrated in Figure 5.6. In this example, SCS results in December 24th because SCD before January 15th is 22 days. Trying to catch transient snow events is a challenging problem because such events can occur in various dimensions and quantities. Therefore, a justified question may be why to calculate SCS and SCM using equations 9 and 10 at all. This question will be addressed to in the discussion since there are significant reasons for the derivation of SCS and especially SCM.

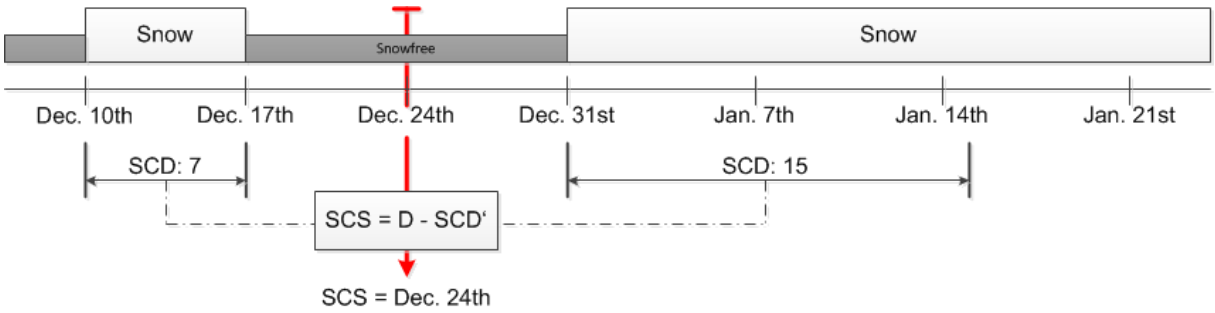

Figure 5.6: Illustration of biased SCS calculation

SCD, SCS, and SCM are calculated for all years from 1985 through 2012. Additionally, SCS is also calculated for 2012/2013 since at the time of writing, January 15th of 2013 had already passed. The results are given in sections 6.2.1 to 6.2.3. Besides single year parameters, mean conditions are also calculated for ten year time spans. Additional products like standard deviations of SCD, SCS, and SCM are derived as well, allowing for an identification of stable and more variable regions.

Another parameter suggested by Wang & Xie (2009) is also prepared for the presented thesis: the SCI (see equation 11). The potential usefulness of this parameter for describing snow cover conditions of a hydrological entity has been addressed to in section 3.4.2. The SCI was initially designed to be calculated from SCD, only. For the presented thesis, two additional SCI results are introduced: Early Season SCI (SCI_{ES}) and Late Season SCI (SCI_{LS}). These products will conform to the respective time periods of SCS and SCM instead of SCD and will be calculated according to equations on and Equation:

$$SCI_{ES} = \sum_{i=0}^{P} A * SCS_i \quad (12)$$

$$SCI_{LS} = \sum_{i=0}^{P} A * SCM_i \quad (13)$$

SCI_{ES} and SCI_{LS} are assumed to provide additional information about the water cycle of a hydrological year: They divide the SCI into two phases: The generation of water within a year (SCI_{ES}) and the release of water after snow melt (SCI_{LS}) – though the validity of these new parameters is still unknown. The application to hydrological catchments of Central Asia and the analysis of the obtained results will reveal the usefulness of the SCI parameters. Results are given in 6.2.4.

5.4 Accuracy assessment of APOLLO snow products

The accuracy of the APOLLO snow cover classification is unknown as already mentioned in section 3.2.1. To assess the accuracy, two approaches are followed: First, a comparison between APOLLO PPL1, PPL3, and Landsat derived snow maps is accomplished. The high resolution snow maps from Landsat already served as ground truth data for several snow cover studies (Hall & Riggs 2007; Huang et al. 2011; Harrison & Lucas 1989) and have confirmed their usefulness. A second approach refers to the snow depth station data from HSDSD, introduced in section 4.5. Though the density of these stations is low, they can be considered independent from cloud coverage and therefore suitable to assess the classification accuracy of the APOLLO snow products.

5.4.1 Using Landsat and MODIS to assess APOLLO snow product accuracy

The snow covered area of Landsat scenes 1 to 18 (see Table 4.5) was derived using a semi-automated classification procedure: The NDSI (see equation 1 in section 3.2.1), which is a good indicator for snow occurrence (Crane and Anderson, 1984) was calculated from Landsat bands 2 and 5 (Table 4.4). Snow cover was assumed for all pixels with NDSI greater 0.4 following an earlier approach by Huang et al. (2011). Chokmani et al. (2010) followed a similar approach, adopting a modified version of the *snowmap* algorithm (which relies on the NDSI, see section 3.2.1) to map snow cover from Landsat. Hüsler et al. (2012) also used Landsat

observation to assess the accuracy of AVHRR snow cover products for Europe. For the presented thesis, each scene was controlled manually and corrected where water bodies, lake ice or cloud cover caused classification errors. The subsequent Landsat snow cover maps were resampled to fit the resolution of the AVHRR data before a comparison between both data sets allowed for detailed accuracy assessment.

A preliminary comparison of APOLLO and Landsat snow maps already revealed that the transition zone between snow covered and snow free area is prone to considerably higher error rates than the more distant area. This behaviour may be caused by the relatively coarse resolution of AVHRR, introducing classification uncertainties for regions with mixed pixels. The geolocation accuracy of AVHRR is a second error source, usually varying between 1-2 pixels when processed by APOLLO (Tungalagsaikhan et al., 2003). Given the pixel size of more than 1,000 m, a shift of 2 AVHRR pixels affects more than 65 Landsat pixels. Therefore, buffer zones are added around the border between snow covered and snow free area in the Landsat scenes. These buffers range 2,000 m in both directions – inside and outside the snow covered area. This procedure was selected to conduct a refined analysis of possible errors. To reveal possible systematic differences between MODIS and APOLLO snow products, the snow maps are compared for the period between February 2000 and April 2000. This step is not directly considered to be part of the accuracy assessment because the MODIS snow cover data faces several inaccuracies itself (as indicated in section 3.2.1). The comparison is intended to give information about the agreement between both products without stating which product is more or less accurate. Projection and resolution of the MODIS data is adjusted to be consistent with the APOLLO results. Beginning with February 2000, the snow cover products from MODIS and AVHRR are compared in intervals of five days. This gap was chosen because the temporal interpolation step used to generate the PPL3 products can comprise up to two days before or after the respective calendar date. Involving these days would eventually lead to a biased weighting of the results. Cloud covered pixels in the MOD10A1 and PPL1 data were treated as data gaps.

The agreement between Landsat, MODIS, APOLLO PPL1, and PPL3 snow maps is investigated additionally for the North-South transect of five Landsat 7 ETM+ scenes from March 4th, 2000 (Landsat scenes 19 to 23 from Table 4.5). Fortunately, these five Landsat scenes are almost cloud free, cover a distance of more than 850 km, and contain the transition zone between snow free and snow covered surface. Furthermore, not only AVHRR (NOAA-14) but also MODIS (Terra) was operational on March 4th, 2000, allowing for the comparison of both products with the independent Landsat source. The results of the comparisons are given in section 6.1

5.4.2 Comparison of snow depth station data with the APOLLO snow product

The HSDSD data introduced in section 4.5 are often exploited for long-term climate studies on a continental scale (e.g. Fallot et al. (1997); Ye et al. (1998); Peings & Douville (2009)). Although station density from HSDSD data is low (Figure 4.3) and the time series of daily observations only runs until 1995, the snow depth information that is contained within the data can be exploited to assess the accuracy of the APOLLO PPL3 snow products. For this purpose, the point data is converted to a raster with the same resolution and projection as the APOLLO products. The snow depth information from the station data (in cm) is transferred to the raster value. This allows for a detailed analysis of possible differences between station and remote sensing data: If errors occur, they are suggested to be related with the snow depth as it was reported by Liang et al. (2008) and Klein & Barnett (2003) for the operational MODIS snow products (see section 3.4.2). However: The comparison of point data with medium resolution raster data faces a few drawbacks. The difference in scale is one possible error source, since the point measurement represents only one small spot within a grid cell of more than 1 km² (in the case of AVHRR) as already described by Derksen, Walker & Goodison (2003). It is known that a grid cell containing more than 50% of snow will be classified as snow covered area within e.g. the MOD10A1 product (Hall et al. 2002). Thus it is possible that station data and snow cover product disagree although they are both correct if treated separately. Another problem observed by Parajka et al. (2010) is the general positioning of stations: For Austria the authors found that most stations are situated within mountain valleys while only very few stations are located on mountain tops or on steep mountain ridges. The same is true for Central Asia: Elevations of HSDSD stations operational until 1995 do not exceed 850 m, totally neglecting the mountainous regions of the south-eastern region of Central Asia. Results of the comparison between APOLLO PPL3 and HSDSD are given in section 6.1.

5.5 Indirect accuracy assessment of cloud free snow products

The reliability of the methods to reduce cloud coverage from the APOLLO and the operational MODIS snow products is an important aspect. Because several steps are applied to the input data (Figure 5.4 in section 5.2), possible errors may propagate through the time series as each step is built upon another. Assessing the accuracy of the applied methods to reduce cloud coverage is therefore a necessary, but yet challenging task: In most cases it is not possible to use remotely sensed data like e.g. Landsat because clouds are present in these sources as well. Snow data from climate stations is not available for Central Asia in sufficient

amount and quality as described in sections 2.1 and 4.5. It is, however, possible to derive an indirect accuracy assessment of the produced, cloud free snow cover data:

The accuracy of each step applied to the input data (Figure 5.4) is known from already conducted studies as reviewed in section 3.2.3. During the application of the cloud reduction scheme, the number of pixels processed by each step is therefore recorded to an accuracy table. This procedure allows the calculation of the theoretical accuracy of the final results, provided that the values from the referred studies also apply to the region of Central Asia.

Another indirect accuracy assessment is accomplished within the framework of the presented thesis: in Europe, comprehensive station data including information about snow depth is available for numerous locations. Therefore, a transferability study is derived, applying a similar cloud reduction scheme to eleven years of MODIS snow cover time series for whole Europe. The study was published in the “Remote Sensing” Journal under the title: *European Snow Cover Characteristics between 2000 and 2011 Derived from Improved MODIS Daily Snow Cover Products* (Dietz et al., 2012b). The ECA&D provides daily snow depth station data on their web page (ECA&D, 2012), 896 of which fell into the study area (Klein Tank et al., 2002). Figure 5.7 shows the distribution of these stations (source of Figure 5.7: Dietz, Wohner, et al. (2012)). SCD is calculated for all stations by summarizing days with snow depth > 0cm and then compared to the SCD derived from the cloud-free MODIS PPL3 time series. Because station data only represents the snow cover status at one point within a MODIS or AVHRR pixel, uncertainties are adhered to the applied method. The problem was already addressed to in section 5.4.2. Results from the transferability study will be presented in section 6.3.

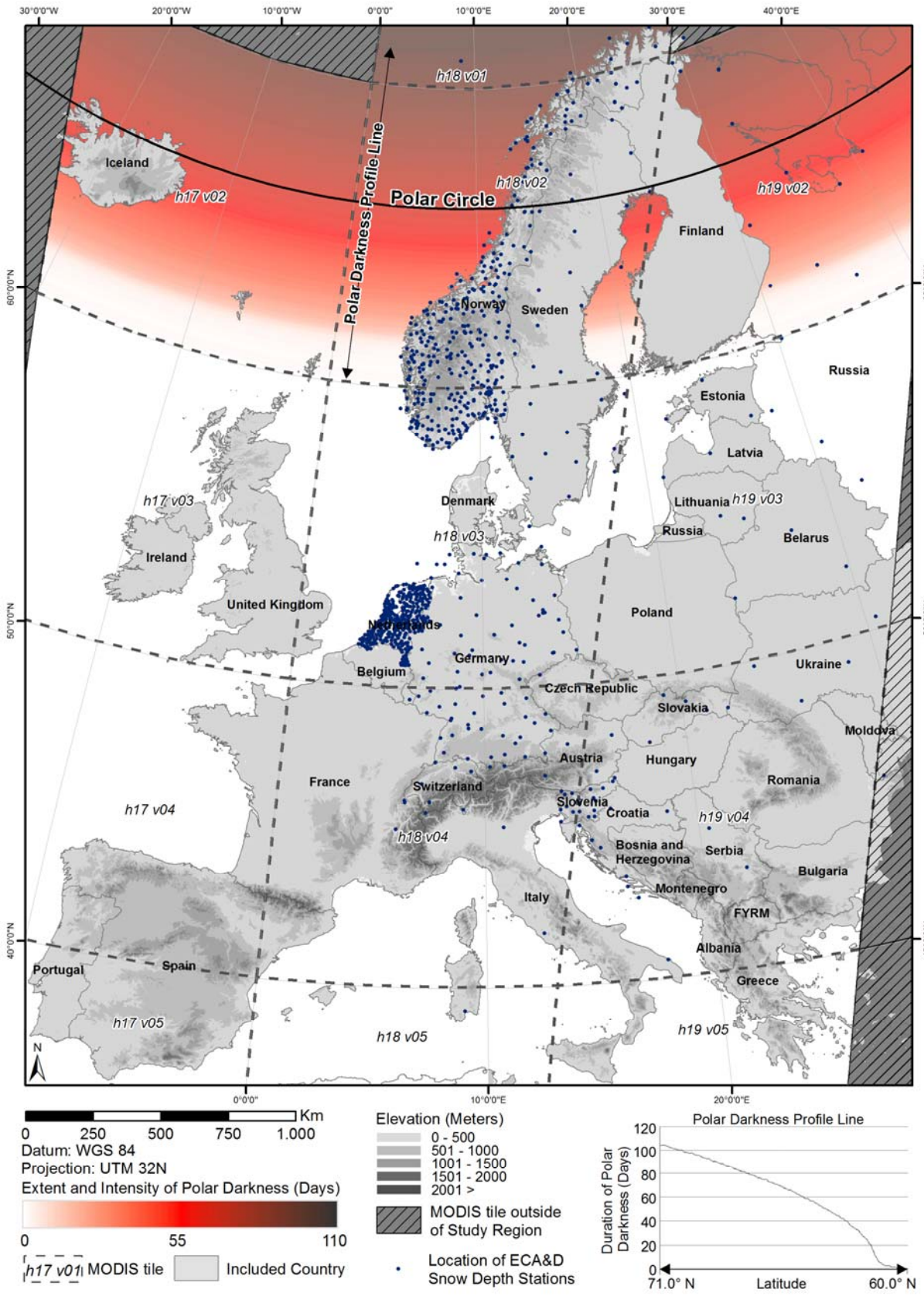

Figure 5.7: Location of ECA&D climate stations (adopted from Dietz, Wohner, et al. (2012))

5.6 Accuracy assessment using field trip data

As already outlined in section 4.5, a field trip was organized within the framework of the CAWa project to support the snow cover processing in December 2010. Snow cover status was recorded at 170 locations along the route. This data source had the potential to estimate the accuracy of the cloud reduction scheme but unfortunately, cloud coverage was relatively low during the time of the field trip. Figure 5.8 illustrates the position of all waypoints with red points referring to cloud free conditions and green points pointing to cloud covered surface.

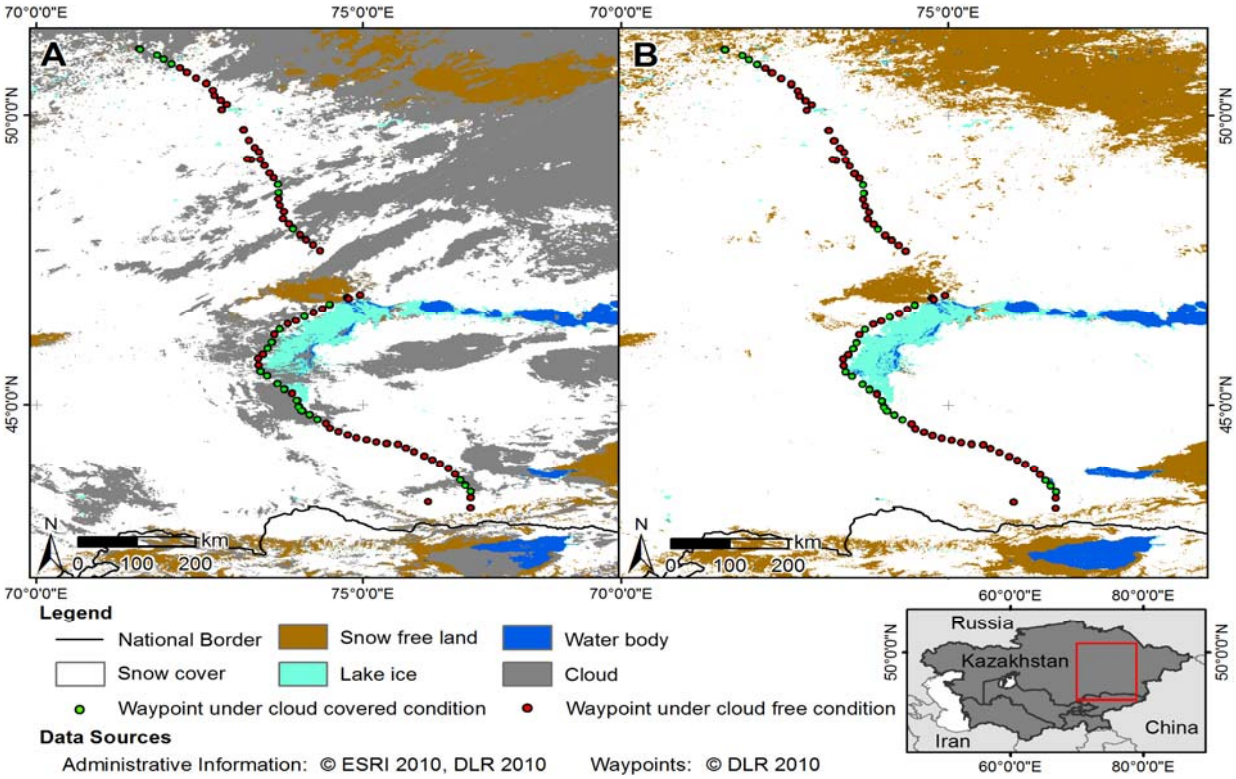

Figure 5.8: Location of waypoints and cloud cover conditions during the field trip

Figure 5.8 “A” represents the original cloud cover conditions in MOD10A1 during December 6th, 2010 while Figure 5.8 “B” includes the PPL3 product of the same date. The snow cover status that was recorded during the field trip is compared to the calculated snow cover status after the cloud reduction scheme has been applied. Only the green points (total number: 20) can be used to assess the accuracy of the cloud reduction scheme. Therefore, the result from this assessment can be considered more or less irrelevant. Anyhow, since these waypoints constitute a quite reliable data source, the findings from this analysis are included in section 6.3. They form only a small brick in the set of accuracy assessments derived for the presented thesis.

6. Results and discussion

All results from the previously described methods are presented and discussed in this section. The time series of the daily snow cover data processed for these results is huge: Beginning with 1986, parameters like SCD, SCS, SCM, and SCI are produced. In theory, snow cover information could be presented for each day between September 1st, 1986 and January 15th, 2013 (~ 9,600 raster products). These single day results may be useful for certain applications but are excluded from section 6. The amount of datasets is too huge to include them here. Therefore, mean conditions, standard deviations, and results aggregated among hydrological and topographical entities are provided within this thesis. The amount of results is still exceptionally large. To include all results within this section in full resolution would still go beyond the scope of the initial intention: To give a distinct overview about Central Asian snow cover conditions. Within section 6, these results will be represented in a more condensed way, combining multiple years of snow cover parameters in only one figure. Some of the presented results have already been published in "International Journal of Remote Sensing" under the title *Snow-cover variability in Central Asia between 2000 and 2011 derived from improved MODIS daily snow-cover products* (Dietz et al., 2013). Only the results from the MODIS time series between 2000 and 2011 are included in this publication. Another manuscript titled *Processing of daily snow cover products from NOAA-AVHRR data for Central Asia using APOLLO* was submitted to "Remote Sensing of Environment" in early 2013. The comments that were received during the review process have proven to be most useful and have in parts also found their way to the presented thesis. Details are included in section 6.1. The presented results also contain an outlook of possible applications and future research opportunities (section 6.4). This outlook is far from being complete but it should help to estimate the potential benefit that is facilitated by developing and maintaining the processing chain that was initiated within the very thesis.

6.1 APOLLO snow cover product and accuracy

After the recoding of all processed AVHRR scenes according to Table 5.2 has been accomplished, a time series of snow cover products is made available that is comparable to the operational MODIS daily snow cover products MOD10A1 and MYD10A1 (except spatial resolution and accuracy). Only those AVHRR scenes have been processed that include at least one pixel with solar elevation > 10° since the APOLLO snow detection scheme only works during daytime. Therefore, not all acquired scenes (Figure 4.1) were exploited to pre-

pare snow cover products. In Figure 6.1, the number of processed AVHRR scenes per year is depicted. The percentage of night scenes reaches 52% in 1990 but usually stays below 30%. In 1994, an onboard calibration system on NOAA-11 failed and a motor current increased, causing jitter in the observations (Huang et al. 2003). Therefore, data from NOAA-11 after September 1994 cannot be processed by APOLLO without serious faults. The respective scenes are flagged as “damaged scenes” in Figure 6.1.

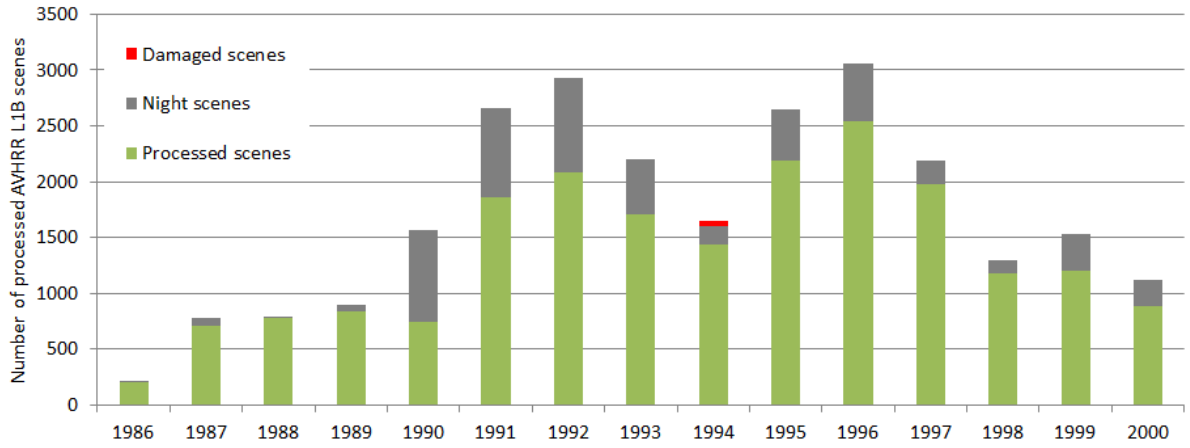

Figure 6.1: Number of processed AVHRR scenes per year

~ 20,300 of the originally available ~ 27,000 AVHRR datasets (75%) have been processed by APOLLO for the presented thesis. The amount of scenes in 1986 is comparably low because the hydrological year, which is used as a basis for the upcoming analyses, starts on September 1st, 1986. Therefore, only 122 days of this year had to be processed. Figure 6.1 gives an overview about the total number of available scenes per year but the spatial distribution of (cloud-free) observations remains unknown. Unlike the MODIS daily snow cover products that are available on a daily basis, AVHRR overpasses are only archived irregularly especially in early years. While for the MODIS product only cloud coverage limits the amount of clear-sky observations (see Figure 5.2 for a typical pattern), the AVHRR data are confined by both, cloud coverage and missing observations. Each year in the time series between 1986 and 2000 is unique with respect to the number and pattern of clear-sky observations. Figure 6.2 and Figure 6.3 contain a summary of the amount of clear-sky observations in the AVHRR time series for each year between 1986 and 1999. 1986 in Figure 6.2 differs from the other years since this year starts in September, therefore containing only 4 months of data. The contrast is stretched to a different intensity for this year (ranging from 0 to 266 instead of a maximum of 800) in order to be able to compare 1986 with the other years.

Figure 6.2 and Figure 6.3 illustrate the difference in data availability between the years. Before 1991, clear-sky observations are rare. The North stands out due to an extremely low amount of useable data. Figure 5.2 already suggested that this area is affected by more intense cloud coverage than the southern parts. The combination of cloud cover and the sparse number of observations poses an additional challenge. The problem affects most products presented in section 6.2, blurring the validity of early year results. Since all available AVHRR scenes have been acquired from the NOAA archive, an alternative data source for the data gaps does not exist. Therefore, the results presented in the next sections can be considered the most substantial and extensive that are feasible from a technical and methodological point of view. Figure 6.2 and Figure 6.3 contain the number of clear-sky observations per year, which must not be confused with the total number of observations. Compared to the MODIS clear-sky data availability, the year between 1991 and 1998 can be considered as equal. In southern Uzbekistan and Turkmenistan, the number of useful AVHRR scenes even exceeds the amount of the MODIS source. 1999 and 1990 contain slightly less cloud-free observations. A sharp edge between only few observations in the North and plenty scenes in the South is noticeable in several years (1989, 1995, 1996, 1998, 1999). The shape of this pattern appears questionable, since it does not always follow the satellite track of ascending and descending orbits. Possible reasons for the data gaps in the North and the patterns in Figure 6.2 and Figure 6.3 will be discussed at the end of section 6.1.

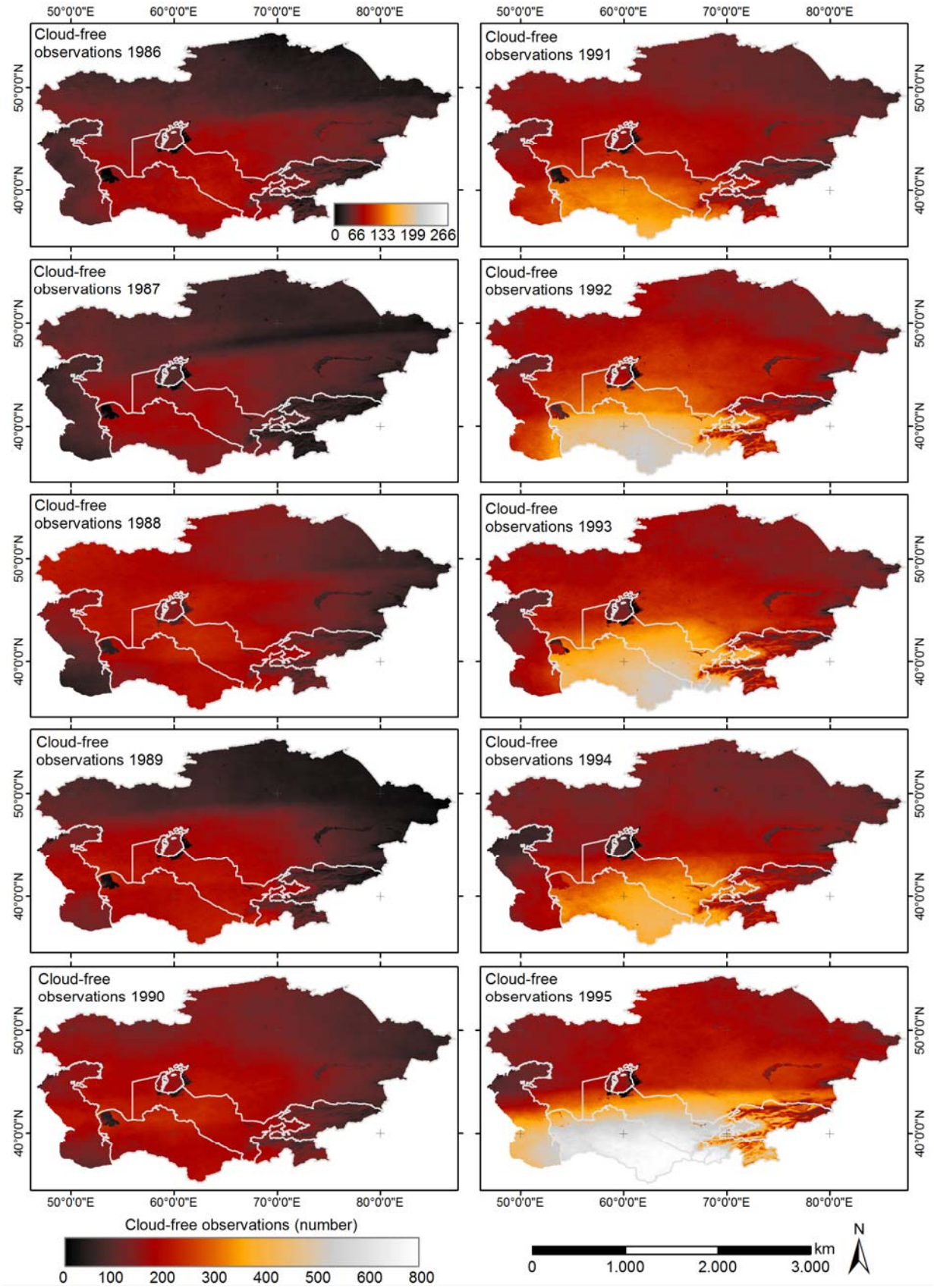

Figure 6.2: Number of clear-sky observations for AVHRR between 1986 and 1995

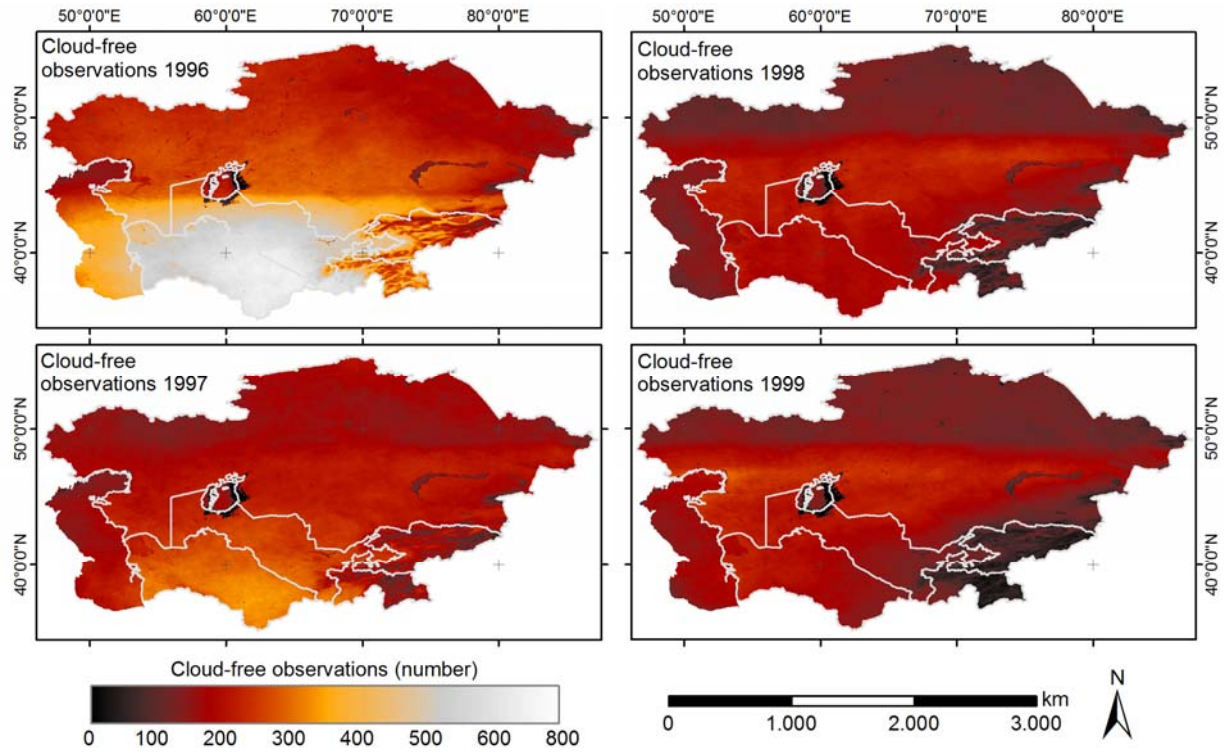

Figure 6.3: Number of clear-sky observations for AVHRR between 1996 and 1999

An example for the original APOLLO PPL1 product was already included in section 5.1 (Figure 5.1). In Figure 6.4, the recoded APOLLO PPL1 product is opposed to the MOD10A1 product of the same date (March 4th, 2000). The cloud patterns of the two products differ significantly. The reason for this difference may emerge from the different observation times of the satellites (NOAA-14 and Terra). Cloud free snow cover patterns are, however, comparable. The APOLLO product seems to misinterpret the ice covered water bodies of Lake Balkhash and Lake Alakol (most eastern water body in Figure 6.4) as cloud covered (Figure 6.4 “A”) while the MODIS product recognizes ice (Figure 6.4 “B”). Problems with water bodies are common for both, AVHRR- and MODIS-derived snow maps. This issue will be discussed in section 6.3 as it affects both sensors likewise.

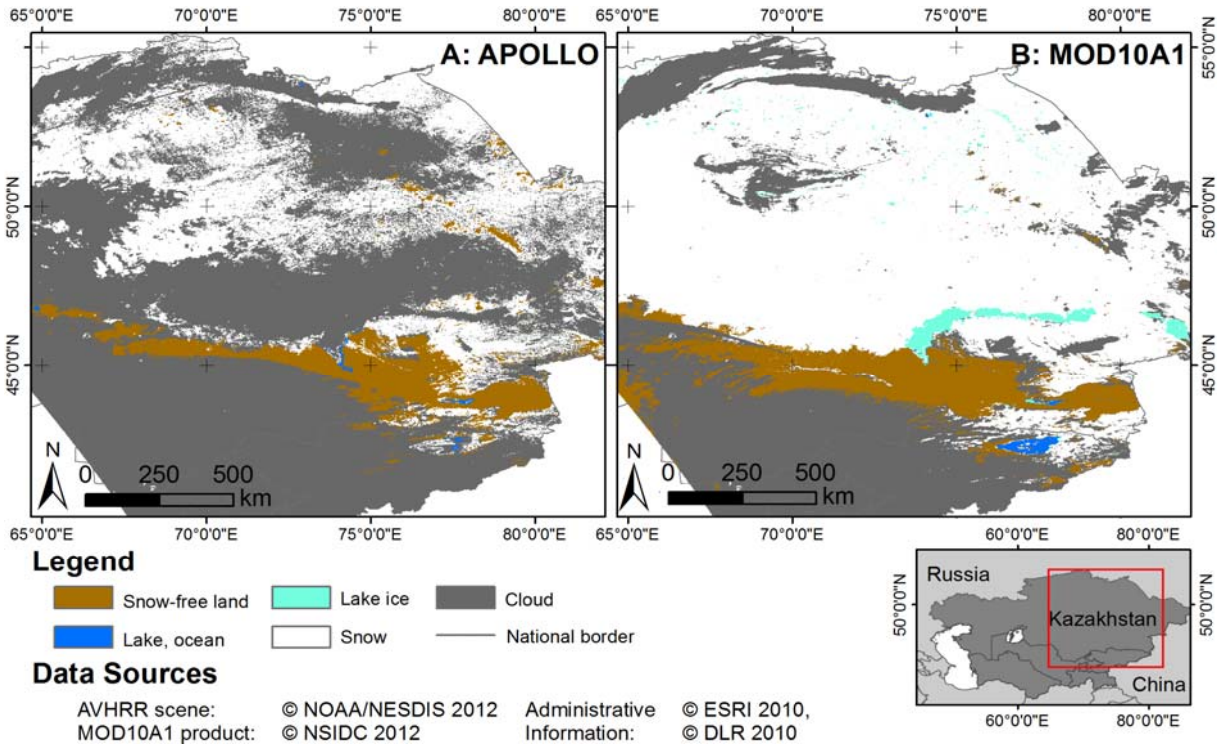

Figure 6.4: APOLLO and MODIS snow products of March 4th, 2000

The accuracy of the APOLLO PPL1 and PPL3 products is assessed using Landsat scenes from different regions, years and seasons (see Table 4.5). The workflow starts with the snow cover classification of appropriate Landsat scenes. Cloud free scenes with a balanced ratio between snow covered and snow free area are desirable because they allow for a detailed assessment of the snow mapping accuracy along the border between snow covered and snow free area – a region that is prone to higher error rates. Reasons for higher errors at the snow border include the relatively coarse resolution of AVHRR (or also MODIS) and the occurrence of patchy snow fields, introducing regions with diverse snow cover fractions and therefore causing over- or underestimation of snow (Jain et al., 2008). More details about fractional snow cover were already described in section 3.2.2.

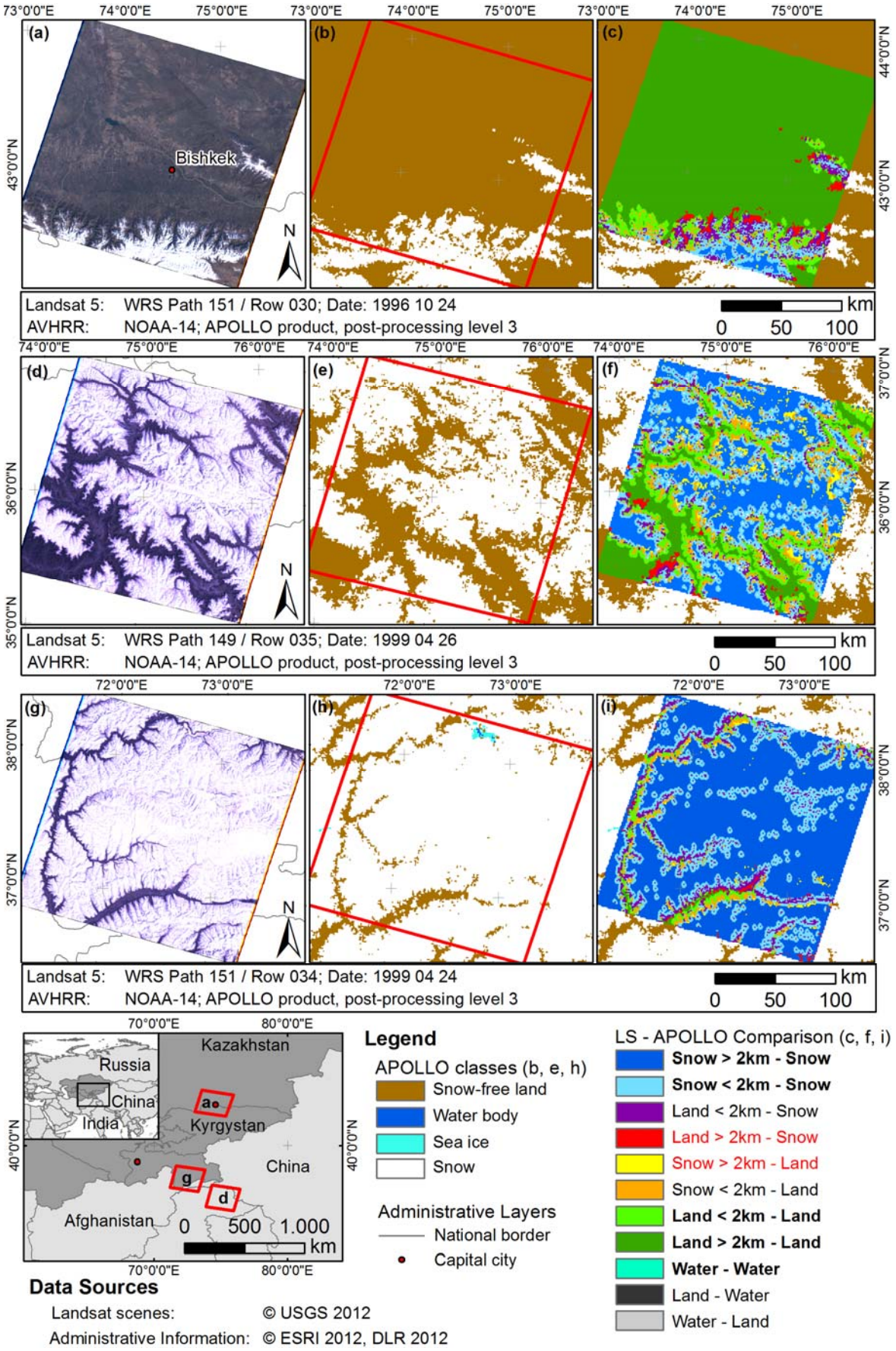

Figure 6.5: Accuracy assessment of APOLLO snow products using Landsat, first example

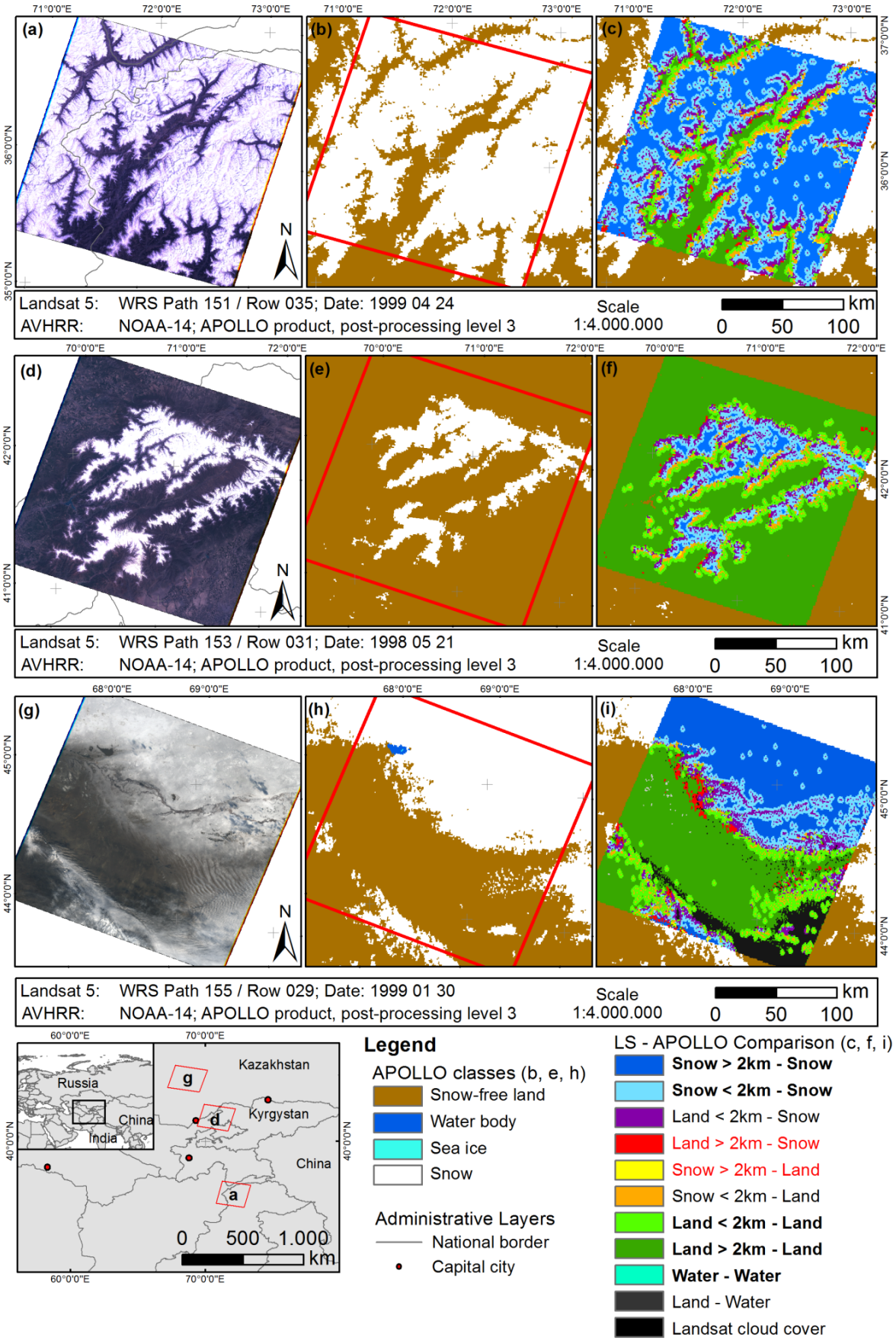

Figure 6.6: Accuracy assessment of APOLLO snow products using Landsat, second example

After snow cover classification, the resolution of the Landsat datasets is adapted to AVHRR in order to be able to compare both products on a pixel basis. APOLLO PPL1, PPL3, and Landsat snow products of the same date are then opposed to each other to estimate the agreement between the sources. The transition zone between snow covered and snow free land is treated separately: A buffer zone of 2 km is added to both sides of the snow border. This allows for a detailed analysis of classification errors within the transition zone. Figure 6.5 and Figure 6.6 illustrate the procedure, depicting the original Landsat scenes (true-colour composite 3-2-1) in the left columns, APOLLO PPL3 of the same date and region in the centre, and the results from the comparison between both products in the right columns. The APOLLO PPL1 product before applying the cloud reduction scheme is also compared to Landsat using the same approach as in Figure 6.5 and Figure 6.6, even though there is no figure included in this section due to clarity. The procedure is conducted for Landsat scenes 1 through 18 from Table 4.5, always comprising comparisons of PPL1 and PPL3 APOLLO snow products.

The results from the comparison between Landsat and the APOLLO snow cover products are combined in two confusion matrixes: Table 6.1 and Table 6.2. The use of confusion matrixes is widely accepted in the remote sensing community and considered to be the standard approach in the accuracy assessment of thematic products (Congalton, 1991; Foody, 2002). The sampling design that was chosen for the accuracy assessment of the presented thesis is simple: Instead of analysing a number of randomly or deliberately distributed sample points, all available pixels are evaluated. This approach may raise the question whether such sample design is representative for all assessed classes. In the case of the presented thesis with only two eminent classes (snow covered and snow free area) and a mean snow cover percentage of ~ 43% in the Landsat scenes used for accuracy assessment (see Table 4.5), these two classes are equally distributed. Therefore, choosing an assessment of all available pixels will not distort the results. The Water/Ice class in Table 6.1 and Table 6.2 is only included for the sake of completeness. This class is prone to considerably high error rates due to the fact that outdated water masks are used for the thematic snow cover products. More details about this problem will be included in section 6.3.

The 2 km buffer zones around the snow border are represented in the fields with grey hachure in Table 6.1 and Table 6.2. It is clearly visible that the accuracy within these zones is lower than outside for both products: PPL1 and PPL3. Overestimation of actual snow cover is only 2.65% outside, but 22.59% inside the buffer zone for PPL1. For snow-free land, only 1.14% overestimation is observed outside the buffer zone, while inside, the rate increases to 30.71%. In PPL3, overestimation of snow cover is higher than for the PPL1 product (7.35%

compared to 2.65% outside, 30.18% compared to 22.59% inside the buffer zone). Underestimation, however, decreases significantly when compared to PPL1 (underestimation of snow in PPL1: 46.45% outside, 58.17% inside buffer zone; PPL3: 3.39% outside, 26.64% inside buffer zone).

Table 6.1: Confusion matrix of Landsat and APOLLO PPL1 snow product

AVHRR PPL1 snow products \ Landsat reference maps	Snow	Land	Snow < 2km	Land < 2km	Water/Ice	Clouds	Total	Users Acc.
Snow	**56417**	1531	0	0	0	0	57948	0.973
Land	2671	**222905**	0	0	266	0	225842	0.986
Snow < 2km	0	0	**42100**	12279	0	0	54379	0.774
Land < 2km	0	0	22289	**50292**	0	0	72581	0.692
Water/Ice	0	401	0	0	**142**	0	543	0.261
Clouds	48925	29713	58288	44883	0	**0**	181809	N/A
Total	108013	254550	122677	107454	408	0	**593102**	
Prod. Acc.	0.522	0.875	0.343	0.468	0.348	N/A		

Overall Accuracy: 62.69% Clear-sky Accuracy: 90.40%
Khat: 0.52 Clear-sky Khat: 0.84

Table 6.2: Confusion matrix of Landsat and APOLLO PPL3 snow product

AVHRR PPL3 snow products \ Landsat reference maps	Snow	Land	Snow < 2km	Land < 2km	Water/Ice	Total	Users Acc.
Snow	**142067**	11268	0	0	0	153335	0.926
Land	4978	**261705**	0	0	630	267313	0.979
Snow < 2km	0	0	**96355**	41636	0	137991	0.698
Land < 2km	0	0	34973	**70045**	0	105018	0.666
Water/Ice	0	1223	0	0	**814**	2037	0.399
Total	147045	274196	131328	111681	1444	**665694**	
Prod. Acc.	0.966	0.954	0.733	0.627	0.563		

Overall Accuracy: 85.77%
Khat: 0.80

One problem in Table 6.1 is the handling of the extensive cloud coverage which is leading to the severe underestimation of snow coverage. Clouds reduce the accuracy of the APOLLO snow products considerably when treated as classification errors (overall accuracy: 62.69%). Clouds are, however, not necessarily errors. If clouds are present during an AVHRR overpass but are missing during the Landsat overpass, the suggested error in the confusion matrix is not valid. The uncertainty in cloud handling is difficult to overcome. It is known – also from the operational MODIS products – that clouds and snow are prone to confusions (see

section 3.2.1). However, an estimation of these confusions remains a challenging task even when examining classification results manually. That is why besides overall accuracy, clear-sky accuracy is included in Table 6.1. This value is calculated using only the cloud free pixels from the confusion matrix. The same approach was used to estimate the accuracy of the operational MODIS snow cover products (e.g. in Wang et al. (2008)). The clear-sky accuracy of 90.4% is only marginally less than the MODIS accuracy of ~93% (Hall & Riggs 2007). After the cloud reduction procedure (Figure 5.4) has been applied to the APOLLO data, the accuracy decreases by around 4.7% (Table 6.2).

Based on the clear-sky accuracy of PPL1 (90.40%) and the overall accuracy of PPL3 (85.77%), the accuracy of all snow cover pixels added since PPL1 is determined to account for 82.50%. This value also constitutes the accuracy of the post-processing steps to produce cloud free daily snow cover datasets outlined in the cloud reduction scheme (Figure 5.4).

The results from Table 6.1 and Table 6.2 depict a generalized view of the accuracy assessment since the analyses from 18 Landsat scenes, comprising different seasons, terrain conditions, and snow cover fractions are combined to only two single tables. The comparison between Landsat and APOLLO snow products can, however, reveal more details. Figure 6.5 and Figure 6.6 demonstrate two additional findings: The snow cover mapping accuracy depends on the snow cover percentage of the area. Furthermore, a geolocation shift of up to two pixels influences overall accuracy, but not the aggregated sum of the snow covered area.

Figure 6.7 contains information about the correlation between snow cover fraction and snow mapping accuracy of the APOLLO PPL3 product. The accuracy of 10x10 (~100 km²) pixel boxes is analyzed and opposed to the snow cover fraction in Figure 6.7. Buffer zones are not considered in this assessment. The accuracy increases nearly linearly with increasing snow cover percentage, reaching ~95% for areas with 100% snow coverage. The reason for the negative outliers in this region is that though the 10x10 pixel boxes are 100% snow covered in Landsat, the box itself may be positioned at the border to snow free land. A shift of only two AVHRR pixels results in the deviations observed at the right edge of Figure 6.7.

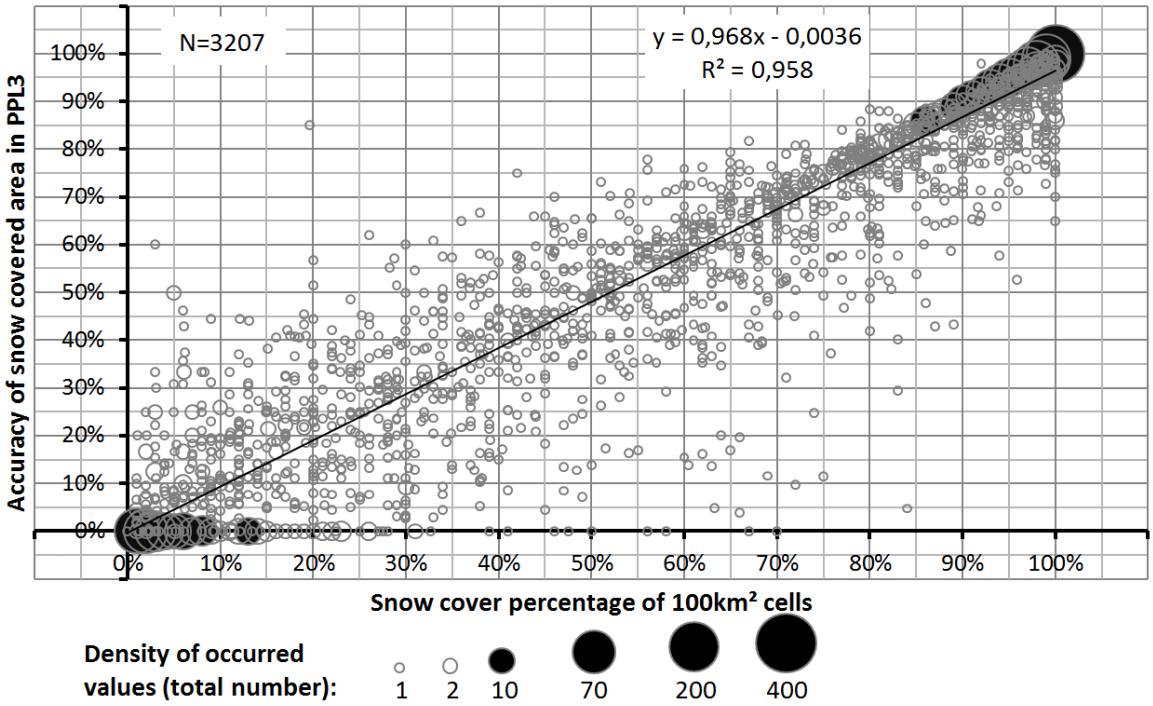

Figure 6.7: Scatterplot of snow cover mapping accuracy compared to snow cover fraction

The impact of the sometimes inaccurate geolocation within the APOLLO snow product is investigated by comparing the snow covered area extent from Landsat with the extent from PPL3. Figure 6.5 “i”, Figure 6.6 “c” and f already suggest that in some observations, a shift of few pixels causes underestimation at one snow-border and overestimation at the opposite snow-border. An analysis of this behavior revealed that these values partially compensate each other, with overestimation of actual snow cover usually prevailing. Although overall accuracy for the investigated Landsat scenes is only 85.77%, the snow cover extent of PPL3 accords with Landsat by 95.55%. The remaining 4.45% add up to the average overestimation of the snow covered area extent from APOLLO PPL3.

The accuracy of the APOLLO snow product is similar to the modified version of SPARC for the European Alps (Hüsler et al., 2012) with a reported clear-sky accuracy of 90%. A drawback of APOLLO suggested by Khlopenkov & Trishchenko (2007) is the comparably high demand on computational resources. This problem was, however, not observed during the processing for the presented thesis (average computational time from Level 1B to APOLLO PPL3: 12 minutes using a Solaris 10 XEN-VM on a SUN FIRE V490 platform with 4 SPARC CPUs and a standard Intel Xeon X5650 workstation with 12GB RAM for post-processing. 20,300 scenes therefore accounted for ~ 170 days of computational time).

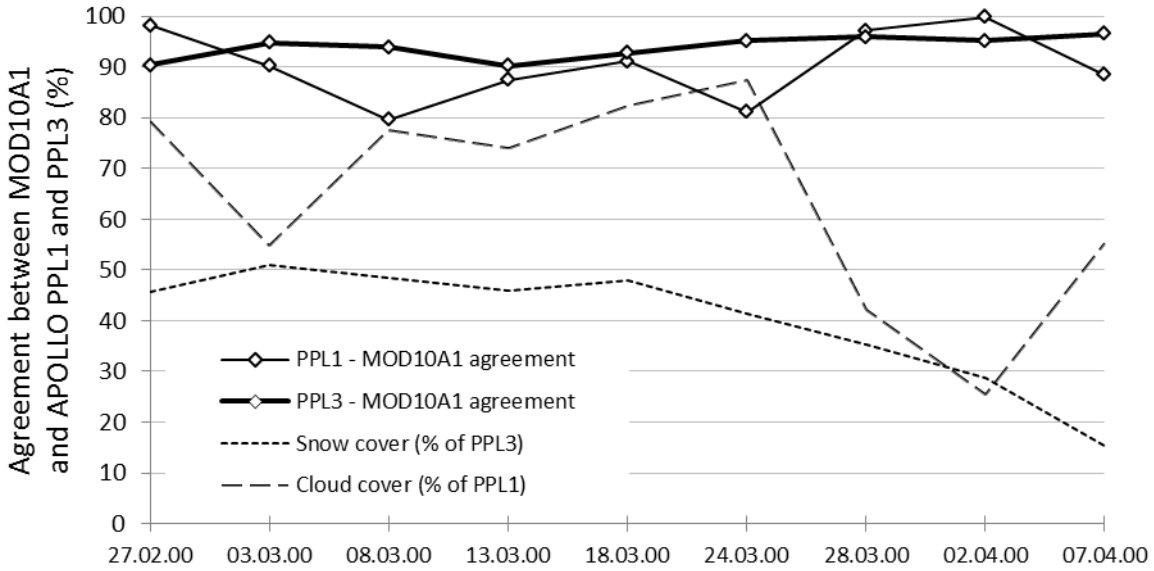

Figure 6.8: Agreement between MOD10A1 and APOLLO PPL1 and PPL3

As described in section 5.4.1, MOD10A1 and APOLLO snow cover products were compared for every fifth day after February 2nd, 2000 and for the full area of Central Asia. The time series only runs until April 7th because snow coverage rapidly depleted afterwards, allowing for no estimation of snow mapping agreement. Figure 6.8 contains the results of the comparison: The agreement for the PPL1 data varies between 80% and 99% (mean: 90.3%) while for PPL3, the mean agreement is 93.8% and never falls below 90%. This is not only the case for winter scenes during February but also during spring time where the snow cover extent is much more variable (as shown by the snow cover plot in Figure 6.8). Cloud cover percentage of PPL1 data is also included in Figure 6.8: Values of 80% and more are not an exception during winter and spring months and confirm the need for the cloud reduction scheme applied in this thesis. It is also eye-catching that the agreement between MOD10A1 and PPL1 decreases noticeably with increasing cloud coverage (e.g. 08.03.00 or 24.03.00 in Figure 6.8). The fact that this relation does not exist for the MOD10A1 - PPL3 comparison indicates that the post-processing steps from the cloud reduction scheme not only remove data gaps caused by cloud coverage, but also improve the overall agreement between the products. Since the MODIS snow cover datasets are accepted as high-quality products, the cloud reduction scheme can be interpreted as an improvement for the snow cover delineation from AVHRR data.

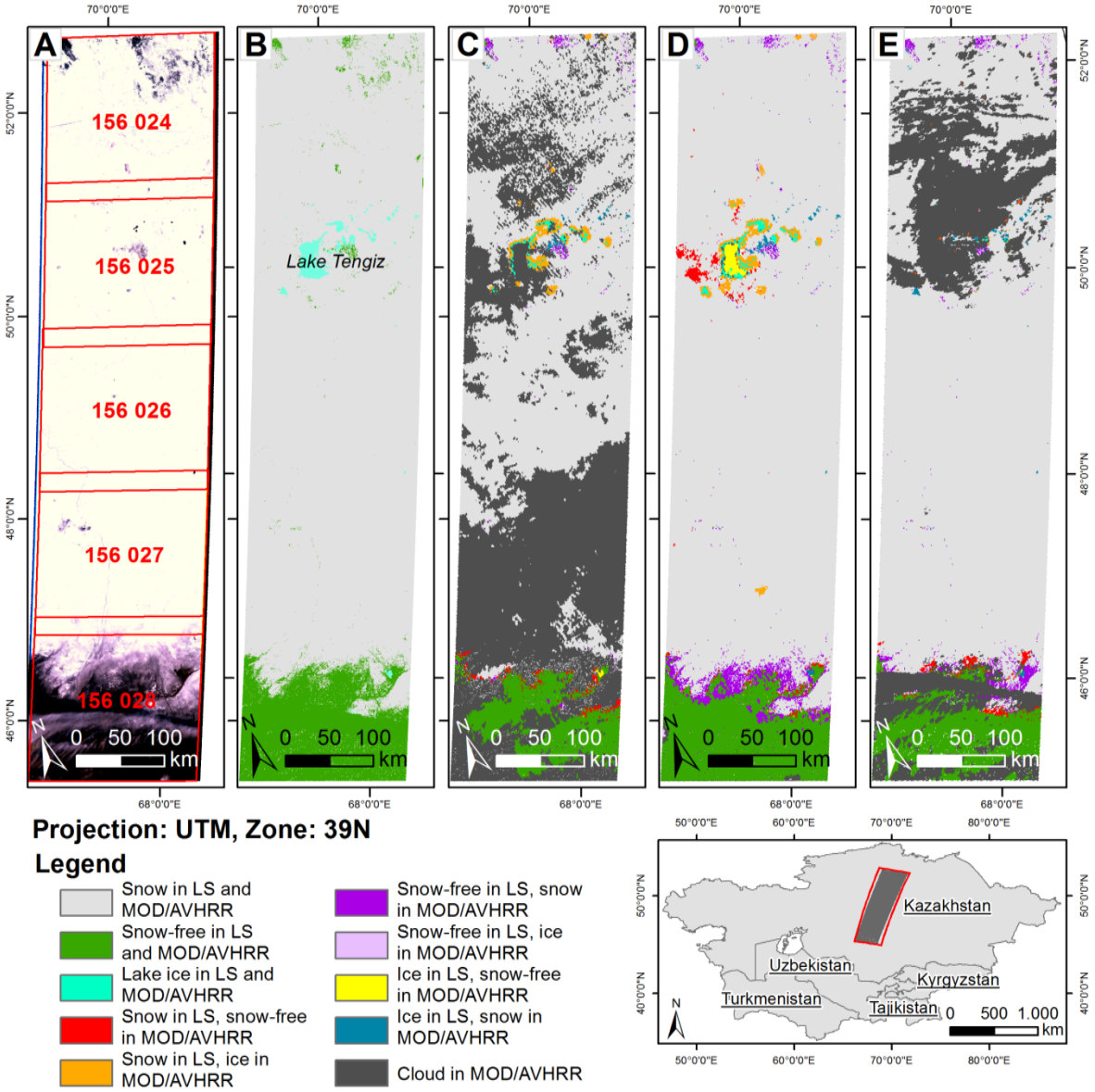

Figure 6.9: Comparison between Landsat (A,B), APOLLO PPL1 (C), PPL3 (D), and MOD10A1 (E)

The comparison with a Landsat transect from March 4th, 2000 is illustrated in Figure 6.9 with the Landsat true-color mosaic in Figure 6.9 “A” and Landsat snow cover classification in Figure 6.9 “B”. The subsequent images depict the results from the comparisons with APOLLO PPL1 (Figure 6.9 “C”), APOLLO PPL3 (Figure 6.9 “D”), and the MOD10A1 mosaic (Figure 6.9 “E”) from the same day. Table 6.3 to 6.5 contain the confusion matrixes of Landsat and the respective snow cover product from Figure 6.9. Cloud patterns are different between MOD10A1 (Figure 6.9 “E”) and APOLLO PPL1 (Figure 6.9 “C”) with observation time at 9:31 UTC for AVHRR and 5:05 UTC for MOD10A1 (both times refer to the beginning of the observation; Study region local time zone: UTC +6h). Observation time of the most southern Land-

sat scene (path 156, row 28) is 3:04 UTC. The pattern of the Cirrus cloud in this scene is clearly visible in the MOD10A1 product, too, ensuring that this cloud cover classification is correct.

The transition zone between snow covered and snow free land is a common error source for both sensors. This is apparent in Figure 6.9 “D” and Figure 6.9 “E”. The lake in the upper half of the scene is covered by clouds in the MOD10A1 product, hindering from the evaluation of this region. In APOLLO PPL1, the lake is classified as cloud cover. Because cloud coverage is persistent in the APOLLO products for more than two days before and after March 4th, 2000, the post-processing step 3 (SRTM snow line definition) is applied to the PPL1 data. This step does not consider the existence of a lake surface at this position, therefore classifying the cloud covered pixels as snow free.

Table 6.3: Confusion matrix of Landsat 7 transect and APOLLO PPL1

PPL1 snow product \ Landsat reference map	Snow	Land	Water/Ice	Clouds	Total	Users Acc.
Snow	**89384**	791	290	0	90465	0.988
Land	827	**11172**	54	0	12053	0.926
Water/Ice	1532	33	**487**	0	2052	0.237
Clouds	65703	12825	1233	**0**	79761	N/A
Total	157446	24821	2064	0	**184331**	
Prod. Acc.	0.567	0.450	0.235	0		

Overall accuracy: 54.81% Clear-sky accuracy: 96.62%

Table 6.4: Confusion matrix of Landsat 7 transect and APOLLO PPL3

PPL3 snow product \ Landsat reference map	Snow	Land	Water/Ice	Clouds	Total	Users Acc.
Snow	**161289**	4619	464	0	166372	0.969
Land	1361	**19928**	685	0	21974	0.906
Water/Ice	1980	95	**777**	0	2852	0.272
Clouds	0	0	0	**0**	0	N/A
Total	164630	24642	1926	0	**191198**	
Prod. Acc.	0.979	0.808	0.403	0		

Overall accuracy: 95.18%

Table 6.5: Confusion matrix of Landsat 7 transect and MOD10A1

MOD10A1 snow	Landsat reference map: Snow	Land	Water/Ice	Clouds	Total	Users Acc.
Snow	**70128**	1094	6	0	71228	0.984
Land	8	**10876**	76	0	10960	0.992
Water/Ice	42	1	**36**	0	79	0.455
Clouds	83966	11903	1623	**0**	97492	N/A
Total	154144	23874	1741	0	**179759**	
Prod. Acc.	0.454	0.455	0.020	0		

Overall accuracy: 45.08% Clear-sky accuracy: 98.50%

The clear-sky accuracy of the MOD10A1 product with 98.5% is slightly higher than the clear-sky accuracy of APOLLO PPL1 (96.6%). Removing the clouds from the APOLLO data only marginally decreases the accuracy to 95.2% for this transect. These values confirm the results from Figure 6.7: Regions with continuous snow coverage are classified with around 95% accuracy. Lakes can cause uncertainties in the classification result, though this is only true for dynamic water bodies with variable extents. Lake Tengiz from Figure 6.9 is one of those highly variable, shallow water bodies that partially dry out in summer months and obtain most of their inflow from snow melt in spring season (Aladin and Plotnikov, 1993).

The last part of the APOLLO snow cover product validation comprises the comparison with the snow depth station data from HSDSD. Details about this dataset were presented in section 4.5 while the approach to compare both products was included in section 5.4.2. Because SCD and SCS from APOLLO are missing for 1994 and HSDSD data records stop in 1995, only the years 1986 to 1993 can be evaluated. Table 6.6 depicts the results from the comparison. The deviation (in days) between station and remote sensing derived SCD are represented in clusters of 5 days to ensure a clearly arranged overview. The number of stations that provide a complete and therefore useable time series of daily measurements varies between 32 in 1986 and 19 in 1990. This number constitutes an inadequate amount of in situ data, given the vast size of the study region. Figure 6.10 illustrates the mean difference between APOLLO PPL3 and HSDSD SCD per year. The results from the comparison show that APOLLO generally overestimates the SCD at more stations than it underestimates. Mean deviations stay below 30 days with largest errors in 1987. Due to the small amount of available stations, the results from this comparison can only be considered as a supplementary extension of the accuracy assessment.

Table 6.6: Result of the comparison between HSDSD and APOLLO PPL3; Number of stations, mean deviation (in days), mean overestimation, and mean underestimation of SCD are included. Deviations are aggregated to clusters of ± 5 days.

Days	1986	1987	1988	1989	1990	1991	1992	1993
-50	2	0	0	0	0	0	0	0
-45	0	1	0	0	0	0	0	0
-40	0	0	1	0	1	0	2	0
-35	0	1	1	0	0	0	0	1
-30	1	1	0	1	0	1	0	0
-25	1	0	0	2	0	0	1	3
-20	1	1	0	1	1	2	0	1
-15	2	1	0	1	1	2	3	1
-10	2	1	2	2	0	4	1	2
-5	2	0	2	2	2	2	3	1
0	4	1	2	3	3	1	2	4
+5	2	3	2	1	3	1	4	2
+10	5	2	5	3	0	4	1	4
+15	3	3	3	2	1	2	1	1
+20	0	1	2	2	2	2	1	3
+25	0	6	4	2	0	0	0	2
+30	3	0	1	2	1	0	3	1
+35	1	1	0	1	3	2	1	2
+40	0	1	3	0	0	1	0	1
+45	1	1	1	1	1	1	1	1
+50	1	1	2	1	0	0	0	0
+55	1	4	0	0	0	0	0	0
Number of stations	32	30	31	27	19	25	24	30
Mean deviation (days)	4.5	16.2	14.0	7.4	8.7	4.8	2.5	6.3
Overestimation	21.4	25.8	17.5	16.1	17.0	13.6	17.5	18.9
Underestimation	-18.1	-26.7	-21.6	-19.2	-17.9	-19.3	-16.8	-17.1

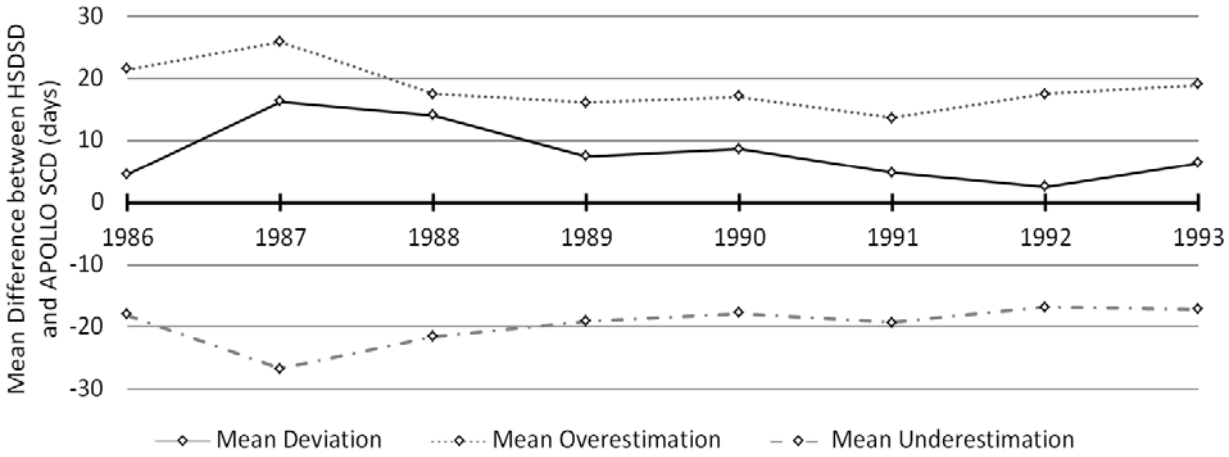

Figure 6.10: Mean difference between HSDSD and APOLLO PPL3 snow cover product per year

Some critical points concerning the AVHRR processing must be reflected that were in parts also noticed during the review process of the APOLLO snow mapping manuscript submitted to “Remote Sensing of Environment”. The accuracy assessment is concentrated on snow maps originating from NOAA-14. The question may arise why the selection of analysed Landsat scenes was not enlarged to cover additional NOAA satellites as well. The answer is simple: There are no Landsat scenes available for years before 1996 that meet the requirements: Low cloud cover while snow coverage is present. A second point is that the channel configuration of AVHRR changed from generation 2 (NOAA-7, -9, -11, -12, -14) to 3 (NOAA-15 and afterwards). Channel 3A was introduced with NOAA-15, providing measurements in the MIR region of the spectrum around 1.61 µm (see Table 4.1) instead of the channel 3B (collecting data at ~ 3.7 µm). The new configuration does not affect the snow cover delineation since the reflective part of channel 3B is calculated within APOLLO. This calculation is just not needed after the introduction of AVHRR generation 3, so APOLLO omits this step. Additionally and because data from NOAA-15 was not available anyway, data from generation 3 satellites are not included in the presented thesis. All data incorporated in this study are therefore processed relying on the measurements from the same spectrum.

Some aspects about the APOLLO snow cover processing and accuracy assessment deserve further discussion: Though it was initially intended to process a continuous time series of daily snow cover data since 1986, several problems occurred that could not completely be solved: Only ~ 75% (20,300) of the acquired AVHRR scenes could be processed (see Figure 6.1). The remaining ~ 25% were night-time observations or damaged scenes. Therefore, the total number of valid AVHRR overpasses stays below 900 per year before 1991. For 1991, where 1,500 raw scenes were available, only 48% could be processed due to an extensive amount of invalid observations. Thus, the years before 1992 are characterized by data gaps especially in the northern parts of Kazakhstan. The area will be marked in red in the snow cover product section 6.2 (Figure 6.11, Figure 6.23, and Figure 6.34). Figure 6.2 and Figure 6.3 illustrate that the availability of clear-sky observations differs significantly between single years and regions: Southern Uzbekistan and Turkmenistan stand out due to considerably more data than the northern parts of Kazakhstan and the mountainous regions. The cloud pattern in the MODIS data (Figure 5.2) already suggested this behavior, but the magnitude of data gaps especially in the years before 1992 exceeds the cloud-induced gaps in the MODIS products considerably. Many observations are missing from the data archive. It appears that the reason for the relatively low number of available AVHRR scenes arises from the fact that overpasses for these regions have never been stored in an archive. No AVHRR receiving station was operational for Central Asia during that time and the LAC data for northern Kazakhstan, from which only 10 minutes can be stored aboard the satellite, was perhaps of less inter-

est to the providers of the data archives than e.g. the regions at the border to Afghanistan or China, where sufficient data is available. If facing the choice between northern Kazakhstan and Russia on the one hand and Afghanistan, Pakistan, and India on the other hand, the decision may have been made in favor of the southern region more often. In 1994, the malfunction of NOAA-11 caused a loss of data after September, hindering a processing of snow cover data. Therefore, SCD and SCS cannot be produced for the hydrological year 1994/1995 while only SCM is unaffected. Although NOAA-12 was operational since 1991, no data is available from this sensor. The reason may be a similar as for the years before 1991 but unfortunately, no information about the true circumstances are provided.

Despite all the existing data gaps, snow cover time series were successfully produced for Central Asia. The accuracy of these snow cover data sets (APOLLO PPL1) is assessed comparing the AVHRR with Landsat snow maps. Cloud covered pixels cause a huge underestimation of snow (Table 6.1). It is not absolutely clear whether this underestimation arises from classification errors or true clouds that may have been present during the observation time of the respective NOAA satellite (which is different than for the Landsat satellite). It is therefore difficult to estimate the actual accuracy. If cloud covered pixels are excluded from the assessment, the clear-sky accuracy reaches 90.4% - only marginally less than the clear-sky accuracy of the MODIS daily snow cover products MOD10A1 (~ 94%). The problem that clouds considerably limit the ability to map snow cover on a daily basis becomes obvious from the statistics in Table 6.1 and Table 6.2. The same is true for the operational MODIS products: Up to 70% of the pixels are contaminated by clouds during January (Figure 5.3), while mean cloud cover percentage can reach more than 50% for north-western Kazakhstan (Figure 5.2). It is impossible to estimate the number of snow covered days per year from these input data – especially due to the fact that cloud coverage concentrates on winter and spring months (Figure 5.3). This was also stated in section 5.2. Table 6.3 and 6.5 show the same: Huge underestimation of snow coverage due to clouds in both products: APOLLO PPL1 and MOD10A1. The cloud reduction scheme (Figure 5.4) was therefore established to estimate the snow cover status below all cloud covered pixels of the time series. Every snow cover product from both sensors – AVHRR and MODIS – was processed with the cloud reduction scheme, providing daily, cloud-free snow cover information for whole Central Asia.

The accuracy of the cloud reduction scheme is difficult to assess for Central Asia because in situ data is only sparsely available for the years before 1995. Fortunately, AVHRR was operational (with data gaps in the North) during this time, making a comparison possible. In situ data from climate stations is generally a good source for daily snow cover information because it is independent from cloud coverage. Thus, the available station data from HSDSD

was exploited for accuracy assessment though number and time span of measurements is relatively small. The comparison between APOLLO PPL3 and the few HSDSD station data revealed that the mean deviation of SCD accounts for 5 – 18 days. The number of useable stations, however, varied between 19 and 32. Given the size of ~ 4,000,000 km², 32 stations (where none is present in the higher mountain regions) is negligible. Results from this comparison are included for the sake of completeness only. The results from the prepared snow cover parameters will be discussed in the following sub chapters of section 6.

6.2 Snow cover parameters for Central Asia

Snow cover parameters include SCD, SCS, SCM, and SCI. They are derived for each hydrological year between 1986/1987 and 2011/2012 (with SCS also for 2012/2013) and constitute the basis for the subsequent discussions. The cloud free daily snow cover products APOLLO PPL3 and the reprocessed MOD10A1/MYD10A1 time series were used as data sources for equations 8 to 11 (section 3.4.2). Unfortunately, snow cover parameters for the hydrological year of 1994/1995 are incomplete because of the missing AVHRR data between September 1994 and January 1995. This affects all derived parameters. Additionally, numerous observations for the years from 1986 to 1992 are missing for the northern part of Central Asia (see Figure 6.2 and Figure 6.3). These data gaps do not affect the mountainous regions in the South nor the hydrological catchments of Amu Darya, Syr Darya, or Lake Balkhash. The following subsections will illustrate each snow cover parameter individually, comprising mean results as well as overviews of each respective year. The results from the MODIS time series (2000 to 2011) have been published within International Journal of Remote Sensing (Dietz et al., 2013). Some of the figures and findings from this publication also found their way to the presented thesis, though the results here comprise a longer time series. An indirect accuracy assessment was also accomplished and published within this article. The results are included in section 6.3. At the end of section 6, an outlook comprising several possible applications of the presented results and findings is added. This outlook provides an insight into the many different opportunities that are given by facilitating the presented results, though it is still far from being complete. Snow cover parameters in medium resolution and derived from daily data offer a wide choice of possible applications on local, regional, and even continental scales. The discussion of each parameter is appended directly to the respective sub-sections.

6.2.1 Snow Cover Duration

SCD was calculated using equation 8 from section 3.4.2 for each hydrological year from 1986/1987 to 2011/2012. 26 single data sets of SCD were prepared for the presented thesis. They are included in Figure 6.11, Figure 6.12, and Figure 6.13. The effect of the malfunction of NOAA-11 in 1994 is clearly visible in Figure 6.12. Based on the single SCD results, 10-year average SCDs are calculated for each decade, beginning with 1986/1987 to 1998/1999 (excluding 1994/1995) and ending with 2002/2003 to 2011/2012. These 10-year averages can be used to analyse single season SCD in comparison to the mean conditions as will be shown in section 6.4.

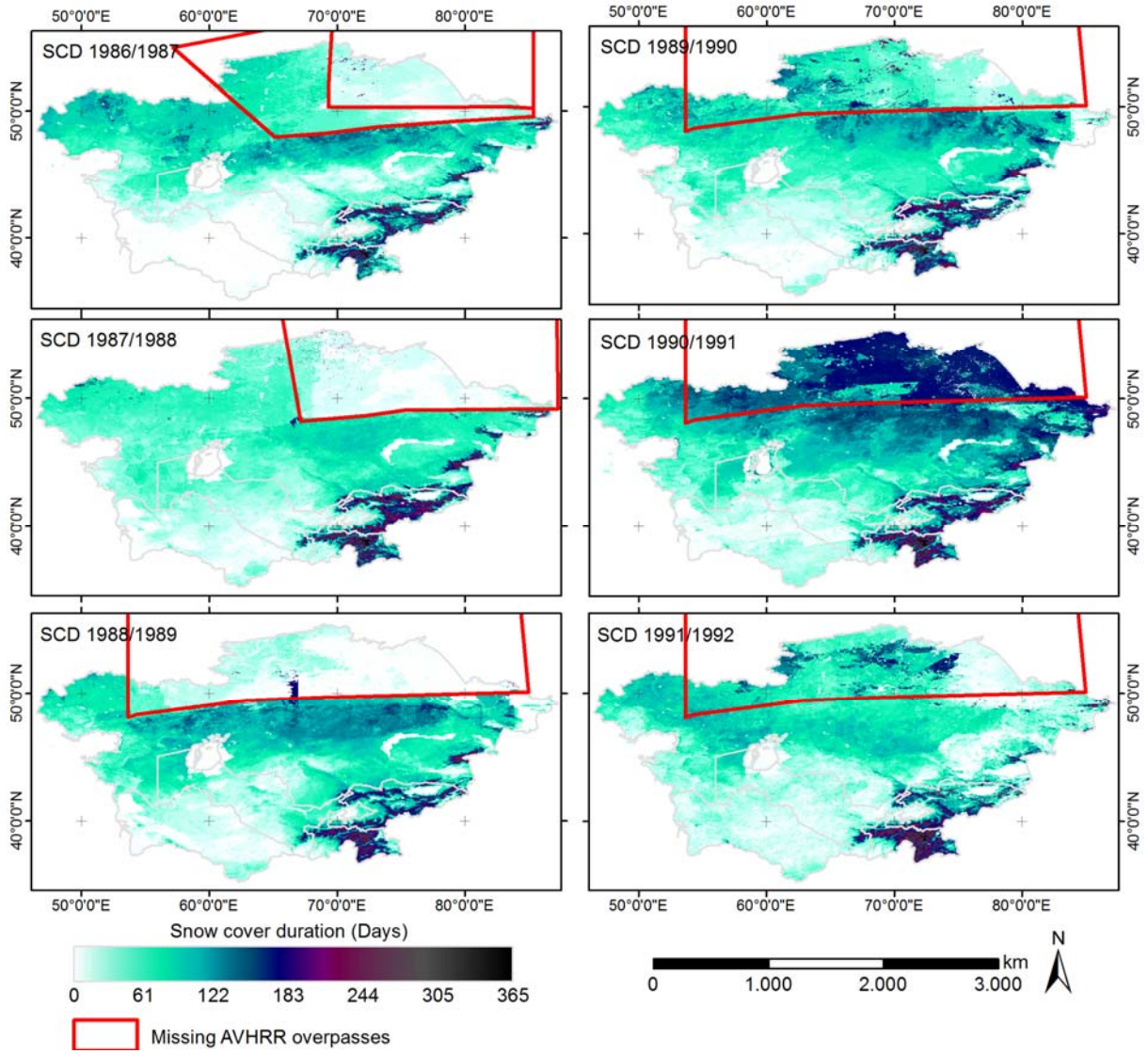

Figure 6.11: SCD for hydrological years 1986/1987 to 1991/1992

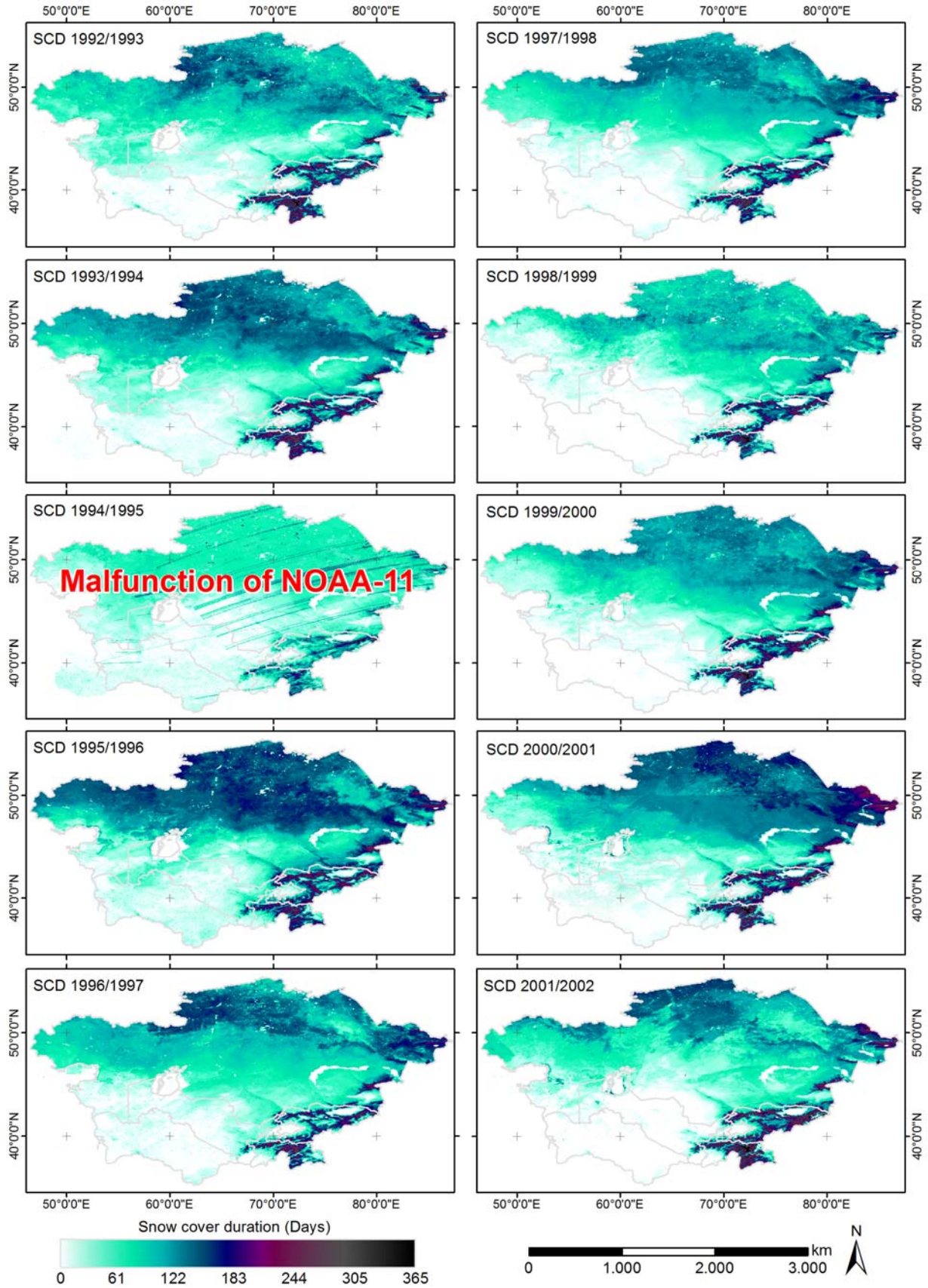

Figure 6.12: SCD for hydrological years 1992/1993 to 2001/2002

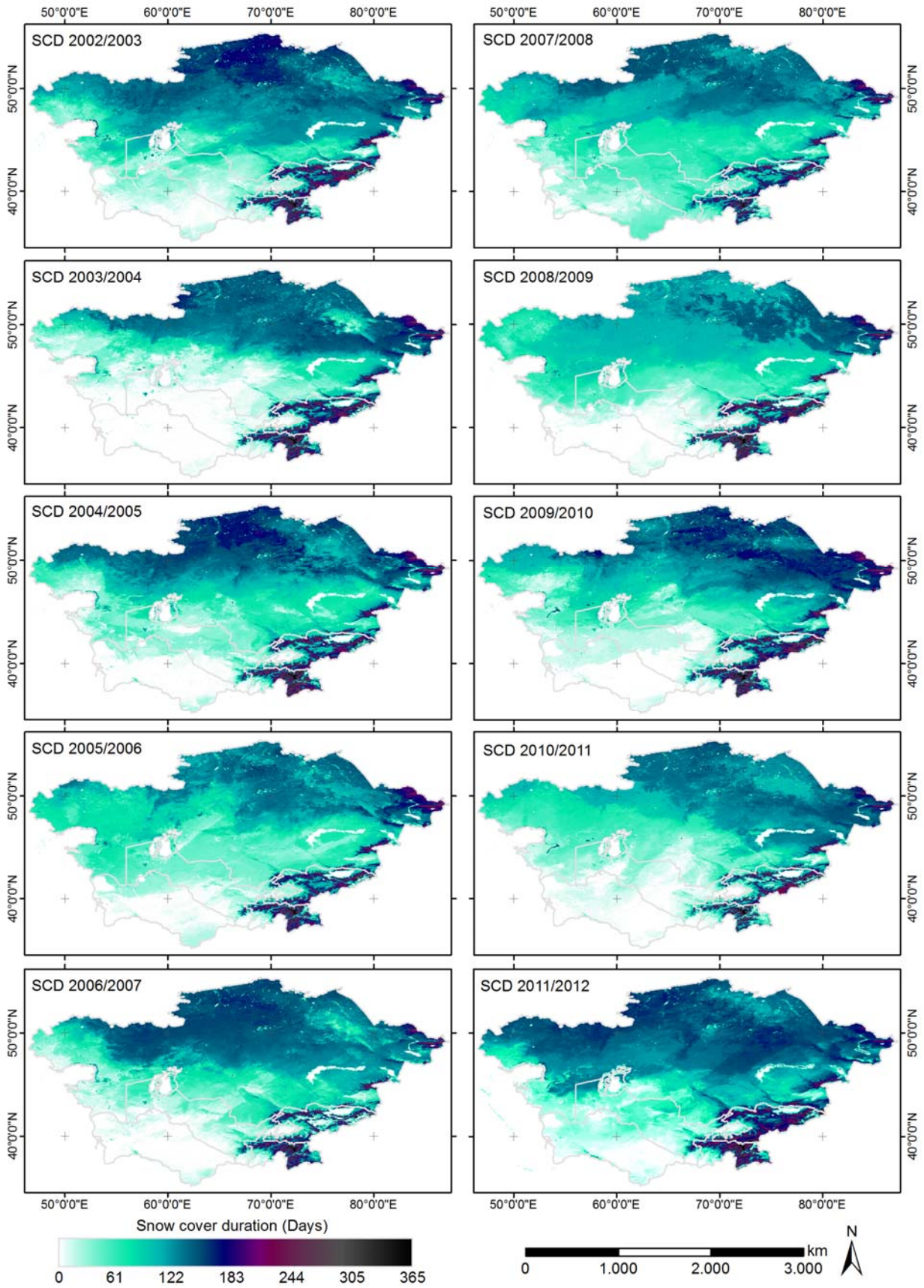

Figure 6.13: SCD for hydrological years 2002/2003 to 2011/2012 (in parts adopted from Dietz et al. (2013))

Additionally, the 10-year averages can be utilized as input parameters for trend calculations. The northern regions with missing observation are excluded from such analyses for the first 6 years as well as 1994/1995. Two examples for 10-year averages are illustrated in Figure 6.14 (1992/1993 to 2001/2002) and Figure 6.15 (2002/2003 to 2011/2012). An example for a trend calculation of SCD will be presented in section 6.4.

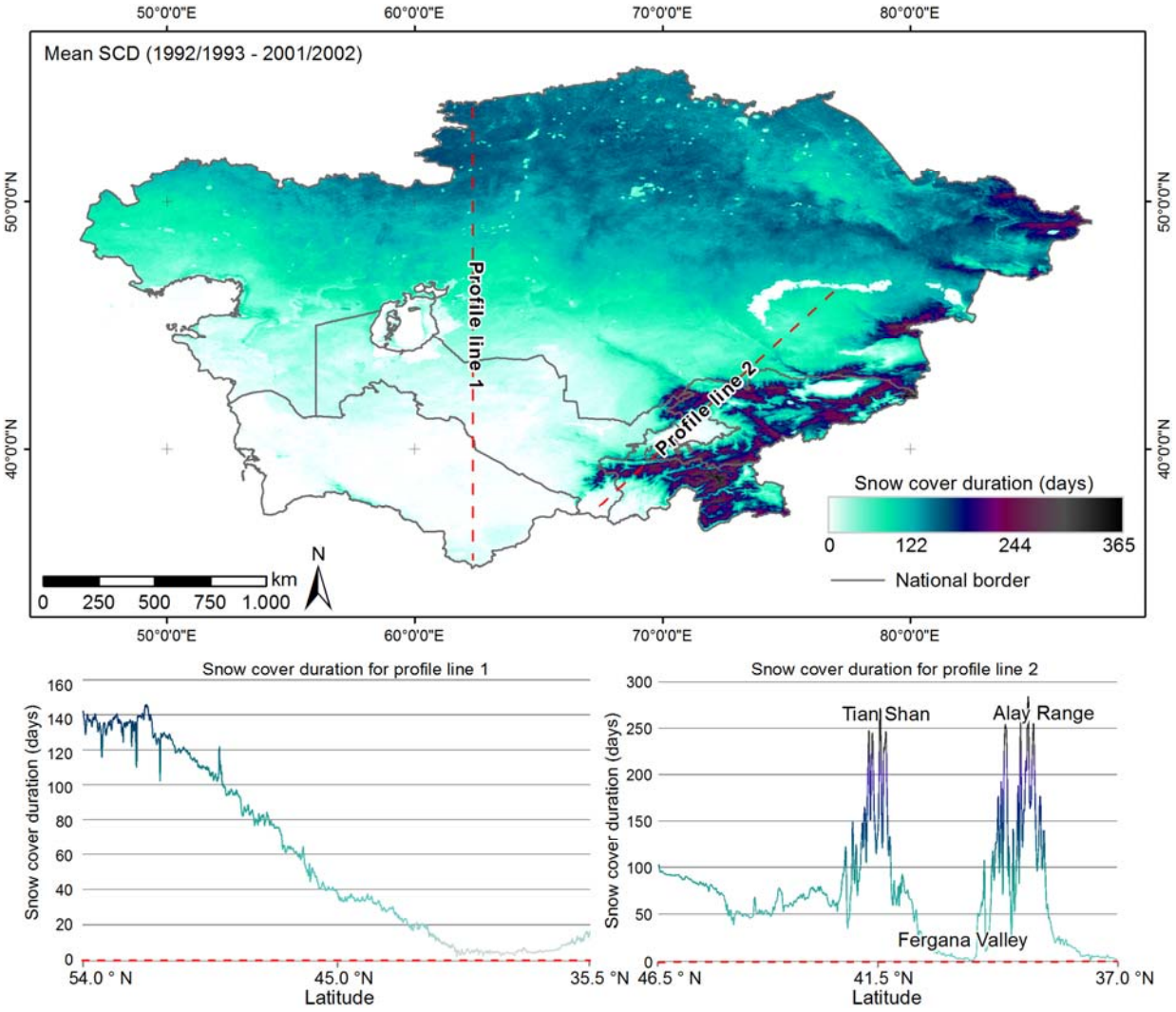

Figure 6.14: Mean SCD for the years 1992/1993 to 2001/2002

Profile lines are prepared in Figure 6.14 and Figure 6.15, transecting the mountainous regions in the South-east (profile line 2) as well as the plains in Turkmenistan, Uzbekistan, and Kazakhstan (profile line 1). The same profile lines will be provided for additional results in the upcoming sections, allowing an easy comparison of changes between snow cover parameters of different years or decades.

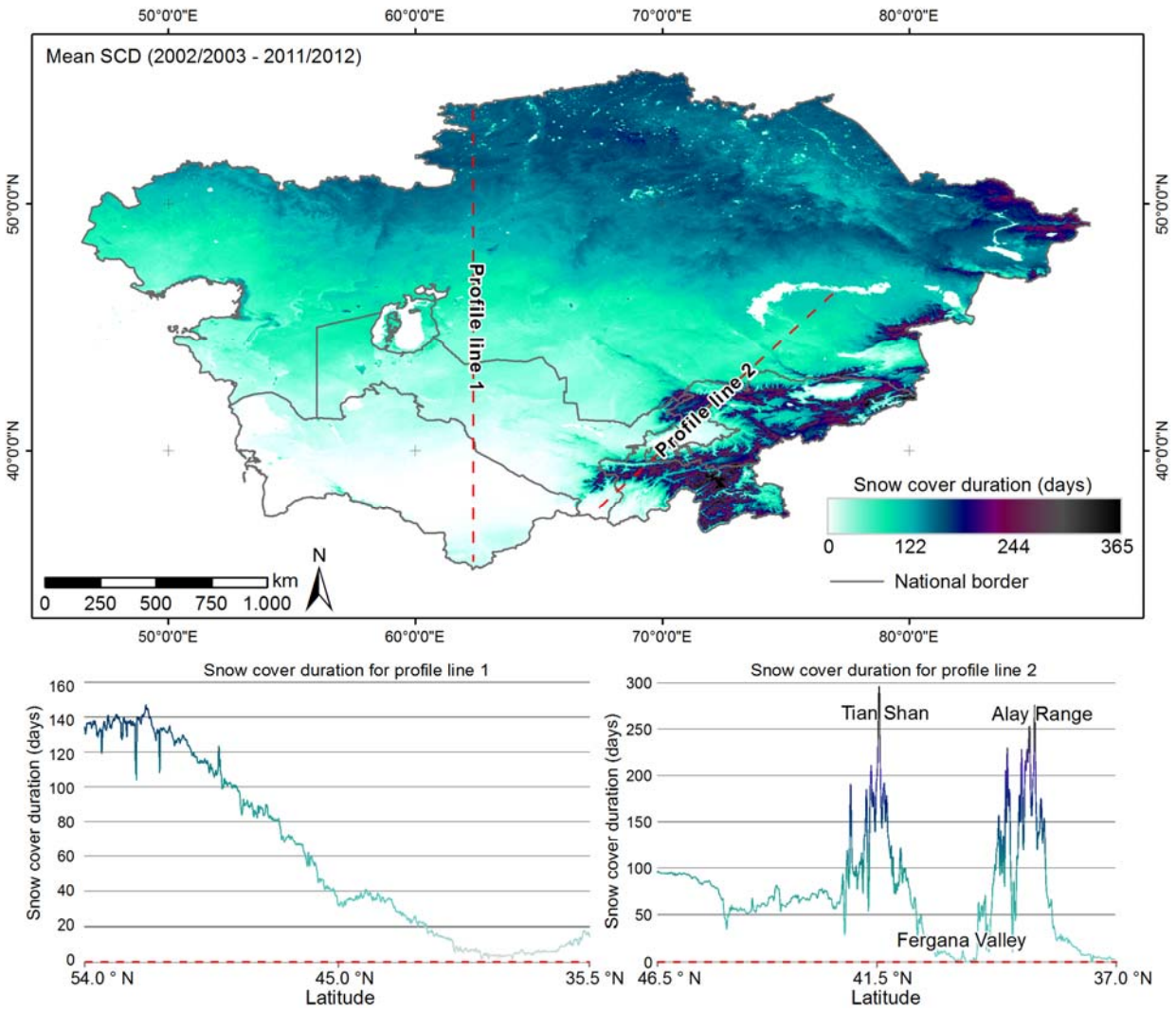

Figure 6.15: Mean SCD for the years 2002/2003 to 2011/2012 (modified from Dietz et al. (2013)).

The mean SCDs and single year SCDs are the first results for the presented thesis. They give a comprehensive overview of Central Asian snow cover conditions for 26 years, which is a unique data set with regards to the provided resolution and amount of utilized input data. The profile lines indicate a clear dependence between SCD and both latitude and elevation.

The variability of SCD can be analysed by calculating the standard deviation of SCD over a given time span. Figure 6.16 and 6.17 give examples for the standard deviation of SCD between 1992/1993 and 2001/2002 and between 2002/2003 and 2011/2012, respectively (equal time spans as SCD in Figure 6.14 and 6.15). Profile lines 1 and 2 are again included in these figures, allowing comparisons with e.g. Figure 6.14 and 6.15. The highest standard deviation exists in the mountainous regions of Pamir and southern Tian Shan mountains.

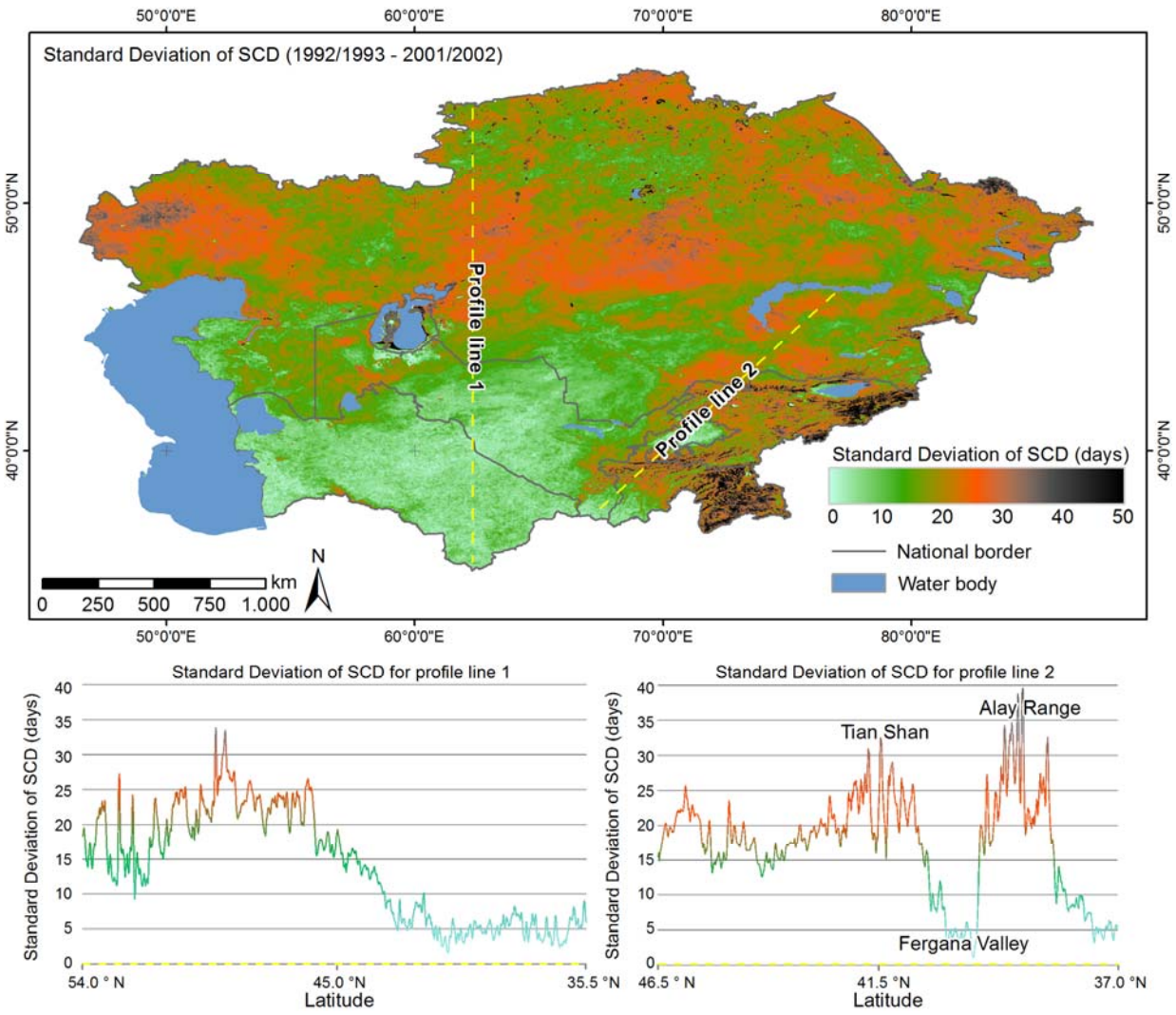

Figure 6.16: Standard Deviation of SCD between 1992/1993 and 2001/2002

The areas around the Aral Sea or the small lake in the East of the Caspian Sea (~45°0'0"N, 54°0'0" E) seem highly variable, too. Regions in the direct proximity of variable water bodies must be treated carefully as already mentioned in section 6.1. SCD is characterized by high variability especially in the central parts of the study area (~ 43° N to 49° N) and in some of the mountainous regions. The exact locations of pixels with high variability are visible from Figure 6.16 and 6.17. The variability in the central regions was not as pronounced between 1992/1993 and 2001/2002 suggesting that possible changes in snow cover characteristics slowly started after 2002/2003. The region with high variability in SCD expanded especially towards the South, while in the North the spatial extent of unstable snow cover conditions nearly stayed the same between 1992/1993 and 2011/2012. Maximum Standard Deviation also increased after 2001/2002, suggesting that the intensity of SCD variability also increased since the beginning of the third millennium.

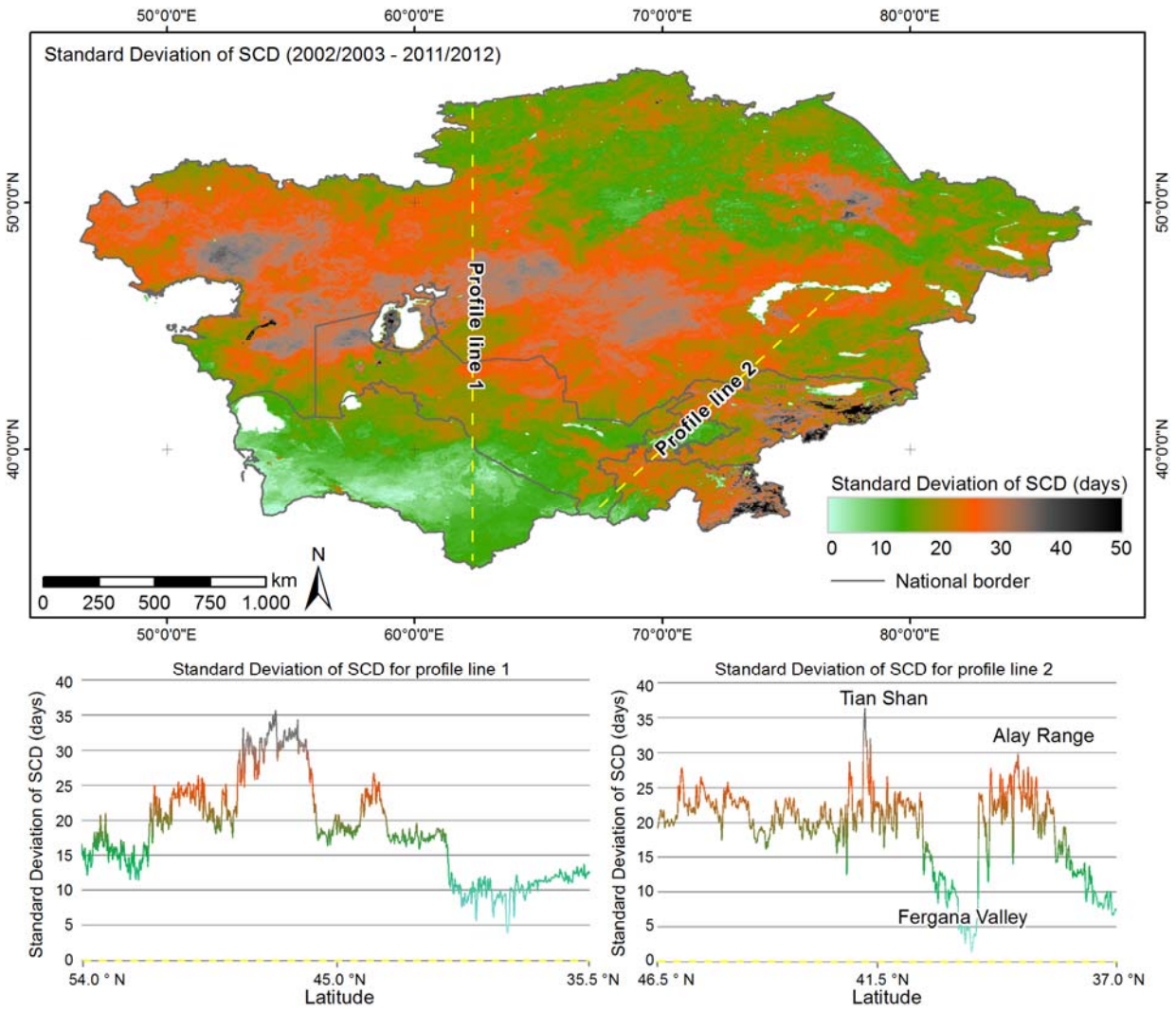

Figure 6.17: Standard Deviation of SCD between 2002/2003 and 2011/2012

Maps of SCD are useful for giving a basic overview about the prevailing snow cover characteristics but against the background of hydrological applications, a catchment-based chart of seasonal SCD is desirable. Therefore, the mean SCD per sub-catchment (Figure 2.2) and year is extracted from the single SCD results. This was accomplished by calculating the mean SCD based on all pixels falling within the area of a sub-catchment. The total number of sub-catchments accounts for 39. These catchments are aggregated into three categories: Up-stream-, Intermediate-, and Downstream-catchments as already highlighted in section 2.1 and Table 2.1, which contains an overview of all entities and their respective affiliations. Figure 6.18 includes the mean SCD per sub-catchment category and year, subdivided into the three major catchments of Amu Darya, Syr Darya, and Lake Balkhash:

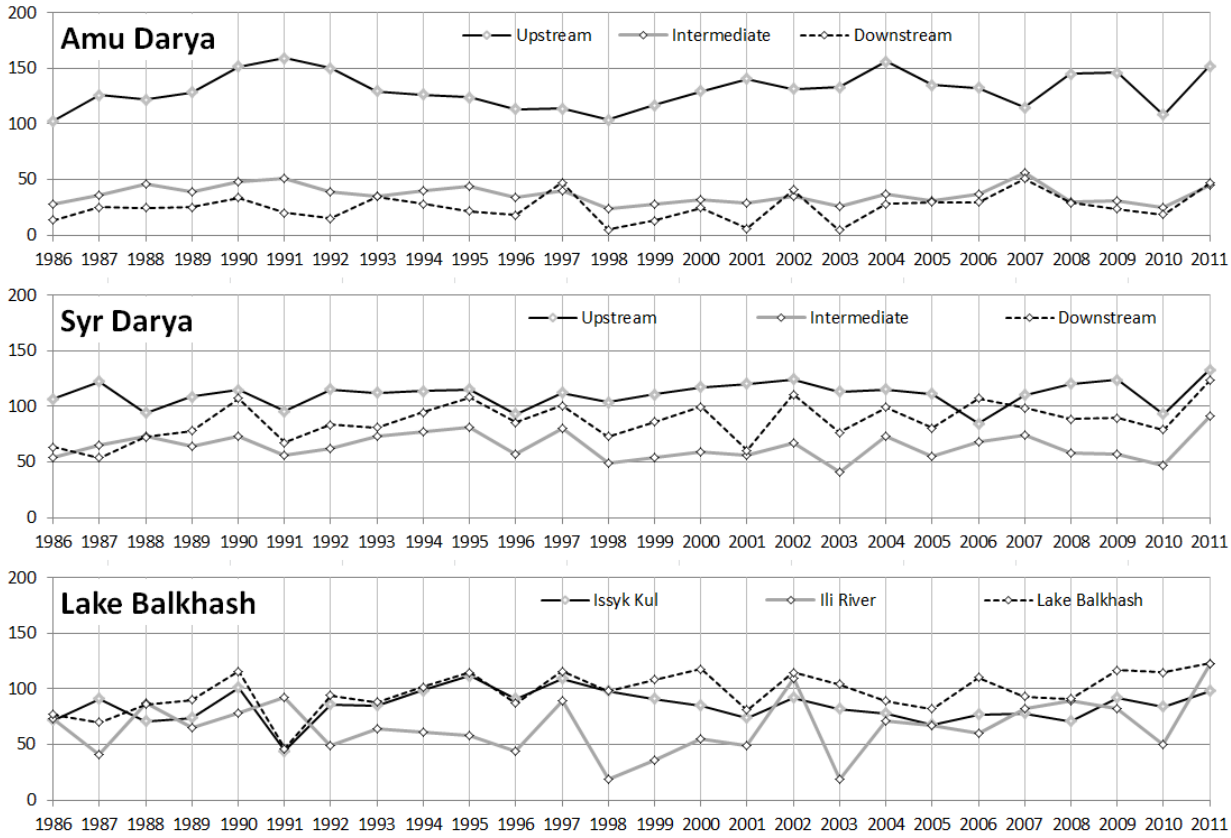

Figure 6.18: SCD for Upstream-, Intermediate-, and Downstream catchments

The vertical axes refer to the mean SCD (in days) while the horizontal axes represent the respective year. Years 1986 to 1991 may be biased for the downstream sub-catchments of Syr Darya River because AVHRR data before 1992 is partially missing for these regions. Values for 1994 are averaged from 1993 and 1995 for all charts in order to avoid data gaps in the time series. However, since SCD can develop very variable even between consecutive years, the results for 1994 should be treated carefully. Figure 6.19 illustrates the mean SCD per mountain catchment for three different time spans: 1986 to 1993, 1994 (actually not 1994 but the mean from 1993 and 1995) to 2003, and 2004 to 2011. This figure allows for an estimation of snow cover development on a sub-catchment scale. The difference between Figure 6.18 and Figure 6.19 is that in Figure 6.18, multiple catchments are aggregated to a single variable for each year. In Figure 6.19, time is aggregated but the spatial entity is conserved. Depending on the research question, both illustrations contain useful information.

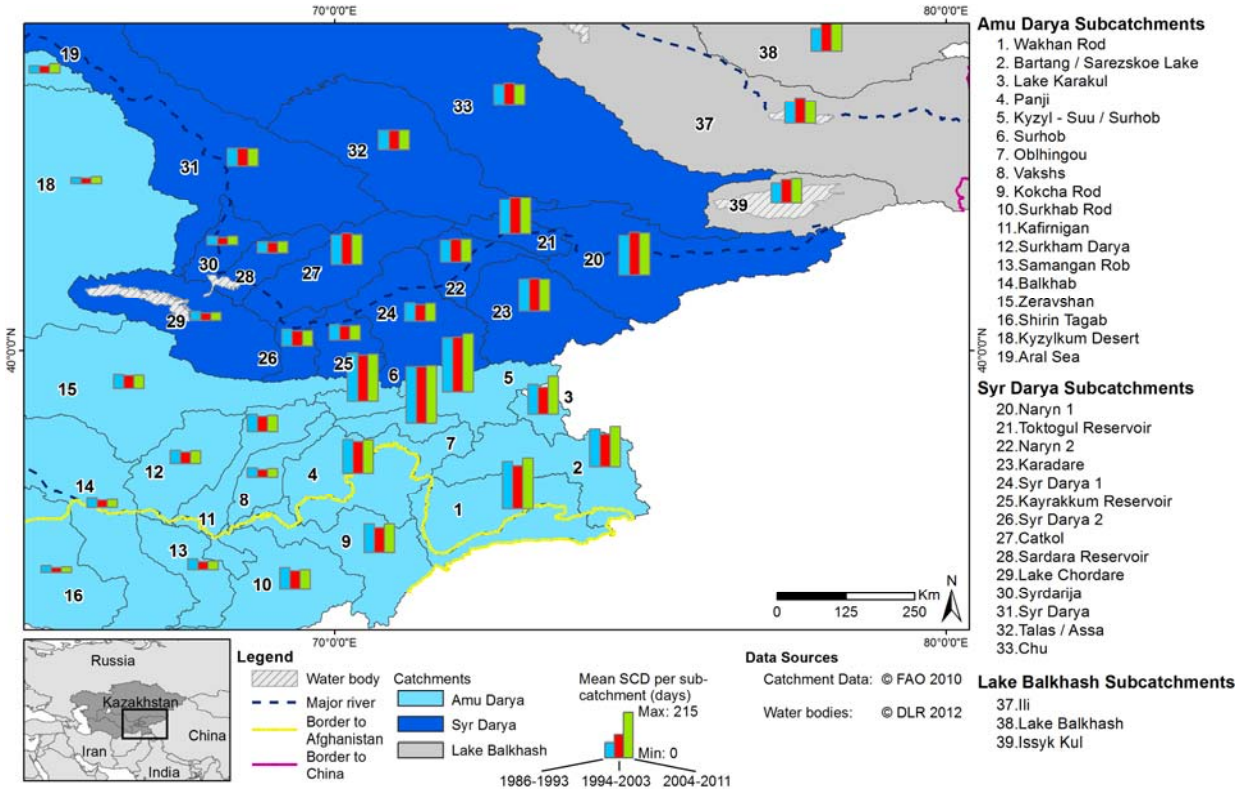

Figure 6.19: Mean SCD per mountain catchment and time span

Figure 6.18 and 6.19 are based on a sub-catchment scale. The catchments constitute closed hydrological entities but differ in size, elevation range, and aspect (see Figure 2.2 and Table 2.1). To identify the effect of changing elevation or aspect on SCD, two additional analyses were derived: Figure 6.20 depicts the SCD per year and elevation zone:

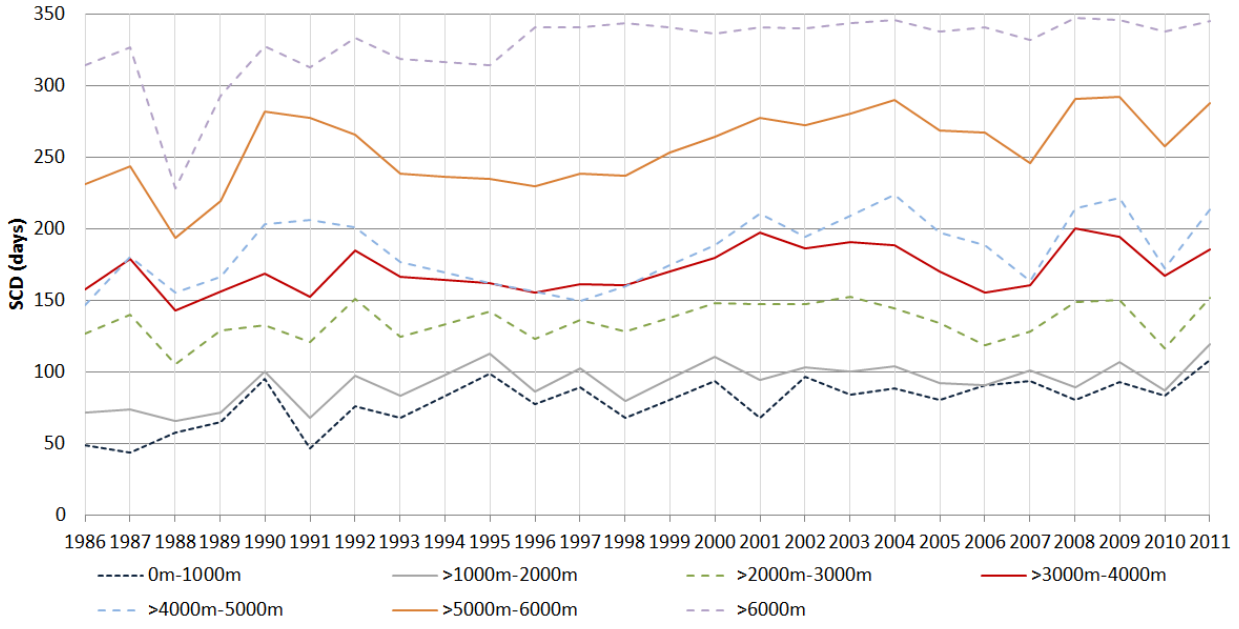

Figure 6.20: SCD per elevation zone and year

Data for 1994 was again averaged from 1993 and 1995 to avoid data gaps in the time series. Results for elevation zone 0 m - 1,000 m and the years 1986 to 1991 in Figure 6.20 are prone to considerable underestimation of SCD due to the missing data in northern Kazakhstan.

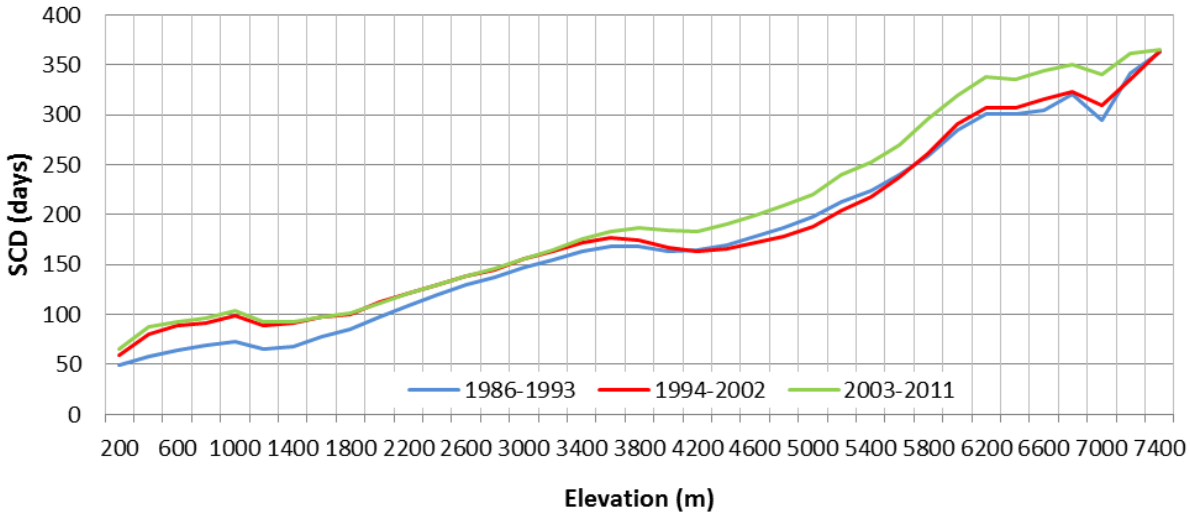

Figure 6.21: SCD as a function of elevation for three different periods

SCD as a function of elevation was also calculated based on the mean SCD for three different periods: 1986-1993, 1994-2002, and 2003-2011. The results from this analysis are illustrated in Figure 6.21. The relatively high variability in SCD for elevation zones above 6,000 m may evolve from the fact that only very few pixels are present in these regions. For AVHRR, only 414 pixels are situated in elevations above 6,000 m (MODIS: 894). This affects all analyses based on elevation (Figure 6.20 as well as Figure 6.21). The trough-like feature between ~3,800 and 4,600 m is eye-catching. SCD increases linearly below and above this zone. Possible reasons for the unusual behaviour within this elevation zone (which will also be present for further results presented in the very section) will be discussed in section 6.2.5.

Slope orientation is another important factor with regards to SCD. This was already discussed in section 2.2. Therefore, SCD is also analysed as a function of slope orientation. Again, different elevation zones are introduced to allow for a distinct differentiation of possible effects originating from elevation. The result of this computation is given in Figure 6.22 and Table 6.7. Only regions above 1,000 m elevation are considered since pixels located in the flat plains may – though characterized by a certain slope orientation – distort the results. The reason is that in the plains, the latitude of a location has more influence on the SCD than the topography. This was already illustrated in Figure 6.15, profile line 1.

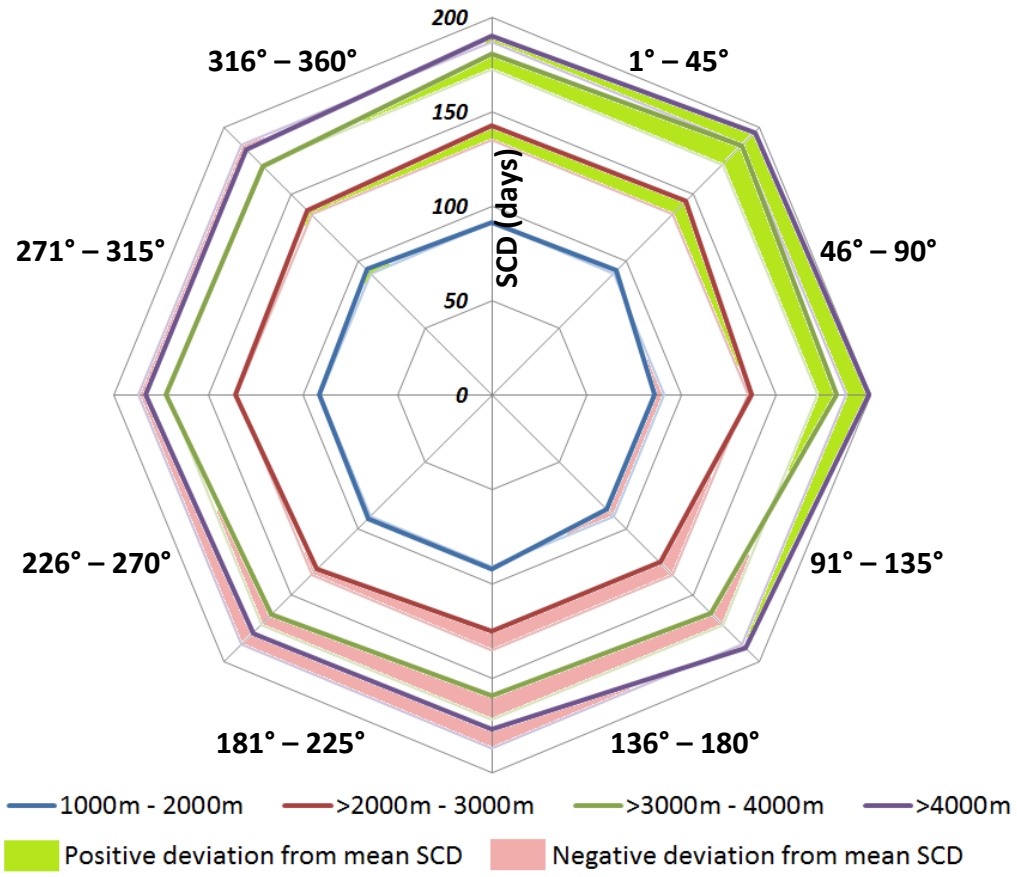

Figure 6.22: Mean SCD as a function of slope orientation and elevation

Table 6.7: Mean SCD per elevation zone and slope aspect (days)

Aspect	1000 to 2000 m	2000 to 3000 m	3000 to 4000 m	> 4000 m
1°-45°	91.1	142.7	180.5	189.8
46°-90°	93.1	145.0	186.6	196.5
91°-135°	85.9	137.0	182.0	199.2
136°-180°	85.5	125.4	163.3	189.2
181°-225°	92.0	124.9	159.3	176.8
226°-270°	92.8	130.7	164.8	178.6
271°-315°	91.5	135.5	172.3	183.1
316°-360°	93.8	137.9	171.0	184.1
Mean	**90.7**	**134.9**	**172.5**	**187.1**
StDev.	**3.0**	**6.9**	**9.2**	**7.5**

The SCD on southern slopes (136°-180°, 181°-225°, 226°-270° in Figure 6.22) is consistently shorter than on northern slopes. This result corresponds to the suggestions given by Severskiy et al. (2000b). The difference is greater in higher elevations (~23 days difference in SCD between northern and southern slopes for elevations above 4,000 m in contrast to only ~8 days between 1,000 m and 2,000 m elevation). The standard deviation of SCD for the different elevation zones is only included in Table 6.7. It equals between 3 days for the lowest elevations and 9 days for the zone between 3,000 and 4,000 m.

6.2.2 Snow Cover Start

Snow cover start (SCS) is calculated using equation 9 in section 3.4.2 for each hydrological year from 1986/1987 to 2012/2013. Settings for the presented processing are described in section 5.3. The results comprise similar products as for SCD in section 6.2.1. Single SCS maps are included in Figure 6.23, 6.24, and 6.25.

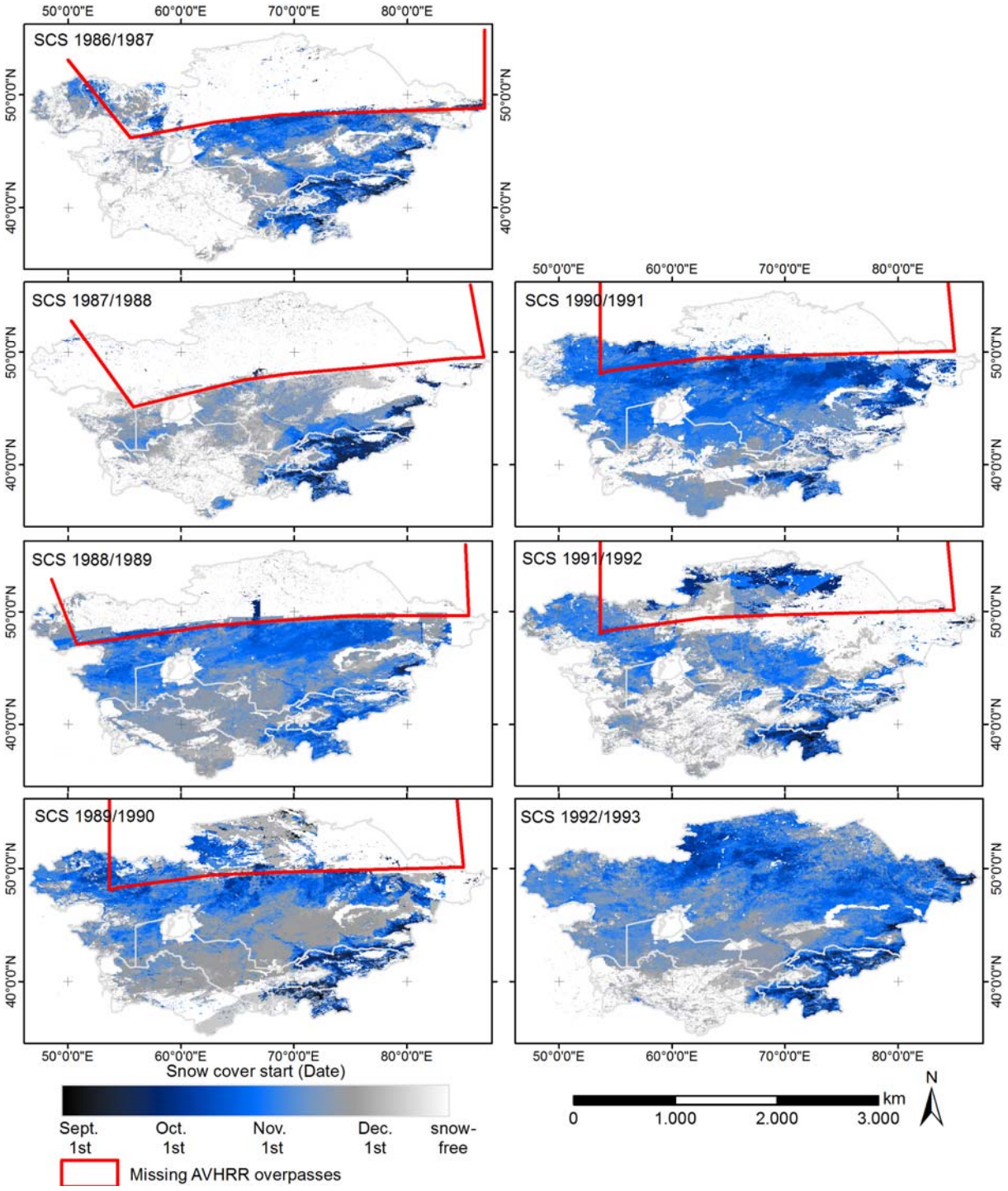

Figure 6.23: SCS for hydrological years 1986/1987 to 1992/1993

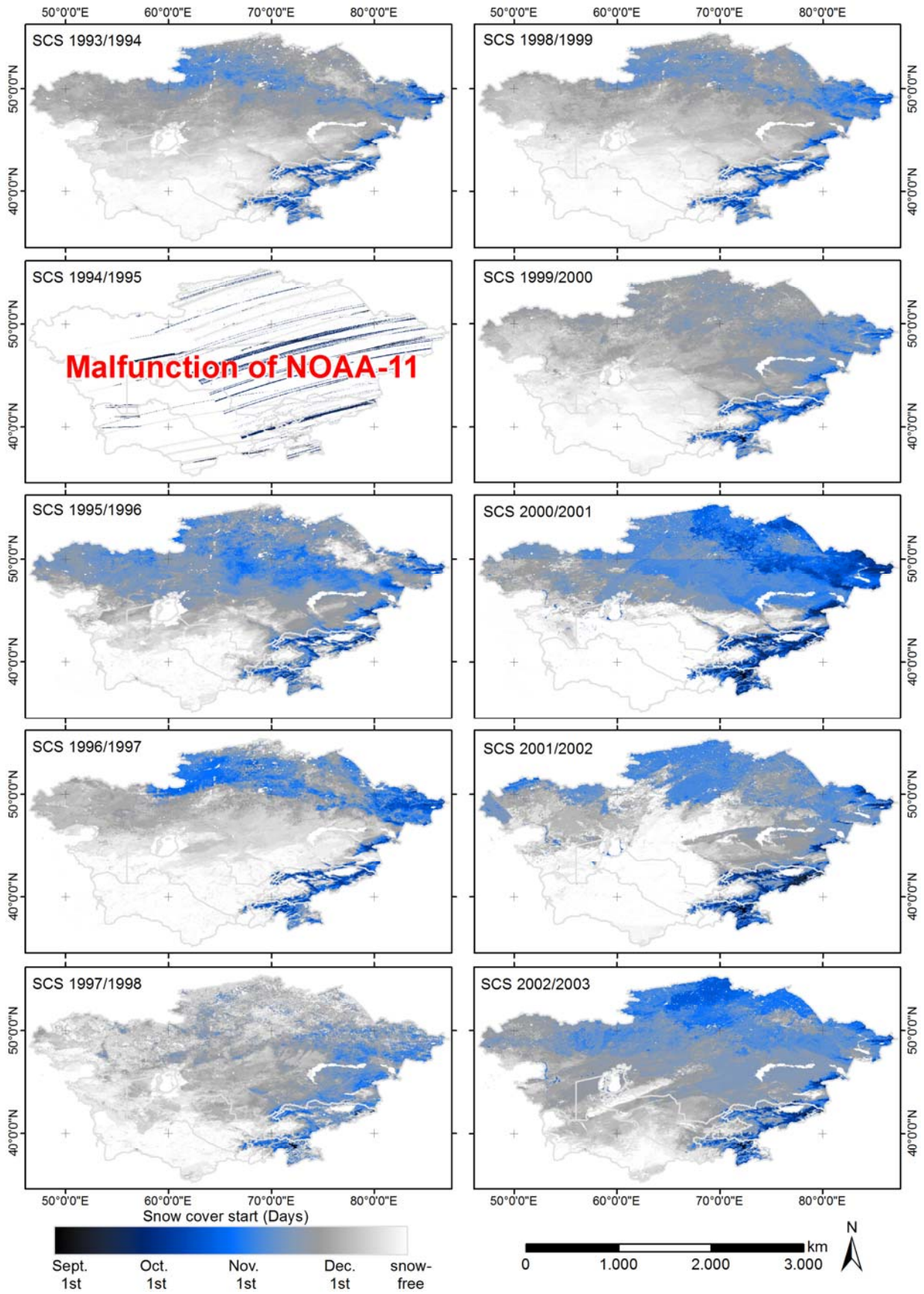

Figure 6.24: SCS for hydrological years 1993/1994 to 2002/2003 (in parts adopted from Dietz et al. (2013))

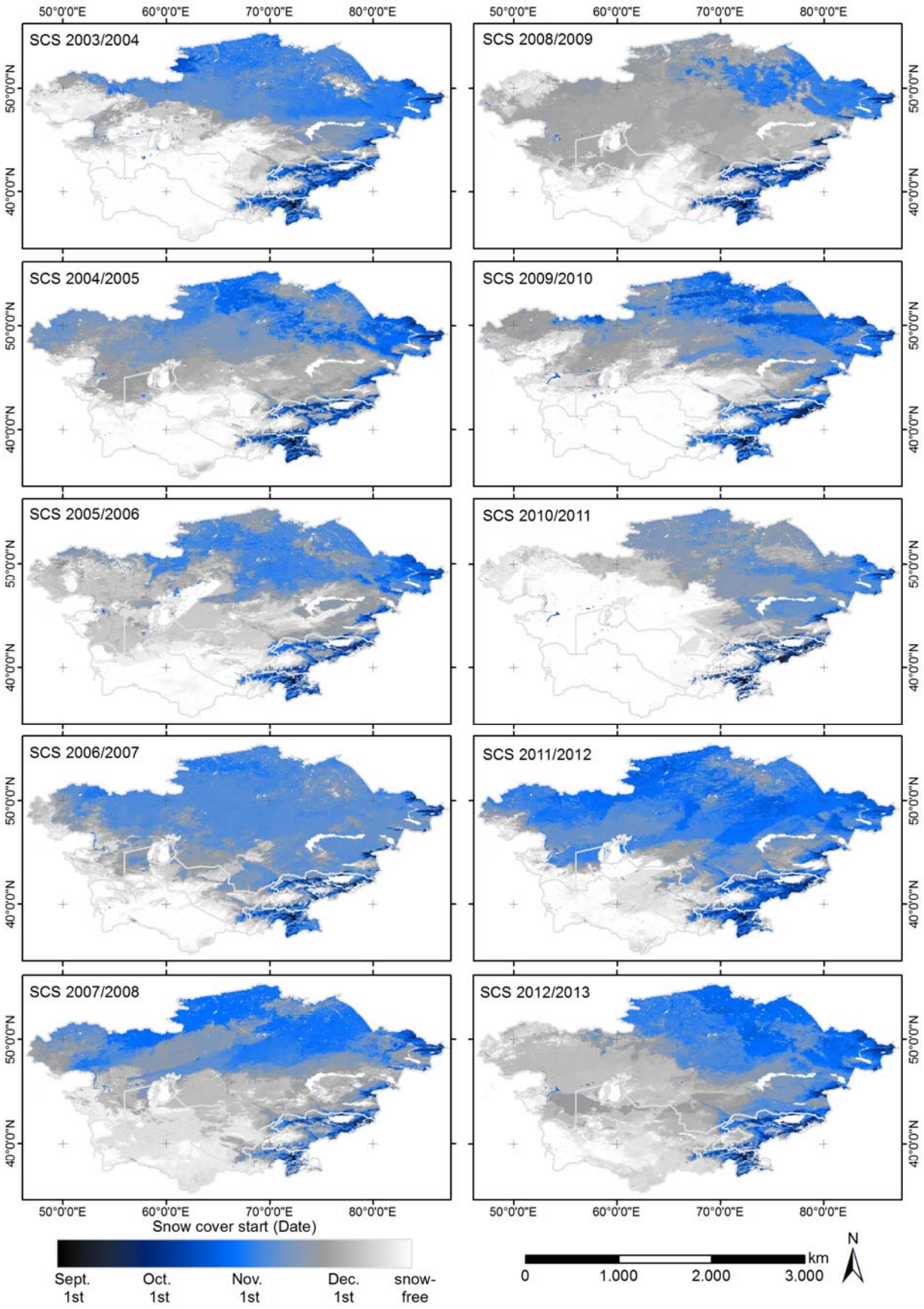

Figure 6.25: SCS for hydrological years 2003/2004 to 2012/2013 (in parts adopted from Dietz et al. (2013))

SCS results contain one more season (2012/2013) than SCD, SCM, and SCI. At the time of writing (and processing), the hydrological year of 2012/2013 was not completely finished, preventing from calculations of the latter parameters. Like SCD in section 6.2.1 so does SCS appear rather variable between single years. The mean SCS (Figure 6.26 for mean SCS between 1992/1993 and 2001/2002, Figure 6.27 for mean SCS between 2002/2003 and 2012/2013) is therefore better suited to describe the typical snow cover conditions during early snow season.

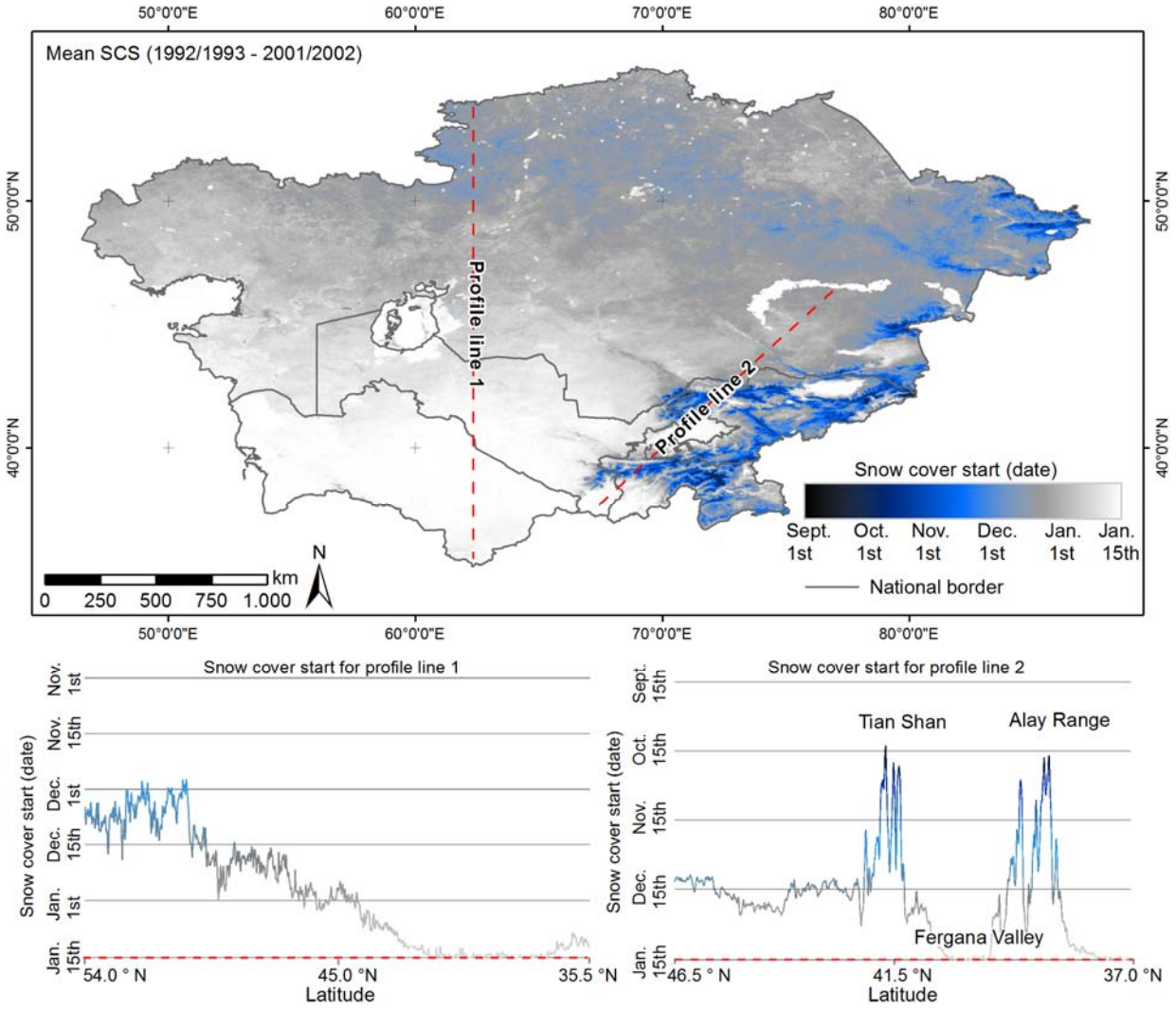

Figure 6.26: Mean SCS for the years 1992/1993 to 2001/2002

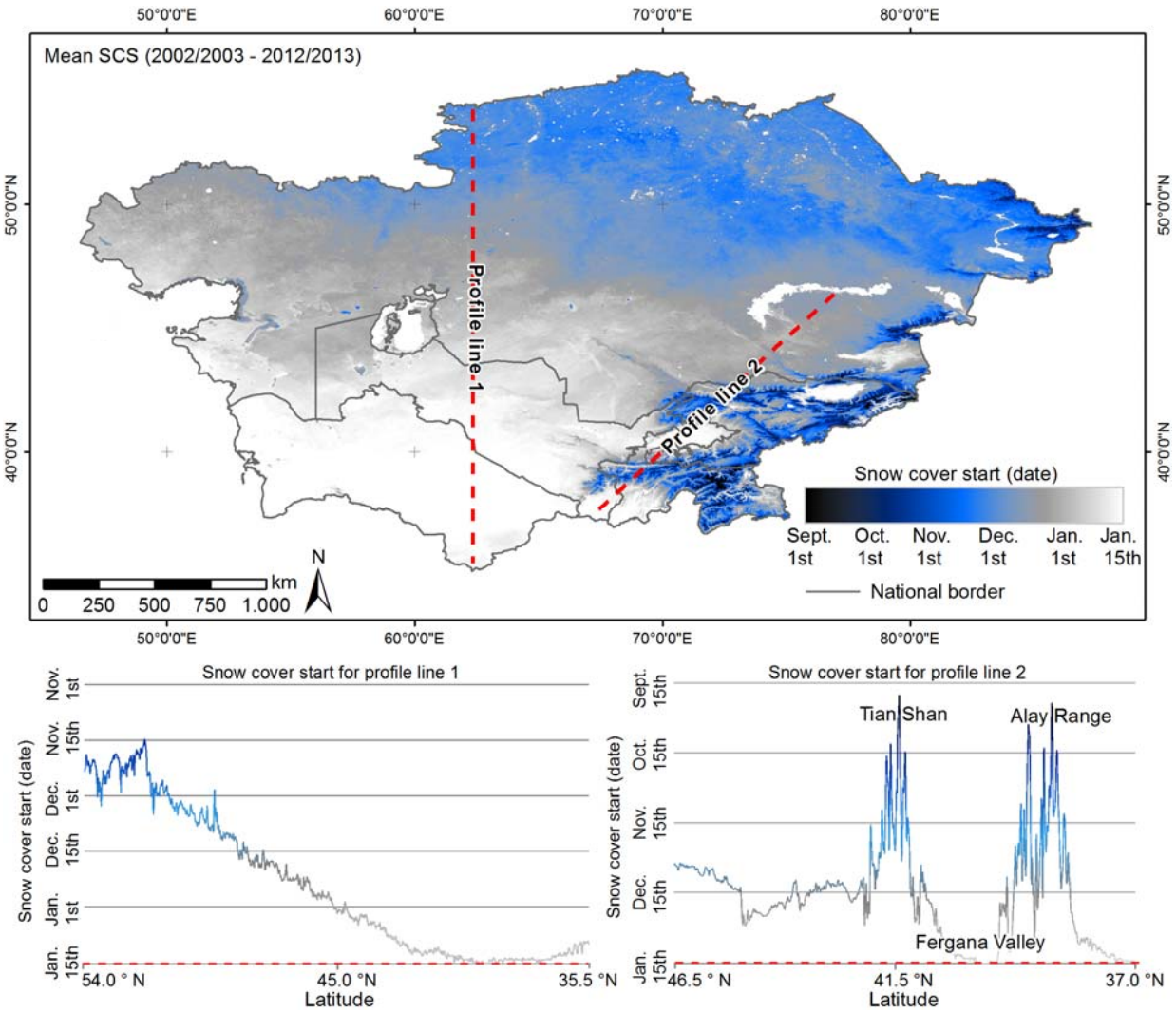

Figure 6.27: Mean SCS for the years 2002/2003 to 2012/2013

Profile lines 1 and 2 are again included in Figure 6.27. They follow the same paths as the respective lines in the SCD results and show similar patterns with a latitudinal dependence of SCS for the plains (profile line 1) and a strong influence of topography in mountainous regions (profile line 2). Snow cover starts during November in the northern plains of Kazakhstan (~54° N), extending southwards by around five days delay per degree latitude. The variability of SCS is again illustrated by calculating the standard deviation of SCS. The results are included in Figure 6.28 (1992/1993 to 2001/2002) and Figure 6.29 (2002/2003 to 2012/2013).

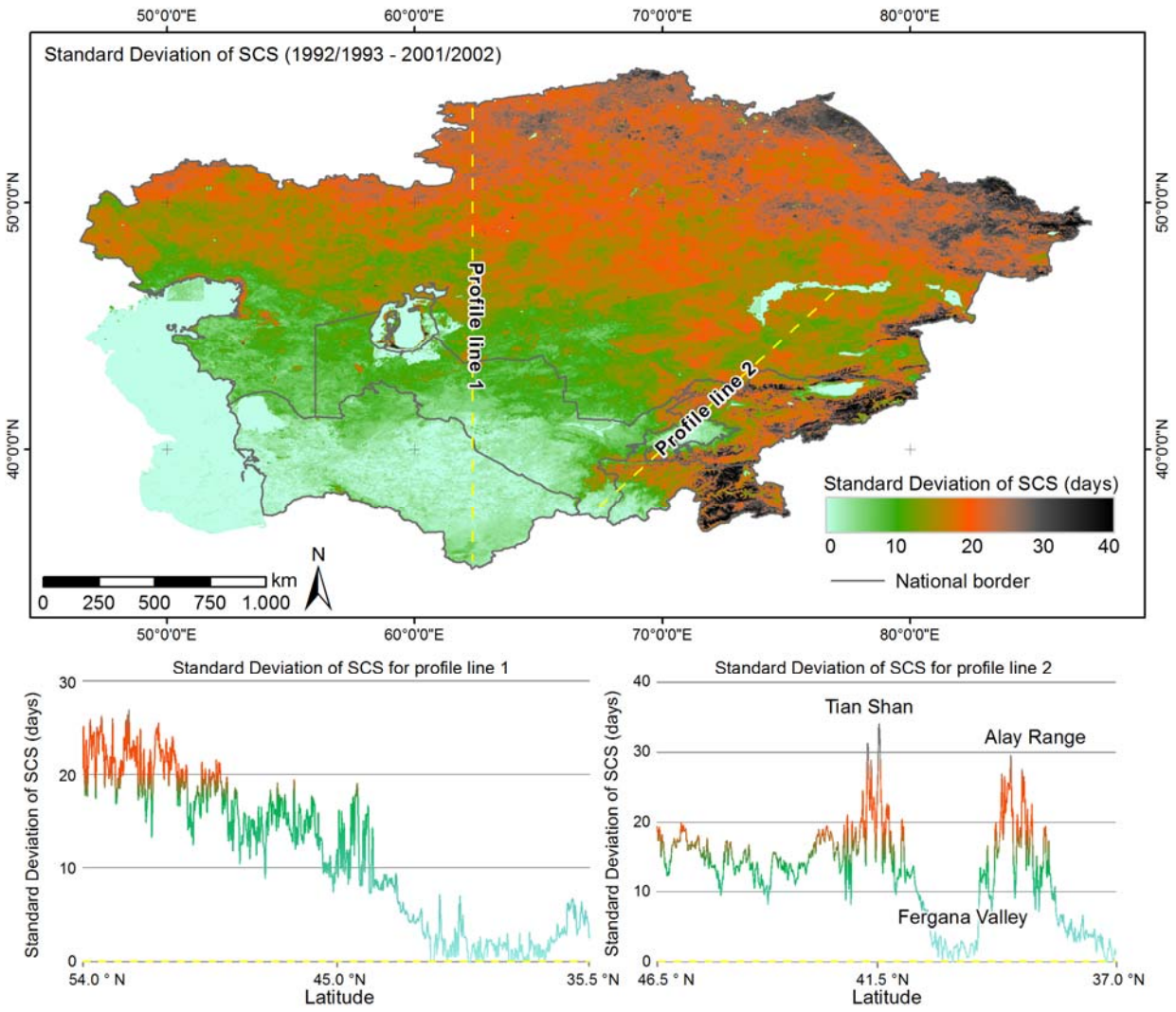

Figure 6.28: Standard Deviation of SCS between 1992/1993 and 2001/2002

The patterns of SCS standard deviation in Figure 6.29 are similar to the ones from the SCD standard deviation (Figure 6.17): Regions with high variability in SCD often show the same behaviour in SCS: This is true for the area northeast of the Caspian Sea as well as the small band between ~45 and 49°N, stretching from the Caspian Sea in the West to the Lake Balkhash in the East. Mountainous regions appear variable, too: Pamir and Tian Shan contain several patches with very high inter-annual SCS variability. Figure 6.30 illustrates the SCS per year and elevation zone (similar to SCD in Figure 6.20): Even the highest zones are affected by relatively high deviations in some years. Possible reasons for this behaviour will be discussed in section 6.2.5.

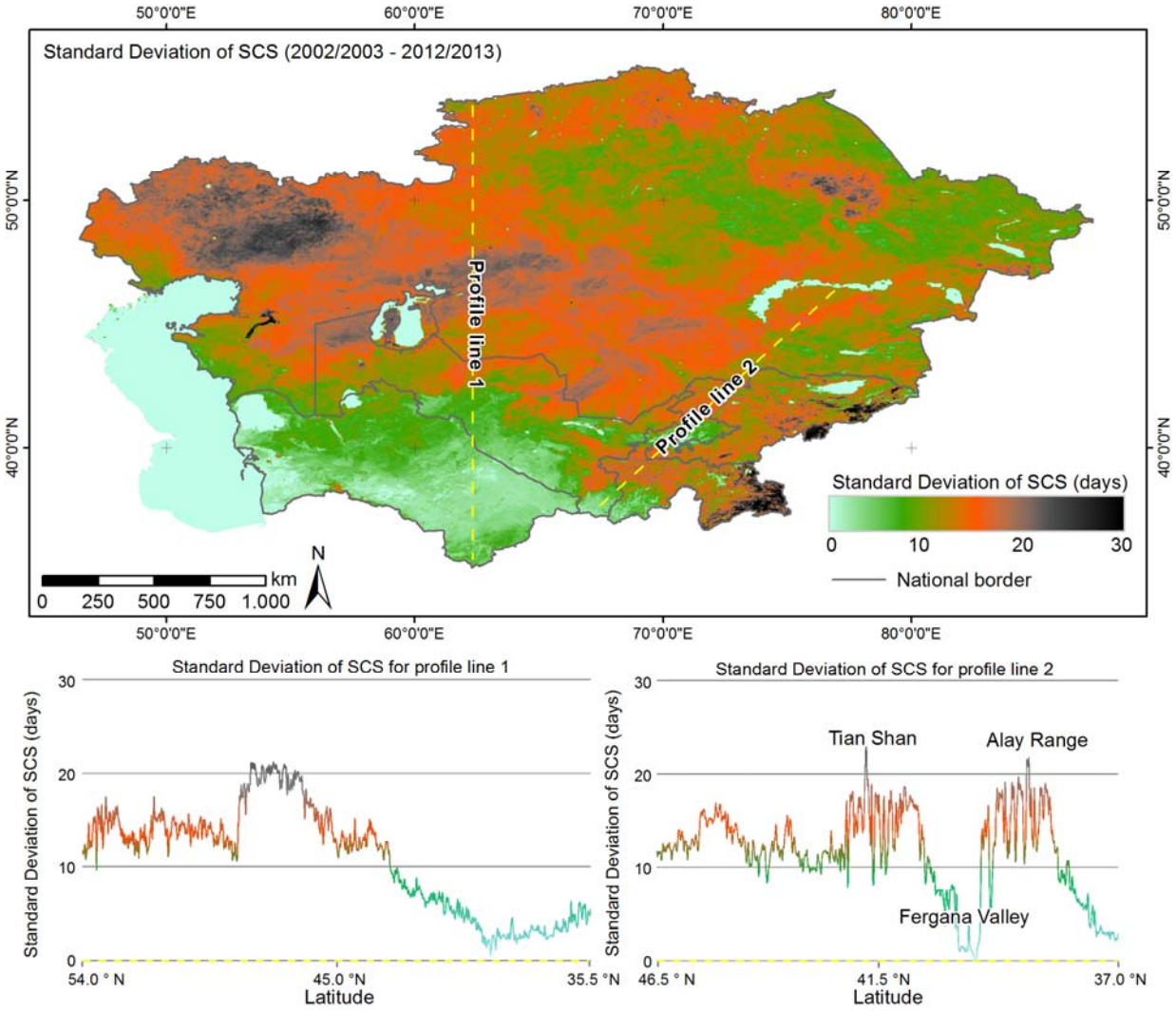

Figure 6.29: Standard Deviation of SCS between 2002/2003 and 2012/2013

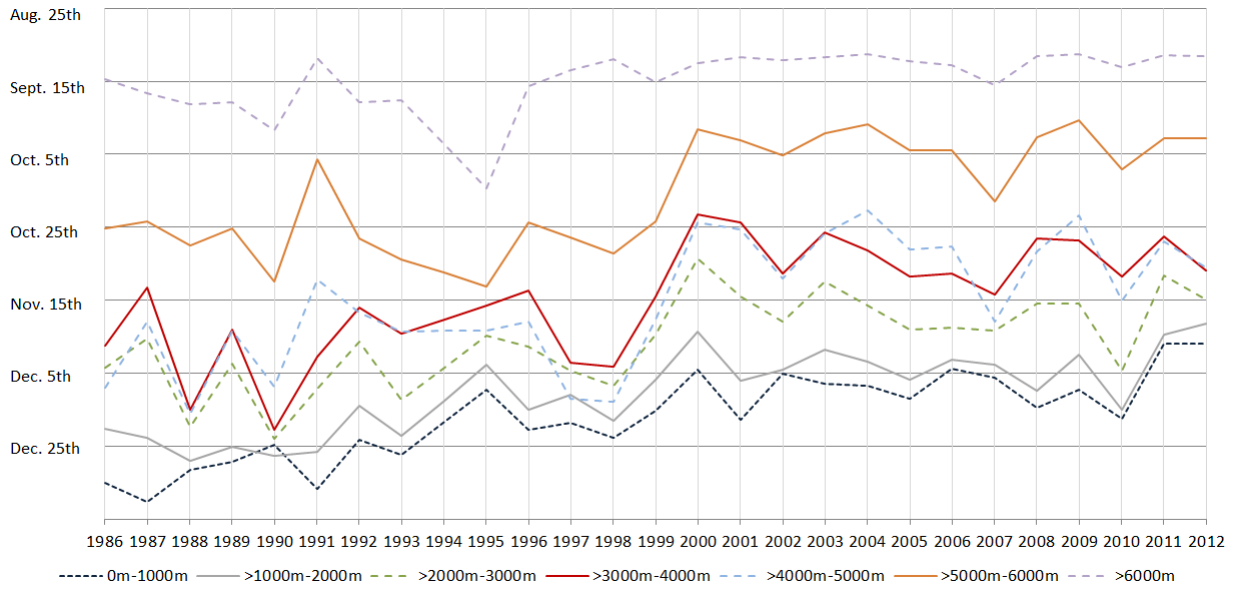

Figure 6.30: SCS per elevation zone and year

When aggregated to longer time periods, a development towards earlier SCS becomes visible from the time series as depicted in Figure 6.31. The periods conform to those from Figure 6.21 (1986-1993 and 1994-2002; 2003-2011 is extended for the SCS variable to 2003-2012). It is clearly visible that snow cover starts 15 to 20 days earlier between 2003 and 2012 than it did between 1986 and 1992. The results for years before 1992 are again uncertain for lower elevation zones due to data gaps in northern Kazakhstan. 1994 was interpolated from 1993 and 1995 for all products presented in section 6.2.2. Additionally, zones above 6,000 m are only represented by ~900 pixels (~180 km²), introducing uncertainties as already mentioned in section 6.2.1. The influence of slope orientation on mean SCS is illustrated in Figure 6.32 and Table 6.8: Snow cover on slopes with orientations towards northern directions starts earlier (~7 days between 2,000 m and 3,000 m, 8 days between 3,000 m and 4,000 m, 5 days above 4,000 m elevation). Between 1,000 m and 2,000 m elevation, SCS begins ~3 days later only for slopes with eastern and south-eastern orientation (91-180°). The variability of mean SCS is low (max. 3.4 days standard deviation for the zone between 3,000 and 4,000 m).

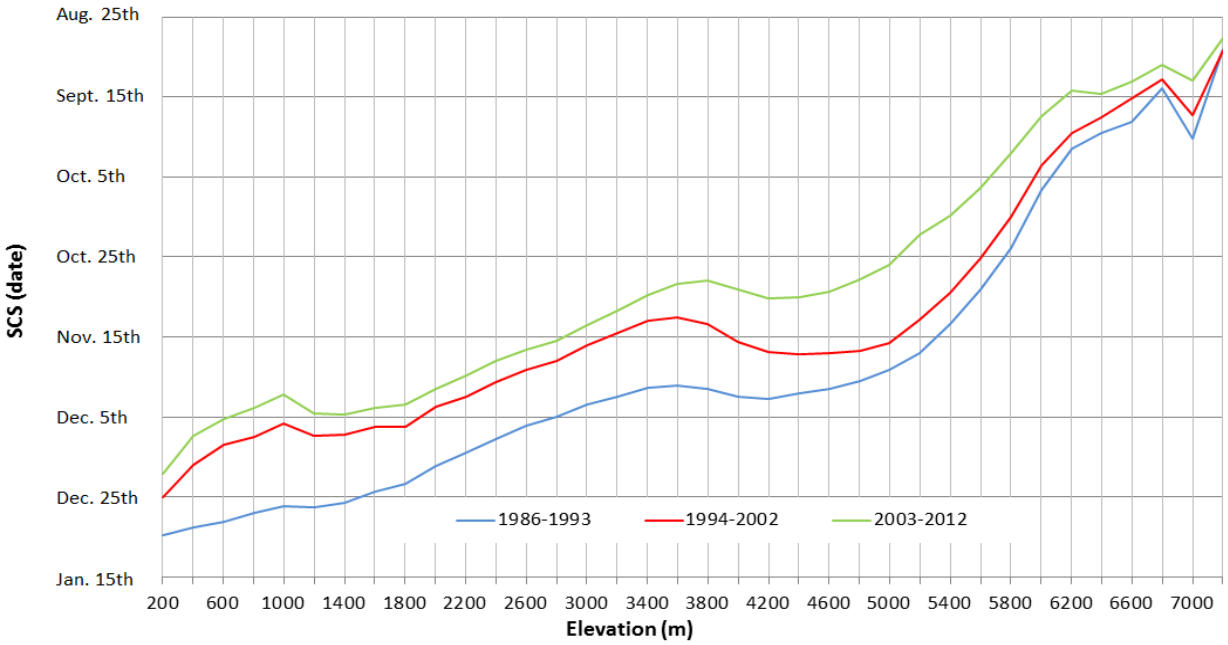

Figure 6.31: SCS as a function of elevation for three different periods

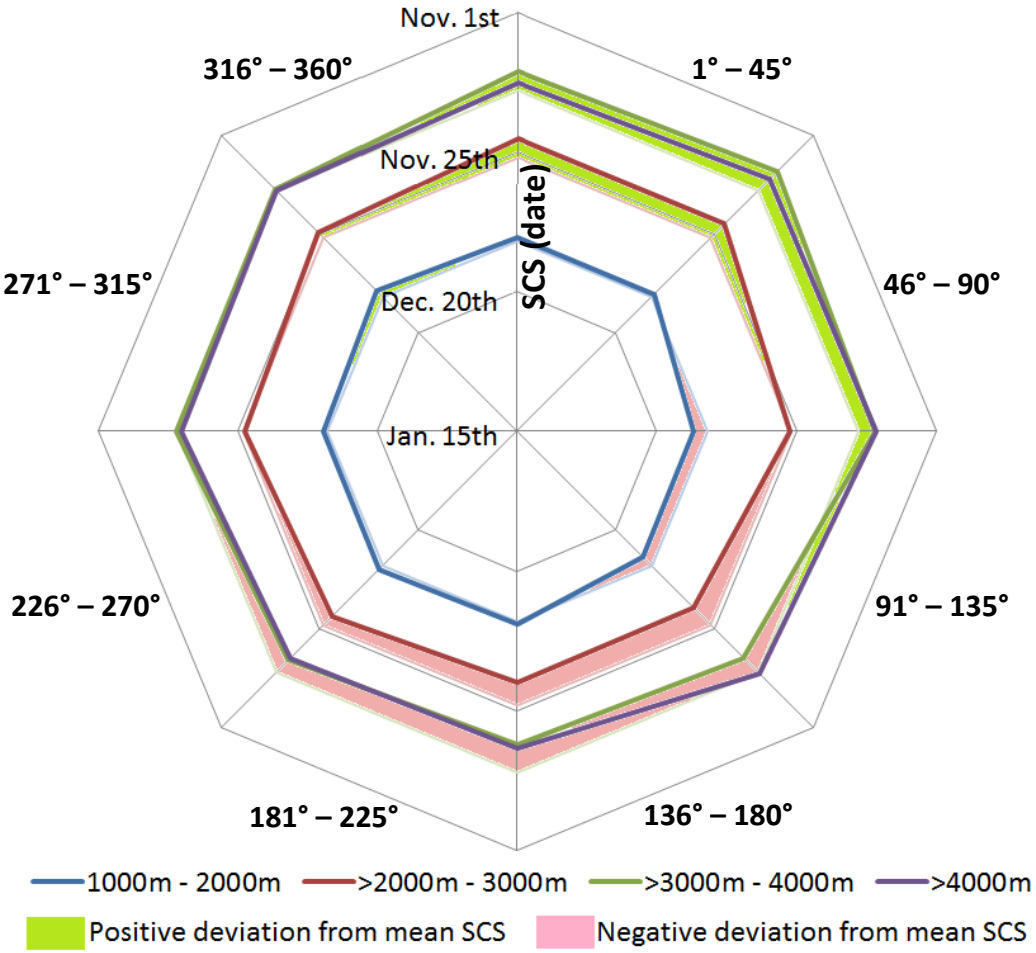

Figure 6.32: Mean SCS as a function of slope orientation and elevation

Table 6.8: Mean SCS per elevation zone and slope aspect (calendar day)

Aspect	1000 to 2000 m	2000 to 3000 m	3000 to 4000 m	> 4000 m
1°-45°	345,2	327,5	315,6	317,5
46°-90°	345,3	327,5	314,1	316,1
91°-135°	348,5	331,2	316,0	315,6
136°-180°	348,3	335,3	322,6	318,7
181°-225°	345,5	335,1	323,9	323,2
226°-270°	345,1	333,2	322,1	322,6
271°-315°	345,4	331,3	319,0	320,0
316°-360°	344,3	329,8	318,7	319,0
Mean	**346,0**	**331,4**	**319,0**	**319,1**
StDev. (days)	**1,4**	**2,9**	**3,4**	**2,6**

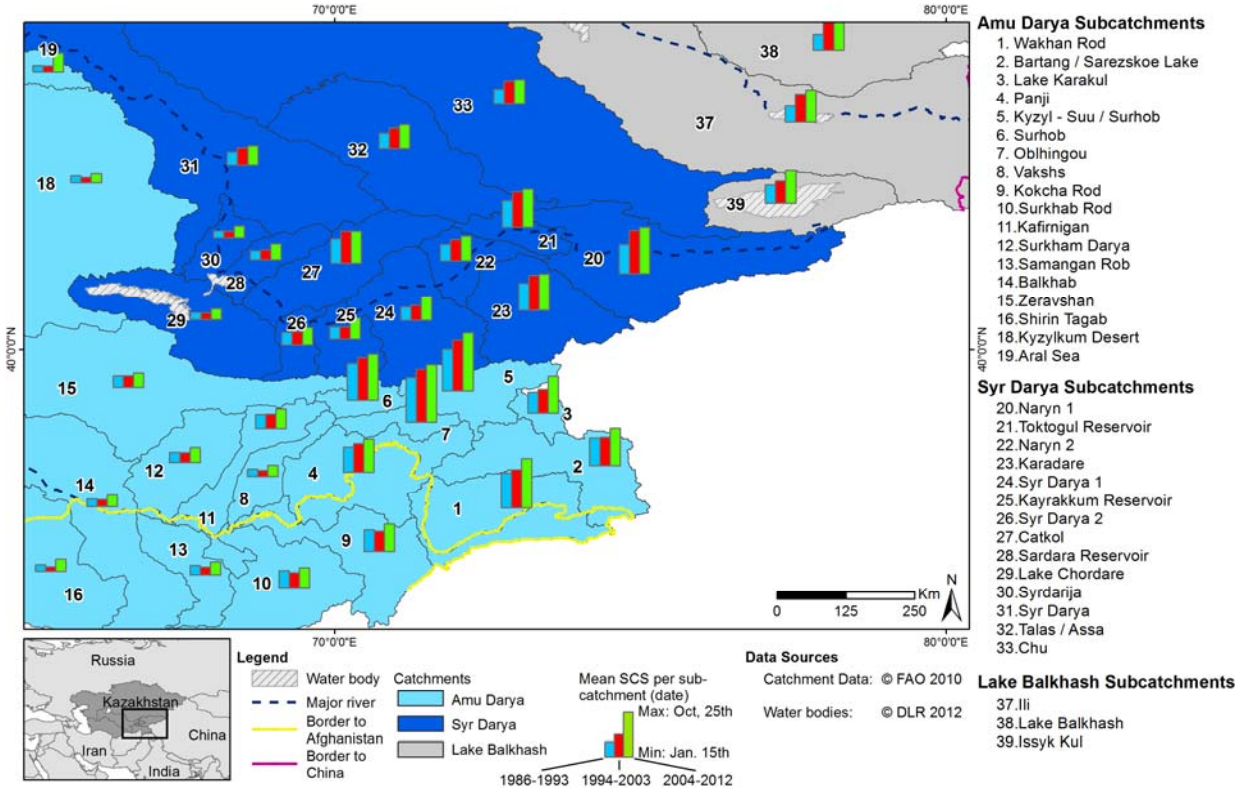

Figure 6.33: Mean SCS per mountain catchment and time span

Similar to Figure 6.19 in section 6.2.1, Figure 6.33 depicts the mean SCS as aggregated to three time spans (1986-1993, 1994-2003, 2004-2012) for the mountain catchments of Amu Darya, Syr Darya, and Lake Balkhash drainage basins. SCS in many of the sub-catchments developed towards earlier dates within the last 26 years. This development stands in contrast to the results from Figure 6.19, where SCD did not change significantly between the observed time spans. Earlier SCS and constant SCD suggest that SCM will also occur earlier. Section 6.2.3 will determine whether this assumption actually applies.

6.2.3 Snow Cover Melt

Snow cover melt is calculated according to equation 10 and the settings described in section 5.3 for each hydrological year between 1986 and 2011.Figure 6.34, 6.35, and 6.36 represent the SCM results for these years. Results for years before 1992 in northern Kazakhstan are uncertain again because of missing observations. The year 1994/1995, however, does not show any of the erroneous patterns already accustomed to from the SCD and SCS results (Figure 6.12, Figure 6.24). The reason is that only data between September 1994 and December 1994 are missing. Since SCM is calculated from January 15th of a hydrological year on, the data gaps caused by the malfunction of NOAA-11 do not affect the SCM result.

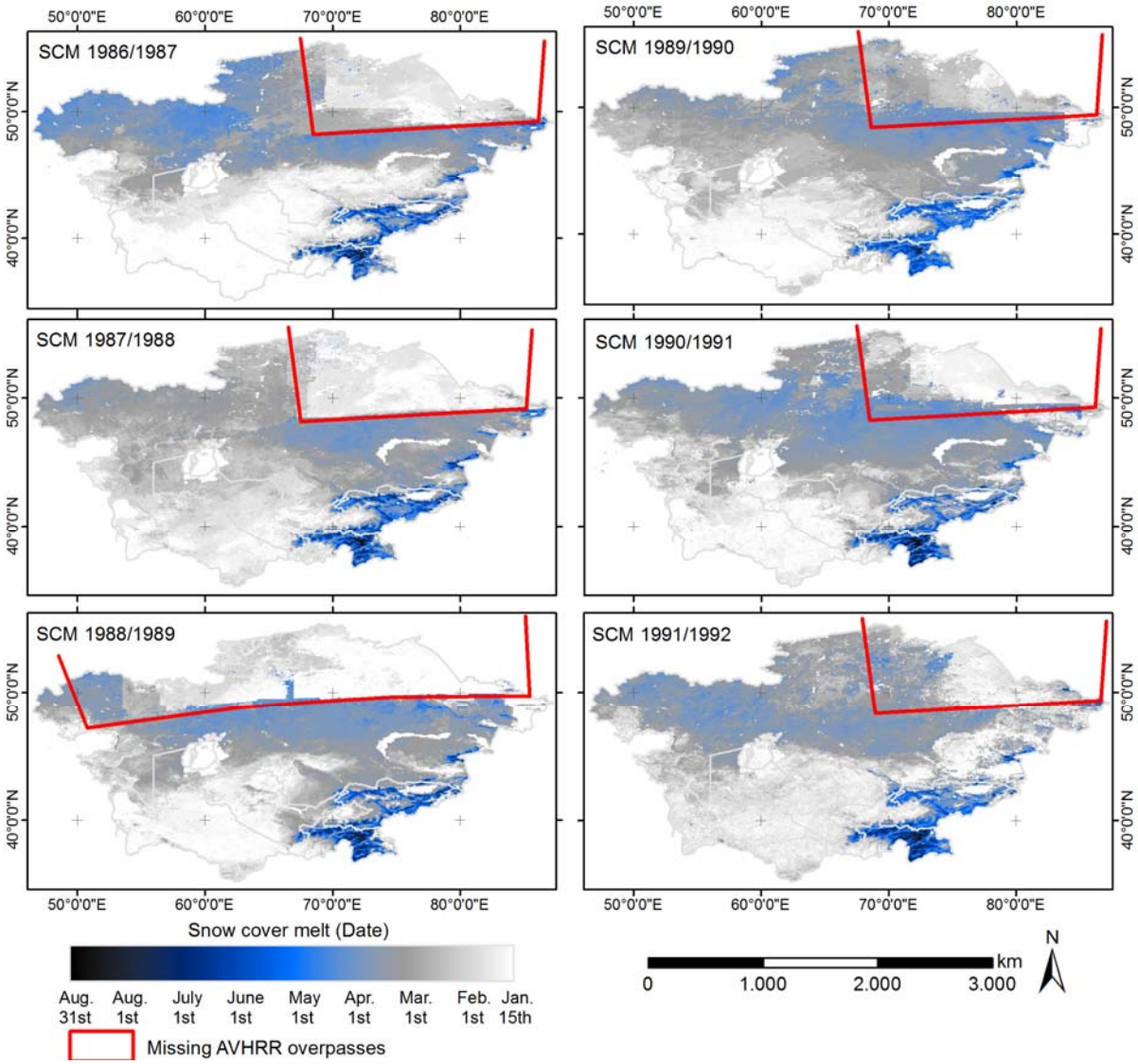

Figure 6.34: SCM for hydrological years 1986/1987 to 1991/1992

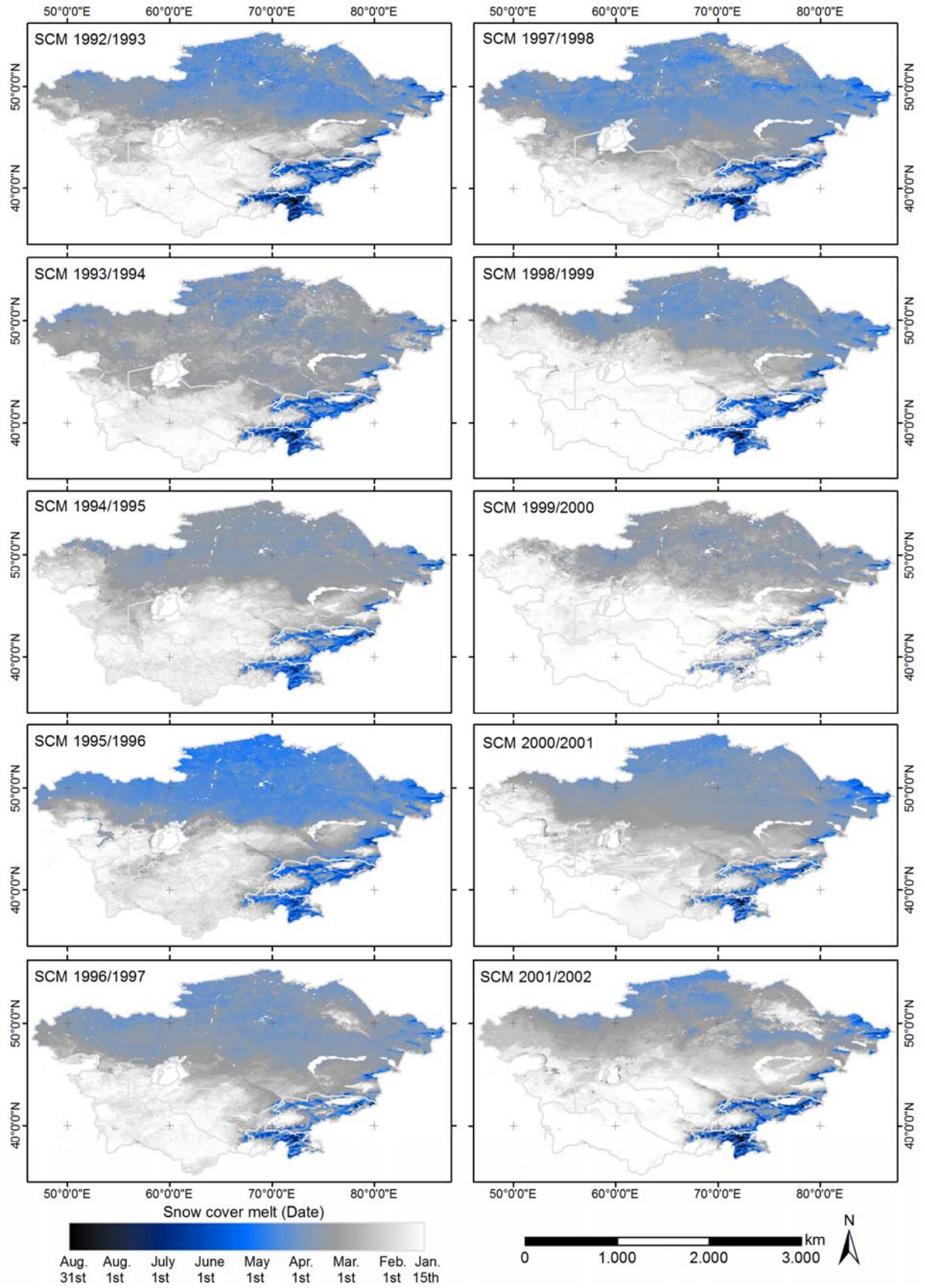

Figure 6.35: SCM for hydrological years 1992/1993 to 2001/2002

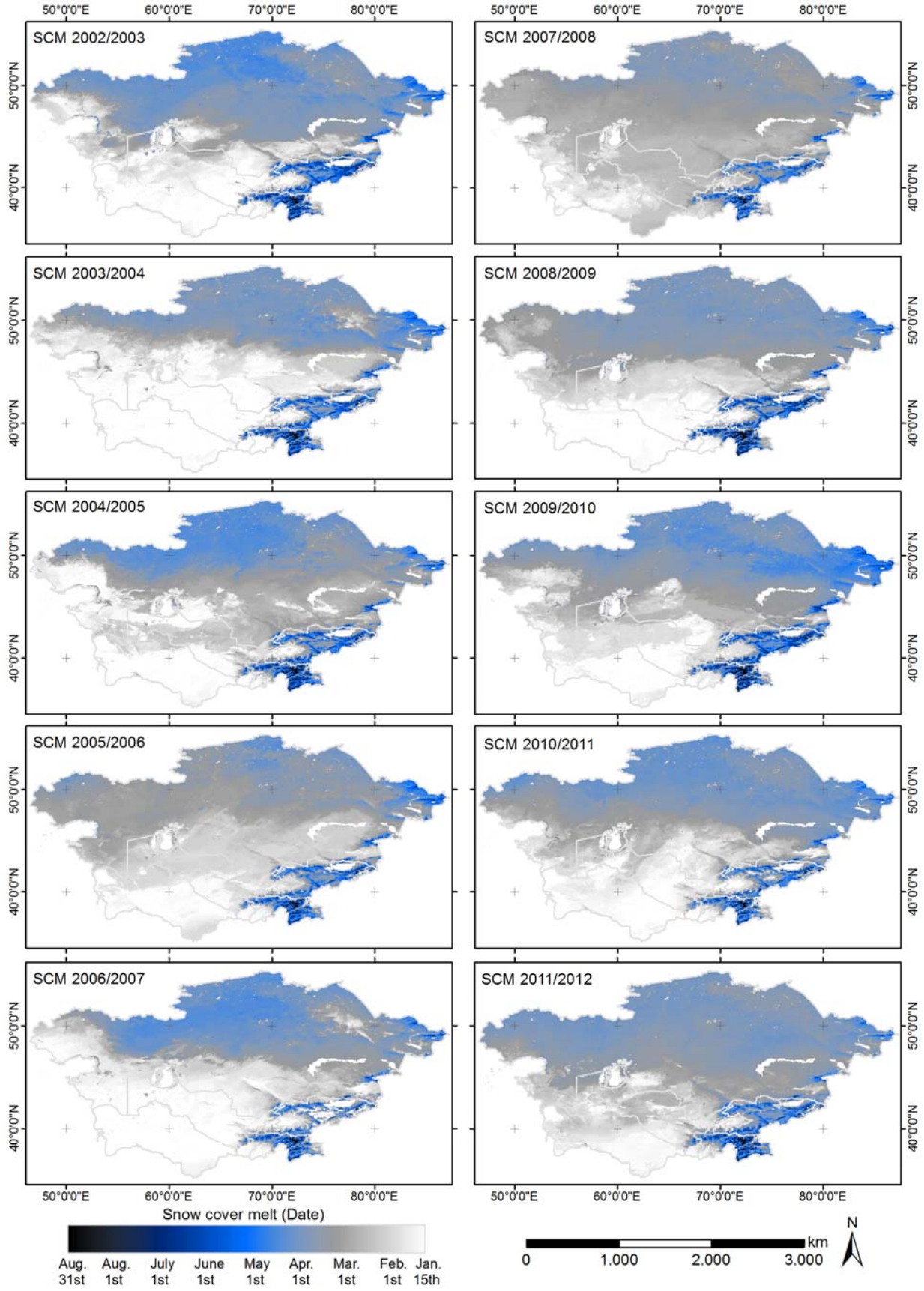

Figure 6.36: SCM for hydrological years 2002/2003 to 2011/2012 (in parts adopted from Dietz et al. (2013))

Mean SCM is provided for the periods from 1992/1993 to 2001/2002 (Figure 6.37) and from 2002/2003 to 2011/2012 (Figure 6.38), again including profile lines 1 and 2. Standard Deviation of SCM is illustrated for the same periods in Figure 6.39 and Figure 6.40.

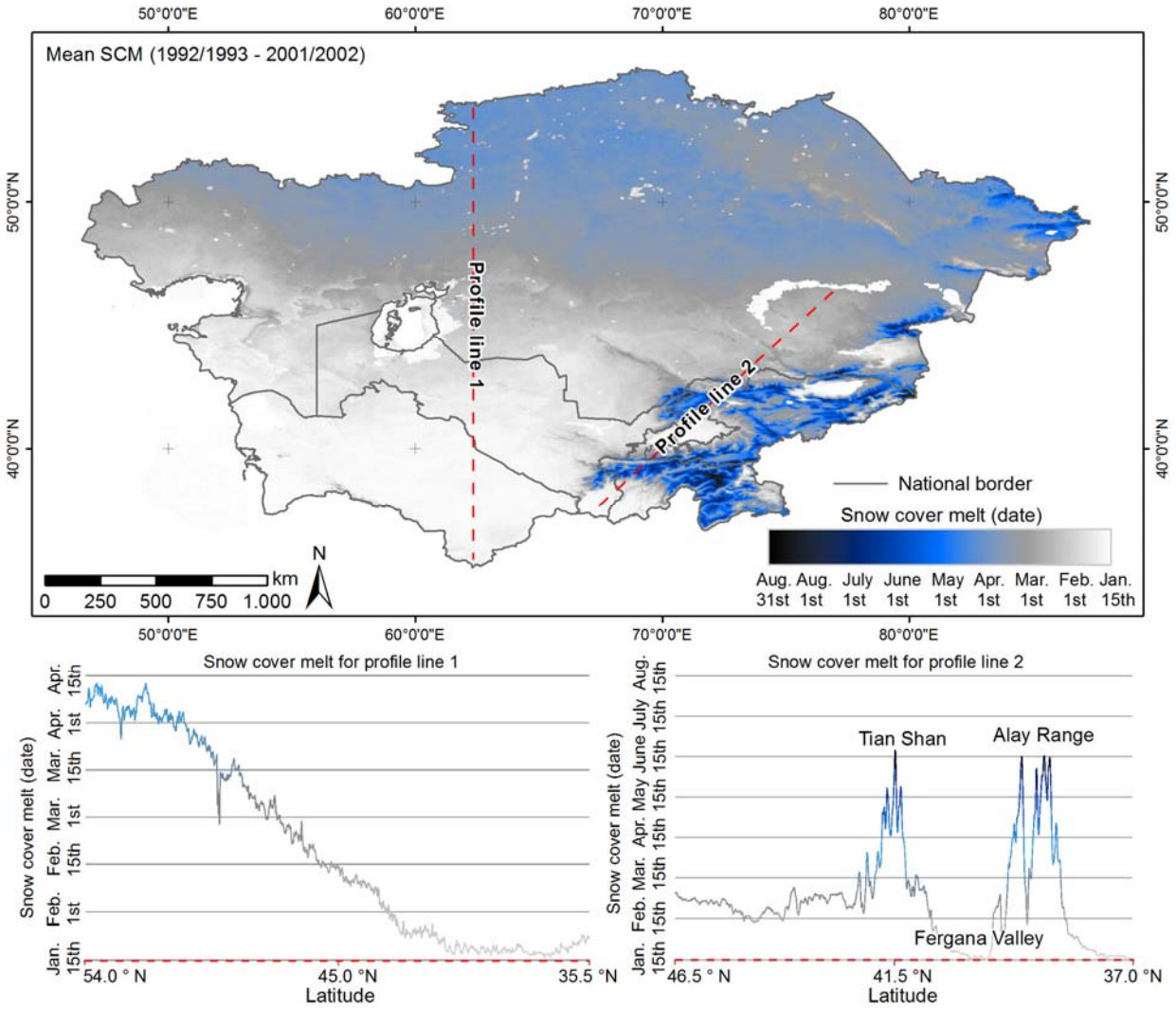

Figure 6.37: Mean SCM for the years 1992/1993 to 2001/2002

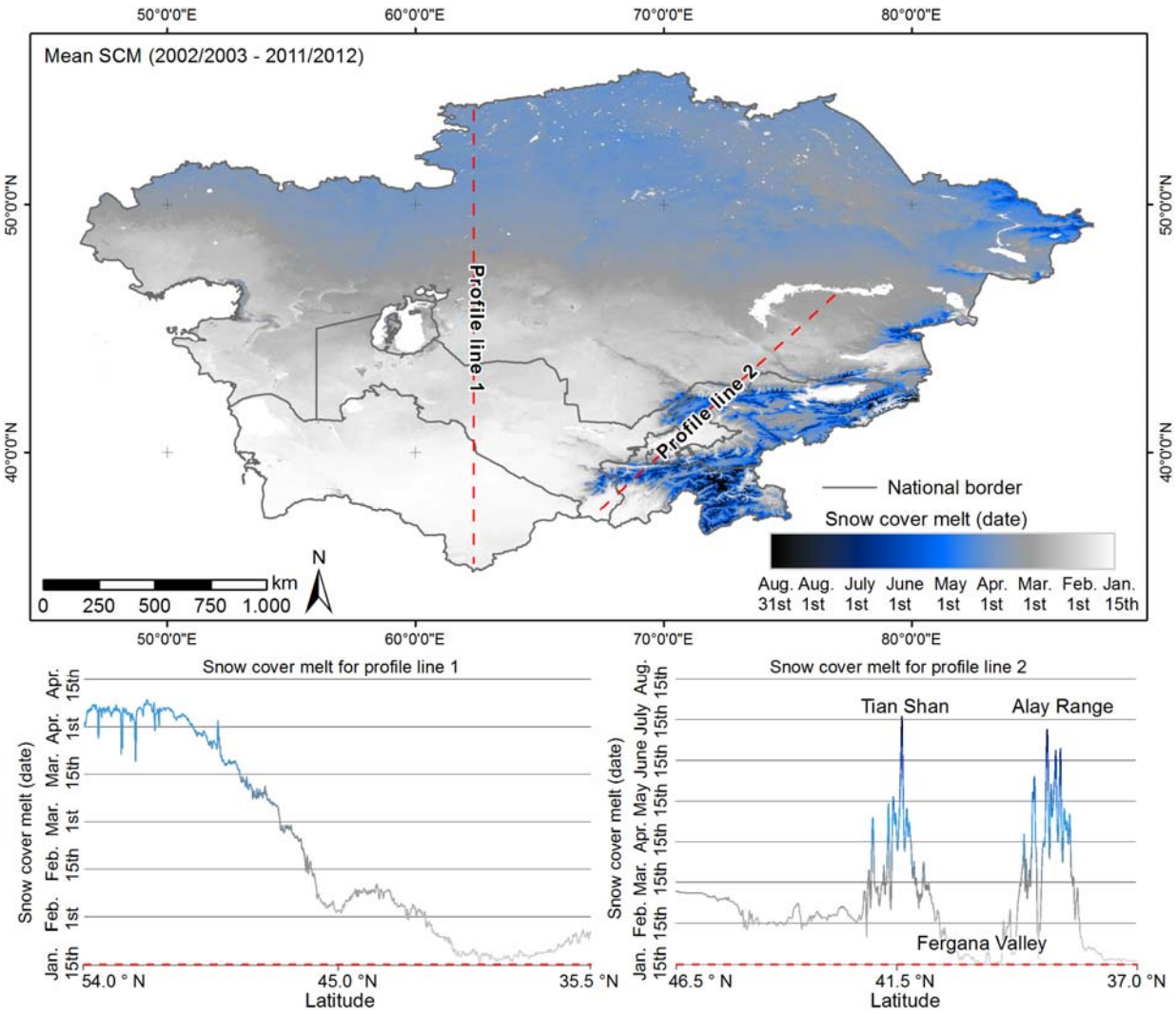

Figure 6.38: Mean SCM for the years 2002/2003 to 2011/2012

As for SCD and SCS, the influence of the topography is also investigated for SCM. Figure 6.41 depicts the SCM per year and elevation zone. Year to year variability is less pronounced than for the respective SCS results in Figure 6.30 but some outliers are recognizable from both graphs, like e.g. the late SCS in 2010/2011 that coincides with an early SCM in 2010/2011. Such agreements between SCS and SCM, however, are no common rule considering the whole time series. Sections 6.2.5 and 6.4 will explore this question in more detail.

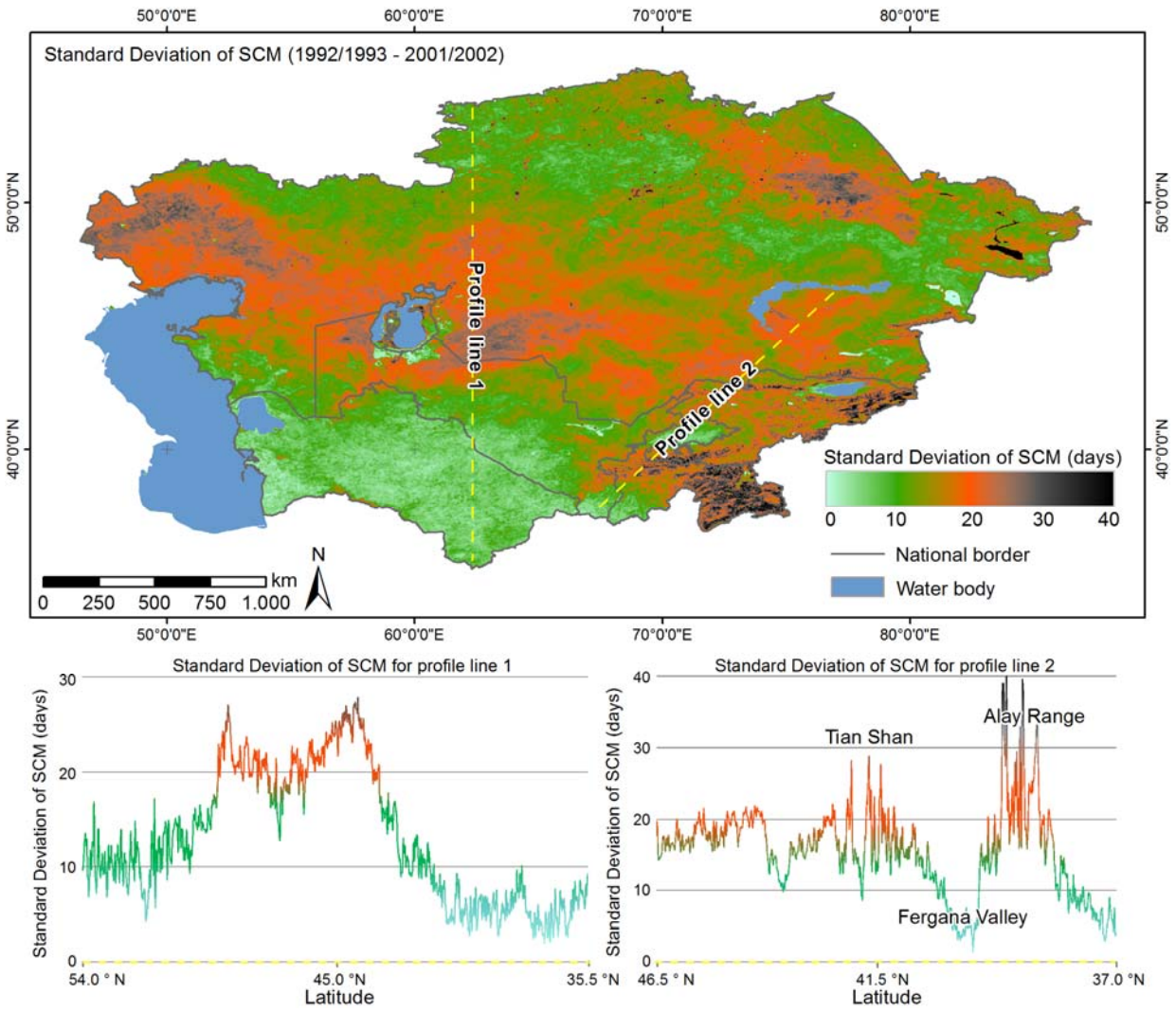

Figure 6.39: Standard Deviation of SCM between 1992/1993 and 2001/2002

The SCM as a function of elevation is illustrated in Figure 6.42 for the same periods as SCD in Figure 6.21 and SCS in Figure 6.31. Snow cover melts up to 12 days earlier during the period between 2003/2004 and 2011/2012 than during 1994/1995 to 2002/2003 while elevation zones above ~1,500 m are more affected than lower regions.

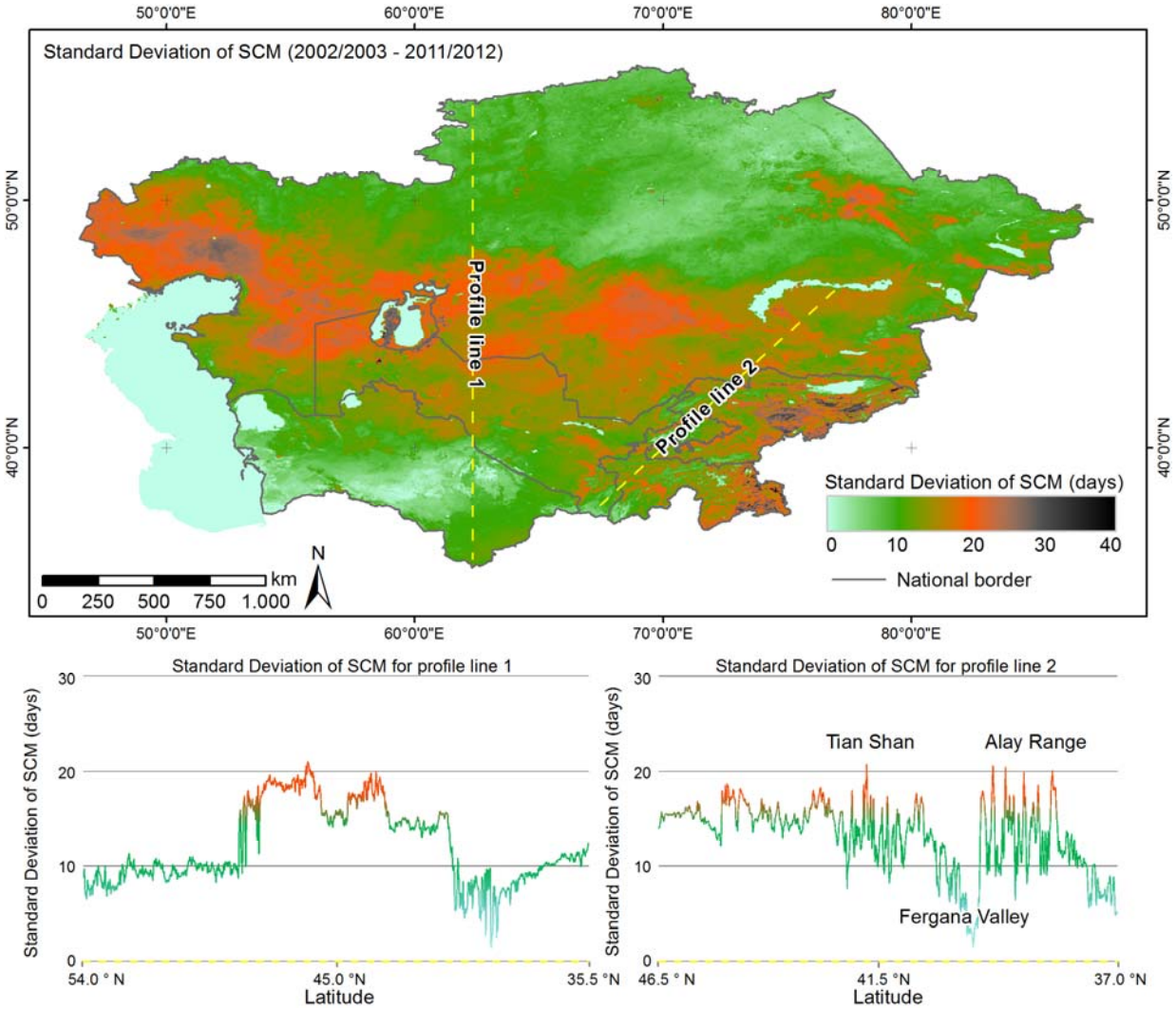

Figure 6.40: Standard Deviation of SCM between 2002/2003 and 2011/2012

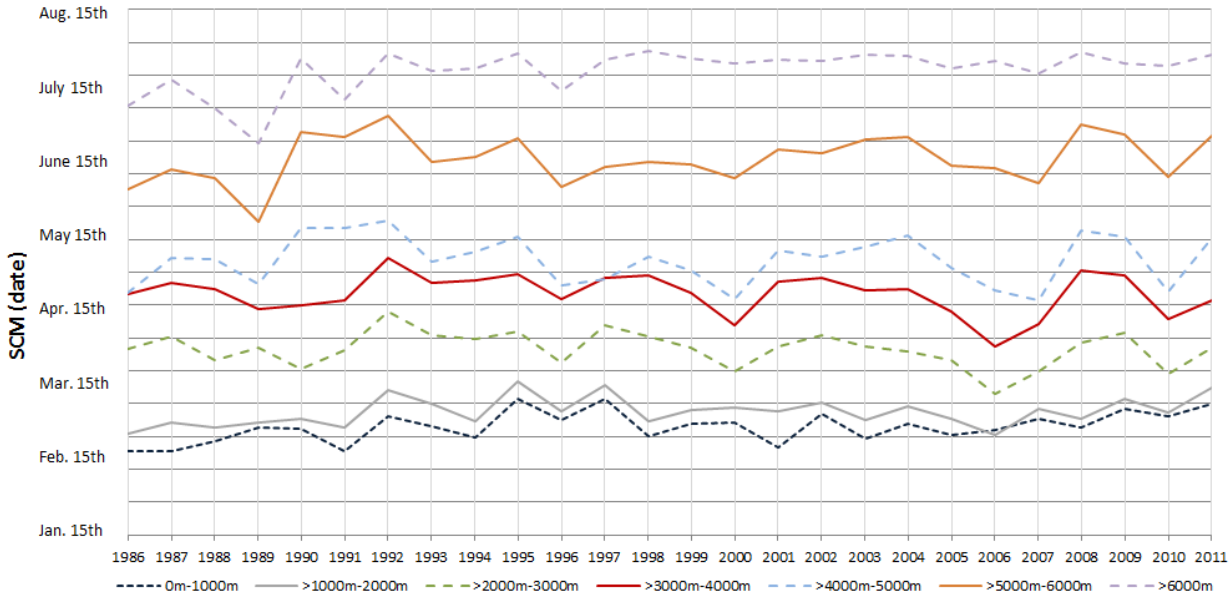

Figure 6.41: SCM per elevation zone and year

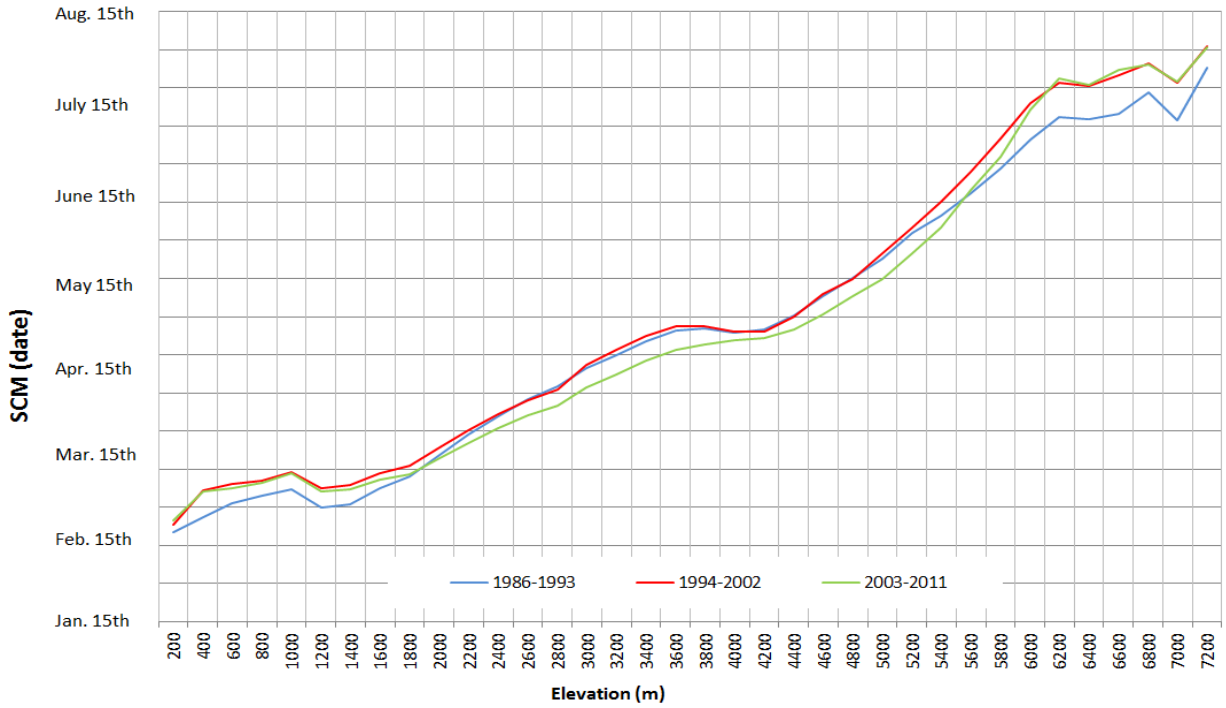

Figure 6.42: SCM as a function of elevation for three different periods

The impact of slope orientation on SCM is depicted in Figure 6.43 and Table 6.9. North- and north-east facing slopes stand out due to later SCM as it was expected. The elevation zone between 1,000 m and 2,000 m constitutes an exception from this rule: here, south-eastern slopes feature earliest SCM dates. The deviations from mean SCM in this zone are, however, very small (± 2 days). Variability is again greatest in the zone between 3,000 and 4,000 m.

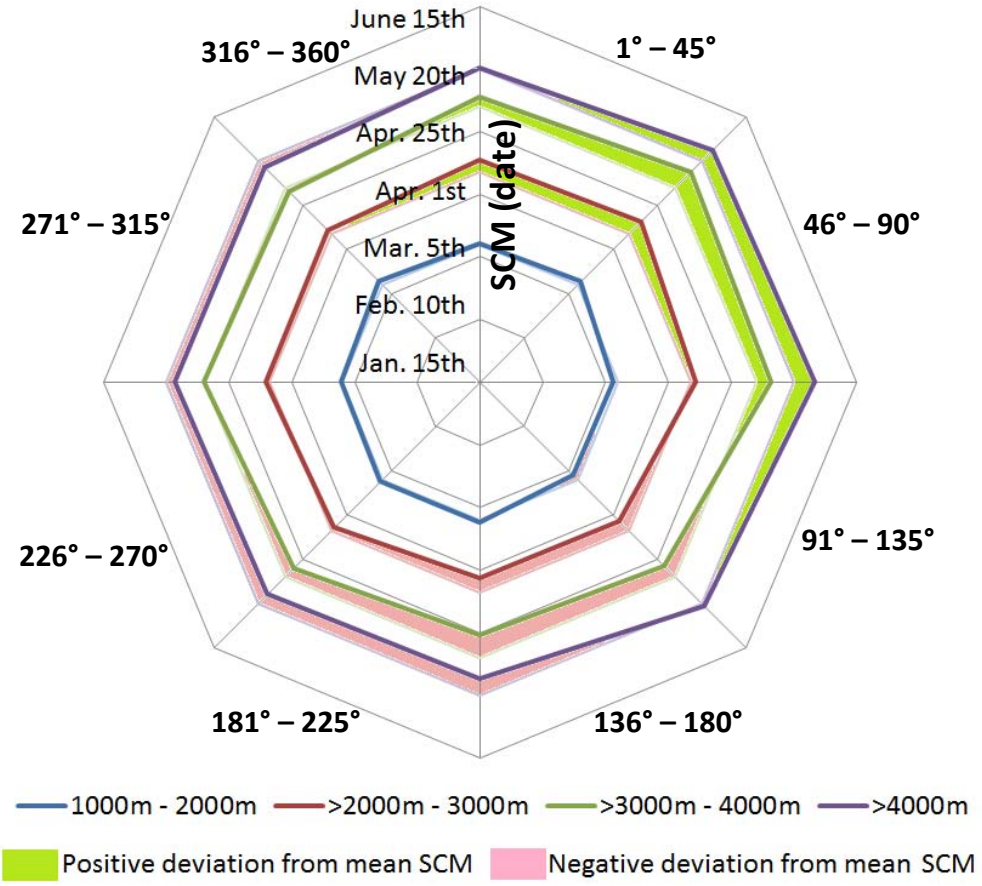

Figure 6.43: Mean SCM as a function of slope orientation and elevation

Table 6.9: Mean SCM per elevation zone and slope aspect (calendar day)

Aspect	1000 to 2000 m	2000 to 3000 m	3000 to 4000 m	> 4000 m
1°-45°	70.1	103.5	128.9	140.7
46°-90°	71.8	105.6	133.7	146.1
91°-135°	67.8	101.1	131.1	148.5
136°-180°	67.2	93.7	118.8	141.3
181°-225°	70.8	93.1	116.2	133.5
226°-270°	71.2	97.1	120.1	134.7
271°-315°	70.3	100.2	124.8	136.4
316°-360°	71.8	101.1	122.9	136.5
Mean	**70.1**	**99.4**	**124.6**	**139.7**
StDev. (days)	**1.6**	**4.2**	**5.8**	**5.1**

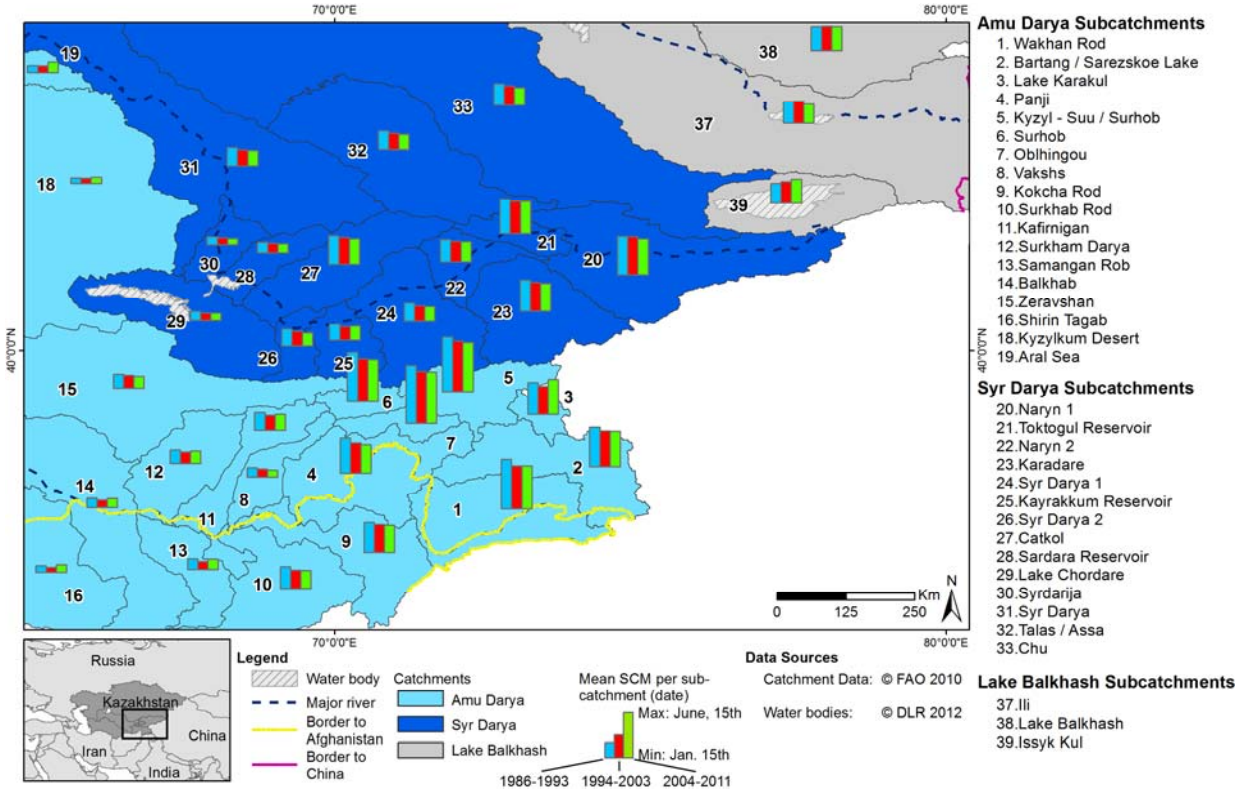

Figure 6.44: Mean SCM per mountain catchment and time span

As in sections 6.2.1 and 6.2.2, mean SCM per mountain catchment and time span is also illustrated here in Figure 6.44. The SCM between 2004 and 2011 occurs earlier in many catchments, as already suggested after investigating mean SCD and SCS in Figure 6.19 and Figure 6.33. Since SCD did not change significantly and SCS started at earlier dates for many catchments, an earlier SCM was assumed as well. Taken together, the shift towards earlier SCS and SCM is an important finding with regards to the hydrological cycle of Central Asia. Possible consequences will be addressed to in the discussion. Not all sub-catchments in Figure 6.44 are characterized by an earlier SCM: Some regions like Toktogul reservoir (21) or Lake Balkhash (39) do not show any change. Lake Karakul (3) and Issyk Kul (39) even indicate a delayed SCM. These sub-catchments all contain large water bodies (in comparison to the total catchment size) that may have an effect on the snow mapping accuracy. This issue will also be discussed in section 6.3.

6.2.4 Snow Cover Index

SCI, SCI_{ES}, and SCI_{LS} were calculated according to equations 11, on , and Equation for all (sub-)catchments already listed in Figure 2.2 and all hydrological years from 1986/1987 to 2011/2012. SCI_{ES} was also derived for 2012/2013. While the SCI is originally only based on the SCD of a hydrological entity, SCI_{ES} and SCI_{LS} are derived from SCS and SCM, respectively. Results are available for each sub-catchment but were aggregated into three categories for section 6.2.4: Downstream-, Intermediate-, and Upstream-catchments – as noted in section 2.1. Figure 6.45, Figure 6.46, and Figure 6.47 represent SCI_{ES}, SCI_{LS}, and SCI, normalized to mean SCI values for the full time series. Illustrating absolute values would compromise the clarity of the figures because values can reach few thousands to several million – always depending on the size of a specific catchment. Additionally, the unit of the SCI (km² days) is uncommon and difficult to rank.

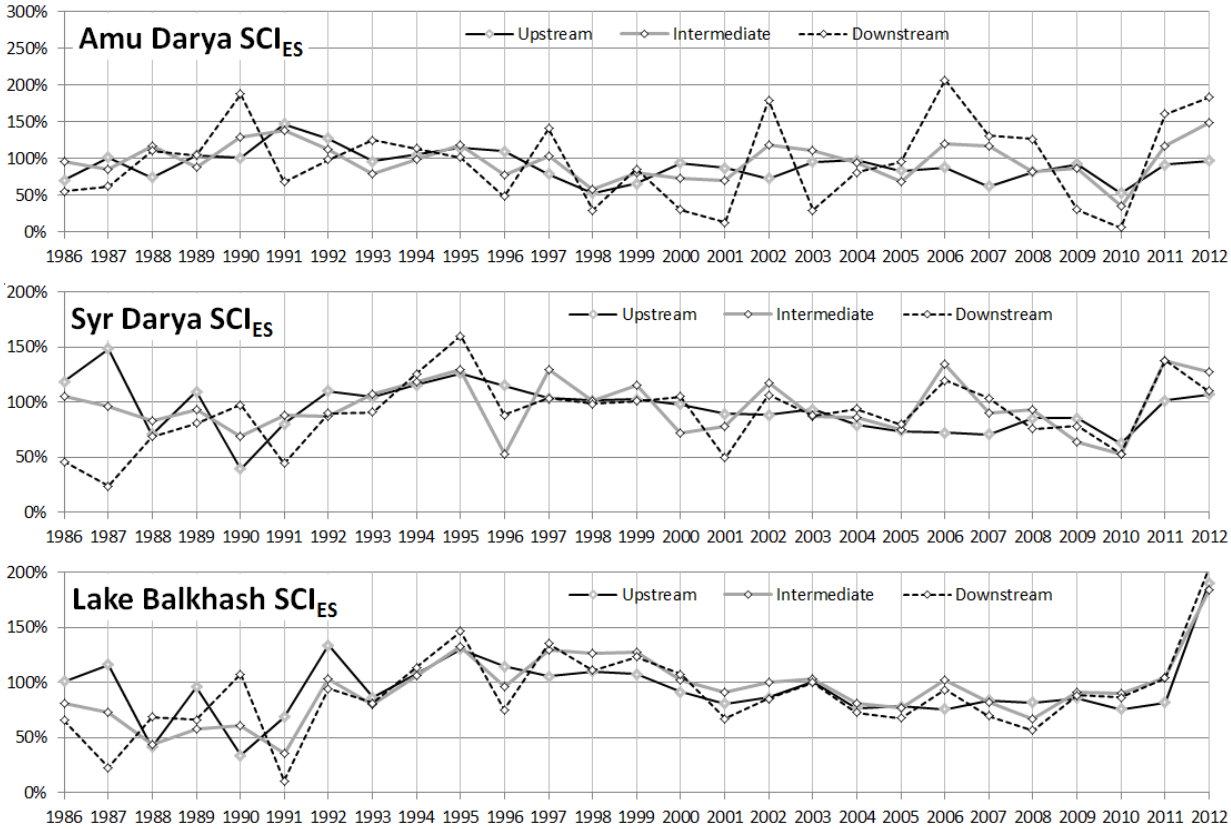

Figure 6.45: SCI_{ES} (% of mean) per sub-catchment and year

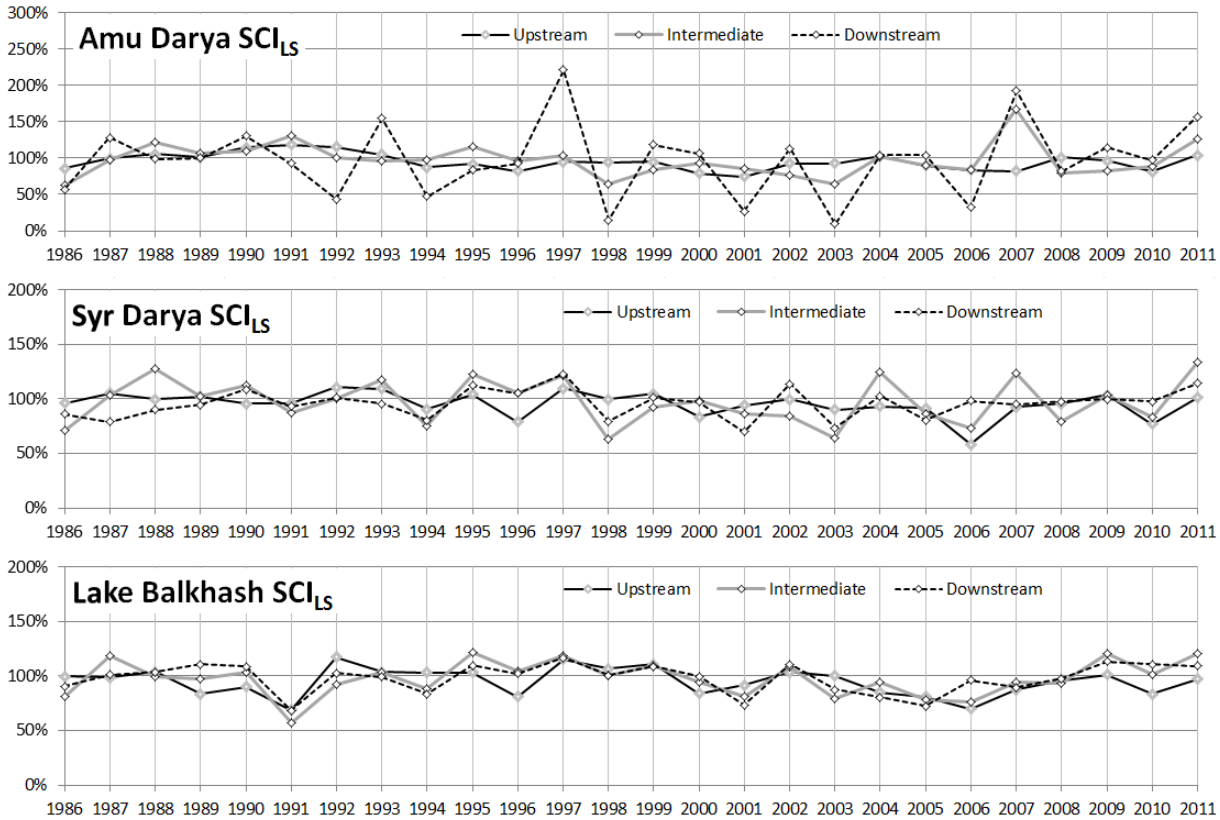

Figure 6.46: SCI_{LS} (% of mean) per sub-catchment and year

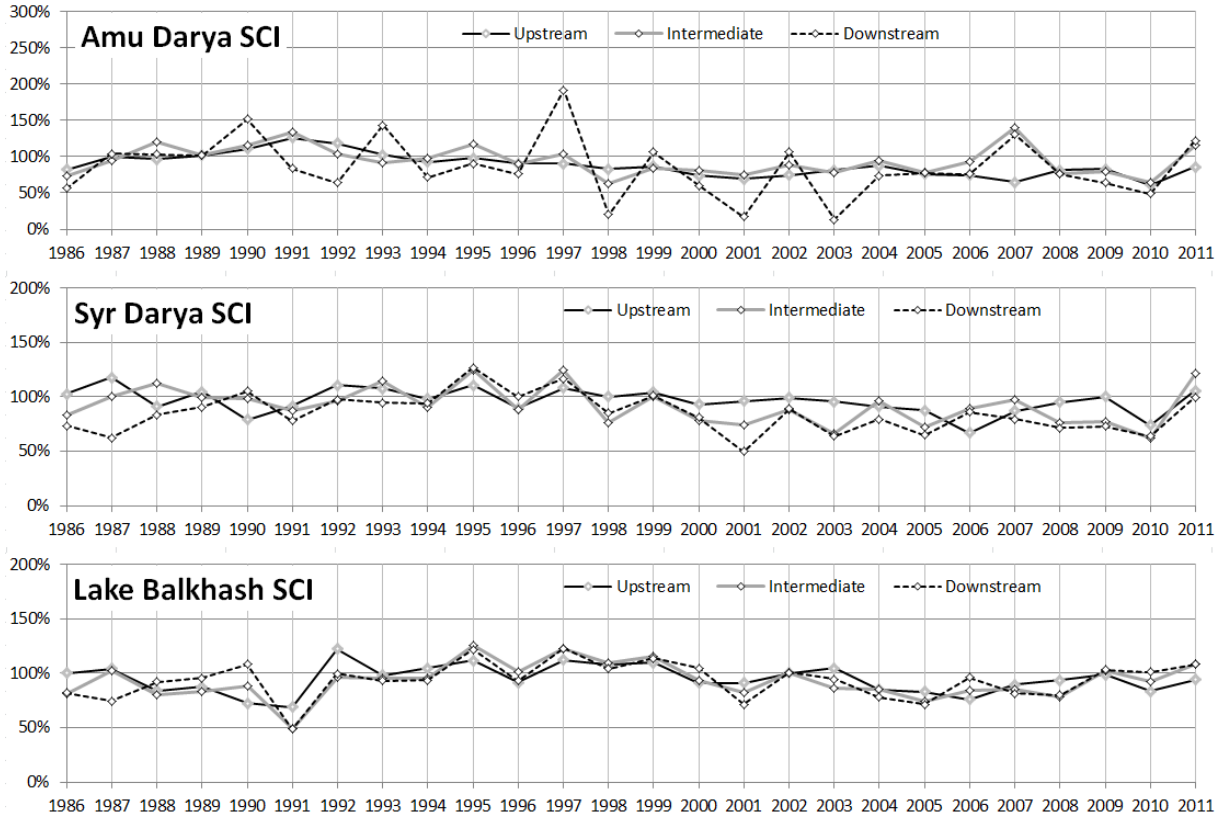

Figure 6.47: SCI (% of mean) per sub-catchment and year

6.2.5 Discussion of snow cover parameters in Central Asia

The analysis of the current status of snow cover characteristics of Central Asia (second aim of the thesis) is made possible by calculating the snow cover parameters (SCD, SCS, SCM, SCI) presented in this thesis (section 6.2). These results are worth a more detailed discussion: SCD is characterized by high variability especially in the central parts of the study area (~ 43° N to 49° N) and in some of the mountainous regions. The exact locations of pixels with high variability are visible from Figure 6.17, that depicts the standard deviation of SCD between 2002/2003 and 2011/2012. The variability in the central regions was not as pronounced between 1992/1993 and 2001/2002 (Figure 6.16), suggesting that possible changes in snow cover characteristics slowly started after 2002/2003. SCS and SCM show variable patterns here, too. These central regions have also been identified by Brown & Mote (2009) to be most sensitive with respect to possible climate changes. This does not automatically implicate that climate change is responsible for a probably lasting change towards longer or shorter SCD. Yet, the findings from Brown & Mote (2009) can be interpreted in a different way: A small band of higher sensitivity between 40° N and 45° N marks a region where only small changes in precipitation or temperature may have severe impacts on the SCD. Mean SCS falls within December for this region (see Figure 6.27) while mean SCM usually occurs between February and March (see Figure 6.38). Figure 2.4, that depicts the mean surface temperature of each month, clearly shows that mean surface temperature in these months (March in particular) is around freezing point. If weather changes towards warmer temperatures, SCD is immediately affected. Precipitation is also a possible source of the high variability because the central regions of the study area are characterized by the lowest precipitation amounts of whole Central Asia especially during autumn and winter seasons (see Figure 2.1). If precipitation is absent, SCS will occur later, directly affecting SCD, as well. Barnett et al. (2005), however, stated in an article published by Nature in 2005, that for regions where the hydrology is dominated by winter snow accumulation (as Central Asia), changes in temperature will have a bigger impact on the on the water management than changes in precipitation.

The high variability in some of the mountainous regions may arise from another fact that is illuminated in Figure 6.48. Figure 6.48 “A” depicts the topography of the region while Figure 6.48 “B” contains the standard deviation of SCD for the same subset of the Central Asian mountains. Pixels with more than 45 days standard deviation are highlighted as polygons with red hachure and opposed to the topography of the surrounding area. Details only become visible in the close up views “a” and “b” of Figure 6.48 where the colour ramp has been stretched in a different contrast. The small valleys enclosed by higher mountain ranges are often characterized by the highest variability in SCD. Figure 6.49 represents a 3D-view of

the Naryn River Valley which is also depicted in Figure 6.48 “a”. The 3D-view visualizes the situation in more detail. It is clearly visible that regions with highest standard deviation of SCD are located in the upstream part of Naryn River Valley as well as a valley identified as Balgart/Small Naryn – a tributary to Naryn River. At this point, a citation taken from Severskiy et al. (2000b) is included in the discussion:

> *“The important factors influencing a distribution of snow cover in mountains are the slope aspect, steepness, character of vegetation, wind snow drift. […] Depending on the actual combinations of the local factors, any of them can be considered as the most important one. So, in the regions with low snow conditions the sharp contrasts in snow distribution because of differences in aspect are typical. In regions with high snow conditions these contrasts become smooth and a dominant factor of an uneven distribution of snow cover is wind or character of vegetation.”*

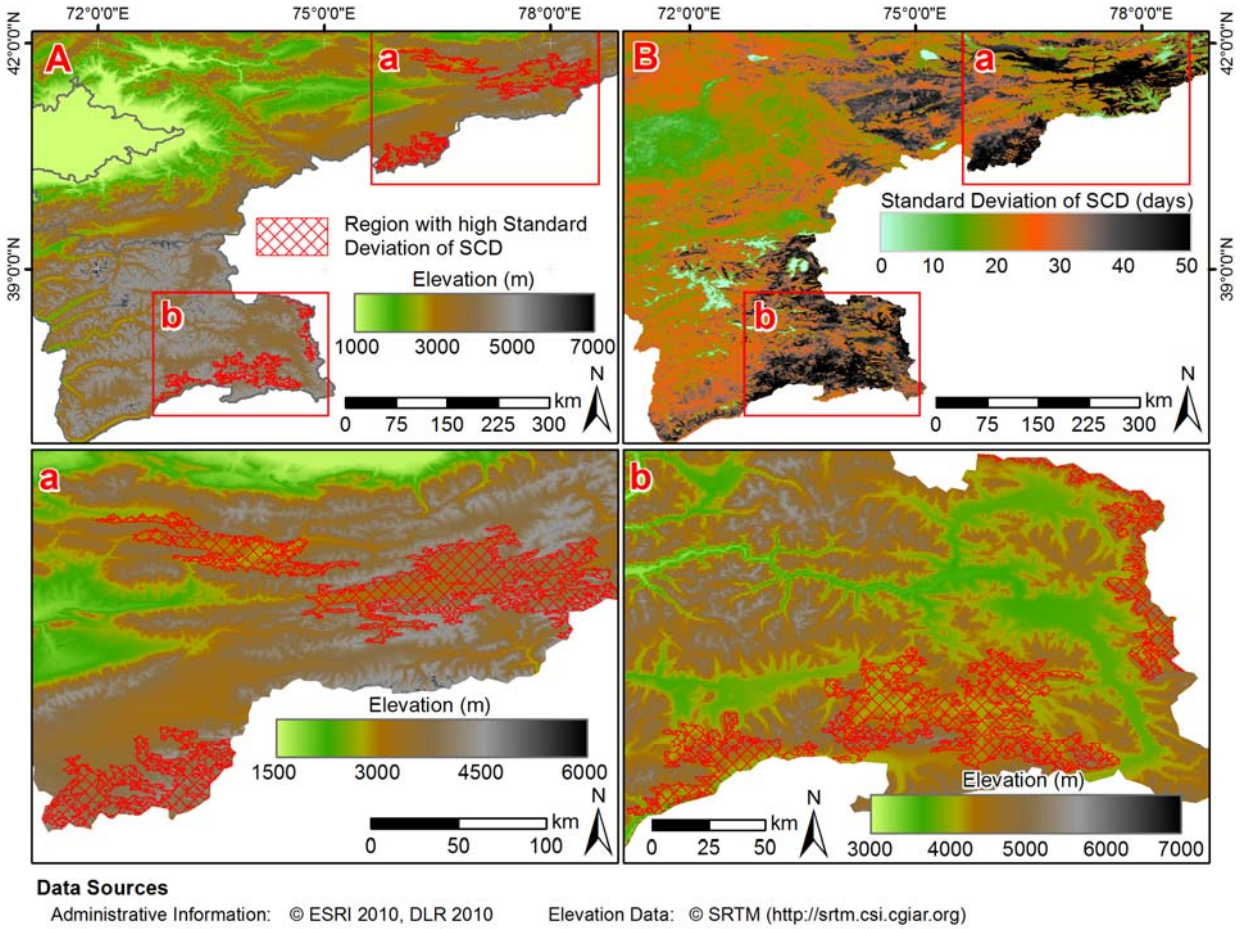

Figure 6.48: Regions with highest standard deviation of SCD (B) compared to topography (B) and details for Tian Shan (a) and Pamir (b)

The high variability of SCD does not argue for factors like slope aspect or steepness of the terrain because these factors are stable and do not change between the years. Land cover consists of bare area and herbaceous vegetation (see Figure 2.5) and is thus also not considered to change significantly between two seasons. Therefore, the factor that is most likely accountable for the high variability is wind. Mountain winds are often directed along the valleys (Severskiy, 1996), redistributing the snow from the surrounding ridges or slopes. Once snow has been transported to the bottom of a valley the SCS is set and SCD begins. In other words: The date of the wind transport is responsible for the beginning of the snow season. This date is much more variable than the beginning of the winter season. It is, however, not possible to prove the validity of the established assumption within the framework of the presented thesis due to the lack of detailed wind information from the study region. It is also noticeable that not all valleys stick out due to high SCD variability. Figure 6.48, Figure 6.17, and Figure 6.16 contain valleys with much lower standard deviation of SCD as well, allowing to classify them as wind or precipitation driven snow regimes, respectively. Such a classification could depend on a threshold like it was applied in Figure 6.48 and Figure 6.49 (more than 45 days standard deviation could form the class “wind driven”, while below the regime may be defined as “precipitation driven”). This classification may be used to define which valleys constitute stable snow cover conditions when planning to construct new reservoirs or hydropower stations.

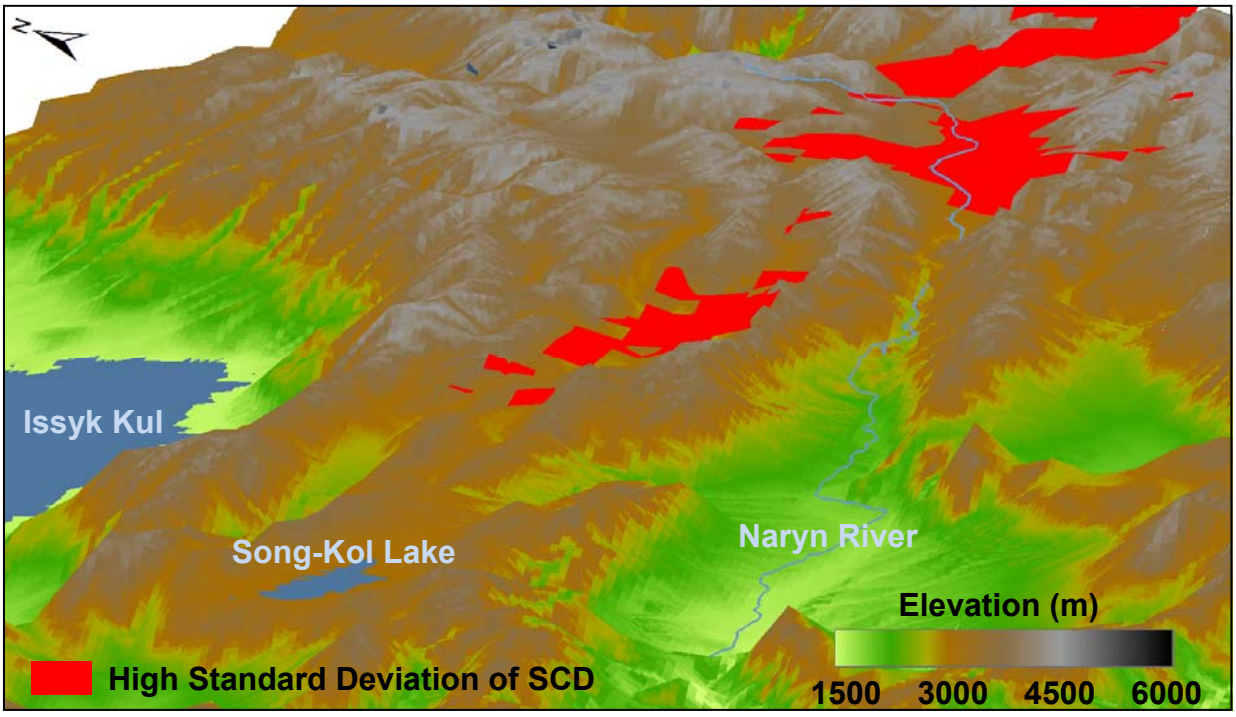

Figure 6.49: 3D-view of detail “a” from Figure 6.48

The mean SCD, SCS, and SCM are illustrated in Figure 6.14 and Figure 6.15, Figure 6.26 and Figure 6.27, Figure 6.37 and Figure 6.38. These figures include profile lines representing the snow cover conditions along a latitudinal transect through the plains of Turkmenistan, Uzbekistan, and Kazakhstan (profile lines 1) as well as the conditions within mountainous terrain (profile lines 2). The mean SCD for the plains is comparable to the result from the large scale snow cover study from Brown & Mote (2009): SCD of up to 140 days per hydrological year for most northern regions, constantly decreasing while moving southwards. The mountainous regions cannot be compared due to the coarse resolution of the global SCD product presented by Brown & Mote (2009).

The change in snowmelt characteristics is of particular interest for hydrological applications such as the management of reservoirs and runoff, as already stated in section 2.1. Siegfried et al. (2011) underlined that a shift towards earlier snowmelt in mountainous terrain is most likely to occur due to climate change and that such a shift would have severe impacts on the runoff regimes of Amu Darya and Syr Darya Rivers. The results presented in section 6.2.3 proof that this shift actually already took place within the last 26 years: In Figure 6.42, the difference between mean SCM from 1994/1995 to 2002/2003 and mean SCM from 2003/2004 to 2011/2012 reaches up to 12 days. Elevation zones above ~1,500 m are affected by this shift while regions situated at lower altitudes stay stable with regards to SCM. In Figure 6.44, earlier SCM can be identified for most upstream sub-catchments of Amu Darya and Syr Darya rivers. This shift in SCM in the upstream catchments potentially influences water availability in the whole study region. Since climate change with increasing temperatures will continue to affect the area (increase of +0.26 to +0.4°C per decade is predicted for mountainous regions (Nogués-Bravo et al., 2007)), the observed shift in SCM is most likely to prolong and intensify throughout the future (as also suggested by Kim et al. (2012)). The projected increase in population with the likewise increasing water demand combines to a tensed situation that puts serious challenges to future water management authorities. At this point, the statement of Glantz (2005) should be recalled that the long-term survival of Central Asia is strongly depending on the flow of Amu Darya and Syr Darya Rivers.

Results from the SCS processing point towards earlier dates of snow cover onset since the beginning of the time series (Figure 6.31 and Figure 6.33), confirming the suggestions of Mokhov et al. (2006). This affects all elevation zones in equal measure. The high variability of SCS in the mountainous regions was already addressed to. The general trend towards earlier SCS in the upstream mountain regions is visible from Figure 6.33: Most sub-catchments are characterized by earlier snow cover onset today when compared to the situation between 1986 and 1992. An unfortunate implication that is directly connected to an earlier SCS will be

illustrated in the very passage: An earlier SCS does not necessarily have a direct influence on the hydrology of the study region. The growing period has already passed in November and the water that is stored within the fresh snow packs will only be released in the upcoming spring and summer months. Therefore, an earlier SCS is of little direct use for water management. It may affect the herders of livestock since earlier snow cover onset will force them to return the animals to their stables and feed them with forage prepared during the growing season. Such small scale implications are not the objective of the thesis. However, since SCS and SCM add to the most common snow cover parameter SCD, changes towards earlier snowmelt will be compensated by earlier SCS. Figure 6.19 confirms that upstream SCD only varied marginally during the last 26 years. This implicates that a shift towards earlier SCM – which is most prevalent for runoff generation – may be concealed when referring to SCD as the most prominent snow cover parameter. This also becomes obvious from Figure 6.21: SCD in this figure remains constant for elevation zones below 3,600 m and even increases above this altitude. When considering only SCD, the most significant development towards earlier SCM may be overlooked. It is therefore of major importance to adhere to all snow cover parameters – SCS, SCM, and SCD – and to establish these parameters as the standard data sets for future snow cover studies.

Many results are presented referring to the snow cover parameters as a function of topography. The elevation plays an important role with regards to onset, duration, and melt of snow. This was already mentioned in section 2.2. Figure 6.21, Figure 6.30, and Figure 6.41 depict the mean snow cover parameters per elevation zone. On average, SCD increases by 4-5 days per 100 m of elevation. Between ~3,700 m and ~4,400 m elevation, a trough-like shape appears in SCS, SCM, and SCD that is rather eye-catching. SCD remains nearly constant in this 700 m wide zone. The reason for this behaviour, however, reveals itself only on a second view. Figure 6.50 illustrates the topography of southern Central Asia, highlighting the elevation zone between 3,700 m and 4,400 m in a red shade. The Pamir Mountains in the South-East of the region comprise a large proportion of this elevation zone. Contrary to Kyrgyzstan, where this zone is situated on the ridges and mountain tops, the area is best described as a valley-like feature, surrounded by higher mountain ranges and peaks in Tajikistan. The Murghab River, running from South-East to North-West into the Sarez Lake, and the Alitchur River, running from East to West and into the Yashikul Lake constitute the centres of these valleys. At this point, Figure 6.48 should be reviewed, referring to regions with high variability of SCD. Together with Figure 6.50 it may give an answer to the question why snow cover parameters depict a trough-like shape between 3,700 m and 4,400 m: The topography of the region prevents from stable snow cover conditions. The high mountain ridges are most likely gathering most of the precipitation while the enclosed valleys only receive snow through wind transport

from the surrounding ranges, which is not a stable feature. Therefore, mean snow cover parameters fall behind what would usually be expected when only examining the linear increase of SCD while moving uphill.

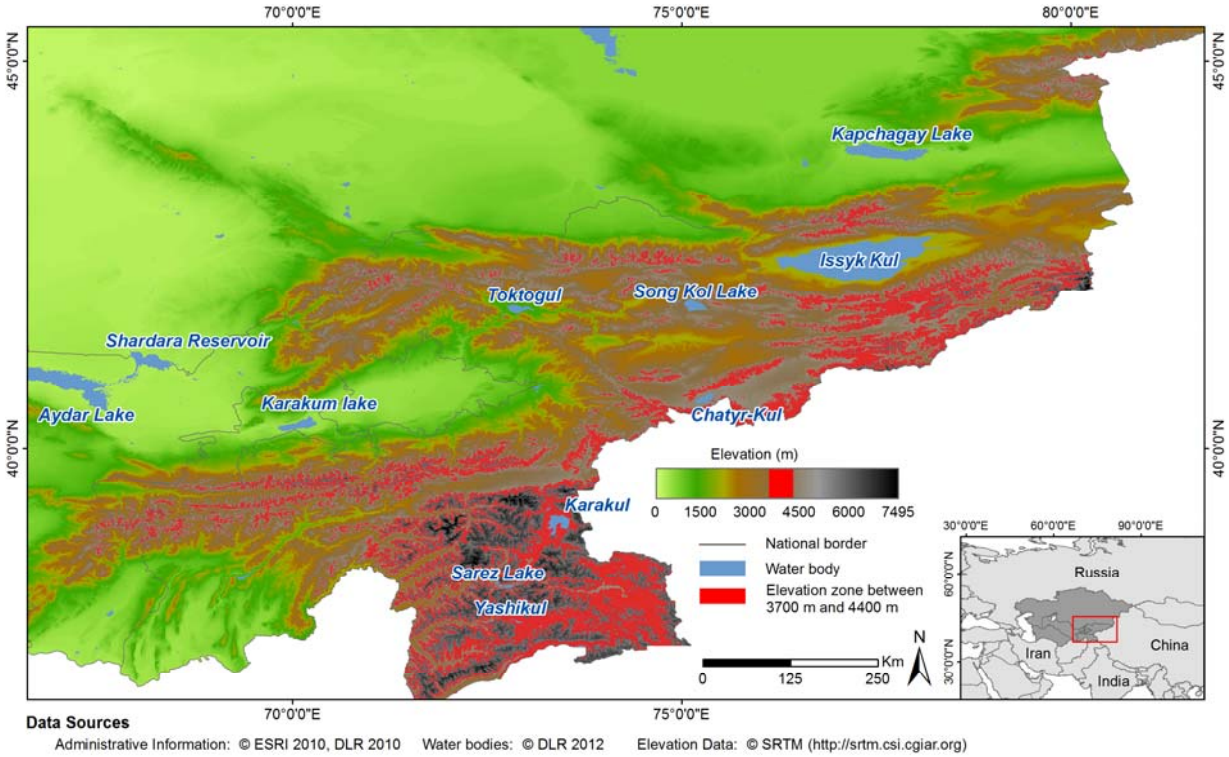

Figure 6.50: Elevation zone between 3,700 m and 4,400 m

Slope orientation of the mountain ranges is another factor influencing snow cover parameters. Figure 6.22, Figure 6.32, and Figure 6.43 illustrate the effect in 45° steps, moving clockwise from 0° to 360°. As expected, snow cover remains longer on north and north-east facing slopes than on southern slopes. It was already stated in section 2.2 that the heat input generated by solar insolation can reach nearly three times higher values for southern than for northern slopes. This leads to a difference in SCD of up to 20 days for elevation zones above 3,000 m, up to 8 days earlier SCS, and up to 15 days later SCM – depending on the elevation zone under investigation. Usually, higher altitude is directly linked with earlier SCS, later SCM, and therefore, longer SCD. SCS constitutes a slight exception from this rule: Above 3,000 m, the elevation has no impact on the beginning of the snow season.

The analysis of snow cover parameters according to elevation zones may appear controversial on a first glance: The mountainous region stretches for more than 10° latitude and 16° longitude. If such a huge area is generalized, climatic variability between potentially different climate zones cannot be considered. This argument would definitely be correct for the

plains of northern Central Asia, as mean temperature and precipitation change according to latitude and longitude. Figure 2.1 (precipitation) and Figure 2.4 (temperature) demonstrate these characteristics. These figures, however, also illustrate that precipitation and temperature in the mountainous regions do not follow the geographical position on the Earth's surface, but they rather change in accordance with the alternating topography. Severskiy et al. (2000b) confirmed that increasing altitude within mountainous regions plays a major role for the distribution of snow. Local differences may still occur but since the presented results are aggregated over time and among elevation zones between one hundred and several hundred meters, the local variability is omitted. This is also a question of clarity: Providing individual results for smaller entities is possible, but it is unfeasible to illustrate the snow cover characteristics and development for each single pixel (just to exaggerate the example), even though the presented datasets would suffice to do so.

6.3 Results from the accuracy assessments

One approach to assess the accuracy of the prepared snow cover products was derived comparing the snow cover status as taken from the cloud-free MODIS product with the field trip data recorded in Kazakhstan between December 6th and 12th, 2010 (Figure 5.8) that was already presented in section 4.5 and 5.6. Unfortunately, only 20 points from the field trip data can be used for the accuracy assessment of the cloud reduction scheme because clear sky was present during the remaining observations. Clouds were removed from all 20 points during the application of the cloud reduction scheme. As a result, 4 of these 20 points assumed a wrong snow cover status. Overestimation of actual snow cover occurred in all those cases. According to this, the accuracy of the cloud-free daily snow cover product adds up to only 80%. However, since only very few field data with cloud cover were available, the results from this assessment must be interpreted with care.

Additional accuracy details of the APOLLO snow cover products were already presented in section 6.1. The comparisons between AVHRR and snow cover products from MODIS or Landsat are a direct and very common way of assessing the accuracy. Similar approaches were followed by many other researchers (e.g. Hüsler et al. (2012), Chokmani et al. (2010), or Jain et al. (2008)) but unfortunately, a direct accuracy assessment of the cloud-free snow cover data prepared for the presented thesis is not possible as explained in section 5.5. In section 6.1, the accuracy of the PPL3 products was assessed comparing the cloud-free snow product with Landsat. This only worked for Landsat scenes with very few cloud covered pixels - which are rare for winter and springs seasons. Therefore, an indirect accuracy assessment was de-

rived, using the theoretical precision of each applied step to reduce the cloud coverage as the basis for the calculation. During the application of the cloud reduction scheme (Figure 5.4), each cloud covered pixel will be processed by one of the successive steps. The accuracy of each method is known from earlier studies (see section 3.2.3). Therefore, tracking the amount of processed pixels and the respective method that was applied to the pixel, a theoretical accuracy of each pixel can be calculated. As a result, each pixel within the final, cloud-free snow cover dataset will have a distinct accuracy that depends on the processing step applied to the pixel. By calculating the mean from all pixels within a single scene and furthermore, a whole year, the accuracy can be derived. This was done for the presented thesis. Figure 6.51 includes examples for three MODIS tiles (see Figure 4.2 for an overview of tile location) and two years: 2004/2005 and 2010/2011.

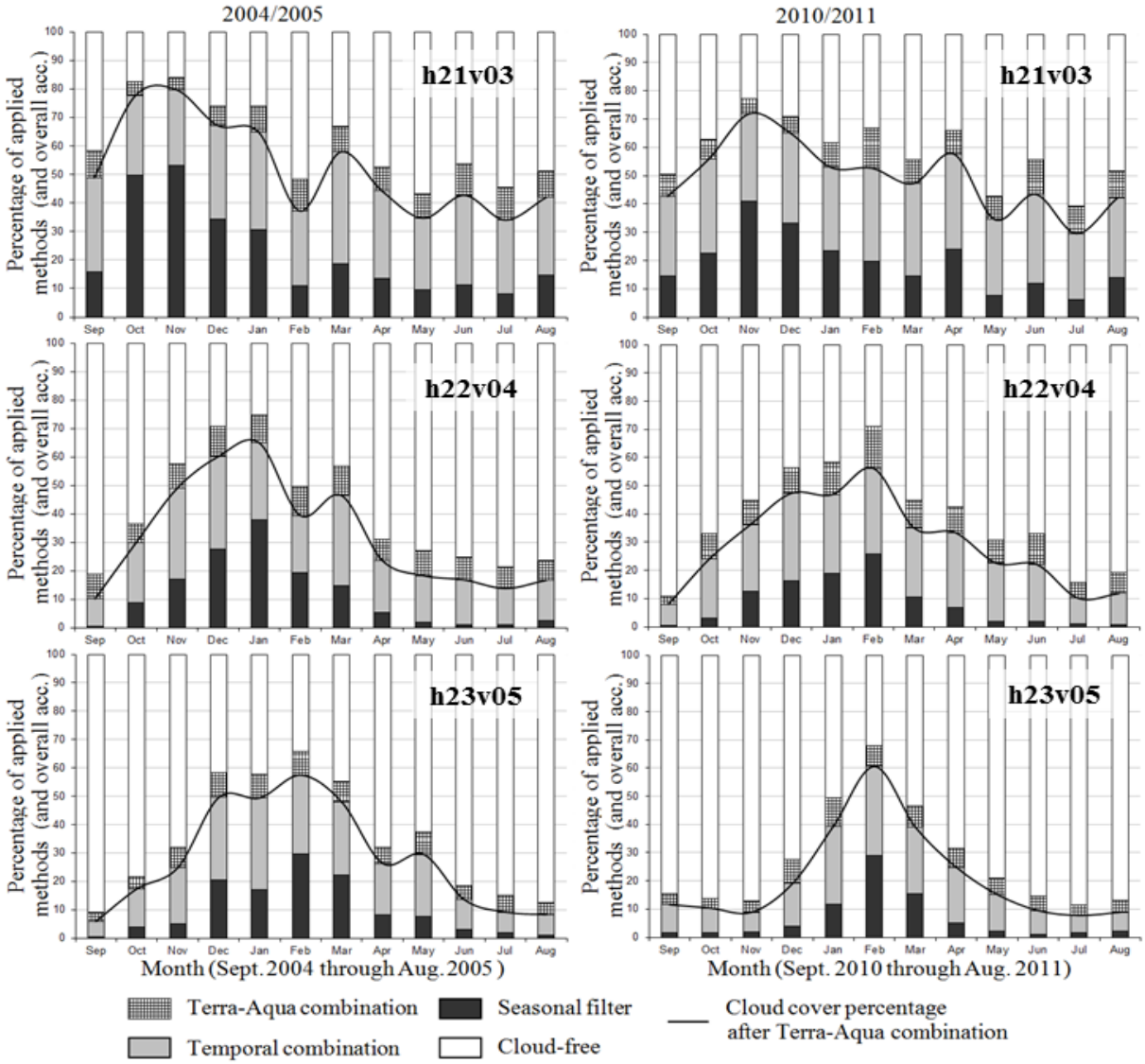

Figure 6.51: Indirect accuracy assessment of cloud-free snow cover data (adopted from Dietz et al. (2013))

The percentage of cloud-free pixels in the original snow cover product (MOD10A1) is given by the white bars: Cloud cover fraction is smallest during summer months for all MODIS tiles. The next bar following below the cloud-free data fraction is the percentage of pixels that was successfully processed applying the combination of MOD10A1 and MYD10A1. The accuracy of these pixels is only marginally less than of the original (MOD10A1) data because of the lower precision of MYD10A1 (~0 to 5%, see Riggs & Hall (2004)). The temporal combination is referred to with the next bar that is represented in a light grey shade: This step is characterized by again lower accuracy than the original data (~90%), which means that the overall accuracy of the final product is altered for each pixel processed by this step. According to Figure 5.4, the snow line detection follows after the temporal combination. This step is missing in Figure 6.51 for a reason: The percentage of processed pixels is generally very low for this step (<2%), affecting the legibility of the figure if included as an additional bar. This does, however,

not imply that the method was omitted: It is applied to all pixels with remaining cloud coverage after the temporal combination. Only after snow line detection, the last cloud reduction step – the seasonal filter – is conducted, which is included in Figure 6.51 as the dark grey bar at the bottom of each graph. Accuracy is lowest for this step (~80%), meaning that each pixel processed by this last step will reduce the overall accuracy of the final product considerably. It is visible from Figure 6.51 that the proportion of applied methods differs for each MODIS tile and year.

The mean accuracy is calculated from all processed years and also shows small variability: The most north-western region (MODIS tile h21v03) is generally characterized by higher cloud coverage, therefore requiring more pixels to be processed by the cloud-reduction scheme. Overall accuracy (as calculated from the indirect accuracy assessment) reaches 89.5% here. In the south-eastern area (MODIS tile h23v05), cloud coverage is consistently lower and therefore, overall accuracy is higher than in the North-west: It accounts for 91.6%. These values only apply to the MODIS time series from 2000 onwards. Because the accuracy of the APOLLO snow cover product (PPL1) is lower than for MOD10A1/MYD10A1, the accuracy of the cloud-free PPL3 data is also reduced. It reaches between 84.2% and 86.5%, with lower values in the northern regions again.

It is not possible to estimate whether over- or underestimation is dominating in the error statistics since only the basic accuracy of each step is known, but not how the occurring errors will be distributed. Station data of snow cover duration would be required to conduct a refined analysis. This is not possible for Central Asia. The transferability study that was already brought up in section 5.5 revealed some additional details about possible error distributions. Figure 6.52 and Figure 6.53 compare SCD, SCS, and SCM derived from cloud-free MODIS snow cover time series with SCD, SCS, and SCM from the ECA&D snow depth stations. As a result of this comparison, overestimation, underestimation, and absolute deviation of snow cover parameters can be estimated. 87% of all investigated pixels were affected by less than 36 days deviation in SCD, SCS, or SCM (10% were affected by error rates between 37 and 72 days, 3% by more than 72 days). Figure 6.52 and Figure 6.53 also show that overestimation of the parameters is usually prevailing (overestimation of SCM in this case stands for a misleadingly later assumed SCM date than in reality). The spatial distribution of emerging errors is, however, not recognizable from Figure 6.52 or Figure 6.53. Thus, an additional analysis was conducted, contrasting deviations in SCD with station latitude and longitude. The ECA&D snow depth stations are distributed between ~ 40° N and 70°N, 3° E and 19° E, but they are not equally distributed. This fact is also visible from Figure 5.7.

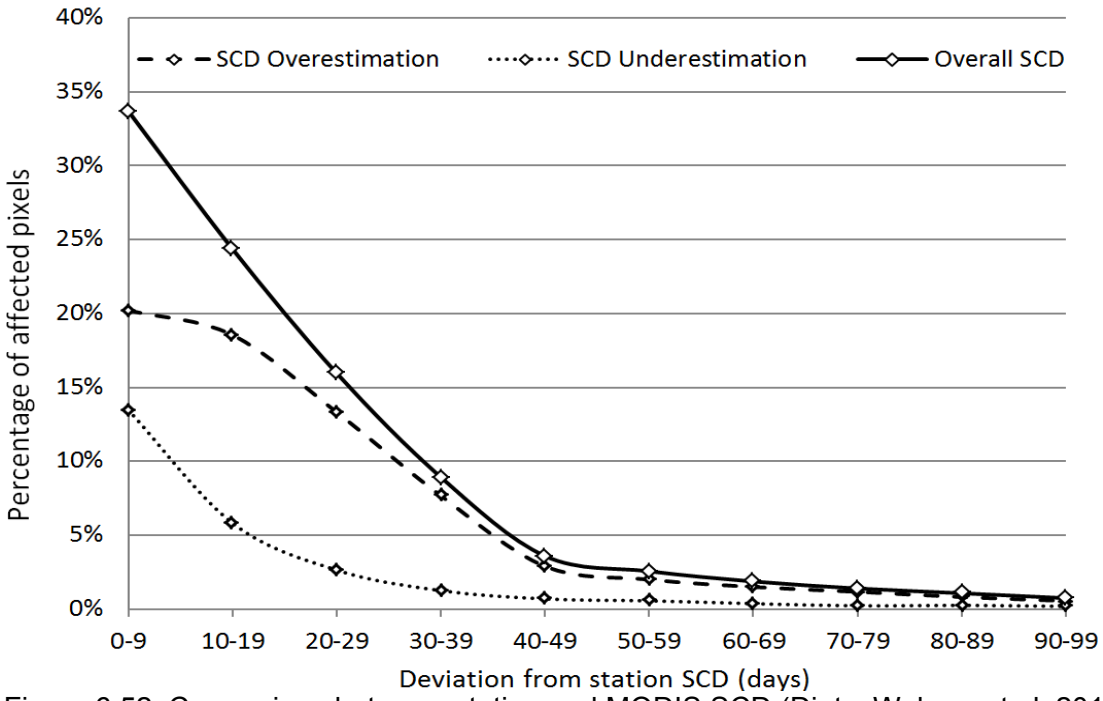

Figure 6.52: Comparison between station and MODIS SCD (Dietz, Wohner et al. 2012)

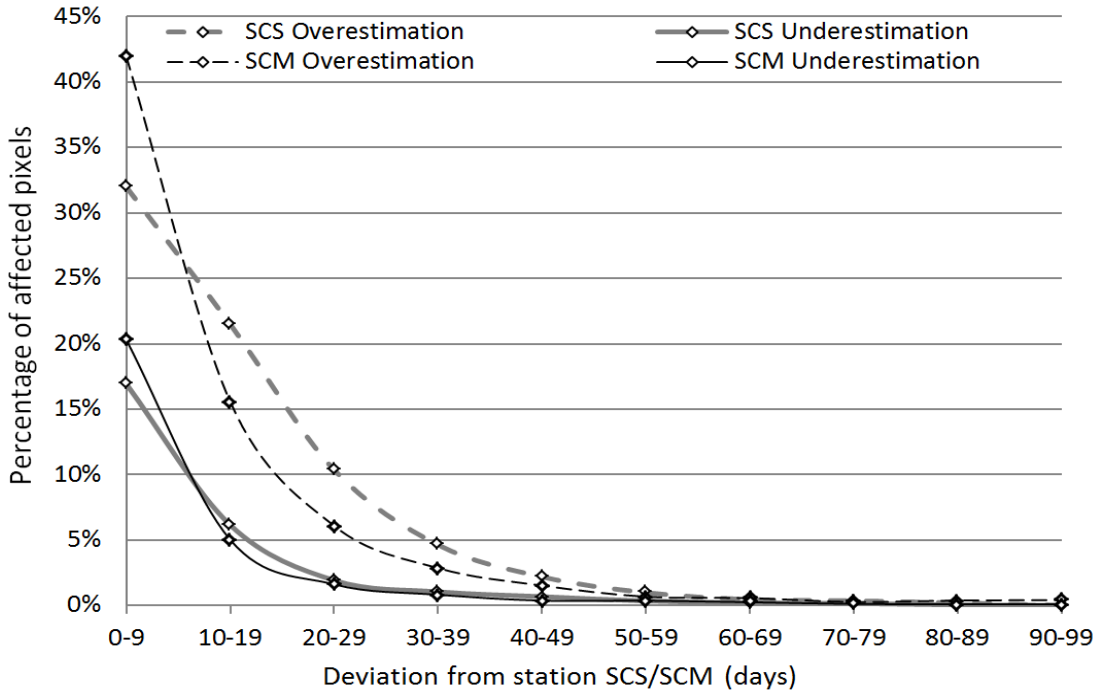

Figure 6.53: Comparison between station and MODIS SCS/SCM (Dietz, Wohner et al. 2012)

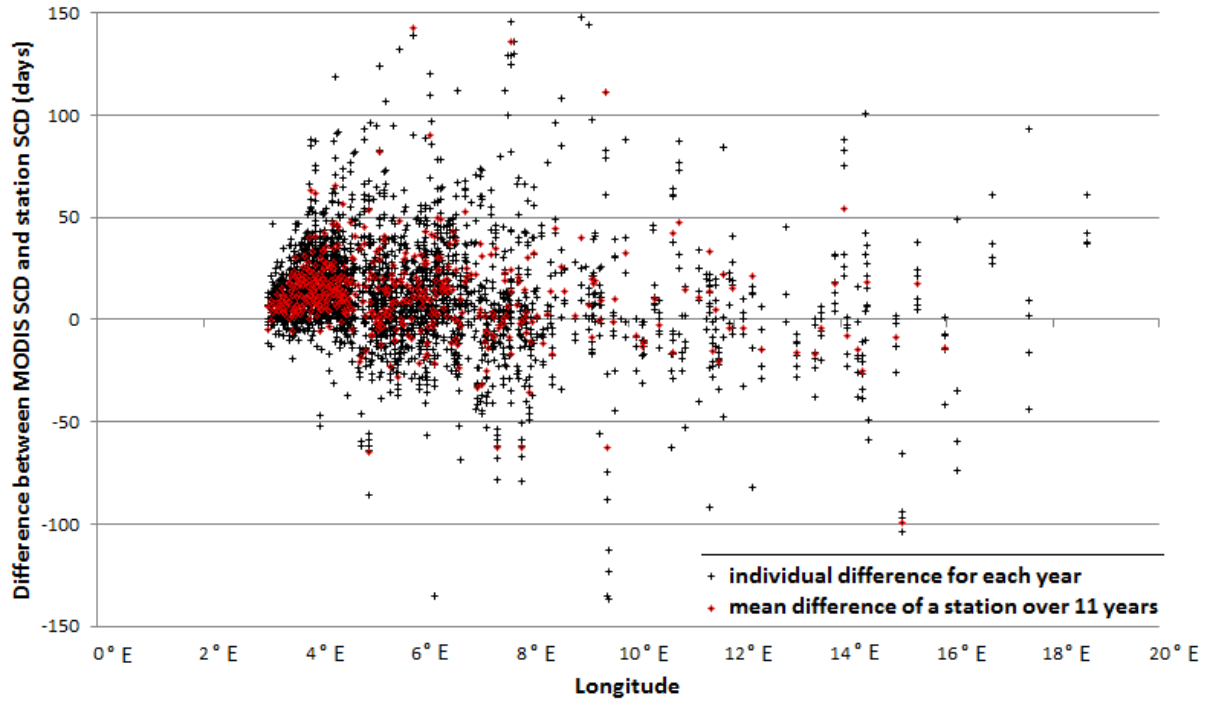

Figure 6.54: SCD differences between MODIS and station data along a longitudinal axis SCM (Dietz, Wohner et al. 2012)

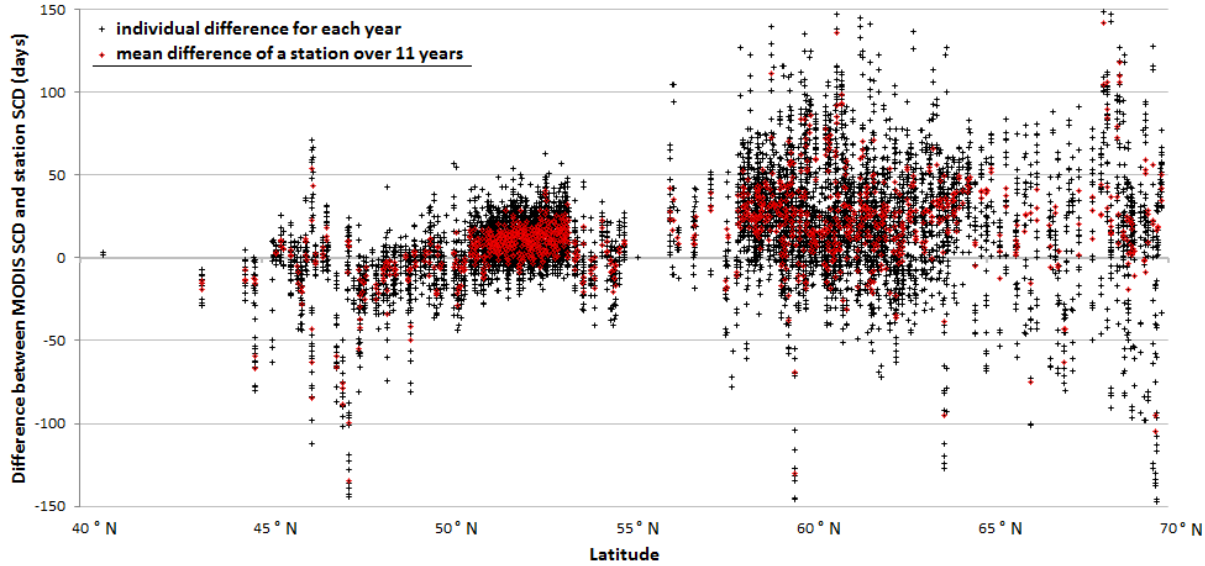

Figure 6.55: SCD differences between MODIS and station data along a latitudinal axis SCM (Dietz, Wohner et al. 2012)

The differences between MODIS- and station-derived SCD along longitudinal and latitudinal axes are illustrated in Figure 6.54 and Figure 6.55 (black crosses stand for single year, red crosses for 11-year mean deviations). The longitude does not seem to affect the accuracy of the SCD results too much. For the latitude, however, the error increases continuously while

moving northwards. The stations north of ~58° N in Figure 6.55 are located in Norway. Here, mean differences between MODIS and station-SCD reach considerable higher values than south of 58°N. Again, overestimation of actual SCD is the prevailing error in both, Figure 6.54 and Figure 6.55. These findings accord with those from Central Asia (see Figure 6.10). The accuracy assessment for Europe – though based on 896 stations – may again be affected by several influences: The stations are not equally distributed over the study area (Figure 5.7). Concentration of stations is highest in the Netherlands, followed by Norway, and Germany. Norway is problematic for several reasons: Polar night is affecting the region, leading to long-term data gaps north of ~ 61° N. The number of continuously missing observations due to polar night reaches more than 100 in most northern Norway. Because sensor combination, temporal interpolation, and snowline detection (steps 1, 2, and 3 from the cloud reduction scheme) cannot help to estimate snow cover status during this period, the last step with the lowest accuracy is used to process huge amounts of pixels. Figure 6.55 proves that deviations between station- and MODIS-derived SCD differ most in northern latitudes. This is not a problem in Central Asia because polar night is not an issue there. A second problem is the relatively high forest cover fraction of Norway's land cover. 27% of the area is covered by forests (Lindstad, 2002), which is 15 times more than the 1.8% of Central Asia (Klein et al. 2012). Because forested areas tend to affect the snow mapping accuracy (see e.g. Hall et al. (2001) and section 3.2.1), it can be assumed that the classification accuracies of MOD10A1, MYD10A1, and APOLLO PPL1 in Central Asia are higher than in Norway, automatically leading to a higher accuracy of the post-processed cloud-free snow cover products (because this is based on the underlying accuracy of the basic snow cover products).

Some uncertainties remain that should be discussed at this point, though some of them were already shortly addressed to during the presentation of the snow cover parameters: One problem may arise from the fact that only 414 AVHRR pixels (894 MODIS pixels) are situated in elevations above 6,000 m. This amount is very low, compared to the remaining elevation zones (5,000 m to 6,000 m: 28,600; 4,000 m to 5,000 m: 153,900; 3,000 m to 4,000 m: 242,600; 2,000 m to 3,000 m: 261,700; 1,000 m to 2,000 m: 607,000; 0 m to 1,000m: 7,616,400; all numbers referring to MODIS pixel scale). It is important to emphasize that results from e.g. Figure 6.21, Figure 6.30, and Figure 6.41 should be interpreted with care for regions above 6,000 m elevation. The abnormal swaying of the plots especially above ~ 6,800 m may arise from the relatively sparse data basis (only 37 MODIS pixels and 18 AVHRR pixels are situated above 6,800 m). Another problem is linked to the pre-processing of the snow cover products – both from AVHRR and MODIS: The classification scheme of APOLLO relies on an internal water mask to detect cloud-free pixels from AVHRR scenes (see Figure 3.7: reflectance test of channel 1 and 2 for land and sea surface, respectively). This implies that

the underlying water mask is up to date. The same is true for the *Snowmap* algorithm producing the MOD10A1 and MYD10A1 snow cover products: It relies on an internal water mask (USGS 1 km land/water mask from 1996) for cloud detection within the MOD35 product, which is then used as a basis for the snow cover classification (Riggs et al. 2006; Hall et al. 2001; Ackerman et al. 2006). The high variability of water bodies in Central Asia is a well-known situation documented by various researchers (Klein et al. 2012; Micklin 2007; Aladin & Plotnikov 1993). The majority of Central Asian lakes experienced a continuous areal decrease since 1975 (Bai et al., 2011). This results in classification uncertainties for areas that were formerly covered by water but have dried out since the generation of the static APOLLO or MODIS water masks. Figure 6.56 compares the APOLLO, MODIS, and 2009 real water body extents (2009 taken from Klein et al. (2012)) against each other. The difference is obvious. Because the area of the Aral Sea decreased considerably during the last decades, classification results from within the erroneous water masks are not reliable. This affects both APOLLO and MODIS products.

Another problem is connected to the spectral channels provided by the AVHRR sensors: There are only five spectral channels available. Even if every other aspect is ignored (geolocation problem, calibration issues, data gaps), the fact that AVHRR channel 1 (VIS: 0.580 – 0.680 µm) has a spectral bandwidth five times as big as the respective MODIS bandwidth (0.545 – 0.565 µm) and channel 3A (MIR: 1.580 – 1.640 µm) is still twice as broad compared to MODIS (1.628 – 1.652 µm) makes clear that an NDSI derived from AVHRR will never be as accurate as the MODIS counterpart. This is something that should always be kept in mind when analysing AVHRR data.

The geolocation uncertainty of AVHRR is a third error source. This was already mentioned in section 6.1 and will be discussed in more detail with regards to the ability of the presented snow cover parameters to map glaciated/permanently snow covered areas (which is not possible for Central Asia using AVHRR data) in section 6.4.

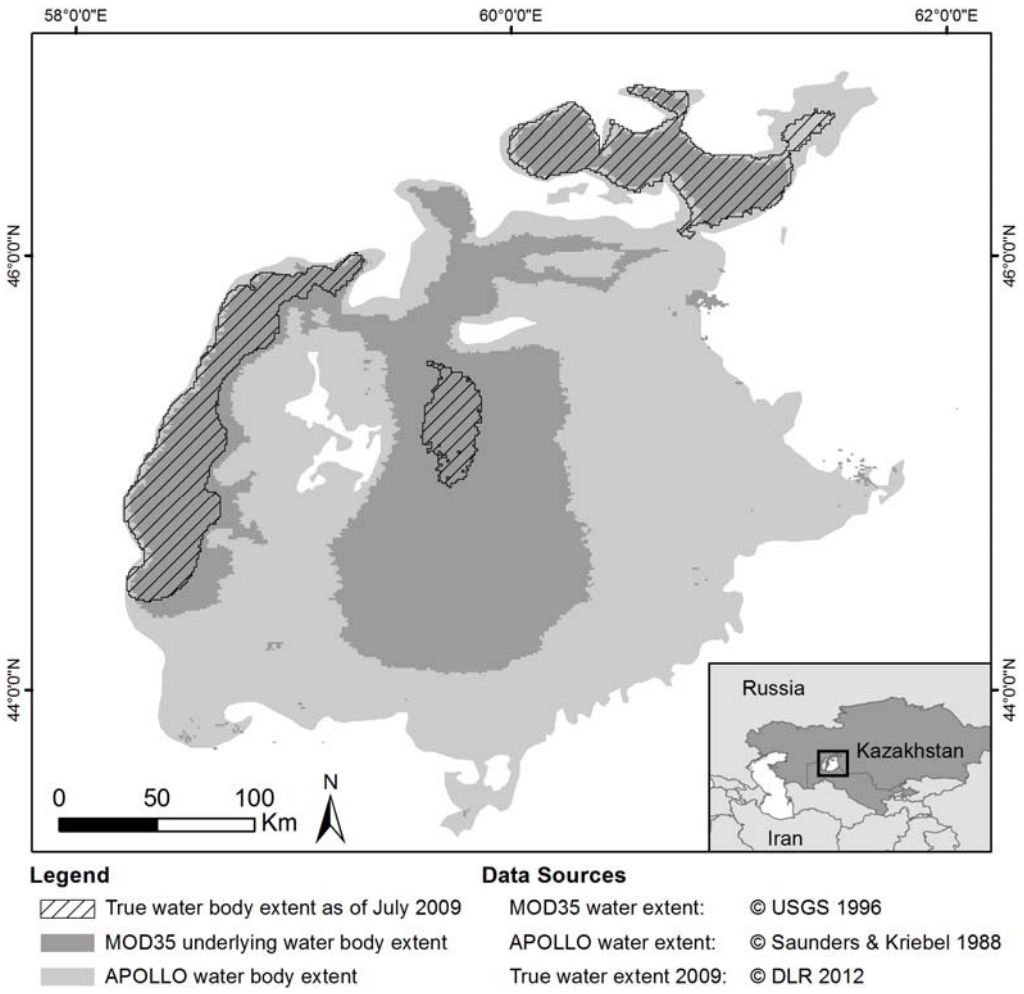

Figure 6.56: Water body extent of APOLLO and MODIS water masks as well as the true water body extent from 2009

Issues that are often discussed when combining and analysing remotely sensed data from different sensors with different resolutions are scaling/rescaling/resampling, mixed pixel handling, resolution variances between the sensors, and error estimation connected to these topics. The transformation from raw orbit to map projection is a necessary evil, introducing possible errors to the satellite data (Khan et al., 1995). Before addressing these problems, one of the primary objectives of the presented thesis should be recalled and kept in mind: To identify the snow cover characteristics of Central Asia – including SCD, SCS, and SCM –, analyse their developments, and estimate possible future impacts. The identification of SCD, SCS, and SCM requires daily and cloud-free data: a fundamental prerequisite that is not up for debate. There is often a trade-off between temporal and spatial resolution but in the presented thesis, the temporal resolution was already carved in stone from the outset. The question is therefore not, whether to prefer one or the other data source but what impact the medium resolution of 1.1 km (AVHRR) or 500 m (MODIS) might have on the final results. Furthermore: Will the switch between AVHRR and MODIS in the year 2000 introduce additional uncertainty due to

the changed sensor resolution? Section 6.1 included a paragraph dealing with the higher error rates in PPL1 (and PPL3) AVHRR snow cover products in the transition zone between snow covered and snow free land. Hall et al. (2002) attested that the *Snowmap* algorithm used to map snow cover for the operational MODIS product only recognizes snow covered areas with at least 50% snow cover fraction. If transferred to the MODIS pixel size of ~ 0.250 km², 50% would mean that at least 0.125 km² of snow covered area are required for a MODIS pixel to be flagged as snow. On the AVHRR scale (pixel size ~ 1.210 km²), around 0.6 km² of the area must be snow covered, if assumed that the 50% fraction is also valid for the APOLLO product (which has not been confirmed so far but appears most likely after accomplishing the accuracy assessment in section 6.1). In general, the over- and underestimations of snow cover will even out – given the vast size of the area and the long time span of the time series. The 50% rule will work in both ways, meaning that a MODIS pixel with only 0.126 km² snow cover will be classified as snow, overestimating the actual snow cover by nearly 50% while in a pixle only covered with 49% of snow, underestimation will occur. This may affect the accuracy of single day results, but level off in the long term. For narrow mountain ridges, however, the difference in pixel size may contribute to an enduring and continuous misinterpretation of true snow cover conditions in AVHRR data when compared to MODIS. If the ridge is too narrow to take more than 50% of the pixel, snow cover that is present on the top of the rigde will not be recognized by the algorithm. Results from sections 6.2.1 to 6.2.3 have demonstrated that elevation plays a significant role for SCD, SCS, and SCM. If an arbitrary elevation range covers less than 50% of an AVHRR pixel, the snow above this elevation and within this pixel will not be recognized after the snow line has passed this elevation. For MODIS, the smaller pixel size automatically leads to a refined snow cover detection: Snow covered ridges too small for AVHRR (e.g. during summer months when valleys are snow-free) may be visible for MODIS' *Snowmap* algorithm, leading to a systematically longer SCD estimation with earlier SCS and later SCM. It is not possible to quantify this effect without exaggerated effort. Section 6.4 will include an outlook on glacier monitoring with MODIS and AVHRR data, constituting a distinct limitaiton of AVHRR's coraser resolution.

Another problem that was also addressed to in section 5.3 is the possibly biased representation of SCS and SCM. The example given in Figure 5.6 explains why a straight-forward solution of the problem is not possible because it would always involve another threshold that would inevitably lead to errors. In my view, the main problem is not the approach of calculating SCS and SCM, but the denomination in "Snow Cover Start/Snow Cover Melt" and the intention to provide one single date for these parameters. This simply does not exist in nature. Transient snow fall with interim snow melt events are a wide spread and common occurrence. The suggestion arising from the presented thesis is therefore to define these two parameters as "Early

Season Snow Cover Duration" (ESSCD or SCD_{ES}), and "Late Season Snow Cover Duration" (LSSCD or SCD_{LS}) – similar to the proposed SCI_{ES} and SCI_{LS} in section 6.2.4. The significance of these parameters is emphasized at various locations - especially when it comes to hydrological applications. Therefore, renaming the variables would reduce the weak spot that is often criticized by scientists (e.g. during the review processes of publications like Dietz, Wohner, et al. (2012) and Dietz et al. (2013)).

One important question has in parts already been answered during the previous discussions but can be extended by a few more aspects: Are there any improvements that could be applied to existing snow mapping algorithms to increase their accuracy? The answer is: Yes, there are. One important aspect has just been mentioned: The static water mask that is included in the processing chain should be replaced with a dynamic one. This water mask could be automatically generated from observations prior to the actually processed snow scene – e.g. comprising one month of reflectances from the NIR. A method to derive water bodies dynamically was presented by Fichtelmann & Borg (2012). This or a similar algorithm may find its way to the operational MODIS and APOLLO methods, replacing the outdated static water masks and all the errors that they cause. Many improvements may come into one's mind when reflecting the APOLLO classification scheme, that appears outdated when compared to newer methods presented in section 3.2. One reason why APOLLO was chosen among the available algorithms was the independence from ancillary data such as precipitation and temperature data. If it was possible to apply a method like SPARC without any additional input data, the results would most likely be more accurate than those from APOLLO. Research is needed to test whether a combination of e.g. theta and SPARC is feasible, where theta will replace the T-test involving surface temperature in SPARC by a three-space vector of AVHRR channels 3, 4, and 5. The drawback of theta is that a reference vector must be selected manually. This step could be accomplished automatically, depending on the results of the SPARC tests processed before. The scores from the two SPARC tests (B- and R-test) can be used to identify some surfaces that are snow covered without any doubt. These areas may serve as reference for those pixels where the classification needs additional information, involving theta and the reference vector derived from the previously defined snow covered pixels. This is, however, just an untested theory.

6.4. Snow cover development and its influence on transboundary water management

Transboundary water management is an important topic in Central Asia and a direct application opportunity of the obtained snow cover results, as the snow cover has an immediate impact on the surface runoff and water availability in Central Asia. Section 2.1 already included some statements about the transboundary water issues that are prevailing among the states of Central Asia. Water scarcity is often portrayed to be a possible trigger for serious future conflicts, not to mention "*water wars*" (as entitled in a book by Younger (2012)). Though the author states that real "*water wars*" have not yet evolved, a statement of Uzbekistan's President Islam Karimov given during an official speech in Astana, Kazakhstan on September 7th, 2012 suggests that this auspicious status is dangling on a string: Within this speech, he threatened Kyrgyzstan and Tajikistan that on-going efforts to establish new hydroelectric power stations upstream of Amu Darya and Syr Darya Rivers could lead to war (Lillis, 2012). (Sehring and Giese, 2011) also reported that many small scale violent incidents already occurred, often connected to the access to water resources. The geopolitical situation in Central Asia is absolutely not the topic of the presented thesis, but with the objective of the CAWa project to "*avoid water conflicts and stabilize the region substantially*" (http://www.cawa-project.net/page/9) in mind it is clear that new findings about potential water resource developments will contribute to this sublime aim. Changed snow cover characteristics - with the shift of up to 12 days towards earlier SCM being one major finding – may pose a challenge difficult to overcome in future water management, especially if the development towards earlier snowmelt proceeds into the future. A figure of the Amu Darya hydrograph at the border of Uzbekistan taken from a publication of Jalilov et al. (2011) will illustrate the relationship: Figure 6.57 depicts the runoff of Amu Darya River as it enters the territory of Uzbekistan. The natural runoff (white line entitled "*no Rogun Dam*") is compared to the situation with the Rogun Dam – a dam intended to be used for hydropower generation at the Vakhsh River - operating (black dotted line). The red line was added to highlight the theoretical effect of earlier snowmelt on the natural runoff: The peak of the annual flow would shift towards an earlier date, which would clearly influence the runoff regime of Vakhsh, and therefore Amu Darya River. Thus, even with an operating Rogun Dam and a correspondent reservoir on site, earlier snowmelt may cause the reservoir to exceed its capacity before the water is needed downstream. The consequence could be that the reservoir must be opened in order to prevent possible damage to the structure, leading to a loss of the most valuable water resource and possibly even flooding events of downstream areas. At the end of the season, the water would then be missing for irrigation (indicated by the blue plot in Figure 6.57). The example of Rogun Dam is just a theoretical demonstration of what could happen due to changed SCM. There are, as mentioned in section

2.1, more than 290 reservoirs in Central Asia and many of them could face similar challenges in the future. Rogun Dam, however, was one of the causes that led to the most provocative comments of Islam Karimov in 2012 about an armed conflict with the upstream countries of Kyrgyzstan and Tajikistan.

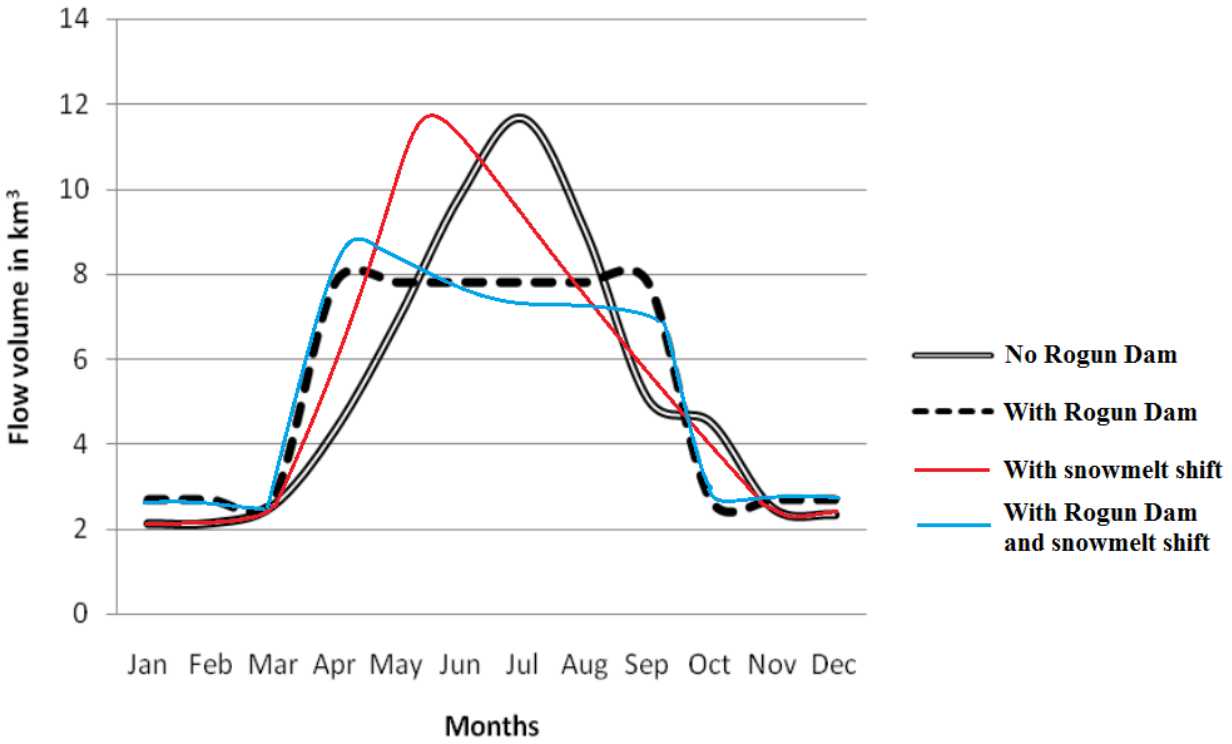

Figure 6.57: Amu Darya hydrograph at the border to Uzbekistan. Modified from the original source of (Jalilov et al., 2011)

(Barnett et al., 2005) summarized the problem on a global scale, being a perfect match for the situation in Central Asia as well: The reservoirs currently operational in the region are not sufficient to adapt to a shift in snow melt and the connected shift in peak runoff. According to the authors, the change in snow cover characteristics may considerably affect the long-term development and water security in Central Asia, as the region's water availability is strongly snow-dominated. (Messner, 2009) emphasizes that the lack of flexibility towards an adaption to changing water contingents may constitute the biggest risk. The influences of climate change on snow cover characteristics in Central Asian Mountains may therefore directly influence the geopolitical stability of the region.

6.5. Outlook on possible applications

Many different products are presented in section 6. Some of them – like mean SCD, SCS, or SCM - can stand for their own while others – like single year results - can be exploited to derive additional information about the snow cover characteristics of Central Asia. Going too much into detail about these applications is beyond the scope of the presented thesis. Some examples will be presented in this section that should encourage scientists to dig deeper into the material:

The first example is the derivation of trend analyses. SCD, SCS, and SCM are suggested to change due to climate change as it was reported from various studies also referred to in sections 3.4.1 and 2.1. To identify regions with ongoing changes – be it towards more or less snow – a trend analysis of the time series can be accomplished. For the presented example, the least-squares linear trend for each pixel within the study region is calculated. Because of the different pixel sizes of MODIS and AVHRR, the resolution of the MODIS snow cover datasets is resampled to be in accordance with the AVHRR cell size. “Nearest Neighbor” is chosen as resampling method as it has been applied successfully for comparative studies between MODIS and AVHRR, before (e.g. Chrysoulakis et al., 2008; Hadjimitsis et al., 2011; Fensholt and Sandholt, 2005). “Nearest Neighbor” can produce subpixel geometric discontinuities (Wolfe et al., 1998) but it is operated comparatively fast (Moreno and Melia, 1994), which is an invaluable advantage when processing huge amounts of data.

The trend analysis is applied to 5-year average SCD maps that were generated prior to the processing to reduce the impact of the single year results that are characterized by considerable variability. Because data before 1992 is missing for northern Kazakhstan, the analysis was only performed for hydrological years after 1991/1992. Figure 6.58 depicts the result of the linear trend analysis: High Mountain and most northern regions are characterized by positive trends while the plains are affected by a decrease of SCD. Figure 6.59 contrasts the SCD trend with elevation and confirms the above statement: Regions below 1,200 m elevation show negative SCD trends while the trend is positive for elevation zones above 1,200 m. The trend towards increased SCD even increases with increasing elevation: +0.1 days of SCD per 200 m between 1992/1993 and 2011/2012. The region above 6,000 m is again prone to uncertainties because only few pixels are located in these altitudes.

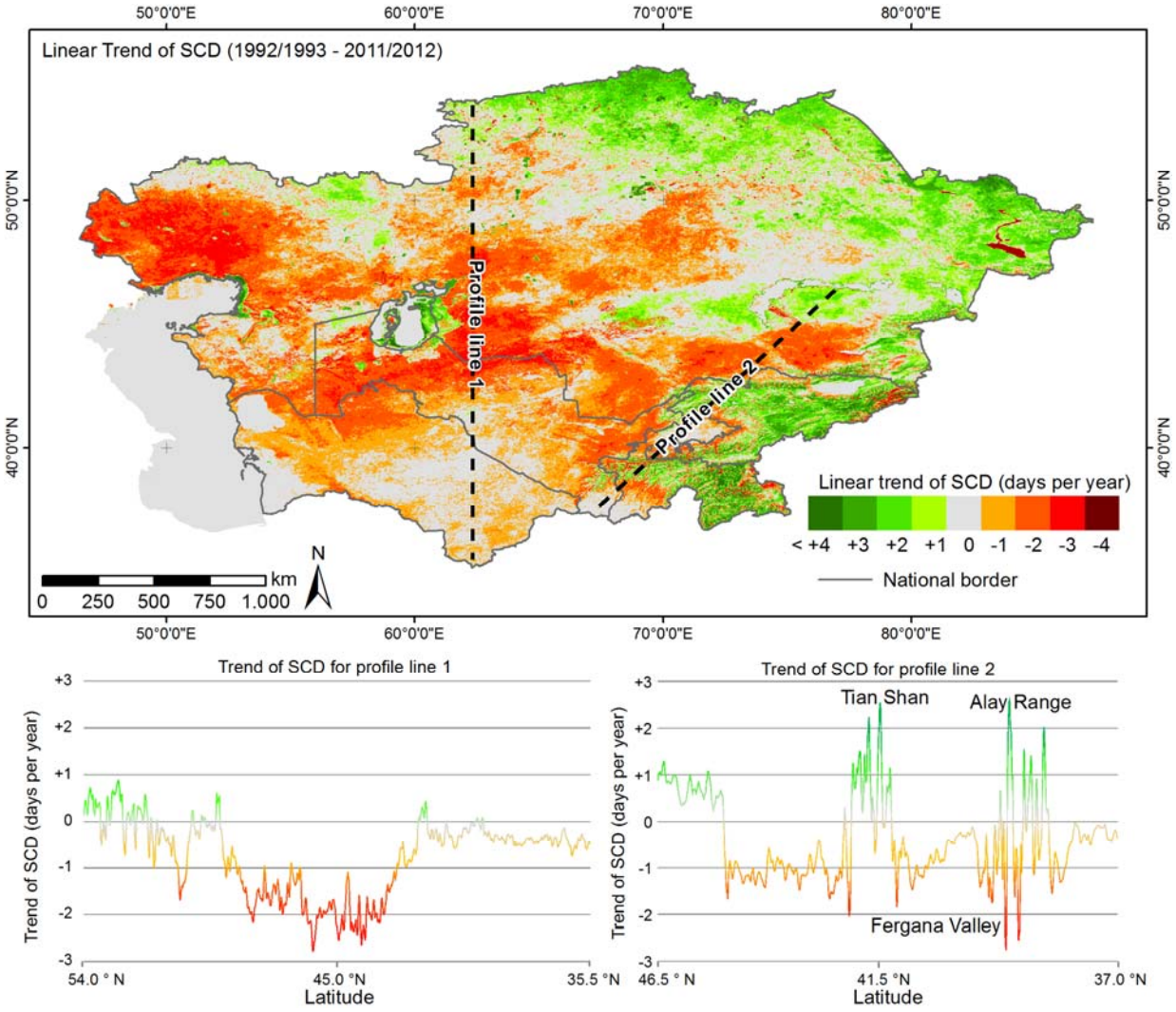

Figure 6.58: Linear trend of SCD for the period from 1992/1993 to 2011/2012

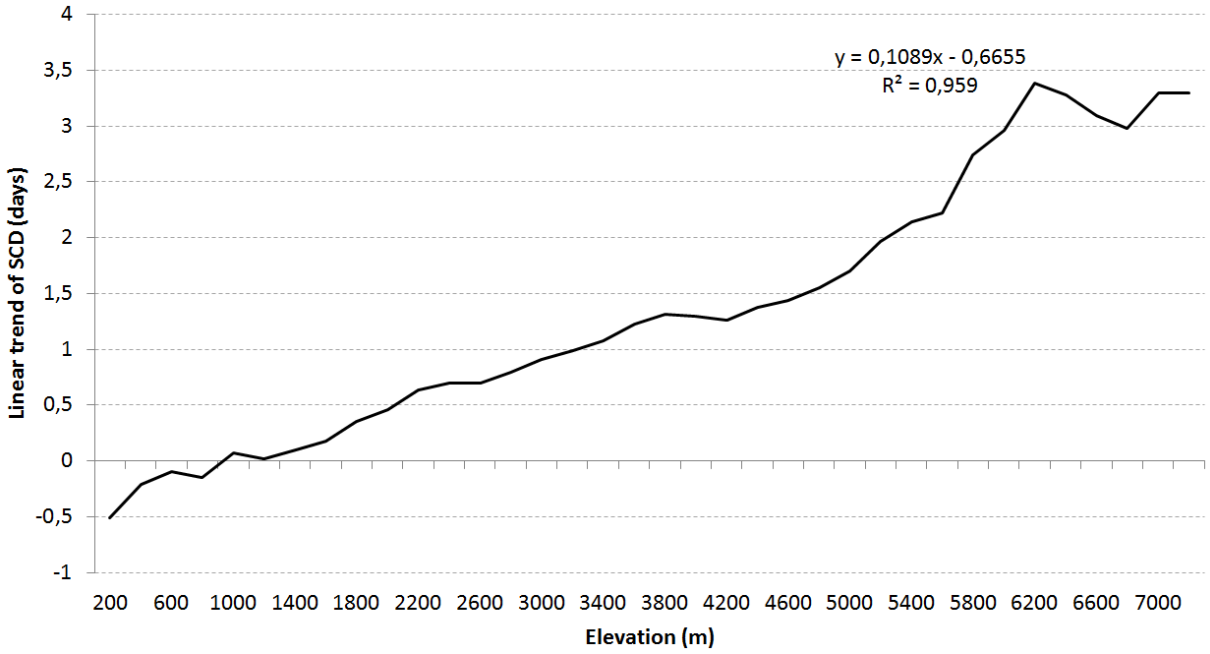

Figure 6.59: Linear trend of SCD between 1992 and 2012 compared to elevation

Some features of the trend map in Figure 6.58 appear questionable: The effect of the different and outdated water masks for APOLLO and MODIS is clearly visible in some of the results. Figure 6.58, depicting the linear trend of SCD from 1992 to 2012, shows a strong negative trend for Lake Zaysan in eastern Kazakhstan (see also Figure 1.2 for information about the exact location of the lake). The origin of this trend is linked to the different water masks behind APOLLO and *Snowmap*: Lake Zaysan is not included as a water body in the APOLLO water mask. Therefore, pixels falling within the area of the lake may be classified as snow, e.g. while the lake is covered by ice (and snow). The MODIS water mask contains Lake Zaysan, thus preventing the MOD10A1 and MYD10A1 products from classifying pixels as snow. Consequently, SCD before the year 2000 may reach much higher values than after 2000, when SCD for the area of Lake Zaysan will always stay zero. The opposite effect can be observed for the Aral Sea region: This lake was much bigger at the beginning of the AVHRR missions, when also the water masks for the APOLLO routines were generated. The effect of the high variability of the Aral Sea on the classification can again be observed in Figure 6.58: The linear trend of pixels falling within the dried out area of the APOLLO water mask (light grey area in Figure 6.56) is characterized by a positive value for SCD – contrary to the surrounding areas where a negative trend is identified. The different extents of the APOLLO and MODIS water masks exactly retrace the shape of this trend feature. This is the reason why water bodies are excluded from the thesis. They cannot be trusted because they are not updated frequently enough.

The patterns of the linear SCD trend between 1992/1993 and 2011/2012 confirm the suggestions from large scale snow cover studies: Positive SCD trends in most northern regions (like e.g. in Brown & Mote (2009) or Fallot et al. (1997)) as well as in mountainous regions above an altitude of ~ 1,500 m. The negative SCD trend that can be observed in the central area again confirms what was proposed by Brown & Mote (2009) and Groisman et al. (2006). The intensity of the derived negative trend in Figure 6.58 even nearly agrees (±1 day) to the values of Brown & Mote (2009), suggesting that the results for the mountainous regions will also apply. This implies that though the significance of the derived linear trend is low, the results are still on the right track. There is, however, one aspect that may influence the validity of the trend estimation in the mountains: The geolocation uncertainty of AVHRR may compromise the accuracy of the SCD results for mountain ranges. This effect may also influence trend calculations for these regions, entailing misleadingly positive trends. It must be noted that the significance of the presented trends is generally low. The high inter-annual variability of SCD (even within the 5-year means) and the comparatively short time series of only 19

years may be some of the reasons. The geolocation uncertainty is certainly the most influencing factor especially in mountainous regions, as SCD can change significantly within very short distances. Shifts of only few pixels already compromise the trend analysis when applied on a per pixel basis. Since the presented trends are only included as an outlook, a detailed analysis of the occurrent uncertainty is omitted.

A second possible application of the processed snow cover products is the analysis of connections between snow and river runoff. Snow cover information has proven to be useful in predicting river runoff before (see studies of Butt & Bilal (2011), Bales et al. (2008), and Blöschl et al. (1991)). The SCI constitutes a promising parameter for this purpose since it gives a comprehensive overview of snow cover characteristics for a whole catchment in just one variable.

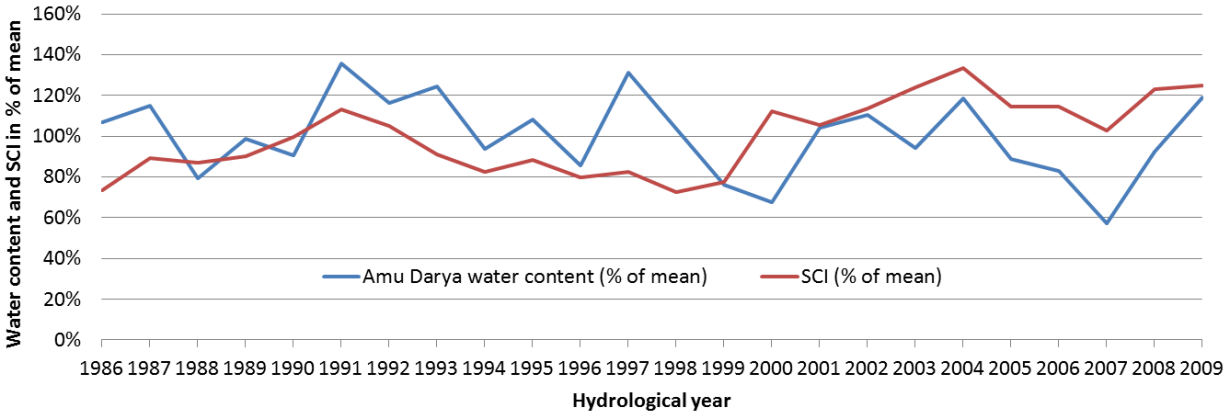

Figure 6.60: Water content of Amu Darya upstream catchments compared to SCI

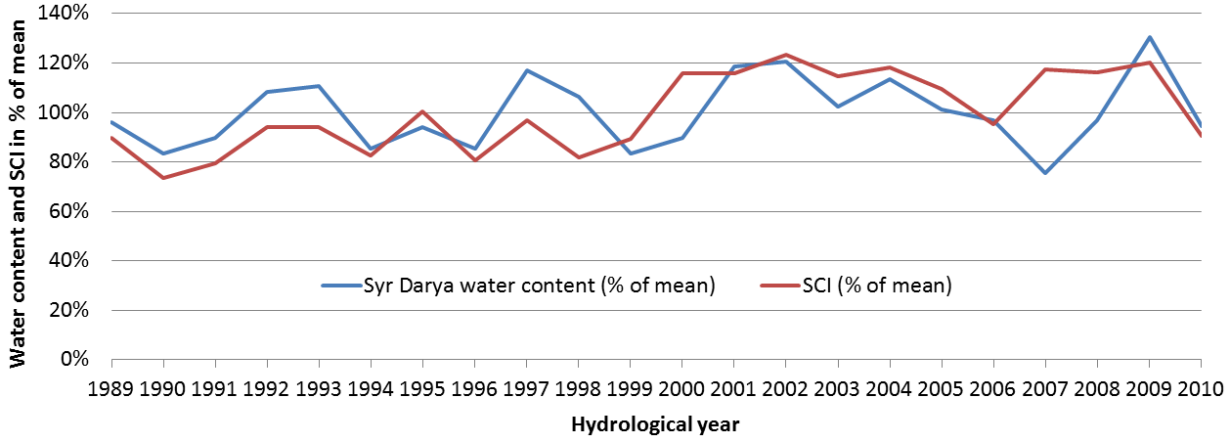

Figure 6.61: Water content of Syr Darya upstream catchments compared to SCI

Figure 6.60 and Figure 6.61 compare the water content of Amu Darya and Syr Darya Rivers (in % of mean km³) with the SCI of the upstream catchments (refer to Figure 2.2 and Figure 3.8 for details about upstream catchment locations). Water content information was taken from the CAWater-info project page (CAWater-Info, 2013), a project that aims to provide

information about water and environmental issues for Central Asia. While SCI and water content seem to be more or less independent for Amu Darya River (r = 0.05), the correlation for Syr Darya is significantly higher (r=0.48).

Results from the SCI calculations are included for early season (SCI_{ES}), late season (SCI_{LS}) and full season (SCI) in section 6.2.4 (Figure 6.45 to Figure 6.47). Because the SCI comprises SCD and snow cover extent both in one parameter, the results can serve as a quick overview about the character of a certain snow season (e.g. “snow rich”, or “snow meagre”). The variability is usually greatest for the downstream catchments, which is perceptible by the oscillating behaviour of the respective charts. Upstream catchments generally deviate no more than 20% from mean SCI conditions (though extreme events like Syr Darya upstream SCI_{ES} in 1987 with 50% higher SCI than under normal conditions can occur). Early season SCI values are characterized by the highest variability among the different SCI classes for upstream, intermediate, and downstream catchments. Again, this is a hint that SCS is generally more unstable than SCM, which is constant particularly in the upstream regions (Figure 6.46). A possible application involving the SCI is presented here: SCI and water content of major rivers in Central Asia correlate with each other – especially in the case of Syr Darya River. For some years, patterns from Amu Darya also agree with the SCI of the upstream catchments (Figure 6.60), but correlation is much higher (r=0.48 compared to r=0.05) for Syr Darya River (Figure 6.61). This is a promising result since the SCI can be calculated at any time within a hydrological year. It is thinkable that information about SCI can be used to predict the water content of e.g. Syr Darya River for the upcoming growing season. Such forecast could be used for the management of reservoirs, irrigation channels, and hydropower generation. If for example a water scarce season is beginning to show in early spring, water management authorities could decide to cut not so productive irrigated areas from water supply or restrict electric power supply to energy intensive industries. Such a decision could be made early enough for the farmers to change the crop type or for the industry to switch to a different shift operation. These are, of course, only suggestions. Before such applications could become operational, more research would be required. However, since water scarcity will intensify in the future, more research is necessary involving all possible fields of water generation – with snow cover constituting no exception. The reason why Amu Darya does not correlate with SCI throughout the time series may be that melt water contribution from glaciers plays a significantly larger role in this catchment (Ososkova et al., 2000). This was also indicated in section 2.1. Another unknown parameter is the extent in which artificial reservoirs contribute to the water content of the investigated rivers. The unusually large deviation between Syr Darya SCI and water content in 2007/2008 (Figure 6.61) may be the direct result of an exceptionally cold winter in this season which led to an increased water consumption for hydropower generation (Libert et al., 2008). If

such an exceptional weather event occurs out-of-band, the SCI can take unusually large values due to the fact that the cold temperatures prevent the snow from melting, leading to longer SCD. Therefore, the SCI should never be used as a sole and universal forecast for runoff, but as an indicator used in combination with additional information sources.

Another example for a possible application of the presented results is the mapping and observation of glaciated/permanently snow covered areas. Medium resolution sensors such as AVHRR or MODIS are usually not suited to map glaciers because the resolution is too coarse. During the realization of the transferability study for Europe (Dietz et al., 2012b) it turned out that larger glaciers can be recognized by MODIS: The size of the Aletsch Glacier in the European Alps is between 81.7 km² to 86.7 km² (Holzhauser et al. 2005; Kelly et al. 2004). The size of this glacier was also derived using the MODIS SCD results (all pixels with mean SCD of 365 days over a 10 year time span are suggested to be glaciated) and the size of the Aletsch Glacier was calculated as 87 km², which is in good agreement to the real extent. Therefore, the same approach can possibly be followed for Central Asia. The mountains of the study region are split in nine different zones in order to be able to assess possible developments in certain regions. Figure 6.62 illustrates these zones, which have been numbered from 1 to 9 to facilitate the upcoming analyses. The number of pixels with 365 snow covered days per hydrological year and glacier zone is now extracted from the time series. As a result, nine charts (one for each zone) are generated, containing the areal extent of permanently snow covered pixels. These charts are depicted in Figure 6.63, Figure 6.64, and Figure 6.65. The single plots are normalized to the mean number of permanently snow covered pixels between 2001/2002 and 2011/2012 to allow for a convenient comparison among the glacier zones. 1994 is again missing from the time series due to gaps in the AVHRR data. Figure 6.63 to Figure 6.65 clearly show that for years prior to the MODIS operational phase, statements about glacier extent appear to be all but impossible. Reasons for this behaviour were in parts already discussed in section 6.3. The following paragraph will contain a more detailed analysis of occurring problems.

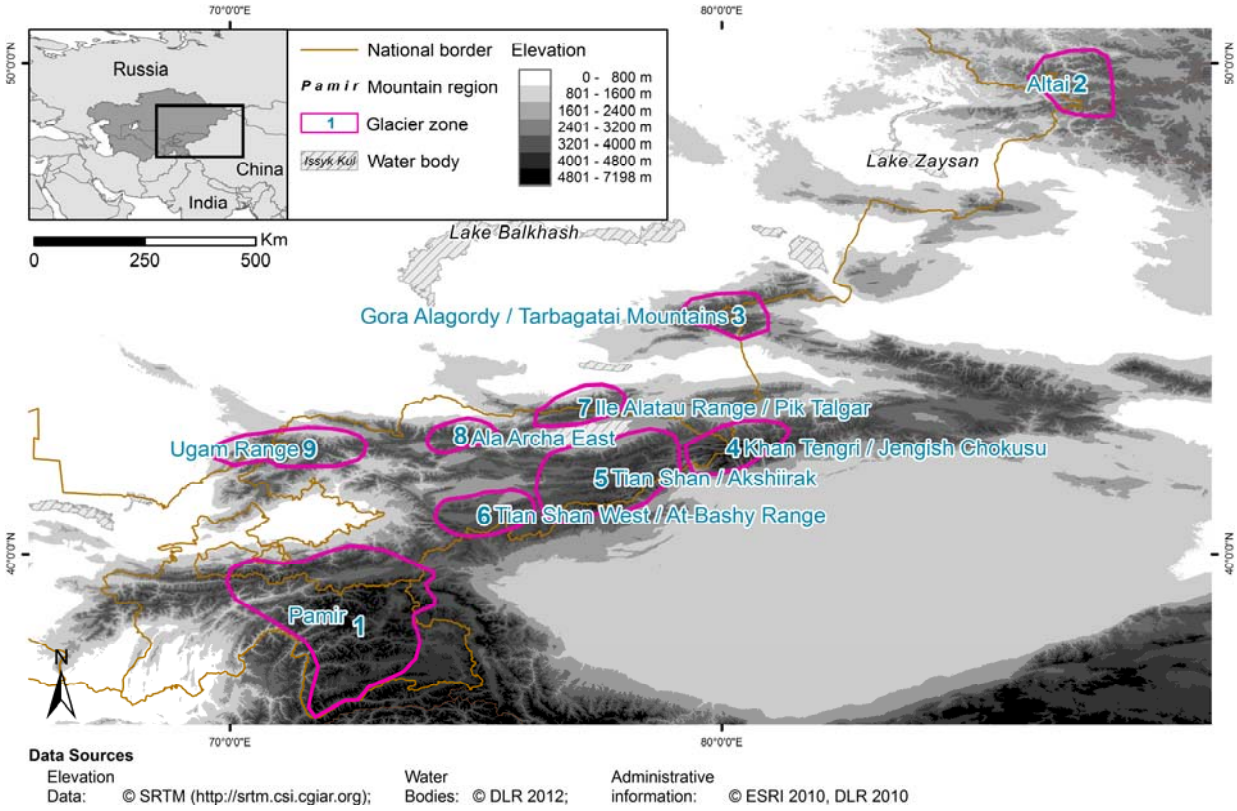

Figure 6.62: Glacier zones of Central Asia

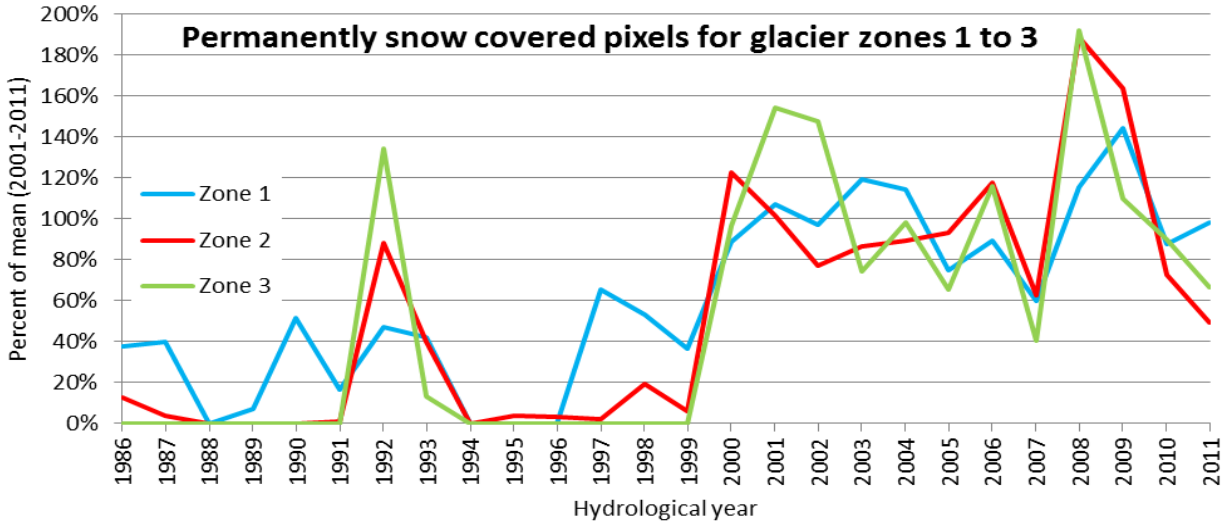

Figure 6.63: Permanently snow covered pixels for glacier zones 1 to 3

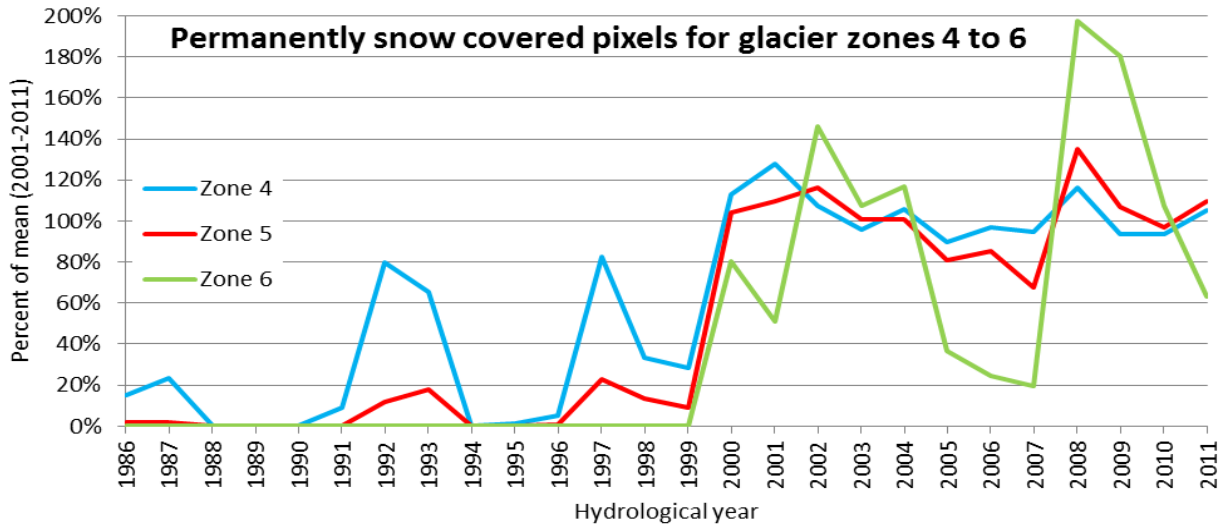

Figure 6.64: Permanently snow covered pixels for glacier zones 4 to 6

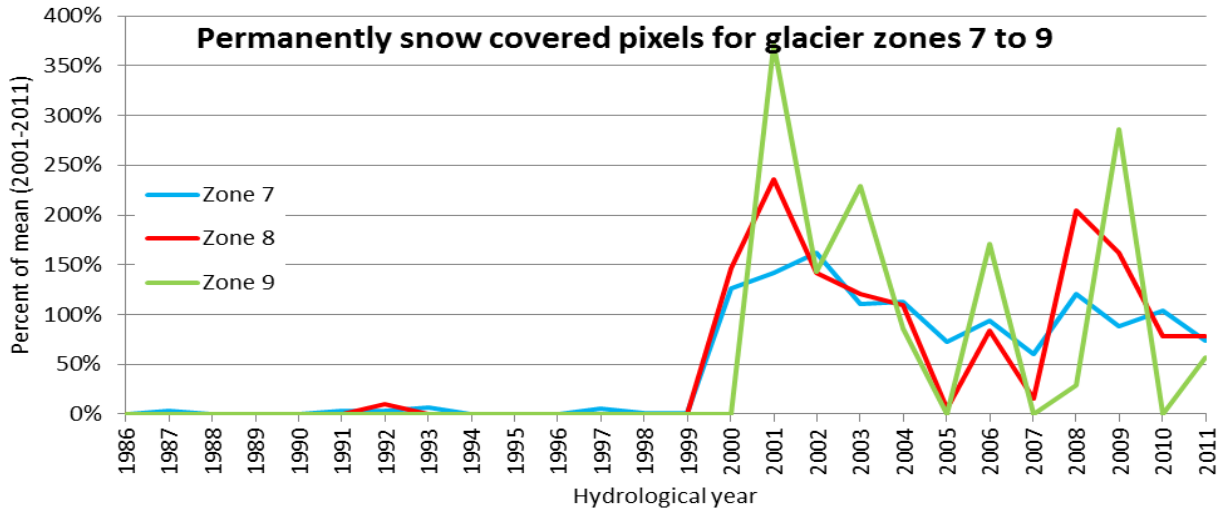

Figure 6.65: Permanently snow covered pixels for glacier zones 7 to 9

Trying to map glaciers with AVHRR and MODIS reveals an apparent limitation of the processed time series: AVHRR snow cover products derived with APOLLO are generally not suited to map glaciers/permanently snow covered areas in Central Asia (see Figure 6.63 to Figure 6.65). The MODIS data beginning with the hydrological year 2000/2001 may constitute a useful tool to map larger, coherent glaciers (as it was also shown by Dietz, Wohner, et al. (2012) for Europe), but AVHRR definitely lacks this capability, which may arise from two reasons: The pixel size of AVHRR is too coarse. Glaciers are often stretched along valleys, building narrow, tubular features. Permanently snow covered mountain tops or ridges are often narrow, too. The pixel size of 1.1 km may be too coarse to catch these snow covered regions – at least at each day during the hydrological year. A few misses already reduce the SCD in an extent too big that the pixel cannot be interpreted as permanently snow covered. This problem was already discussed in section 6.3 and it was also stated there that MODIS' 500 m

resolution may detect considerably more snow covered pixels in mountainous terrain. Comparing both data sources and trying to combine them will inevitably produce biased results. Another problem is again the sometimes inaccurate geolocation of ±1-2 pixels of AVHRR data (Tungalagsaikhan et al., 2003). Given that a snow covered pixel on a narrow mountain ridge was correctly classified as snow covered from APOLLO, then a shift of 2 pixels in only very few summer time observations would prevent the final SCD product to reach 365 days. This problem does not exist for the MODIS time series since here, the geolocation accuracy is not an issue. Unfortunately, it is impossible to accomplish a manual adjustment of the AVHRR data. The number of datasets is too huge (~20,300) for this task. The geolocation uncertainty is, however, not a serious problem for most hydrological applications – given that the scale of the respective catchment is not too small. If the SCD of one pixel is underestimated by a few days, the neighbouring pixels will most likely be overestimated for this shortage. Errors will even out, producing correct results on a catchment/elevation zone/SCI scale – yet another reason why the SCI is a promising parameter. A comparison between APOLLO PPL3 and Landsat snow maps in section 6.1 confirmed that though the overall accuracy of the PPL3 data only reaches ~ 85.7%, the areal extent between Landsat and PPL3 snow maps agrees by 95,5%. Figure 6.63 to 6.65 illustrate that some of the glaciated regions show a more or less constant areal fraction of permanently snow covered pixels for the MODIS time series: Glacier zones 1 (Pamir), 4 (Khan Tengri/Jengish Chokusu), and 5 (Tian Shan/Akshiirak) only deviate slightly around the 100% margin. This suggests that MODIS may be capable of identifying permanently snow covered regions in these zones. Glacier zones 8 (Ala Archa East) and 9 (Ugam Range) are examples for the contrary: Here, an identification of glaciated pixel is not even possible with MODIS' 500m pixel size. A promising approach exists to map snow cover with MODIS at 250 m resolution, possibly improving the capability to detect even narrower snow covered areas (Notarnicola et al., 2013a, 2013b). This algorithm, however, is not in an operational stage at the moment and requires a lot of additional input data.

Another potential application that is made available by providing the presented snow cover parameters is the analysis of single snow cover seasons with respect to mean conditions. The SCD of each specific year can be compared with the 5-year, 10-year, or the full time series average to identify regions with abnormal snow conditions. This can be a helpful tool when analysing possible effects of especially harsh or mild winter seasons. In Figure 6.66, the SCD of 2011/2012 is compared to the mean SCD between 2002/2003 and 2011/2012. The exceptionally long SCD for large regions of Central Asia in this season is eye-catching. Values of up to two months above average can be identified for parts of Kazakhstan, Uzbekistan, and the border area between Kyrgyzstan and Tajikistan. A newsletter article from April 2012 confirms that the season 2011/2012 stood out due to the harshest winter with longest snow cover

since 1968 (Igoe, 2012), which finally also caused the death of 25,000 livestock in Kyrgyzstan. Figure 6.66 illustrates that in Kyrgyzstan - especially in the western and south-western regions - SCD was up to 60 days longer than normal (see also profile line 2 north and south of Ferga-na Valley). This accords with what was reported in the article. Comparisons between single seasons and mean conditions are possible for all snow cover parameters including SCS, SCM, SCD, and even SCI. Many of such examples were included in the publication about snow cover variability in Central Asia derived from improved MODIS snow cover data (Dietz et al., 2013). They are not depicted here because Figure 6.66 should already suffice to clarify what opportunities are offered once a complete time series of snow cover parameters be-comes available.

In the presented example, 2011/2012 SCD was also selected because it is the most up to date season and therefore of augmented interest. The question is: Can information provided by remotely sensed data help to prevent/mitigate such consequences as the livestock loss in this season in the future? Is it possible to develop an early warning system that recognized such situations early enough for the herders to react? The answer is possibly: Not directly. A long term weather forecast would perhaps be more useful but even then, details about spring time SCM are difficult to foretell during autumn. Anyhow, the presented results can help in a different way: Figure 6.66 gives a clear inventory of SCD deviations. The same could easily be provided for SCS and SCM. This information may serve as the basis for refund-ing/reimbursement of affected herders/farmers. Given the government would install a compen-sation fund for those herders that suffered most, Figure 6.66 could serve as a tool to identify the locations where the help is needed most urgently. If the farmers had an insurance, the insurance company may also resort to products like Figure 6.66 to assess whether a petitioner is eligible to make an application for reimbursement or not. Again, these are just suggestions about possible utilizations of the presented results. More research would be needed to prove the connection between livestock mortality and SCD deviations before such products could be used in the future.

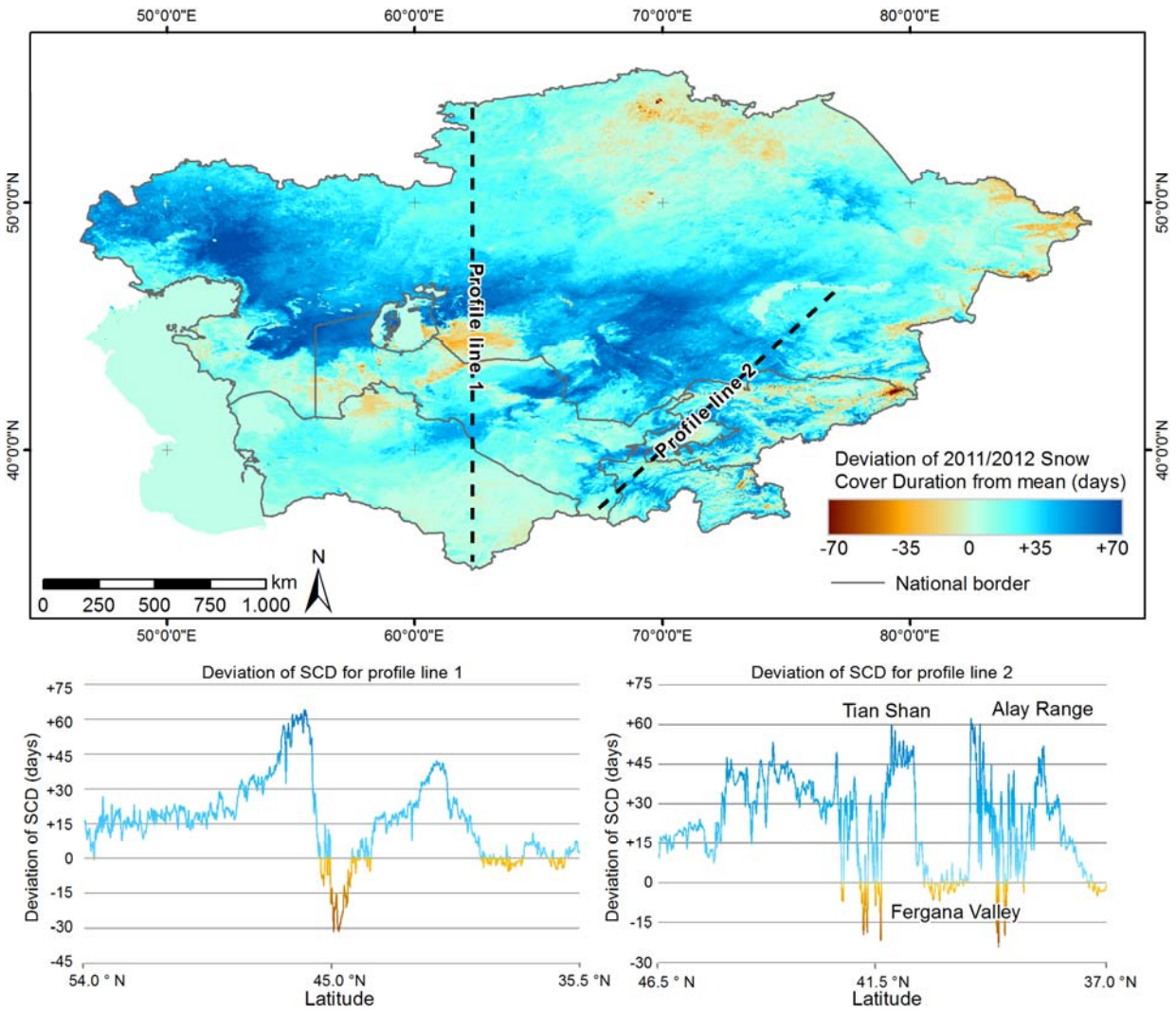

Figure 6.66: Deviation of 2011/2012 SCD from mean SCD between 2002/2003 and 2011/2012

An additional outlook is the possible application of the established processing chain to different regions. The transferability study for Europe already demonstrated that the cloud reduction scheme can be applied to regions outside of Central Asia as well (Dietz et al., 2012b). The configuration, development, testing, and improvement of the processing environment are most unappreciative tasks since they require a good deal of time. This effort is usually not reflected in publications because only the results are of interest for the scientific community. However, once the system is running it is possible to extent the study region to any dimension. Figure 6.67 is an example of what is possible once a system is established and running. 55 MODIS tiles were acquired for 12 years of daily data, including both, Terra and Aqua platforms. Around 441,000 single tiles have been processed to produce Figure 6.67 – a unique view on Eurasian snow cover conditions that has never been presented in this resolution (500 m). The results from the transferability study (Dietz et al., 2012b) and from the presented the-

sis and the publication about Central Asian snow cover variability (Dietz et al., 2013) were stitched together with the remaining parts of Eurasia to create a continuous overview of the mean SCD from eleven years of observation. Figure 6.67 is depicted in an orthographic projection that is centred on Central Asia (Longitude of centre: 65° E; Latitude of centre: 46° N). Though not illustrated here it is clear that SCS, SCM, and SCI may also be derived from the time series, allowing analyses on any scale from local, over regional, to continental. Figure 6.67 has the potential to serve as the basis for many future studies, comprising hydrological, geographical, climatological, and cryospherical backgrounds. With the modified APOLLO processing chain also at hand, it would be possible to extend the time series of daily, cloud-free, medium resolution snow cover data back to at least mid-1980s (in some regions even late 1970s, always depending on the available data archive), relying on AVHRR LAC or HRPT data.

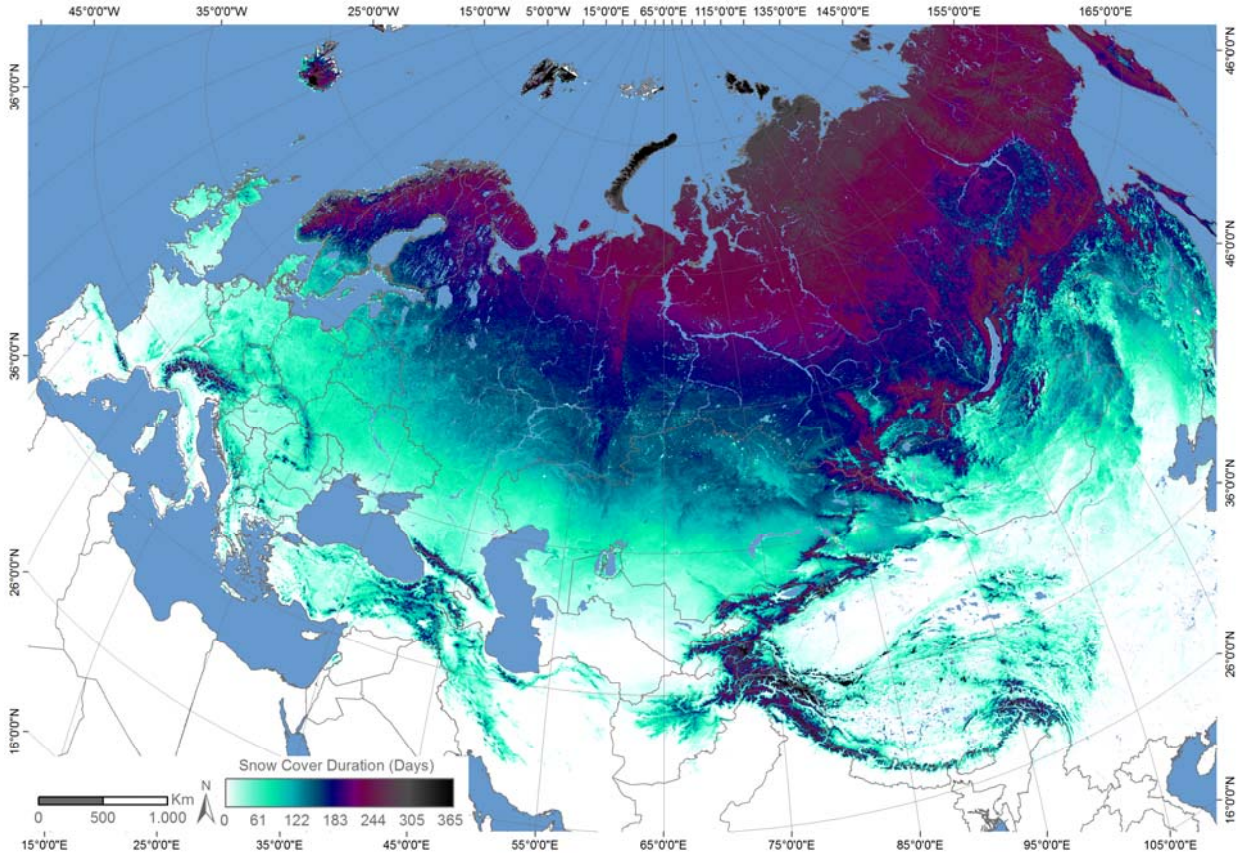

Figure 6.67: Mean Snow Cover Duration (2000/2001 to 2010/2011) for Eurasia

The time-consuming development of the applied processing chains was already mentioned in this section. Some background about the development of the applied processing chains will now be illuminated, before possible transferability opportunities are discussed: It was clear from the early beginning on that the establishment of a time series of daily snow

cover data in medium resolution, for an area of 4,000,000 km² and for 26 years would be a most challenging task. Many studies exist based on the exploitation of MODIS data: Vegetation, biomass, SST, LST, land cover, forest fires, sea ice - the list could be extended over several lines. The intention of the presented thesis was never to enqueue in a collection of studies all relying on the same, somehow convenient MODIS source. These data come in a regular grid, are available each day, have been pre-processed and georeferenced to constitute a high quality data source that is ready to use for most applications. Processing AVHRR LAC Level 1B data has not much in common with the analysis of MODIS data. Those familiar with the subject don't need any further explanation but unfortunately, knowledge and experience in dealing with raw AVHRR data is not very widespread, leading to potential misunderstandings and false expectations. The accuracy of AVHRR-derived parameters will never meet the MODIS-quality. Reasons for this circumstance were already explained in this section. The way from raw L1B data to the PPL3 snow cover product presented in the very thesis is long: APOLLO was initially not set to process LAC data. Many modifications had to be done and tested, followed by many updates and improvements. The results finally came in a binary data format without georeferencing being applied to the data. Post-processing routines were developed to be able to construct geo-lookup-tables for each single scene, consuming a lot of development and processing time. It is easy to look at figures like Figure 6.5 or Figure 6.6 and point to the obvious pixel shift in the APOLLO PPL3 product. The question may arise why these shifts have not been corrected during post-processing or why there was no atmospheric correction applied to the AVHRR data. The answer is simple: It was just impossible to accomplish all these tasks. The presented time series is unique with regards to the resolution, length, and coverage. It is the longest time span that was possible to establish – for the region and beyond. Till the date of writing, no similar study was ever heard of. Hence, the established processing chain should be used for different study regions as well. Figure 6.67 is a good example of what is possible when referring to the cloud reduction scheme (Figure 5.4). Full Eurasia comprising more than 440,000 MODIS snow cover product files was processed for this figure. Mean SCD between 2000/2001 and 2010/2011 is illustrated, putting Central Asia in relation to the rest of the continent. Many potential future studies could evolve from this map: The effects of large scale weather anomalies on SCD, detailed inventories of snow induced albedo-fluctuations of the Earth's surface, accompanied by the effects on the radiation budget, or small scale studies of single hydrological catchments. Most of Russia's runoff regime is snowmelt dominated (Barnett et al. 2005). Studies of single year snow cover characteristics in comparison with river runoff data may produce interesting results. Furthermore, and if North America is also added, the connection between snow cover parameters on both continents could be studied on a medium resolution data basis. Some additional aspects were already

mentioned: Further research on hydrological implications including runoff and water management, decision support for the distribution of water for irrigation, and early warming potential in years where the SCI is extraordinary low in upstream drainage basins. Few concrete applications have already evolved since the beginning of the study in 2010: The results from the transferability study in Europe (Dietz et al., 2012b) have been requested and incorporated for the creation of an avalanches hazard map for Europe (ESPON Natural hazard maps update, 2012). Additionally, a project for “Assessing Climate impacts on the Quantity and quality of Water” (ACQWA) showed increased interest in the snow cover time series derived from AVHRR data for Kyrgyzstan, which are planned to be used for the validation of climate and hydrological models (Acqwa 2013; Dedieu, personal communication). Finally, snow cover information processed for the presented thesis are also of interest for improving runoff models for Chon Kemin Valley, Kyrgyzstan within the framework of a PhD thesis accomplished at the University of Bern, Switzerland (Sorg, personal communication), relying basically on a publication by Huss et al. (2008).

The results presented in this thesis offer plenty of additional application opportunities not extended in detail within this outlook: The influence of the observed snowmelt shift (Figure 6.42) on forest health is one aspect that could be investigated in the future: It was reported by Trujillo et al. (2012) that earlier snowmelt resulted in increased tree mortality and reduced maximum NDVI for elevation zones between 1,700 m and 2,600 m in the Western US. According to the authors, such implications are common for mid-latitude mountain regions around the globe. Schlaepfer et al. (2012) state that shifts in snowmelt conditions within snow dominated precipitation regimes may substantially affect the water balance of the area. Similar consequences can be expected for Central Asia, as well. Another research field is the effect of SCS, SCM, and SCD on general NDVI and Biomass values in a given ecosystem. Peng et al. (2010) already pointed to the positive effect of snow cover (and snow depth) on vegetation growth. Grippa et al. (2005) confirmed that snow variability has a significant impact on summer NDVI in central Siberia (~ 65°N) – which is located just north of the study regions of the presented thesis. It would be possible to analyse the correlation between snow cover and biomass for Central Asia by combining the presented results with estimates about vegetation net primary productivity, relying e.g. on the study of Eisfelder et al. (2012) for Kazakhstan. With the outlook of Figure 6.67 in mind it is clear that the already mentioned application examples can be applied to any given region. Changes in snow cover characteristics have effects on regions outside of Central Asia, too. Many countries like Norway or Switzerland depend on melt water for electric power production (Vikhamar & Solberg 2003; Beniston 1997; Cherry et al. 2005). Snow cover changes on a sub-catchment scale could be analysed using the processing chain that was developed within the presented thesis. The connection between Eurasian SCS and

snow cover parameters in North America (as reported by Cohen & Saito (2003) and Saito et al. (2001)) could be investigated relying on Figure 6.67 as well.

There is, however, one very important aspect, affecting all presented results but those referring to hydrological applications in particular: Although SCD, SCS, SCM, and SCI can be calculated for any given spatial or temporal entity, all these parameters can by definition never include information about the snow depth/SWE. The snow depth may range from 5 cm to 50 cm – the satellite will only discriminate between 1: snow, and 0: no snow (metaphorically speaking). For some applications, this limitation is not an eminent issue. When evaluating the radiation budget of the Earth's surface for example, the albedo of snow covered areas is the same for deep and shallow snow (With some exceptions of course: if snow depth is not sufficient to cover the full ground, the albedo will decrease. Additionally, if exceptionally deep snow melts, its albedo will decrease because refractory black carbon/soot will accumulate in the upper snow layer during the melt process, reducing the reflectance of the snow surface (Ramanathan and Carmichael, 2008; Sterle et al., 2013)). When analysing the effects of climate change on snow cover parameters, most of them can also be examined without knowledge about the depth of the snowpack (though it would be very interesting to have this additional parameter, of course). As soon as statements about hydrological implications are formulated, it should always be kept in mind that information about the water content of the snowpack is not available from optical sensors. Section 3.2 gave a comprehensive overview about the topic and also introduced to passive microwave sensors as a possible source to estimate SWE – along with all the restrictions that are connected with this sensor type. These data are not suited to analyse snow cover conditions in the mountainous regions, which makes them useless for the analysis of Central Asian water issues.

One aspect that was included in the introduction and aims of the presented thesis but not discussed in detail is the orientation towards the GCOS target requirements regarding snow cover product's temporal (daily) and spatial (1 km, 100m in complex terrain) resolution. The benefits of snow cover products fulfilling these requirements are described as follows by GCOS (WMO and GCOS, 2011):

- *"Better estimate of planetary albedo*
- *Indicator of changes in precipitation and temperature regimes*
- *Assessment and improvement of regional and global climate-model performance*
- *Provision of a key indicator of climate change in cold seasons/regions*

- *Assessment of changes in seasonally-frozen ground"*

When going through these points with the results presented in the thesis at hand, those items referring to a more regional scale can thoroughly be approved: The daily data allows for a distinct designation of SCS, SCM, and SCD. Changes of only several days become visible while analysing the time series. The shift of 12 days towards earlier SCM (Figure 6.42) may have been ignored or underestimated using 8-day composites of snow cover extents. Therefore, daily estimations of snow cover are an invaluable data source worth the processing effort undertaken within this thesis. The required spatial resolution is justified as well, the very thought of the complex snow cover conditions in the mountainous regions in mind. It would be impossible to determine the particular characteristics of variable snow cover conditions in e.g. the narrow mountain valleys (see Figure 6.48 and Figure 6.50) using coarse resolution (e.g. 25 km pixel size) data. Additionally, analyses on a catchment- and especially sub-catchment-scale are made available that would have been prevented using coarse resolution snow cover data. These data can be used as an indicator for precipitation and/or temperature changes only because the temporal and spatial resolutions are high enough (though in the mountains an even higher resolution is desirable). The third point from the list – assessment and improvement of climate model performance – can also be stated as confirmed – keeping the results of SCD in mind: Durations taken from Brown & Mote (2009) coincide with results obtained in the thesis. A band of higher sensitivity between 40°N and 45°N in this study is superimposable with the band of negative SCD trends (Figure 6.58), though a more detailed analysis is still needed to assure validity. The obtained results from the mountainous regions could help to improve climate models for complex terrain. This comprises also point four: Provision of a key indicator of climate change: SCD and SCM change for a reason. This reason is definitely linked to changed temperature and/or precipitation characteristics (especially in mountainous terrain). The fact that snow melts earlier above ~1,500 m is a clear indicator for increased temperatures, also confirming the assumptions of Nogués-Bravo et al. (2007) and Diaz et al. (2003). However, only by providing medium resolution, daily and cloud-free snow cover time series for more than 25 years, the exact locations, elevation zones, and extents of changes are made visible. This may be of particular value for the decision makers in place: The effects of a changing climate on water availability have in parts been made visible on a medium resolution. Future developments are foreseeable, allowing for decisions to be made now – and be it only for the conclusion that additional research is required to create more confidence.

7. Conclusions

Four research questions have been expressed at the beginning of the presented thesis: Which snow mapping techniques for remotely sensed data exist? How are the snow cover conditions in Central Asia characterized? How did these conditions develop within the last 26 years and under the influence of climate change? And finally: How may the future of Central Asian snow cover characteristics look like (accompanied by which effects on the region's hydrology)? All these questions were investigated during the realization of the presented thesis.

A review about available snow mapping techniques has been accomplished, examining approaches, potentials, and limitations of different sensor types, revealing that observations made from medium resolution optical remote sensing sensors are best suited to meet the study demands. Accordingly, 27,000 AVHRR scenes and 66,000 MODIS snow cover products were acquired and processed (while only ~20,300 AVHRR scenes and all MODIS products were utilized for the study) for the years between 1986 and 2013, including pre-processing of the raw AVHRR L1B data and post-processing of the complete time series of daily data to remove cloud coverage. Based on these cloud-free snow cover data, parameters like Snow Cover Duration, Snow Cover Start, Snow Cover Melt, and Snow Cover Index are presented both for single years and also longer time spans. These results are provided for the full ~ 4,000,000 km² as areal datasets as well as in an aggregated form, divided among elevation zones or river catchments. Taken all together, the results for Central Asia draw an unambiguous picture of how changes in temperature and precipitation regimes affect snow cover characteristics in an area that is highly depending on snow as a major source of fresh water: In the plains of Central Asia, snow cover duration is longest (~ 140 days per year) for the most northern parts of Kazakhstan. Long term changes that can be identified from the time series prepared within the presented thesis point towards an increase of Snow Cover Duration in this region, primarily triggered by earlier snow cover onset. The central parts of the study area are characterized by shorter Snow Cover Duration which continuously reduces with decreasing latitude. In these regions, the trend is characterized by a negative sign, suggesting that Snow Cover Duration will most likely further decrease in the future between 40°N and 45°N. In the mountains of Central Asia, Snow Cover Duration increased above an altitude of ~ 3,600 m while it remained stable below. Snow Cover Melt occurs up to 12 days earlier above ~1,500 m and Snow Cover Start begins earlier in all elevation zones (with largest shifts in altitudes between ~4,000 m and 5,200 m). Snow remains up to 20 days longer on north-facing slopes (depending on the elevation) when compared to south- and south-west facing slopes. This behaviour is the direct result of the different solar insulation characteristics which vary accord-

ing to slope direction and steepness of the terrain. The variability of Snow Cover is investigated by analysing the standard deviation of the parameters. Highest variability is identified for the central plains as well as in valleys within the mountainous terrain. In the central regions, snow cover conditions are unstable and can differ significantly between single years, leading to the high variability in this area. In the mountains, the high standard deviation of Snow Cover Duration appears questionable on a first glance as the temperature stays way below freezing point during winter and early spring season. A closer investigation reveals that the regions with most variable Snow Cover Duration are located within valleys surrounded by high mountain ridges. Although no in situ information about wind speed or direction is available, it can be suggested that wind transport of snow is the major cause for the high variability: Parameters like land cover, slope, aspect, or temperature do not change significantly enough to explain standard deviations of 50 days or more.

The changed snow cover characteristics of earlier Snow Cover Start and earlier Snow Cover Melt constitute most considerable results of the thesis and are the direct consequence of increased temperatures in the mountainous regions. The shift towards earlier Snow Cover Melt may have wide-ranging effects on the ecosystem as it influences the water balance of the whole region. Earlier release of the water that is stored within the snowpack directly leads to a shift of the runoff regime. This poses a serious challenge to the future water management authorities as this development will most likely consolidate and even aggravate, following a proceeding change in climate conditions – temperature increase in particular. Shifts in Snow Cover Melt will affect the snow melt dominated hydrology, influencing reservoir and irrigation management. Already existing transboundary water issues will most likely be exacerbated by this development, as well. As the population grows, more water is consumed for irrigation and hydropower generation. Export of energy to foreign countries will also extend in the future. Monitoring of actual snow cover conditions therefore emerges to be of particular importance as it may allow for the forecast of forthcoming runoff water amounts. Comparisons between the Snow Cover Index and water content of major river catchments demonstrate that correlations exist for some rivers. Further studies in this direction appear worthwhile.

New parameters like Early Season and Late Season Snow Cover Index and new denominations of Snow Cover Start/Snow Cover Melt as Early/Late Season Snow Cover Duration are proposed, whose scientific benefit is still to be proven. Against the background of the presented thesis and the experiences from the in parts already published results, these new/renamed parameters appear promising and expedient.

Other possible applications of the prepared snow cover information are presented. Single year snow cover parameters may be compared to the mean (normal) conditions, identify-

ing regions with exceptionally long or short, early or late snow cover on the ground. Such analyses can help to recognize areas where the deviations from mean conditions may have effects on vegetation, which is influenced by Snow Cover Duration and the date of Snow Cover Melt. The application of the developed processing schemes to different regions is another possibility. The scheme is in an operational status, allowing for fast and efficient post-processing of snow cover data all over the globe.

Limitations do exist caused by the relatively coarse resolution of AVHRR (1.1 km), hindering from precise mapping of glaciated areas and/or permanently snow covered regions. The geolocation uncertainty of 2 pixels adds to the problem, constituting conclusions on a pixel basis a difficult task. The aggregation of the obtained results on a sub-catchment scale eliminates this problem, as the pixel-wise uncertainty can be compensated. Additional problems exist due to the static and often outdated water masks that form essential components within the snow detection algorithms. Because water body extents in Central Asia partially varied considerably over the last 26 years, snow cover detection for these dynamic water bodies does not produce reliable results. A possible future improvement of snow detection algorithms therefore includes the use of dynamically updated water masks instead of static versions.

The presented results, comprising time series of daily, cloud-free, medium resolution snow cover data from 26 years are unique with regards to the spatial and temporal resolution. Chances are that the approach followed within the presented thesis will be adopted for different regions throughout the world since they offer, for the first time, insight in long term snow cover changes on a sub-catchment scale. Regions with snow dominated hydrology are distributed north of 45° N all around the globe (except Central and Western Europe), legitimating similar studies as presented within the very thesis.

References

A

Ackerman, S., Frey, R., Strabala, K., Liu, Y., Gumley, L. and Baum, B.: Discriminating clear-sky from cloud with MODIS ATBD (MOD35), 2010.

Ackerman, S., Strabala, K., Menzel, P., Frey, R., Moeller, C., Gumley, L., Baum, B., Wetzel Seemann, S. and Zhang, H.: Discriminating Clear-Sky from Cloud with MODIS Algorithm Theoretical Basis Document (MOD35), 2006.

Acqwa: ACQWA project page, [online] Available from: http://www.acqwa.ch/index.php?option=com_content&view=category&layout=blog&id=10&Itemid=26 (Accessed 8 March 2013), 2013.

Adam, J. C., Hamlet, A. F. and Lettenmaier, D. P.: Implications of global climate change for snowmelt hydrology in the twenty-first century, Hydrological Processes, 23, 962–972, doi:10.1002/hyp, 2009.

Aizen, V. B., Aizen, E. M. and Kuzmichonok, V. a: Glaciers and hydrological changes in the Tien Shan: simulation and prediction, Environmental Research Letters, 2(4), 1–10, doi:10.1088/1748-9326/2/4/045019, 2007.

Aizen, V. B., Aizen, E. M., Melack, J. and Dozier, J.: Climatic and Hydrologic Changes in the Tien Shan , Central Asia, Journal of Climate, 10, 1393–1404, 1997.

Aizen, V. B., Aizen, E. M. and Melack, J. M.: Climate, Snow Cover, Glaciers, and Runoff in the Tien Shan, Central Asia, Journal of the American Water Resources Association, 31(6), 1113–1129, doi:10.1111/j.1752-1688.1995.tb03426.x, 1995.

Aizen, V. B., Kuzmichenok, V. a., Surazakov, A. B. and Aizen, E. M.: Glacier changes in the central and northern Tien Shan during the last 140 years based on surface and remote-sensing data, Annals of Glaciology, 43(1), 202–213, doi:10.3189/172756406781812465, 2006.

Akyürek, Z. and Sorman, A. Ü.: Monitoring snow-covered areas using NOAA- AVHRR data in the eastern part of Turkey, Hydrological Sciences Journal, 47(2), 243–252, 2002.

Aladin, N. V. and Plotnikov, I. S.: Large saline lakes of former USSR: a summary review, Hydrobiologia, 267, 1–12, doi:10.1007/BF00018787, 1993.

Amlien, J.: Remote sensing of snow with passive microwave radiometers - A review of current algorithms, Oslo, Norway, 2008.

Aoki, T., Aoki, T. and Fukabori, M.: Effects of snow physical parameters on spectral albedo and bidirectional reflectance of snow surface, Journal of Geophysical Research, 105, 219–236, 2000.

Aoki, T., Motoyoshi, H., Kodama, Y., Yasunari, T. J. and Sugiura, K.: Variations of the snow physical parameters and their effects on albedo in Sapporo, Japan, Annals of Glaciology, 46(1994), 375–381, 2007.

Armstrong, R.: Historical Soviet Daily Snow Depth Version 2 (HSDSD), NSIDC, Boulder, Colorado USA, Available from: http://nsidc.org/data/g01092.html (Accessed 12 October 2012) 1999.

Armstrong, R. L. and Brodzik, M. J.: Recent northern hemisphere snow extent - A comparison of data derived from visible and optical satellite sensors.pdf, Geophysical Research Letters, 28(19), 3673–3676, 2001.

Armstrong, R. L. and Brodzik, M. J.: Northern Hemisphere EASE-Grid Weekly Snow Cover and Sea Ice Extent Version 3, Boulder, Colorado USA: NSIDC, 2005.

Armstrong, R., Raup, B., Khalsa, S. J. S., Barry, R., Kargel, J., Helm, C. and Kieffer, H.: GLIMS glacier database, Boulder, Colorado USA: NSIDC, 2011.

Awan, U. K., Tischbein, B., Conrad, C., Martius, C. and Hafeez, M.: Remote Sensing and Hydrological Measurements for Irrigation Performance Assessments in a Water User Association in the Lower Amu Darya River Basin, Water Resources Management, 25(10), 2467–2485, doi:10.1007/s11269-011-9821-2, 2011.

B

Bai, J., Chen, X., Li, J., Yang, L. and Fang, H.: Changes in the area of inland lakes in arid regions of central Asia during the past 30 years, Environmental monitoring and assessment, 178, 247–256, doi:10.1007/s10661-010-1686-y, 2011.

Bales, R. C., Dressler, K. A., Imam, B., Fassnacht, S. R. and Lampkin, D.: Fractional snow cover in the Colorado and Rio Grande basins, 1995–2002, Water Resources Research, 44(1), 1–10, doi:10.1029/2006WR005377, 2008.

Barnett, T. P., Adam, J. C. and Lettenmaier, D. P.: Potential impacts of a warming climate on water availability in snow-dominated regions., Nature, 438, 303–309, doi:10.1038/nature04141, 2005.

Barnett, T. P., Dümelin, L., Schlese, U., Roeckner, E. and Latif, M.: The effect of Eurasian snow cover on regional and global climate variations, Journal of Atmospheric Sciences, 46(5), 661–685, 1989.

Barrett, A. P.: National Operational Hydrologic Remote Sensing Center SNOw Data Assimilation System (SNODAS) Products at NSIDC, NSIDC Special Report #11, 2003.

Barry, R. G.: Snow Cover, in Terrestrial essential Climate Variables, edited by R. Sessa and H. Dolman, pp. 20–21, FAO GTOS-52, Rome, Italy, 2008.

Beniston, M.: Variations of Snow Depth and Duration in the Swiss Alps over the last 50 Years: Links to Changes in large-scale Climatic Forcings, Climatic Change, 36, 281–300, 1997.

Bernauer, T. and Siegfried, T.: Climate change and international water conflict in Central Asia, Journal of Peace Research, 49(1), 227–239, doi:10.1177/0022343311425843, 2012.

Bernier, P. Y.: Microwave Remote Sensing of Snowpack Properties: Potential and Limitations, Nordic Hydrology, 18, 1–20, 1987.

Blöschl, G., Kirnbauer, R. and Gutknecht, D.: Distributed Snowmelt Simulations in an Alpine Catchment 1. Model Evaluation on the Basis of Snow Cover Patterns, Water Resources Research, 27(12), 3171–3179, 1991.

Bormann, K. J., McCabe, M. F. and Evans, J. P.: Satellite based observations for seasonal snow cover detection and characterisation in Australia, Remote Sensing of Environment, 123, 57–71, doi:10.1016/j.rse.2012.03.003, 2012.

Bormann, K., McCabe, M. and Evans, J.: A New Approach to Snow Detection in Australia using MODIS & Landsat TM, Proceedings of the 34th International Symposium on Remote Sensing of Environment, Sydney, Australia, April 10-15 2011, pp. 2007–2010.

Brown, R. D.: Northern Hemisphere Snow Cover Variability and Change , 1915 – 97, Journal of Climate, 13, 2339–2355, 2000.

Brown, R. D. and Mote, P. W.: The Response of Northern Hemisphere Snow Cover to a Changing Climate*, Journal of Climate, 22(8), 2124–2145, doi:10.1175/2008JCLI2665.1, 2009.

Bulygina, O. N., Groisman, P. Y., Razuvaev, V. N. and Korshunova, N. N.: Changes in snow cover characteristics over Northern Eurasia since 1966, Environmental Research Letters, 6(4), 045204, doi:10.1088/1748-9326/6/4/045204, 2011.

Butt, M. J. and Bilal, M.: Application of snowmelt runoff model for water resource management, Hydrological Processes, 25(24), 3735–3747, doi:10.1002/hyp.8099, 2011.

C

Callaghan, T. V., Johannsson, M., Brown, R. D., Groisman, P. Y., Labba, N. and Radionov, V.: Snow, Water, Ice and Permafrost in the Arctic, in AMAP Report to the Arctic Council chapter 4, p. 59., 2011.

Cavalieri, D., Parkinson, C., Gloersen, P. and Zwally, H. J.: Sea Ice Concentrations from Nimbus-7 SMMR and DMSP SSM/I-SSMIS Passive Microwave Data, Version 1.0. Boulder, Colorado USA: NSIDC, 1996.

CAWater-Info: CAWater-info, [online] Available from: http://www.cawater-info.net/index_e.htm (Accessed 17 November 2012), 2013.

Chang, A. T. C., Foster, J. L. and Hall, D. K.: Nimbus-7 smmr derived global snow cover parameters, Annals of Glaciology, 9, 39–44, 1987.

Chang, A. T. C., Kelly, R. E. J., Josberger, E. G., Armstrong, R. L., Foster, J. L. and Mognard, N. M.: Analysis of Ground-Measured and Passive-Microwave-Derived Snow Depth Variations in Midwinter across the Northern Great Plains, Journal of Hydrometeorology, 6, 20–33, 2005.

Chang, A. T. C. and Rango, A.: Algorithm Theoretical Basis Document (ATBD) for the AMSR-E Snow Water Equivalent Algorithm, , 1–49, 2000.

Chang, A. T. C. and Tsang, L.: A Neural Network Approach to Inversion of Snow Water Equivalent from Passive Microwave Measurements, Nordic Hydrology, 23, 173–182, 1992.

Che, T., Li, X., Jin, R., Armstrong, R. and Zhang, T.: Snow depth derived from passive microwave remote-sensing data in China, Annals of Glaciology, 49(1990), 145–154, 2008.

Cherry, J., Cullen, H., Visbeck, M., Small, A. and Uvo, C.: Impacts of the North Atlantic Oscillation on Scandinavian Hydropower Production and Energy Markets, Water Resources Management, 19(6), 673–691, doi:10.1007/s11269-005-3279-z, 2005.

Chokmani, K., Dever, K., Bernier, M., Gauthier, Y. and Paquet, L.: Adaptation of the SNOW-MAP algorithm for snow mapping over eastern Canada using Landsat-TM imagery, Hydrological Sciences Journal, 55(4), 649–660, 2010.

Choudhury, B. J. and Chang, A. T. C.: Two-Stream Theory of Spectral Reflectance of Snow, IEEE Transactions on Geoscience Electronics, 17, 63–68, 1979.

Chrysoulakis, N., Kamarianakis, Y., Xu, L., Mitraka, Z. and Ding, J.: Combined use of MODIS, AVHRR and radiosonde data for the estimation of spatiotemporal distribution of precipitable water, Journal of Geophysical Research, 113, 1–18, doi:10.1029/2007JD009255, 2008.

Clifford, D.: Global estimates of snow water equivalent from passive microwave instruments: history, challenges and future developments, International Journal of Remote Sensing, 31(14), 3707–3726, doi:10.1080/01431161.2010.483482, 2010.

Cohen, J. L. and Saito, K.: Eurasian snow cover, more skillful in predicting U.S. winter climate than the NAO/AO?, Geophysical Research Letters, 30(23), 1–4, doi:10.1029/2003GL018053, 2003.

Congalton, R. G.: A Review of Assessing the Accuracy of Classifications of Remotely Sensed Data, Remote Sensing of Environment, 37, 35–46, 1991.

Conrad, C., Dech, S. W., Hafeez, M., Lamers, J., Martius, C. and Strunz, G.: Mapping and assessing water use in a Central Asian irrigation system by utilizing MODIS remote sensing products, Irrigation and Drainage Systems, 21, 197–218, doi:10.1007/s10795-007-9029-z, 2007.

Cowan, P. J.: Geographic usage of the terms Middle Asia and Central Asia, Journal of Arid Environments, 69(2), 359–363, doi:10.1016/j.jaridenv.2006.09.013, 2007.

Crane, R. G. and Anderson, M. R.: Satellite discrimination of snow/cloud surfaces, International Journal of Remote Sensing, 5(1), 213–223, doi:10.1080/01431168408948799, 1984.

D

Dahe, Q., Shiyin, L. and Peiji, L.: Snow Cover Distribution, Variability, and Response to Climate Change in Western China, Journal of Climate, 19, 1820–1833, 2006.

Dankers, R. and De Jong, S. M.: Monitoring snow-cover dynamics in Northern Fennoscandia with SPOT VEGETATION images, International Journal of Remote Sensing, 25(15), 2933–2949, doi:10.1080/01431160310001618374, 2004.

Dech, S. W., Meisner, R. E., Tungalagsaikhan, P., Popp, T. and Thomas, W.: Operational Generation of AVHRR-Based Level3 Products at the German Remote Sensing Data Centre : Status and Perspectives, in Proceedings of the 1997 International Geoscience and Remote Sensing Symposium IGARSS'97, pp. 1505–1508, 3.-8. August 1997, Singapore., 1997.

Dech, S. W., Tungalagsaikhan, P., Preusser, C. and Meisner, R. E.: Operational value-adding to AVHRR data over Europe: methods, results, and prospects, Aerospace Science and Technology, 2(5), 335–346, doi:10.1016/S1270-9638(98)80009-6, 1998.

Derksen, C.: The contribution of AMSR-E 18.7 and 10.7 GHz measurements to improved boreal forest snow water equivalent retrievals, Remote Sensing of Environment, 112(5), 2701–2710, doi:10.1016/j.rse.2008.01.001, 2008.

Derksen, C., Walker, A. and Goodison, B.: A comparison of 18 winter seasons of in situ and passive microwave-derived snow water equivalent estimates in Western Canada, Remote Sensing of Environment, 88(3), 271–282, doi:10.1016/j.rse.2003.07.003, 2003a.

Derksen, C., Walker, A., LeDrew, E. and Goodison, B.: Combining SMMR and SSM / I Data for Time Series Analysis of Central North American Snow Water Equivalent, Journal of Hydrometeorology, 4, 304–316, 2003b.

Diaz, H. F., Grosjean, M. and Graumlich, L.: Climate Variability and Change in High Elevation Regions: Past, Present and Future, Climatic Change, 59(Chapter 13), 1–4, 2003.

Diebold, A. and Sehring, J.: From the Glaciers to the Aral Sea - Water Unites, 1st ed., Trescher Verlag., 2012.

Dietz, A. J., Kuenzer, C. and Conrad, C.: Snow-cover variability in central Asia between 2000 and 2011 derived from improved MODIS daily snow-cover products, International Journal of Remote Sensing, 34(11), 3879–3902, 2013.

Dietz, A. J., Kuenzer, C., Gessner, U. and Dech, S.: Remote sensing of snow – a review of available methods, International Journal of Remote Sensing, 13, 4094–4134, 2012a.

Dietz, A. J., Wohner, C. and Kuenzer, C.: European Snow Cover Characteristics between 2000 and 2011 Derived from Improved MODIS Daily Snow Cover Products, Remote Sensing, 4(8), 2432–2454, doi:10.3390/rs4082432, 2012b.

Domine, F., Albert, M., Huthwelker, T., Jacobi, H.-W., Kokhanovsky, A. A., Lehning, M., Picard, G. and Simpson, W. R.: Snow physics as relevant to snow photochemistry, Atmospheric Chemistry and Physics Discussions, 7, 5941–6036, doi:10.5194/acpd-7-5941-2007, 2007.

Dong, J., Walker, J. P. and Houser, P. R.: Factors affecting remotely sensed snow water equivalent uncertainty, Remote Sensing of Environment, 97(1), 68–82, doi:10.1016/j.rse.2005.04.010, 2005.

Dozier, J.: Spectral Signature of Alpine Snow Cover from the Landsat Thematic Mapper, Remote Sensing of Environment, 28, 9–22, 1989.

Dozier, J. and Marks, D.: Snow Mapping and Classification from Landsat Thematic Mapper Data, Annals of Glaciology, 9, 97–103, 1987.

Dozier, J. and Painter, T. H.: Multispectral and Hyperspectral Remote Sensing of Alpine Snow Properties, Annual Review of Earth and Planetary Sciences, 32(1), 465–494, doi:10.1146/annurev.earth.32.101802.120404, 2004.

Dye, D. G.: Variability and trends in the annual snow-cover cycle in Northern Hemisphere land areas, 1972-2000, Hydrological Processes, 16, 3065–3077, doi:10.1002/hyp.1089, 2002.

E

ECA&D: European Climate Assessment & Dataset, [online] Available from: http://eca.knmi.nl (Accessed 31 July 2012), 2012.

Eisfelder, C., Kuenzer, C., Dech, S. and Buchroithner, M. F.: Comparison of Two Remote Sensing Based Models for Regional Net Primary Productivity Estimation—A Case Study in Semi-Arid Central Kazakhstan, IEEE Journal of Selected Topics in Applied Earth Observations and Remote Sensing, (99), 1–14, doi:10.1109/JSTARS.2012.2226707, 2012.

F

Fallot, J.-M., Barry, R. G. and Hoogstrate, D.: Variations of mean cold season temperature , precipitation and snow depths during the last 100 years in the former Soviet Union (FSU), Hydrological Sciences, 42(3), 301–327, 1997.

Fensholt, R. and Sandholt, I.: Evaluation of MODIS and NOAA AVHRR vegetation indices with in situ measurements in a semi-arid environment, International Journal of Remote Sensing, 26(12), 2561–2594, doi:10.1080/01431160500033724, 2005.

Fernandes, R. and Zhao, H.: Mapping Daily Snow Cover Extent over Land Surfaces using NOAA AVHRR Imagery, in Proceedings of the 5th EARSeL Workshop: Remote Sensing of Land Ice and Snow, pp. 1–8, Bern, 11-13 February., 2008.

Fichtelmann, B. and Borg, E.: A New Self-Learning Algorithm for Dynamic Classification of Water Bodies, in Computational Science an Its Applications - ICCSA 2012, Part III, edited by B. Murgante, O. Gervasi, S. Misra, N. Nedjah, A. M. A. C. Rocha, D. Taniar, and B. O. Apduhan, pp. 457–470, Springer, Salvador de Bahia, Brazil., 2012.

Fisher, P. F. and Pathirana, S.: The evaluation of fuzzy membership of land cover classes in the suburban zone, Remote Sensing of Environment, 34(2), 121–132, doi:10.1016/0034-4257(90)90103-S, 1990.

Foody, G. M.: Status of land cover classification accuracy assessment, Remote Sensing of Environment, 80, 185–201, 2002.

Foster, J. L., Chang, A. T. C. and Hall, D. K.: Derivation of Snow Water Equivalent in Boreal Forests Using Microwave Radiometry, Arctic, 44(1), 147–152, 1991.

Foster, J. L., Hall, D. K., Chang, A. T. C., Rango, A., Wergin, W. and Erbe, E.: Effects of Snow Crystal Shape on the Scattering of Passive Microwave Radiation, IEEE Transactions on Geoscience and Remote Sensing, 37(2), 1997–2000, 1999.

Foster, J. L., Hall, D. K., Eylander, J. B., Riggs, G. a., Nghiem, S. V., Tedesco, M., Kim, E., Montesano, P. M., Kelly, R. E. J., Casey, K. a. and Choudhury, B.: A blended global snow product using visible, passive microwave and scatterometer satellite data, International Journal of Remote Sensing, 32(5), 1371–1395, doi:10.1080/01431160903548013, 2011.

Foster, J. L., Liston, G. E., Koster, R., Essery, R., Behr, H., Dumenil, L., Verseghy, D., Thompson, S., Pollard, D. and Cohen, J.: Snow cover and snow mass intercomparisons of general circulation models and Remotely Sensed Datasets, Journal of Climate, 9, 409–426, 1996.

Foster, J. L., Sun, C., Walker, J. P., Kelly, R., Chang, A., Dong, J. and Powell, H.: Quantifying the uncertainty in passive microwave snow water equivalent observations, Remote Sensing of Environment, 94(2), 187–203, doi:10.1016/j.rse.2004.09.012, 2005.

Frei, A. and Lee, S.: A comparison of optical-band based snow extent products during spring over North America, Remote Sensing of Environment, 114(9), 1940–1948, doi:10.1016/j.rse.2010.03.015, 2010.

Frei, A. and Robinson, D. A.: Northern Hemisphere Snow Extent: Regional Variability 1972-1994, International Journal of Climatology, 19, 1535–1560, 1999.

G

Gafurov, A. and Bárdossy, A.: Cloud removal methodology from MODIS snow cover product, Hydrology and Earth System Sciences, 13, 1361–1373, 2009.

Gao, Y., Xie, H., Lu, N., Yao, T. and Liang, T.: Toward advanced daily cloud-free snow cover and snow water equivalent products from Terra–Aqua MODIS and Aqua AMSR-E measurements, Journal of Hydrology, 385(1-4), 23–35, doi:10.1016/j.jhydrol.2010.01.022, 2010.

GCOS: GCOS web page, [online] Available from: http://www.wmo.int/pages/prog/gcos/index.php?name=AboutGCOS (Accessed 20 November 2012), 2012.

Gesell, G.: An algorithm for snow and ice detection using AVHRR data An extension to the APOLLO software package, International Journal of Remote Sensing, 10(4-5), 897–905, doi:10.1080/01431168908903929, 1989.

Giese, E. and Moßig, I.: Klimawandel in Zentralasien, Discussion Paper/Zentrum für Internationale Entwicklungs- und Umweltforschung, Justus-Liebig-Universität Gießen, (17), 70, 2004.

Glantz, M. H.: Water, Climate, And Development Issues in the Amu Darya Basin, Mitigation and Adaptation Strategies for Global Change, 10, 23–50, 2005.

Granit, J., Jägerskog, A., Löfgren, R., Bullock, A., Gooijer, G. De, Pettigrew, S. and Lindström, A.: Regional Water Intelligence Report Central Asia, Stockholm, Sweden., 2010.

Grippa, M., Kergoat, L., Le Toan, T., Mognard, N. M., Delbart, N., L'Hermitte, J. and Vicente-Serrano, S. M.: The impact of snow depth and snowmelt on the vegetation variability over central Siberia, Geophysical Research Letters, 32, 2–5, doi:10.1029/2005GL024286, 2005.

Grody, N. C. and Basist, A. N.: Global identification of snowcover using SSM/I measurements, IEEE Transactions on Geoscience and Remote Sensing, 34(1), 237–249, 1996.

Groisman, P. and Soja, A. J.: Ongoing climatic change in Northern Eurasia: justification for expedient research, Environmental Research Letters, 4(4), 1–7, doi:10.1088/1748-9326/4/4/045002, 2009.

Groisman, P. Y., Karl, T. R. and Knight, R. W.: Changes of Snow Cover, Temperature, and Radiative Heat Balance over the Northern Hemisphere, Journal of Climate, 7, 1633–1656, 1994a.

Groisman, P. Y., Karl, T. R. and Knight, R. W.: Observed Impact of Snow Cover on the Heat Balance and the Rise of Continental Spring Temperatures, Science, 263, 198–200, 1994b.

Groisman, P. Y., Knight, R. W., Razuvaev, V. N., Bulygina, O. N. and Karl, T. R.: State of the Ground: Climatology and Changes during the Past 69 Years over Northern Eurasia for a Rarely Used Measure of Snow Cover and Frozen Land, Journal of CLimate, 19, 4933–4955, 2006.

Gurt, M.: Turkmenistan plans $1 billion expansion of cotton industry, Reuters, 17th October, 2012.

Gutzler, D. S. and Rosen, R. D.: Interannual Variability of Wintertime snow cover across the Northern Hemisphere, Journal of Climate, 5, 1441–1447, 1992.

H

Hadjimitsis, D., Mitraka, Z., Gazani, I., Retalis, a., Chrysoulakis, N. and Michaelides, S.: Estimation of spatio-temporal distribution of precipitable water using MODIS and AVHRR data: a case study for Cyprus, Advances in Geosciences, 30, 23–29, doi:10.5194/adgeo-30-23-2011, 2011.

Hadley, O. L. and Kirchstetter, T. W.: Black-carbon reduction of snow albedo, Nature Climate Change, 2(6), 437–440, doi:10.1038/nclimate1433, 2012.

Hall, D. K., Foster, J. L. and Chang, A. T. C.: Measurement and Modeling of Microwave Emission from Forested Snowfields in Michigan, Nordic Hydrology, 13, 129–138, 1982.

Hall, D. K., Foster, J. L., Salomonson, V. V., Klein, a. G. and Chien, J. Y. L.: Development of a technique to assess snow-cover mapping errors from space, IEEE Transactions on Geoscience and Remote Sensing, 39(2), 432–438, doi:10.1109/36.905251, 2001a.

Hall, D. K. and Martinec, J.: Remote Sensing of Ice and Snow, Chapman & Hall, London, 1985.

Hall, D. K., Montesano, P. M., Foster, J. L., Riggs, G. A., Kelly, R. E. J. and Czajkowski, K.: Preliminary Evaluation of the AFWA-NASA Blended Snow-Cover Product over the Lower Great Lakes region, in 64th Eastern Snow Conference, pp. 1–6, St. Johns, Newfoundland, Canada., 2007.

Hall, D. K., Riggs, A. G. and Salomonson, V. V.: Algorithm Theoretical Basis Document (ATBD) for the MODIS snow and sea ice-mapping algorithms, , 45, 2001b.

Hall, D. K. and Riggs, G. A.: Accuracy assessment of the MODIS snow products, Hydrological Processes, 21, 1534–1547, doi:10.1002/hyp, 2007.

Hall, D. K., Riggs, G. a., Foster, J. L. and Kumar, S. V.: Development and evaluation of a cloud-gap-filled MODIS daily snow-cover product, Remote Sensing of Environment, 114(3), 496–503, doi:10.1016/j.rse.2009.10.007, 2010.

Hall, D. K., Riggs, G. A. and Salomonson, V. V: Development of Methods for Mapping Global Snow Cover Using Moderate Resolution Imaging Spectroradiometer Data, Remote Sensing of Environment, 54, 127–140, 1995.

Hall, D. K., Riggs, G. A., Salomonson, V. V, Digirolamo, N. E. and Bayr, K. J.: MODIS snow-cover products, Remote Sensing of Environment, 83, 181–194, 2002.

Harrison, A. R. and Lucas, R. M.: Multi-spectral classification of snow using NOAA AVHRR imagery, International Journal of Remote Sensing, 10(4-5), 907–916, doi:10.1080/01431168908903930, 1989.

Helfrich, S. R., Mcnamara, D., Ramsay, B. H., Baldwin, T. and Kasheta, T.: Enhancements to, and forthcoming developments in the Interactive Multisensor Snow and Ice Mapping System (IMS), Hydrological Processes, 21, 1576–1586, doi:10.1002/hyp, 2007.

Hijmans, R. J., Cameron, S. E., Parra, J. L., Jones, P. G. and Jarvis, A.: Very high resolution interpolated climate surfaces for global land areas, International Journal of Climatology, 25(15), 1965–1978, doi:10.1002/joc.1276, 2005.

Hollinger, J. P., Peirce, J. L. and Poe, G. a.: SSM/I instrument evaluation, IEEE Transactions on Geoscience and Remote Sensing, 28(5), 781–790, doi:10.1109/36.58964, 1990.

Holzhauser, H., Magny, M. and Zumbühl, H. J.: Glacier and lake-level variations in west-central Europe over the last 3500 years, The Holocene, 15(6), 789–801, 2005.

Hosaka, M., Nohara, D. and Kitoh, A.: Changes in Snow Cover and Snow Water Equivalent Due to Global Warming Simulated by a 20km-mesh Global Atmospheric Model, SOLA (Scientific Online Letters on the Atmosphere), 1, 93–96, doi:10.2151/sola., 2005.

Http://www.cawa-project.net/: CAWa project homepage, [online] Available from: http://www.cawa-project.net/ (Accessed 20 November 2012)

Http://www.seaspace.com/: TeraScan, [online] Available from: http://www.seaspace.com/ (Accessed January 7th, 2013) (Accessed 7 January 2013)

Huang, J., Fu, Q., Zhang, W., Wang, X., Zhang, R., Ye, H. and Warren, S. G.: Dust and Black Carbon in Seasonal Snow Across Northern China, Bulletin of the American Meteorological Society, 92(2), 175–181, doi:10.1175/2010BAMS3064.1, 2011a.

Huang, L. K., Cebula, R. P., Taylor, S. L., Deland, M. T., Mcpeters, R. D. and Stolarski, R. S.: Determination of NOAA-11 SBUV / 2 radiance sensitivity drift based on measurements of polar ice cap radiance, International Journal of Remote Sensing, 24(2), 305–314, doi:10.1080/01431160110113133, 2003.

Huang, X., Liang, T., Zhang, X. and Guo, Z.: Validation of MODIS snow cover products using Landsat and ground measurements during the 2001–2005 snow seasons over northern Xinjiang, China, International Journal of Remote Sensing, 32(1), 133–152, doi:10.1080/01431160903439924, 2011b.

Hüsler, F., Jonas, T., Wunderle, S. and Albrecht, S.: Validation of a modified snow cover retrieval algorithm from historical 1-km AVHRR data over the European Alps, Remote Sensing of Environment, 121, 497–515, doi:10.1016/j.rse.2012.02.018, 2012.

Huss, M., Farinotti, D., Bauder, A. and Funk, M.: Modelling runoff from highly glacierized alpine drainage basins in a changing climate, Hydrological Processes, 22, 3888–3902, doi:10.1002/hyp, 2008.

Hyvärinen, O., Eerola, K., Siljamo, N. and Koskinen, J.: Comparison of Snow Cover from Satellite and Numerical Weather Prediction Models in the Northern Hemisphere and Northern Europe, Journal of Applied Meteorology and Climatology, 48(6), 1199–1216, doi:10.1175/2008JAMC2069.1, 2009.

I

Ibatullin, S., Yasinsky, V. and Mironenkov, A.: The Impact of Climate Change on Water Resources in Central Asia. Sector report no. 6, Almaty, Kazakhstan., 2009.

Igoe, M.: Kyrgyzstan: Harsh Winter Triggers Mass Livestock Deaths, Eurasianet, 16th April, 2012.

J

Jain, S. K., Goswami, A. and Saraf, a. K.: Accuracy assessment of MODIS, NOAA and IRS data in snow cover mapping under Himalayan conditions, International Journal of Remote Sensing, 29(20), 5863–5878, doi:10.1080/01431160801908129, 2008.

Jalilov, S., Desutter, T. M. and Leitch, J. A.: Impact of Rogun dam on downstream Uzbekistan agriculture, International Journal of Water Resources and Environmental Engineering, 3(8), 161–166, 2011.

Jarvis, A., Reuter, H. I., Nelson, A. and Guevara, E.: Hole-filled SRTM for the globe Version 4, available from the CGIAR-CSI SRTM 90m Database (http://srtm.csi.cgiar.org), 2008.

Josberger, E. G. and Mognard, N. M.: A passive microwave snow depth algorithm with a proxy for snow metamorphism, Hydrological Processes, 16(8), 1557–1568, doi:10.1002/hyp.1020, 2002.

Jylhä, K., Fronzek, S., Tuomenvirta, H., Carter, T. R. and Ruosteenoja, K.: Changes in frost, snow and Baltic sea ice by the end of the twenty-first century based on climate model projections for Europe, Climatic Change, 86, 441–462, doi:10.1007/s10584-007-9310-z, 2008.

K

Karaev, B. Z.: Water diplomacy in central asia, The Middle East Review of International Affairs, 9(1), 63–69, 2005.

Kelly, M. A., Kubik, P. W., Von Blanckenburg, F. and Schlüchter, C.: Surface exposure dating of the Great Aletsch Glacier Egesen moraine system, western Swiss Alps, using the cosmogenic nuclide10Be, Journal of Quaternary Science, 19(5), 431–441, doi:10.1002/jqs.854, 2004.

Kelly, R.: The AMSR-E Snow Depth Algorithm: Description and Initial Results, Journal of The Remote Sensing Society of Japan, 29(1), 307–317, 2009.

Kelly, R. E., Chang, a. T., Tsang, L. and Foster, J. L.: A prototype AMSR-E global snow area and snow depth algorithm, IEEE Transactions on Geoscience and Remote Sensing, 41(2), 230–242, doi:10.1109/TGRS.2003.809118, 2003.

Kerr, R. A.: Can Northern Snow Foretell Next Winter's Weather?, Science, 300, 1865–1866, 2003.

Khan, B., Hayes, L. W. B. and Cracknell, A. P.: The effects of higher-order resampling on AVHRR data, International Journal of Remote Sensing, 16(1), 147–163, 1995.

Khan, V. M. and Holko, L.: Snow cover characteristics in the Aral Sea Basin from different data sources and their relation with river runoff, Journal of Marine Systems, 76(3), 254–262, doi:10.1016/j.jmarsys.2008.03.012, 2009.

Khlopenkov, K. V. and Trishchenko, A. P.: SPARC: New Cloud, Snow, and Cloud Shadow Detection Scheme for Historical 1-km AVHHR Data over Canada, Journal of Atmospheric and Oceanic Technology, 24(3), 322–343, doi:10.1175/JTECH1987.1, 2007.

Khromova, T. E., Osipova, G. B., Tsvetkov, D. G., Dyurgerov, M. B. and Barry, R. G.: Changes in glacier extent in the eastern Pamir, Central Asia, determined from historical data and ASTER imagery, Remote Sensing of Environment, 102(1-2), 24–32, doi:10.1016/j.rse.2006.01.019, 2006.

Kim, Y., Kimball, J. S., Zhang, K. and McDonald, K. C.: Satellite detection of increasing Northern Hemisphere non-frozen seasons from 1979 to 2008: Implications for regional vegetation growth, Remote Sensing of Environment, 121, 472–487, doi:10.1016/j.rse.2012.02.014, 2012.

King, M. D., Tsay, S. C., Platnick, S. E., Wand, M. and Liou, K. N.: Cloud Retrieval Algorithms for MODIS: Optical Thickness, Effective Particle Radius and Thermodynamic Phase, in MODIS Algorithm Theoretical Basis Document No. ATBDMOD- 05 MOD06 – Cloud Product, pp. 1–83, NASA, Washington, DC., 1997.

Kipshakbaev, N., Sarsembekov, T., Valentini, K., Kholmatov, A. and Krasnova, I.: Diagnostic Report on Water Resources in Central Asia., 2004.

Klein, A. G. and Barnett, A. C.: Validation of daily MODIS snow cover maps of the Upper Rio Grande River Basin for the 2000–2001 snow year, Remote Sensing of Environment, 86(2), 162–176, doi:10.1016/S0034-4257(03)00097-X, 2003.

Klein, A. G., Hall, D. K. and Nolin, A. W.: Development of a prototype snow albedo algorithm for the NASA MODIS Instrument, in 57th Eastern Snow Conference, pp. 143–158, Syracuse, New York, USA., 2000.

Klein, A. G., Hall, D. K. and Riggs, G. a.: Improving snow cover mapping in forests through the use of a canopy reflectance model, Hydrological Processes, 12(1011), 1723–1744, doi:10.1002/(SICI)1099-1085(199808/09)12:10/11<1723::AID-HYP691>3.3.CO;2-U, 1998.

Klein, I., Gessner, U. and Kuenzer, C.: Regional land cover mapping and change detection in Central Asia using MODIS time-series, Applied Geography, 35, 219–234, doi:10.1016/j.apgeog.2012.06.016, 2012.

Klein Tank, a. M. G., Wijngaard, J. B., Können, G. P., Böhm, R., Demarée, G., Gocheva, A., Mileta, M., Pashiardis, S., Hejkrlik, L., Kern-Hansen, C., Heino, R., et al.: Daily dataset of 20th-century surface air temperature and precipitation series for the European Climate Assessment, International Journal of Climatology, 22(12), 1441–1453, doi:10.1002/joc.773, 2002.

König, M., Winther, J. and Isaksson, E.: Measuring Snow and Glacier Ice Properties from Satellite, Reviews of Geophysics, 39(2001), 1–27, 2001.

Kotlyakov, V. M. and Dolgushin, L. D.: Possibility of artificial augmentation of melting by surface dusting of glaciers (results of Soviet Investigations), in The Role of snow and ice in hydrology: proceedings of the Banff Symposia, pp. 1421–1426, IAHS AISH Publ. 107, 1973.

Kriebel, K. T., Gesell, G., Kästner, M. and Mannstein, H.: The cloud analysis tool APOLLO: Improvements and validations, International Journal of Remote Sensing, 24(12), 2389–2408, doi:10.1080/01431160210163065, 2003.

Kukla, G. and Robinson, D.: Accuracy of Snow and Ice Monitoring, Glaciological Data Report, GD-5, 91–97, 1979.

L

Lemke, P., Ren, J., Alley, R. B., Allison, I., Carrasco, J., Flato, G., Fujii, Y., Kaser, G., Mote, P., Thomas, R. H. and Zhang, T.: Observations: Changes in Snow, Ice and Frozen Ground, in Climate Change 2007: The Physical Science Basis. Contributions of Working Group 1 to the Fourth Assessment Report of the Intergovernmental Panel on Climate Change, edited by S. Solomon, D. Qin, M. Manning, Z. Chen, M. C. Marquis, K. Averyt, M. Tignor, and H. L. Miller, pp. 337–383, Cambridge, U.K and New York, USA., 2007.

Levinson, D. H. and Lawrimore, J. H.: State of the Climate in 2007, Bulletin of the American Meteorological Society, 89(7), 1–179, 2007.

Liang, T., Huang, X., Wu, C., Liu, X., Li, W., Guo, Z. and Ren, J.: An application of MODIS data to snow cover monitoring in a pastoral area: A case study in Northern Xinjiang, China, Remote Sensing of Environment, 112(4), 1514–1526, doi:10.1016/j.rse.2007.06.001, 2008a.

Liang, T., Zhang, X., Xie, H., Wu, C., Feng, Q., Huang, X. and Chen, Q.: Toward improved daily snow cover mapping with advanced combination of MODIS and AMSR-E measurements, Remote Sensing of Environment, 112, 3750–3761, doi:10.1016/j.rse.2008.05.010, 2008b.

Libert, B., Orolbaev, E. and Steklov, Y.: Water and Energy Crisis in Central Asia, China and Eurasia Forum Quarterly, 6(3), 9–20, 2008.

Lillis, J.: Uzbekistan Leader Warns of Water Wars in Central Asia, Inside The Cocoon - Central Asia Today, 7th September, 2012.

Lindstad, B. H.: A Comparative Study of Forestry in Finland , Norway , Sweden , and the United States , with Special Emphasis on Policy Measures for Nonindustrial Private Forests in Norway and the United States., 2002.

Lioubimtseva, E. and Henebry, G. M.: Climate and environmental change in arid Central Asia: Impacts, vulnerability, and adaptations, Journal of Arid Environments, 73(11), 963–977, doi:10.1016/j.jaridenv.2009.04.022, 2009.

Lissens, G., Kempeneers, P., Fierens, F. and Van Rensbergen, J.: Development of Cloud, Snow, and Shadow Masking Algorithms for VEGETATION Imagery, in IEEE International Geoscience and Remote Sensing Symposium, pp. 834–836, Honolulu, Hawaii, USA, 24-28 July 2000., 2000.

Liston, G. E. and Hiemstra, C. a.: The Changing Cryosphere: Pan-Arctic Snow Trends (1979–2009), Journal of Climate, 24(21), 5691–5712, doi:10.1175/JCLI-D-11-00081.1, 2011.

Loarie, S. R., Duffy, P. B., Hamilton, H., Asner, G. P., Field, C. B. and Ackerly, D. D.: The velocity of climate change., Nature, 462, 1052–1057, doi:10.1038/nature08649, 2009.

Lucas, R. M. and Harrison, A. R.: Snow observation by satellite : A review, Remote Sensing Revi, 4(2), 285–348, doi:10.1080/02757259009532109, 1990a.

Lucas, R. M. and Harrison, A. R.: Snow observation by satellite: A review, Remote Sensing Reviews, 4(2), 285–348, doi:10.1080/02757259009532109, 1990b.

Luojus, K., Pulliainen, J., Takala, M., Derksen, C., Rott, H., Nagler, T., Solberg, R., Wiesmann, A., Metsämäki, S., Malnes, E. and Bojkov, B.: Investigating the Feasibility of the Globsnow Snow Water Equivalent Data for Climate Research Purposes, in IEEE International Geoscience and Remote Sensing Symposium, vol. 19, pp. 4851–4853, Honolulu, Hawaii, USA, 25-30 July, 2010., 2010a.

Luojus, K., Pulliainen, J., Takala, M. and Lemmetyinen, J.: Snow Water Equivalent (SWE) product guide - European Space Agency Study Contract Report., 2010b.

M

Markus, T., Powell, D. C. and Wang, J. R.: Sensitivity of passive microwave snow depth retrievals to weather effects and snow evolution, IEEE Transactions on Geoscience and Remote Sensing, 44(1), 68–77, doi:10.1109/TGRS.2005.860208, 2006.

Massom, R. A.: Satellite Remote Sensing of Polar Regions: Applications, Limitations and Data Availability, Belhaven Press, University of Cambridge., 1991.

Mätzler, C.: Meteorolog E and Atmospheric Physics Passive Microwave Signatures of Landscapes in Winter, Meteorol. Atmos. Phys., 54, 241–260, 1994.

Mätzler, C. and Wegmüller, U.: Dielectric properties of freshwater ice at microwave frequencies, Journal of Physics D: Applied Physics, 20, 1623–1630, 1987.

Maurer, E. P., Rhoads, J. D., Dubayah, R. O. and Lettenmaier, D. P.: Evaluation of the snow-covered area data product from MODIS, Hydrological Processes, 17(1), 59–71, doi:10.1002/hyp.1193, 2003.

Maxson, R. W., Allen, M. W. and Szeliga, T. L.: Theta - Image Classification by Comparison of Angles Created Between Multi-Channel Vectors and an Empirically Selected Reference Vector, NOHRSC, Chanhassen, Minnesota, USA, 7, 1998.

Meehl, G. a., Covey, C., Taylor, K. E., Delworth, T., Stouffer, R. J., Latif, M., McAvaney, B. and Mitchell, J. F. B.: THE WCRP CMIP3 Multimodel Dataset: A New Era in Climate Change Research, Bulletin of the American Meteorological Society, 88(9), 1383–1394, doi:10.1175/BAMS-88-9-1383, 2007.

Messner, D.: Klimawandel und Wasserkrisen der Zukunft, Sicherheit und Frieden, 27(3), 167–174, doi:10.5771/0175-274x-2009-3-167, 2009.

Metsamaki, S., Anttila, S., Markus, H. and Vepsalainen, J.: A feasible method for fractional snow cover mapping in boreal zone based on a reflectance model, Remote Sensing of Environment, 95(1), 77–95, doi:10.1016/j.rse.2004.11.013, 2005.

Meyer, P., Itten, K. I., Kellenberger, T., Sandmeier, S. and Sandmeier, R.: Radiometric correction of topographically induced effects on Landsat TM data in an Alpine environment, ISPRS Journal of Photogrammetry and Remote Sensing, 48, 17–28, 1993.

Micklin, P.: The Aral Sea Disaster, Annual Review of Earth and Planetary Sciences, 35(1), 47–72, doi:10.1146/annurev.earth.35.031306.140120, 2007.

Miller, S. D. and Lee, T. F.: Satellite-Based Imagery Techniques for Daytime Cloud / Snow Delineation from MODIS, Journal of Applied Meteorology, 44, 987–997, 2005.

Mokhov, I. I., Roeckner, E., Semenov, V. a. and Khon, V. C.: Possible regional changes in precipitation regimes in northern Eurasia in the 21st century, Water Resources, 33(6), 702–710, doi:10.1134/S009780780606011X, 2006.

Molotch, N. P. and Margulis, S. A.: Estimating the distribution of snow water equivalent using remotely sensed snow cover data and a spatially distributed snowmelt model: A multi-resolution , multi-sensor comparison, Advances in Water Resources, 31(11), 1503–1514, doi:10.1016/j.advwatres.2008.07.017, 2008.

Moreno, J. F. and Melia, J.: An Optimum Interpolation Method Applied to the Resampling of NOAA AVHRR Data, IEEE Transactions on Geoscience and Remote Sensing, 32(1), 131–151, 1994.

Muntán, E., Garcia, C., Oller, P., Marti, G., Garcia, A. and Gutiérrez, E.: Reconstructing snow avalanches in the Southeastern Pyrenees, Natural Hazards and Earth System Sciences, 9, 1599–1612, 2009.

N

NASA: Landsat 7 Science Data Users Handbook, 2006.

Nature_Protection_Ministry_Republic_of_Kazakhstan: Drought Management and mitigation assessment for Kazakhstan, phase two: Regional vulnerability and capacity assessment survey, Almaty, Kazakhstan., 2006.

Nghiem, S. V., Steffen, K., Neumann, G. and Huff, R.: Mapping of ice layer extent and snow accumulation in the percolation zone of the Greenland ice sheet, Journal of Geophysical Research, 110, 1–13, doi:10.1029/2004JF000234, 2005.

Nghiem, S. V. and Tsai, W.: Global Snow Cover Monitoring With Spaceborne Ku-band Scatterometer, IEEE Transactions on Geoscience and Remote Sensing, 39(10), 2118–2134, 2001.

NOAA: Comprehensive Large Array-data Stewardship System, [online] Available from: http://www.class.noaa.gov (Accessed 18 September 2012), n.d.

NOAA/NESDIS: NOAA Polar Orbiter Data User's Guide, [online] Available from: http://www.ncdc.noaa.gov/oa/pod-guide/ncdc/docs/podug/index.htm (Accessed 22 July 2012), 1998.

NOAA/NESDIS: NOAA KLM User's Guide with NOAA-N, -N' Supplement, [online] Available from: http://www.ncdc.noaa.gov/oa/pod-guide/ncdc/docs/klm/index.htm (Accessed 23 July 2012), 2009.

Nogués-Bravo, D., Araújo, M. B., Errea, M. P. and Martínez-Rica, J. P.: Exposure of global mountain systems to climate warming during the 21st Century, Global Environmental Change, 17, 420–428, doi:10.1016/j.gloenvcha.2006.11.007, 2007.

Notarnicola, C., Duguay, M., Moelg, N., Schellenberger, T., Tetzlaff, A., Monsorno, R., Costa, A., Steurer, C. and Zebisch, M.: Snow Cover Maps from MODIS Images at 250 m Resolution, Part 1: Algorithm Description, Remote Sensing, 5(1), 110–126, doi:10.3390/rs5010110, 2013a.

Notarnicola, C., Duguay, M., Moelg, N., Schellenberger, T., Tetzlaff, A., Monsorno, R., Costa, A., Steurer, C. and Zebisch, M.: Snow Cover Maps from MODIS Images at 250 m Resolution, Part 2: Validation, Remote Sensing, 5(4), 1568–1587, doi:10.3390/rs5041568, 2013b.

NSIDC: NSIDC website, Cold Land Processes Field Experiment (CLPX) [online] Available from: http://nsidc.org/data/clpx/ (Accessed 28 February 2013), 2013.

O

Ososkova, T., Gorelkin, N. and Chub, V.: Water Resources of Central Asia and Adaptation Measures for Climate Change, Environmental Monitoring and Assessment, 61, 161–166, 2000.

P

Painter, T. H., Rittger, K., McKenzie, C., Slaughter, P., Davis, R. E. and Dozier, J.: Retrieval of subpixel snow covered area, grain size, and albedo from MODIS, Remote Sensing of Environment, 113(4), 868–879, doi:10.1016/j.rse.2009.01.001, 2009.

Parajka, J. and Blöschl, G.: Validation of MODIS snow cover images over Austria, Hydrology and Earth System Sciences, 10, 679–689, 2006.

Parajka, J. and Blöschl, G.: Spatio-temporal combination of MODIS images – potential for snow cover mapping, Water Resources Research, 44, 1–13, 2008.

Parajka, J., Pepe, M., Rampini, a., Rossi, S. and Blöschl, G.: A regional snow-line method for estimating snow cover from MODIS during cloud cover, Journal of Hydrology, 381(3-4), 203–212, doi:10.1016/j.jhydrol.2009.11.042, 2010.

Peings, Y. and Douville, H.: Influence of the Eurasian snow cover on the Indian summer monsoon variability in observed climatologies and CMIP3 simulations, Climate Dynamics, 34(5), 643–660, doi:10.1007/s00382-009-0565-0, 2009.

Peng, S., Piao, S., Ciais, P., Fang, J. and Wang, X.: Change in winter snow depth and its impacts on vegetation in China, Global Change Biology, 16(11), 3004–3013, doi:10.1111/j.1365-2486.2010.02210.x, 2010.

Pepe, M., Brivio, P. a., Rampini, a., Nodari, F. R. and Boschetti, M.: Snow cover monitoring in Alpine regions using ENVISAT optical data, International Journal of Remote Sensing, 26(21), 4661–4667, doi:10.1080/01431160500206635, 2005.

Pulliainen, J.: Mapping of snow water equivalent and snow depth in boreal and sub-arctic zones by assimilating space-borne microwave radiometer data and ground-based observations, Remote Sensing of Environment, 101(2), 257–269, doi:10.1016/j.rse.2006.01.002, 2006.

Pulliainen, J. and Hallikainen, M.: Retrieval of Regional Snow Water Equivalent from Space-Borne Passive Microwave Observations, Remote Sensing of Environment, 75(00), 76–85, 2001.

Pulliainen, J., Karna, J.-P. and Hallikainen, M.: Development of geophysical retrieval algorithms for the MIMR, IEEE Transactions on Geoscience and Remote Sensing, 31(1), 268–277, doi:10.1109/36.210466, 1993.

Pulliainen, J. T., Grandell, J. and Hallikainen, M. T.: Retrieval of Surface Temperature in Boreal Forest Zone from SSM/I Data, IEEE Transactions on Geoscience and Remote Sensing, 35(5), 1188–1200, 1997.

Pulliainen, J. T., Grandell, J. and Hallikainen, M. T.: HUT Snow Emission Model and its Applicability to Snow Water Equivalent Retrieval, IEEE Transactions on Geoscience and Remote Sensing, 37(3), 1378–1390, 1999.

Q

Qobilov, T., Pertziger, F. and Vasilina, L.: Operational technology for snow-cover mapping in the Central Asian mountains using NOAA-AVHRR data, Remote Sensing and Hydrology, 267, 76–80, 2001.

R

Rabus, B., Eineder, M., Roth, A. and Bamler, R.: The shuttle radar topography mission—a new class of digital elevation models acquired by spaceborne radar, ISPRS Journal of Photogrammetry and Remote Sensing, 57(4), 241–262, doi:10.1016/S0924-2716(02)00124-7, 2003.

Räisänen, J.: Warmer climate: less or more snow?, Climate Dynamics, 30(2-3), 307–319, doi:10.1007/s00382-007-0289-y, 2007.

Rakhmatullaev, S., Huneau, F., Le Coustumer, P., Motelica-Heino, M. and Bakiev, M.: Facts and Perspectives of Water Reservoirs in Central Asia: A Special Focus on Uzbekistan, Water, 2, 307–320, doi:10.3390/w2020307, 2010.

Ramanathan, V. and Carmichael, G.: Global and regional climate changes due to black carbon, Nature Geoscience, 1, 221–227, 2008.

Ramsay, B. H.: The interactive multisensor snow and ice mapping system, Hydrological Processes, 12, 1537–1546, 1998.

Ranchin, T. and Wald, L.: FUSION OF HIGH SPATIAL AND SPECTRAL RESOLUTION IMAGES: THE ARSIS CONCEPT AND ITS IMPLEMENTATION Thierry RANCHIN and Lucien WALD, Photogrammetric Engineering & Remote Sensing, 66(1), 49–61, 2000.

Rango, a.: Spaceborne remote sensing for snow hydrology applications, Hydrological Sciences Journal, 41(4), 477–494, doi:10.1080/02626669609491521, 1996.

Raup, B. H., Racoviteanu, A., Khalsa, S. J. S., Helm, C., Armstrong, R. and Arnaud, Y.: The GLIMS Geospatial Glacier Database: a New Tool for Studying Glacier Change, Global and Planetary Change, 56, 101–110, 2007.

Richter, G.: Development of snow studies in the USSR, in General Assembly of Helsinki - Snow and Ice Commission, pp. 69–73, Helsinki, Finland, 25.07 - 06.08.1960., 1960.

Riggs, G. A., Hall, D. K. and Salomonson, V. V: MODIS Snow Products User Guide to Collection 5, Available from: http://nsidc.org/data/docs/daac/modis_v5/dorothy_snow_doc.pdf (accessed 20 January 2013), 1–80, 2006.

Riggs, G. and Hall, D. K.: Snow Mapping with the MODIS Aqua Instrument, in 61st Eastern Snow Conference, pp. 81–84, Portland, Maine, USA., 2004.

Rittger, K., Painter, T. H. and Dozier, J.: Assessment of methods for mapping snow cover from MODIS, Advances in Water Resources, 1–14, doi:10.1016/j.advwatres.2012.03.002, 2012.

Robinson, D. A.: Monitoring Northern Hemisphere Snow Cover, Snow Watch ’92: Detection Strategies for Snow and Ice, Glaciological Data Report, GD-25, 1–25, 1993.

Robinson, D. A., Dewey, K. F. and Heim, R. R.: Global Snow Cover Monitoring: An Update, Bulletin of the American Meteorological Society, 74, 1689–1696, 1993.

Rodell, M. and Houser, P. R.: Updating a Land Surface Model with MODIS-Derived Snow Cover, Journal of Hydrometeorology, 5, 1064–1075, 2004.

Rodríguez, E., Morris, C. S., Belz, J. E., Chapin, E. C., Martin, J. M., Daffer, W. and Hensley, S.: An Assessment of the SRTM Topographic Products, Technical Report JPL D-31639, Pasadena, California, USA., 2005.

Romanov, P., Gutman, G. and Csiszar, I.: Automated Monitoring of Snow Cover over North America with Multispectral Satellite Data, Journal of Applied Meteorology, 39, 1866–1880, 2000.

Rosenthal, W. and Dozier, J.: Automated mapping of montane snow cover at subpixel resolution from the Landsat Thematic Mapper, Water Resources Research, 32(1), 115–130, 1996.

Rott, H.: Remote sensing of snow, in Large Scale Effects of Seasonal Snow Cover (Proceedings of the Vancouver Symposium), pp. 279–290, IAHS Publ. no.166, Vancouver., 1987.

Rott, H. and Nagler, T.: Capabilities of ERS-1 SAR for snow and glacier monitoring in alpine areas, in Proceedings of the Second ERS-1 Symposium, pp. 965–970, ESA SP-361., 1994.

Rott, H. and Nagler, T.: Intercomparison of snow retrieval algorithms by means of spaceborn microwave radiometry, in Passive Microwave Remote Sensing of Land-Atmosphere Interactions, edited by B. J. Choudhury, Y. H. Kerr, E. G. Nijoku, and P. Pampaloni, pp. 227–243, Zeist: VSP., 1995.

S

Saito, K., Cohen, J. and Entekhabi, D.: Evolution of Atmospheric Response to Early-Season Eurasian Snow Cover Anomalies, Monthly Weather Review, 129(11), 2746–2760, doi:10.1175/1520-0493(2001)129<2746:EOARTE>2.0.CO;2, 2001.

Salminen, M., Pulliainen, J., Metsämäki, S., Kontu, A. and Suokanerva, H.: The behaviour of snow and snow-free surface reflectance in boreal forests: Implications to the performance of snow covered area monitoring, Remote Sensing of Environment, 113(5), 907–918, doi:10.1016/j.rse.2008.12.008, 2009.

Salomonson, V. . and Appel, I.: Estimating fractional snow cover from MODIS using the normalized difference snow index, Remote Sensing of Environment, 89(3), 351–360, doi:10.1016/j.rse.2003.10.016, 2004.

Salomonson, V. V. and Appel, I.: Development of the Aqua MODIS NDSI fractional snow cover algorithm and validation results, IEEE Transactions on Geoscience and Remote Sensing, 44(7), 1747–1756, doi:10.1109/TGRS.2006.876029, 2006.

Saunders, R. W. and Kriebel, K. T.: An improved method for detecting clear sky and cloudy radiances from AVHRR data, International Journal of Remote Sensing, 9(1), 123–150, doi:10.1080/01431168808954841, 1988.

Savitskaya, D.: Statistical picture of climate changes in Central Asia : Temperature , precipitation , and river flow, in International Environmental Modelling and Software Society (iEMSs) 2010 International Congress on Environmental Modelling and Software Modelling for Environment's Sake, Fifth Biennial Meeting, edited by D. A. Swayne, W. Yang, A. A. Voinov, A. Rizzoli, and T. Filatova, p. 8, Ottawa, Canada., 2010.

Schlaepfer, D. R., Lauenroth, W. K. and Bradford, J. B.: Consequences of declining snow accumulation for water balance of mid-latitude dry regions, Global Change Biology, 18(6), 1988–1997, doi:10.1111/j.1365-2486.2012.02642.x, 2012.

Schneider, U., Becker, A., Ziese, M. and Rudolf, B.: Global Precipitation Analysis Products of the GPCC, , 1–12, 2010.

Sehring, J. and Giese, E.: Global Environmental Change and Conflict Potential in Central Asia, in Coping with Global Environmental Change, Disasters and Security - Threats, Challenges, Vulnerabilities and Risks. Hexagon Series on Human and Environmental Security and Peace, vol. 5, edited by H. G. Brauch, Ü. Oswald-Spring, C. Mesjasz, J. Grin, P. Kameri-Mbote, B. Chourou, P. Dunay, and J. Birkmann, pp. 525–534, Springer, Berlin - Heidelberg - New York., 2011.

Serreze, M. C., Holland, M. M. and Stroeve, J.: Perspectives on the Arctic's shrinking sea-ice cover., Science (New York, N.Y.), 315, 1533–1536, doi:10.1126/science.1139426, 2007.

Severskiy, I. V, Blagoveshchenskiy, V. P., Severskiy, S. I., Pimankina, N. V, Zichu, X., Zhizhong, Z. and Ruji, H.: Chapter 1. Natural Conditions for Avalanche Formation, in Snow Cover and Avalanches in Tien Shan Mountains, edited by I. V Severskiy and X. Zichu, pp. 9–28, VAC Publishing House, Almaty, Kazakhstan, 2000a.

Severskiy, I. V, Blagoveshchenskiy, V. P., Severskiy, S. I., Pimankina, N. V, Zichu, X., Zhizhong, Z. and Ruji, H.: Chapter 3. Influence of local factors on the distribution of snow cover in mountains, in Snow Cover and Avalanches in Tien Shan Mountains, edited by I. V Severskiy and X. Zichu, pp. 91–106, VAC Publishing House, Almaty, Kazakhstan, 2000b.

Severskiy, I. V.: Distribution of Snow Cover in the Mountains of Central Asia, in International Conference on Ecohydrology of High Mountain Areas, pp. 405–412, Kathmandu, Nepal., 1996.

Siegfried, T., Bernauer, T., Guiennet, R., Sellars, S., Robertson, A. W., Mankin, J., Bauer-Gottwein, P. and Yakovlev, A.: Will climate change exacerbate water stress in Central Asia?, Climatic Change, 112(3-4), 881–899, doi:10.1007/s10584-011-0253-z, 2011.

Simic, A., Fernandes, R., Brown, R., Romanov, P. and Park, W.: Validation of VEGETATION, MODIS, and GOES+ SSM/I snow-cover products over Canada based on surface snow depth observations, Hydrological Processes, 18(6), 1089–1104, doi:10.1002/hyp.5509, 2004.

Sirguey, P., Mathieu, R., Arnaud, Y., Khan, M. M., Chanussot, J. and Member, S.: Improving MODIS Spatial Resolution for Snow Mapping Using Wavelet Fusion and ARSIS Concept, IEEE Transactions on Geoscience and Remote Sensing, 5(1), 78–82, 2008.

Solberg, R. and Andersen, T.: An Automatic System for Operational Snow-Cover Monitoring in the Norwegian Mountain Regions, in Proceedings of the International Geoscience and Remote Sensing Symposium, pp. 2084–2086, Pasadena, CA, USA, 8-12 August 1994, 1994.

Solberg, R., Koren, H. and Amlien, J.: A review of optical snow cover algorithms, Norsk Regnesentral Norwegian Computing Center Publication number SAMBA/40/06, 2006.

Solberg, R., Wangensteen, B., Amlien, J., Koren, H., Metsämäki, S., Nagler, T., Luojus, K. and Pulliainen, J.: A new Global Snow Extent Product Based on ATSR-2 and AATSR, in Proceedings of the 2010 IEEE International Geoscience and Remote Sensing Symposium, 25-30 July 2010, p. 4, Honolulu, Hawaii, USA., 2010a.

Solberg, R., Wangensteen, B., Metsämäki, S., Nagler, T., Sandner, R., Rott, H., Wiesmann, A., Luojus, K., Kangwa, M. and Pulliainen, J.: GlobSnow Snow Extent Product Guide Product

Version 1.0, European Space Agency Study Contract Report ESRIN Contract 21703/08/I-EC, 19, 2010b.

Solberg, R., Wangensteen, B., Rudjord, O., Metsämäki, S., Nagler, T., Sandner, R., Müller, F., Rott, H., Wiesmann, A., Luojus, K., Kangwa, M., et al.: GlobSnow Snow Extent Product Guide - Product Version 1.2., 2011.

Sterle, K. M., McConnell, J. R., Dozier, J., Edwards, R. and Flanner, M. G.: Retention and radiative forcing of black carbon in eastern Sierra Nevada snow, The Cryosphere, 7(1), 365–374, doi:10.5194/tc-7-365-2013, 2013.

Stieglitz, M., Déry, S. J., Romanovsky, V. E. and Osterkamp, T. E.: The role of snow cover in the warming of arctic permafrost, Geophysical Research Letters, 30(13), 1–4, doi:10.1029/2003GL017337, 2003.

Stowe, L. L., Davis, P. A. and McClain, P. E.: Scientific Basis and Initial Evaluation of the CLAVR-1 Global Clear / Cloud Classification Algorithm for the Advanced Very High Resolution Radiometer, Journal of Atmospheric and Oceanic Technology, 16, 656–681, 1998.

Strickman, R. and Porkka, M.: Water and Social Changes in Central Asia: Problems related to Cotton Production in Uzbekistan, in Central Asian Waters - Social, economic, environmental and governance puzzle, edited by M. M. Rahaman and O. Varis, pp. 105–116, Helsinki University of Technology - TKK, Helsinki, Finland, 2008.

Strozzi, T., Teatini, P. and Tosi, L.: TerraSAR-X reveals the impact of the mobile barrier works on Venice coastland stability, Remote Sensing of Environment, 113(12), 2682–2688, doi:10.1016/j.rse.2009.08.001, 2009.

Sturm, M., Holmgren, J. and Liston, G.: A Seasonal Snow Cover Classification System for Local to Global Applications, Journal of Climate, 8, 1261–1283, 1995.

Surazakov, A. B., Aizen, V. B., Aizen, E. M. and Nikitin, S. a: Glacier changes in the Siberian Altai Mountains, Ob river basin, (1952–2006) estimated with high resolution imagery, Environmental Research Letters, 2(4), 045017, doi:10.1088/1748-9326/2/4/045017, 2007.

T

Tait, A. B.: Estimation of Snow Water Equivalent Using Passive Microwave Radiation Data, Remote Sensing of Environment, 64, 286–291, 1998.

Tedesco, M. and Miller, J.: Northern Hemisphere Snow-Covered Area Mapping: Optical Versus Active and Passive Microwave Data, IEEE Geoscience and Remote Sensing Letters, 4(2), 221–225, doi:10.1109/LGRS.2006.888842, 2007.

Thurman, M.: Natural Disaster Risks in Central Asia : A Synthesis Table of Contents, , (April), 2011.

Tischbein, B., Manschadi, A., Conrad, C., Hornidge, A.-K., Bhaduri, A., Ul Hassan, M., Lamers, J. and Vlek, P.: Adapting to Water Scarcity – Constraints and Opportunities for Im-

proving Irrigation Management in Khorezm , Uzbekistan, Water Science & Technology, 13(2), 337–348, 2013.

Trujillo, E., Molotch, N. P., Goulden, M. L., Kelly, A. E. and Bales, R. C.: Elevation-dependent influence of snow accumulation on forest greening, Nature Geoscience, 5(10), 705–709, doi:10.1038/ngeo1571, 2012.

Tungalagsaikhan, P., Günther, K. P., Gesell, G., Dech, S. W. and Ruppert, T.: Operational processing of AVHRR data at DFD, in Publikationen der Deutschen Gesellschaft für Photogrammetrie, Fernerkundung und Geoinformation: Vorträge, 23. Wissenschaftlich- Technische Jahrestagung der DGPF, 9.-11. Sept. 2003, Bochum, Bd. 12, pp. 435–449., 2003.

U

Ulaby, F., Moore, R. and Fung, A.: Microwave Remote Sensing, 1st ed., Addison-Wesley, Reading, MA., 1981.

UNECE: Our waters: Joining hands across borders. First Assessment of Transboundary Rivers, Lakes and Groundwaters., 2007.

UNEP, UNDP, OSCE and NATO: Environment and Security - Transforming risks into cooperation, 2005.

USGS: Landsat : A Global Land-Imaging Mission, Sioux Falls, South Dakota, USA., 2012.

V

Vikhamar, D. and Solberg, R.: Subpixel mapping of snow cover in forests by optical remote sensing, Remote Sensing of Environment, 84, 69–82, 2002.

Vikhamar, D. and Solberg, R.: Snow-cover mapping in forests by constrained linear spectral unmixing of MODIS data, Remote Sensing of Environment, 88(3), 309–323, doi:10.1016/j.rse.2003.06.004, 2003.

Vinogradov, S. and Langford, V. P. E.: Managing transboundary water resources in the Aral Sea Basin : in search of a solution, International Journal of Global Environmental Issues, 1(3/4), 345–362, 2001.

W

Wang, L., Derksen, C. and Brown, R.: Detection of pan-Arctic terrestrial snowmelt from QuikSCAT, 2000–2005, Remote Sensing of Environment, 112(10), 3794–3805, doi:10.1016/j.rse.2008.05.017, 2008a.

Wang, L., Sharp, M., Brown, R., Derksen, C. and Rivard, B.: Evaluation of spring snow covered area depletion in the Canadian Arctic from NOAA snow charts, Remote Sensing of Environment, 95(4), 453–463, doi:10.1016/j.rse.2005.01.006, 2005.

Wang, X. and Xie, H.: New methods for studying the spatiotemporal variation of snow cover based on combination products of MODIS Terra and Aqua, Journal of Hydrology, 371(1-4), 192–200, doi:10.1016/j.jhydrol.2009.03.028, 2009.

Wang, X., Xie, H. and Liang, T.: Evaluation of MODIS snow cover and cloud mask and its application in Northern Xinjiang, China, Remote Sensing of Environment, 112(4), 1497–1513, doi:10.1016/j.rse.2007.05.016, 2008b.

Wang, X., Xie, H. and Liang, T.: Development and assessment of combined Terra and Aqua MODIS snow cover products in Colorado, Journal of Applied Remote Sensing, 3, 1–15, 2009.

Wang, Z. and Bovik, A. C.: A Universal Image Quality Index, IEEE Signal Processing Letters, 1–4, 2002.

Watson, R. T., Zinyowera, M. C. and Moss, R. H.: An assessment of vulnerability, Summary for Policymakers: The Regional Impacts of Climate Change, A special report of IPCC Working Group II, published for the Intergovernmental Panel on Climate Change., Cambridge, U.K., 1998.

Winther, J.-G., Gerland, S., Orbaek, J. B., Ivanov, B., Blanco, A. and Boike, J.: Spectral reflectance of melting snow in a high Arctic watershed on Svalbard: some implications for optical satellite remote sensing studies, Hydrological Processes, 13, 2033–2049, 1999.

WMO and GCOS: Systematic Observation Requirements For Satellite-Based Data Products for Climate - 2011 Update, GCOS - 154., WMO GCOS, Geneva, Switzerland., 2011.

Wolfe, R. E., Roy, D. P. and Vermote, E.: MODIS land data storage, gridding, and compositing methodology: Level 2 grid, IEEE Transactions on Geoscience and Remote Sensing, 36(4), 1324–1338, doi:10.1109/36.701082, 1998.

Y

Ye, H., Cho, H. and Gustafson, P. E.: The Changes in Russian Winter Snow Accumulation during 1936 – 83 and Its Spatial Patterns, Journal of Climate, 11, 856–863, 1998.

Yesserkepova, I.: Forest and climate change in Eastern Europe and Central Asia, in Forests and Climate Change Working paper 8, edited by C. Matyas, pp. 63–75, FAO, Rome, 2010.

Younger, P. L.: Water - All that matters, planetearth, London., 2012.

Z

Zeng, Q., Cao, M., Feng, X., Liang, F., Chen, X. and Sheng, W.: A study of spectral reflection characteristics for snow , ice and water in the north of China, Hydrological Applications of Remote Sensing and Remote Sensing Data Transmission, 145, 451–262, 1983.

Zhang, Y., Yan, S. and Lu, Y.: Snow Cover Monitoring Using MODIS Data in Liaoning Province, Northeastern China, Remote Sensing, 2(3), 777–793, doi:10.3390/rs2030777, 2010.

Zhao, H. and Fernandes, R.: Daily snow cover estimation from Advanced Very High Resolution Radiometer Polar Pathfinder data over Northern Hemisphere land surfaces during 1982–2004, Journal of Geophysical Research, 114(D5), 1–14, doi:10.1029/2008JD011272, 2009.

Eidesstattliche Erklärung

Hiermit versichere ich an Eides statt, dass ich meine Dissertation mit dem Titel

Central Asian Snow Cover Characteristics between 1986 and 2012 derived from Time Series of Medium Resolution Remote Sensing Data

eigenständig angefertigt und keine anderen als die von mir angegebenen Quellen und Hilfsmittel benutzt habe.

Die vorgelegte Dissertation wurde bisher bei keinem anderen Prüfungsverfahren in gleicher oder ähnlicher Form eingereicht; sie ist nicht identisch mit einer von mir verfassten Magister-, Diplom-, Master-, Bachelor- oder Zulassungsarbeit.

Die meinem Promotionsverfahren zugrunde liegende Promotionsordnung sowie die Studienordnung für die Fakultät für Geowissenschaften der Universität Würzburg sind mir bekannt.

Würzburg, den ……..

(Andreas Dietz)